IJBM

International Journal of

BIOMEDICINE

ISSN 2158-0510

Available online at
www.ijbm.org

INTERNATIONAL JOURNAL OF BIOMEDICINE

Aims and Scope: *International Journal of Biomedicine (IJBM)* publishes peer-reviewed articles on the topics of basic, applied, and translational research on biology and medicine. Original research studies, reviews, hypotheses, editorial commentary, and special reports spanning the spectrum of human and experimental and tissue research will be considered. All research studies involving animals must have been conducted following animal welfare guidelines such as the National Institutes of Health (NIH) Guide for the Care and Use of Laboratory Animals, or equivalent documents. Studies involving human subjects or tissues must adhere to the Declaration of Helsinki and Title 45, US Code of Federal Regulations, Part 46, Protection of Human Subjects, and must have received approval of the appropriate institutional committee charged with oversight of human studies. Informed consent must be obtained.

International Journal of Biomedicine endorses and behaves in accordance with the codes of conduct and international standards established by the Committee on Publication Ethics (COPE).

International Journal of Biomedicine (ISSN 2158-0510) is published four times a year by International Medical Research and Development Corp. (IMRDC), 6308, 12 Avenue, Brooklyn, NY 11219 USA

Customer Service: International Journal of Biomedicine, 6308, 12 Avenue, Brooklyn, NY 11219 USA; Tel: 1-917-740-3053; E-mail: editor@ijbm.org

Manuscript Submission: Original works will be accepted with the understanding that they are contributed solely to the Journal, are not under review by another publication, and have not previously been published except in abstract form. Accepted manuscripts become the sole property of the Journal and may not be published elsewhere without the consent of the Journal. A form stating that the authors transfer all copyright ownership to the Journal will be sent from the Publisher when the manuscript is accepted; this form must be signed by all authors of the article. All manuscripts must be submitted through the International Journal of Biomedicine`s online submission and review website. Authors who are unable to provide an electronic version or have other circumstances that prevent online submission must contact the Editorial Office prior to submission to discuss alternate options (editor@ijbm.org).

IJBM

INTERNATIONAL JOURNAL OF BIOMEDICINE

ISTH 2022 CONGRESS LONDON

JULY 9-13

ISTH2022.ORG

IJBM

INTERNATIONAL JOURNAL OF BIOMEDICINE

www.ijbm.org

Volume 12 Issue 1 March 2022

CONTENTS

Online-Only Articles

READER SERVICES

ins
International
Neuromodulation
Society

INS 15TH WORLD CONGRESS

21 - 26 MAY 2022, BARCELONA, SPAIN

BARCELONA

ins-congress.com

ICNMD 2022

17TH INTERNATIONAL CONGRESS ON NEUROMUSCULAR DISEASES

5 - 9 July 2022 Brussels, Belgium

26th EACMFS CONGRESS

27-30 September 2022

MADRID - SPAIN

European Association for
Cranio - Maxillo - Facial Surgery

www.eacmfs.org www.eacmfs-congress.com

International Journal of Biomedicine 12(1) (2022) 9-18
http://dx.doi.org/10.21103/Article12(1)_RA1

REVIEW ARTICLE

INTERNATIONAL JOURNAL OF BIOMEDICINE

Modern Technologies of Endoscopic Hemostasis in the Treatment of Ulcer Gastroduodenal Bleeding: A Literature Review

Evgeniy F. Cherednikov PhD, ScD[1]; Sergey V. Barannikov[1], PhD; Igor S. Yuzefovich[1], PhD; Aleksandr V. Chernykh[1], PhD, ScD; Tatyana A. Berezhnova[1], PhD, ScD; Galina V. Polubkova[1], PhD; Igor N. Banin[1,2], PhD; Yuri V. Maleev[3], PhD, ScD; Evgeniy S. Ovsyannikov[1*], PhD, ScD; Irina A. Shkurina[1]

[1]Voronezh State Medical University named after N.N. Burdenko
[2]Voronezh City Clinical Emergency Hospital №1
[3]Voronezh Basic Medical College
Voronezh, Russia

Abstract

The treatment of upper gastrointestinal bleeding (UGIB) remains one of the complex problems of clinical practice. In the structure of UGIB, 30%-60% of cases are occupied by bleeding of ulcerative etiology. Success in treating patients with ulcerative gastroduodenal bleeding is possible only with the use of an integrated approach that includes endoscopic, medicinal, endovascular, and surgical hemostasis technologies. In contrast, endoscopic hemostasis (EH) is crucial in the treatment of such patients. The use of modern advances in endoscopy can significantly improve the treatment results of patients with UGIB, reducing the number of operations and mortality in this severely affected group of patients. Modern therapeutic endoscopy has a wide arsenal of tools that can reliably stop bleeding. They differ from each other in the nature of impact, effectiveness, availability, safety, and cost. This article presents an overview of the technological and clinical features of hemostasis, modern views on the choice and application of methods of EH for ulcerative gastroduodenal bleeding.(**International Journal of Biomedicine. 2021;12(1):9-18.**)

Key Words: gastrointestinal hemorrhage • endoscopic hemostasis • peptic ulcer disease • powdered hemostatic systems

For citation: Cherednikov EF, Barannikov SV, Yuzefovich IS, Chernykh AV, Berezhnova TA, Polubkova GV, Banin IN, Maleev YuV, Ovsyannikov ES, Shkurina IA. Modern Technologies of Endoscopic Hemostasis in the Treatment of Ulcer Gastroduodenal Bleeding: A Literature Review. International Journal of Biomedicine. 2022;12(1):9-18. doi:10.21103/Article12(1)_RA1

Abbreviations

AGDU, acute gastroduodenal ulcers; **APC**, argon-plasma coagulation; **EH**, endoscopic hemostasis; **GIB**, gastrointestinal bleeding; **LDA**, low-dose aspirin; **NSAIDs**, non-steroidal anti-inflammatory drugs; **OTSC**, over-the-scope-clip; **PUD**, peptic ulcer disease; **PRP**, platelet-rich plasma; **UGIB**, upper gastrointestinal bleeding.

Introduction

The treatment of UGIB is a serious problem of global clinical practice, which is due to the high rates of morbidity and mortality in this pathology. From 40 to 150 cases of gastrointestinal bleeding (GIB) per 100,000 population are registered annually. The overall mortality in this pathology is at a high level and reaches extremely high figures (40%) with the development of recurrent hemorrhage. From an economic point of view, this problem is also very acute, which is associated with the enormous costs of healthcare systems for the treatment of GIB patients.[1-5]

The largest number of cases in the structure of UGIB falls on the share of bleeding of ulcerative etiology – 30%-60% of cases. PUD of the stomach and duodenum is a chronic recurrent disease with various variants of the course, characterized by

the formation of an ulcerative defect in the mucous membrane and submucosal layer, due to a local inflammatory-necrotic process with an imbalance of intragastric factors of aggression and defense.

PUD is chronic, often recurrent, affecting the young and able-bodied. The progression of PUD is inevitably combined with the development of its complications, in the structure of which the first place is occupied by UGIB (40%-51%), developing in every 10 patients with PUD.[6,7]

Gastroduodenal ulcers can also form due to factors unrelated to the pathogenesis of PUD. These lesions of the gastrointestinal tract are commonly referred to as acute or "symptomatic" gastroduodenal ulcers (AGDU), which have a clear connection with provoking factors with a short history of the development of the disease. According to recent publications, more than half of UGIBs of ulcerative etiology develop as a result of AGDU, rather than PUD, and the number of patients with bleeding from AGDU increases from year to year. Bleeding from AGDU is most common in elderly patients, in patients with burns, after severe surgical interventions, with acute myocardial infarction, cardiovascular insufficiency, uremia, sepsis, and other urgent conditions. The occurrence of this formidable complication in patients with urgent conditions significantly worsens the results of their treatment and often leads to fatal outcomes.[8,9]

One of the types of AGDU is drug ulceration of the stomach and duodenum, the so-called drug ulcers or gastropathy. They are most often formed with the prolonged, uncontrolled intake of anticoagulants, LDA, NSAIDs, glucocorticosteroids, etc.[10-12]

Success in the treatment of patients with ulcerative gastroduodenal bleeding, according to many authors, is possible only with the use of an integrated approach. The main factors determining the successful treatment of patients with ulcerative bleeding are EH, drug-induced hemostasis, and endovascular and surgical hemostasis. At the same time, conservative methods of stopping UGID are of crucial importance in the treatment of such patients, in which EH is of leading importance, and surgical treatment should be performed only in cases when all the possibilities of conservative treatment have been exhausted.[13,14] In this regard, the study of modern methods of EH of UGIB is of particular relevance.

General issues for technologies of EH of UGIB

Endoscopy for UGIB is the most significant endoscopic procedure. Urgent endoscopic examination of the upper digestive tract plays an important role both in the diagnosis and in the treatment of GID. There is no doubt that the decisive role in providing highly qualified care to patients with UGIB belongs to EH and preventing the resumption of GIB. The use of therapeutic endoscopy in patients with UGIB of ulcerative etiology, especially in patients with severe concomitant pathology, and severe blood loss, avoids surgical treatment and reduces overall mortality.[15-17]

Modern endoscopy has a wide arsenal of tools that can reliably stop bleeding. They differ from each other in the nature of impact, effectiveness, availability, safety, and cost. The ideal remedy for EG in UGIB should meet the following requirements: reliable mechanical compression of the bleeding vessel; protection of ulcers from the aggressive effects of gastric contents; the possibility of its application through an endoscope; high hemostatic properties that persist against the background of various coagulopathies; a large area of contact with blood and bleeding surface; presence of sorption, adhesive and plastic properties; long-term preservation on the surface of the bleeding source; positive effect on trophic and regenerative processes; antimicrobial effect; absence of antigenic and toxic properties; safety during application; cheapness; and ease of production and application.[18-20]

The main methods of EH include injection therapy, thermal therapy, mechanical therapy, topical therapy, and combined methods. The choice of the EH method depends on the etiology, localization of the source of hemorrhage, type of UGID, features of the bleeding lesion, the experience of the endoscopist, and technical equipment of the clinic. At the same time, not only implementing primary hemostasis, but also, most importantly, preventing the resumption of bleeding is crucial in the endoscopic treatment of GIB.[21-23]

Injection therapy

Injection EH is the most common method of stopping UGIB and requires only an endoscopic injector and a solution for injecting the source of hemorrhage, which determines the simplicity, accessibility, and cheapness of using this method of hemostasis. When using drugs for the purpose of injection hemostasis, it is necessary that the drug meet certain requirements: low absorption rate, no locally damaging effect on tissue, availability, and low cost of the drug. Most often, a solution of epinephrine in dilution 1:10000/1:20000, 5% solution of aminocaproic acid, 1% solution of hydrogen peroxide, 5% ascorbic acid, ethanolamine, thrombin, sodium tetradecyl sulfate, etc. are used as a hemostatic agent for injection therapy. The mechanism of action of injection therapy consists in compressing the source of bleeding by infiltrate created during paravasal administration of the medicinal solution, as well as by pharmacological mechanisms of action of the injected drugs.[24]

Most often, in clinical practice, pricking the source of bleeding with epinephrine in a dilution of 1:10000 or 1:20000 is used. Injection therapy with epinephrine leads to bleeding stoppage due to infiltrative compression of the eroded vessel, spasm of the eroded vessels, and stimulation of platelet aggregation at the bleeding site. The injection is made into the submucosa and/or directly into the base of the ulcer in four zones around the eroded vessel in an amount of 0.5 ml to 2 ml of epinephrine solution (1:10000). At the same time, it is important to retreat from the border of the bleeding vessel at least 3 mm. The disadvantages of this method include: within a short period of time, the infiltrate created by the injection resolves, vasospasm is stopped, which leads to the development of a recurrence of hemorrhage. In this regard, this method of EH in the form of monotherapy is not recommended.[25,26]

In recent years, solutions of sclerosants have been actively used for EH: 96% ethanol, ethanolamine, sodium tetradecyl sulfate, polydicanol, etc. The mechanism of action of sclerosants consists in the dehydration and fixation of the wall of the damaged vessel to the surrounding tissues, which leads to the destruction of the endothelial cells of the vessel

and the formation of a dense thrombus. At the same time, the use of sclerosants has a number of significant drawbacks: firstly, the administration of the drug in small doses is often insufficient, and secondly, hemostasis is achieved due to vascular thrombosis, tissue necrosis and inflammation at the injection site, which can lead to perforation of the organ wall (1-3% of cases). These drugs should be used with caution in small quantities due to the fear of developing deep tissue necrosis.[27,28]

Another class of injectable agents is tissue adhesives, which include thrombin, fibrin, and cyanoacrylate adhesives that clog the site of hemorrhage. Fibrin glue consists of two components: human fibrinogen with coagulation factor XIII and an activator solution containing human thrombin, which are in two separate syringes. During hemostasis, these two components are mixed by agents, which leads to the formation of a clot, thereby simulating the final phase of the physiological cascade of blood clotting. Fibrin glue is commercially used in Europe for EH in bleeding ulcers and varicose veins. It should be noted that the procedure for hemostasis is quite complicated and requires some experience. In some cases, if the glue technology is used incorrectly, glue polymerization is possible in the lumen of the injector or in the working channels of the endoscope, which can lead to damage to endoscopic equipment and failure in hemostasis of UGIB.[29]

A promising method is injectable hemostasis by pricking a bleeding ulcer defect with platelet-rich autoplasm (PRP) of the patient. PRP is obtained immediately before the procedure by centrifugation of the patient's blood. Introducing PRP into the submucosal layer of the periulcer zone for a long time creates compression by infiltration of tissues due to edema, which leads to persistent hemostasis and prevents the development of relapses. In addition, PRP contains autogenic "growth factors" that stimulate intensive recovery of the affected area of the mucous and submucosal layers of the stomach and duodenum. PRP is injected in a volume of 2 ml endoscopically into the submucosal layer of the periulcer zone. The method provides stable hemostasis and significantly reduces the number of relapses, which contributes to improving the quality of life of patients and reducing treatment costs. However, this method is also not without drawbacks: the preparation of PRP requires a certain amount of time, which is not always possible in patients in critical condition; to obtain PRP requires specialized systems that are not always available in clinical practice. In addition, there are no randomized controlled clinical trials showing the effectiveness of this method of EH.[30,31]

It should be noted that none of the types of solutions for endoscopic injection hemostasis has significant pronounced advantages and cannot be used as the "gold standard" of endoscopic treatment.

Thermal therapy

Thermal therapy methods of EH are widely used in clinical practice. The mechanism of action of these methods of hemostasis consists of the use of thermal energy in order to coagulate eroded vessels and stop bleeding. Laser photocoagulation, diathermocoagulation, radiofrequency ablation, and APC have become the most widespread.[32]

One of the methods of thermal therapy of UGIB is laser photocoagulation. As a method of EH, laser coagulation uses laser radiation in order to create coagulation necrosis in the area of the source of GIB. High-power lasers of more than 10 watts are used. The effectiveness of laser photocoagulation in UGID is observed in 80%-90% of cases; the frequency of relapses after successful coagulation is high, reaching 28%. The advantage of laser coagulation is contactless, but this method has technical limitations. Thus, with continued jet bleeding, the blood coming from the eroded vessel scatters the laser beam, thereby weakening the coagulating effect. In the presence of a clot on the surface of the ulcerative defect, it is also impossible to provide laser hemostasis. To stop bleeding with continued bleeding, it is necessary to increase the radiation power and exposure time, which, in turn, increases the risk of perforation. The way out of this problem was the use of contact laser coagulation, but at the same time, the main advantage of this method is lost – it's non-contact. The high cost of using laser photocoagulation, in the presence of other disadvantages of this method, limits the possibility of its use in clinical practice.[33-37]

The most common method of EH is diathermocoagulation. There are several ways to use it: unipolar or bipolar electrocoagulation, multipolar diathermocoagulation, and liquid diathermocoagulation. In bipolar diathermocoagulation, hemostasis is achieved by the formation of coagulation necrosis between two located electrodes when an electrical circuit is closed. During coagulation, a blood clot forms in the vessel, both directly at the site of coagulation and throughout, due to the spread of the zone of coagulation necrosis. When using monopolar coagulation, tissue damage is more extensive and deep than when using the bipolar method. In this regard, it is advisable to use bipolar diathermocoagulation with bleeding from small vessels, and with bleeding from larger vessels, the monopolar method is preferred. Despite the many advantages of diathermocoagulation, this method is not without drawbacks. One of the most formidable complications when using it is deep necrosis of the organ wall, which can lead to perforation.

The method of diathermocoagulation is a contact method, and when the electrocautery is withdrawn, bleeding may resume due to the separation of the formed thrombus.[38,39]

The solution to the main drawback of the electrocoagulation method in the form of sticking the electrode to the source of bleeding was a method of "liquid" diathermocoagulation, developed by the staff of the Department of Faculty Surgery of the Voronezh N.N. Burdenko State Medical University. Coagulation of the bleeding source when using "liquid" diathermocoagulation occurs through an electrolyte, which makes it possible to coagulate the bleeding vessel directly without subsequent separation of the electrode from the coagulation scab. In addition, this method is more gentle and causes less damage to surrounding tissues than traditional electrocoagulation.[40,41]

An alternative to the electrocoagulation method is heater probe thermocoagulation, which consists in cauterizing the source of bleeding with a heated aluminum cylinder-probe coated with Teflon.

Closing the electrical circuit leads to the aluminum cylinder heating to 150 degrees. With the help of a red-hot tip, the source of bleeding is cauterized, resulting in coagulation hemostasis. The use of Teflon as a sprayer reduces the possibility of tissue burning to the probe and increases the effectiveness of this method. However, this method is also a contact method, and the possibility remains that the coagulation scab will be separated during its application. In addition, local exposure to high temperature leads to deep destructive processes forming in the area surrounding the source of bleeding tissues, which worsens the reparative processes in the area of ulcerative defect and is a prerequisite for the development of repeated bleeding.[42-44]

Argon-plasma coagulation (APC) is an effective non-contact method of EH. It is based on the application of high-frequency electric current in the flow of ionized argon. The absolute advantage of this method is that it is a non-contact mode since the impact is made at a distance of 2mm to 10mm from the source of hemorrhage, and when removing the electrode, there is no threat of clot separation. In addition, the coagulation depth does not exceed 3 mm, which avoids the possibility of perforation of the organ wall. The disadvantage of APC is the high cost of the equipment, which limits the possibilities of its use. The effectiveness of primary EH when using APC reaches 95%-98%, but the occurrence of hemorrhagic relapses, even after a successful primary stop of bleeding, reaches 12.5%-15% of cases, which may be due to the effect of coagulation on the source of bleeding, as well as the lack of protection of the coagulation scab from the aggressive environment of gastric juice.[45-48]

The method of radiofrequency ablation, based on the effect of radio waves, has become widespread. When using radiofrequency ablation, radiofrequency evaporation of tissues occurs by forming a surface layer of necrosis. With this method, the electrode remains cold all the time and does not cause burns to the surrounding tissues. The effect of coagulation is also associated with vasoconstriction and evaporation of an intercellular fluid, which leads to additional spasms of the eroded vessels. The advantage of radiofrequency ablation is its safety and low risk of perforating the organ wall. Radiofrequency ablation allows for primary EH in 95%-97% of cases, but the recurrence rate remains high (10%-13% of cases), which is explained by disadvantages similar to APC.[49,50]

Mechanical therapy

One of the effective methods of EH in UGIB is clipping, which consists in squeezing the source of bleeding with the endoscopic hemoclips (endoclips). Hemoclips can be used for active bleeding of Forrest IA-IB, in the presence of thrombosed vessels of the Forrest IIA ulcerative defect area, as well as for closing perforations and fistulas. They were first introduced into clinical practice in Japan, and later their use expanded after certain technical improvements. Currently, the use of endoclips is considered a safe and effective method of EH - an alternative to surgical treatment of patients.[51,52]

The mechanism of hemostasis with the use of endoclips is similar to the mechanism of surgical stitching of a bleeding vessel. The clip is carried out through the instrumental channel of the endoscope and fixed with a clip on the base of the vessel, while achieving a reliable stoppage of bleeding. There is a direct clipping – when the clip is applied directly to the base of the bleeding vessel; and indirect – the capture of the vessel together with the tissues surrounding the source of bleeding. Endoscopic clips directly squeeze the source of bleeding without causing tissue damage. The available clips differ in several functions (opening and closing, turning the clip, disposable or not) with a total minimum channel size (2.8mm). Their jaw length varies from 9mm to 11mm, which makes them ideal for defects from 10mm to 15mm. The advantage of clipping is its effectiveness in stopping bleeding from large eroded vessels, and its effectiveness in patients with severe hypocoagulation. Currently, a large number of devices for endoscopic clipping with different hole diameters, ease of rotation, and the possibility of re-opening have been developed. However, the disadvantages of this method of EH include technical complexity, which requires high training of endoscopists. Hemoclips are difficult to use in hard-to-reach areas, such as the small curvature of the stomach, the cardia and the posterior wall of the duodenum. With large and callous ulcers, in which the defect tissues are dense and rigid, the imposition often fails to completely compress the source of bleeding when clips are applied, which can lead to insufficient hemostasis or repeated bleeding. It should be noted that even after successful endoclipping, bleeding relapses occur in 1.8%-37% of cases.[53,54]

A modern variant of endoscopic clips is the "over-the-scope-clip" (OTSC) system. Due to their design, size, and high compression force, the OTSC system can be much better fixed in chronic callous ulcerative defects. The OTSC system is effective in 84.9% of cases, and is also effective in the difficult localization of ulcers in the posterior wall of the duodenum. These results show that the OTSC system is a possible method of choice for patients who are at high risk for an operation.[55-57]

Topical therapy

The topical therapy method of EH is one of the earliest in therapeutic endoscopy. For application to the surface of a bleeding ulcer, vasoconstrictive and hemostatic drugs are used: Thrombin, Firrogen, Caprofer, Amifer, Feracril, Fibrin, medical adhesives, etc. However, adhesive compositions have water-repellent properties; the rejection of the polymer film from the bleeding defect occurs within a few hours to one day, so the time of its therapeutic effect is sharply limited. At the same time, it should be noted that film-forming polymers do not have local hemostatic properties, and implementing the therapeutic procedure itself has certain difficulties.[58-60]

The advantages of using the topical therapy method are ease of use, easier access to complex anatomical zones of the gastroduodenal region, not necessarily accurate targeting of the source of hemorrhage, the possibility of covering large bleeding eroded surfaces with decaying tumors of the digestive tract. At the same time, the effectiveness of the application of EH methods to stop ongoing ulcerative bleeding is considered low. However, the possibility of protecting the ulcerative defect from aggressive factors of gastric and duodenal contents allows this method to be widely used in order to prevent recurrence of bleeding.[61-63]

In recent years, an increasing number of publications have appeared in the literature on the use of modern powdered hemostatic systems TC-325 (Hemospray; Cook Medical Inc., Winston-Salem, NC, USA), EndoClot (EndoClot Plus Inc., Santa Clara, CA, USA) for EH of GIB. The use of powdered hemostatic systems shows promising results in the treatment of patients with UGIB.[64]

Hemospray (TC-325) is a granular, inorganic, natural, mineral absorbent powder made from a material known as bentonite clay (aluminum phyllosilicate). TC-325 has high biocompatibility, is even edible, does not contain organic substances, and has strong absorbent properties. The drug is applied to the source of gastroduodenal bleeding in powder form using a device powered by CO2 cartridges under pressure. The mechanism of action is based on the absorption of water from the surrounding tissues by TC-325 powder, which becomes an adhesive aggregate that creates a mechanical barrier over the bleeding site. After application, Hemospray naturally exfoliates from the surface of the source of hemorrhage and is removed within 1 to 3 days after insufflation. The effectiveness of Hemospray with continued bleeding reaches from 75% to 95%, while the recurrence rate of hemorrhage reaches 8.8% to 22.8%.[65,66]

Another biocompatible hemostatic powder system for flexible endoscopy is EndoClot. EndoClot is a powdered polysaccharide hemostatic system, the chemical substrate of which is dextran, obtained from starch, which manufacturers call "absorbable modified polymers." EndoClot has been specially developed as a powdered hemostatic agent for the treatment of GIB. The mechanism of hemostasis when using EndoClot is based on the chemical properties of dextran, the ability to adsorb blood, thereby concentrating clotting factors and cellular elements on the surface of the granules, which accelerates the clotting process. A comparative study conducted by Vitali et al.[67] showed that Hemospray and Endoclot powders are equally effective as local hemostatics in the treatment of GIB, without differences in short-term or long-term success and repeated bleeding.

The use of powdered hemostatic systems is not possible with spurting hemorrhage FIA, since these hemostatic agents are washed off by a stream of blood and cannot attach to the source of hemorrhage. Clinical studies have shown that the use of these drugs is possible as an intermediate option for temporary hemostasis, since they are safe and effective, but have a temporary effect. It should be noted that sufficient experience has not yet been accumulated in the clinical use of the hemostatic systems Hemospray and EndoClot, which would require larger-scale, randomized controlled clinical trials to determine the effectiveness of their use in clinical practice.[68,69]

The Voronezh City Specialized Center for the Treatment of Patients with GIB has been using powdered granular sorbents (Aseptisorb, Aseptisorb-A, Aseptisorb-D, Sefadex, etc.) for the endoscopic treatment of UGIB for 30 years. The founder of sorption-insufflation therapy of GIB is professor EF Cherednikov.[70-72]

According to scientists in this field, the mechanism of hemostatic action of granular sorbents consists of sorption, absorption, and concentration of platelet and coagulation factors on the surface of sorbent granules. Granular sorbents are chemically neutral compounds that can be used without causing damage to the mucous membrane of the digestive tract. Having a high adhesive activity, granular sorbents are retained in the area of bleeding defects for 3-5 days, after which they are naturally removed from the digestive tract. The application of the sorbent promotes cytoprotective protection of the source of hemorrhage from the aggressive effects of gastric and duodenal contents, creating conditions for the healing of gastroduodenal ulcers. A number of sorbents are endowed with additional pharmacological properties – antiseptic, analgesic, proteolytic, etc.– which expands the indications and effectiveness of their use. However, the use of granular sorbents in the form of monotherapy can lead to repeated bleeding, which the authors attribute to their insufficient hemostatic activity.[73-75]

The improvement of the sorption-insufflation direction of endoscopic treatment of GIB was the combined use of granular sorbents with local hemostatics. In an experimental clinical study conducted on 15 laboratory animals and 115 patients with bleeding from gastroduodenal ulcers, a team of scientists from Voronezh N.N. Burdenko State University showed the effectiveness of granular sorbent Aseptisorb-D in combination with powdered hemostatic in treating ulcerative UGIB, which allowed for final hemostasis in 94.9% of cases, with a recurrence rate of 5.1%.[76-78]

S.V.Barannikov and co-authors used combined endoscopic insufflation of granular sorbent Aseptisorb-A in combination with PRP of patients in an experimental clinical study with a morphological examination of the processes of reparative regeneration of gastroduodenal ulcers. It has been shown that the use of the developed technology based on sorption cytoprotection of ulcerative defects in combination with the use of biologically active hemostatic PRP containing autogenic growth factors contributes to the achievement of final hemostasis in 96.5% of cases, reduces the frequency of resumption of bleeding to 3.5%, while reducing the time and improving the quality of healing of gastroduodenal ulcers.[79-81]

Combined EH

To increase the reliability of EH in ulcerative UGIB, a combination of several methods of stopping bleeding that complement each other is used. This method is called combined EH. The most commonly used injection therapy is used in combination with thermal therapy (APC, diathermocoagulation, laser photocoagulation, etc.). Combination therapy (dual therapy), that is, infiltration in combination with coagulation of the bleeding source, or mechanical compression using hemoclips, remains the optimal endoscopic therapy recommended in the main international clinical guidelines for the treatment of GIB patients.[82,83]

The Cochrane review in 2014 evaluated the results of 19 randomized clinical trials involving 2033 patients and concluded that the use of dual endoscopic therapy significantly reduces the risk of bleeding recurrence and the need for emergency surgical treatment, compared with monotherapy with epinephrine injection therapy. The mortality of patients with gastric bleeding was also lower in the group of combined

EH; the results were not statistically significant. Similar results have been demonstrated in some other meta-analyses. Thus, scientists came to the conclusion that injection therapy with epinephrine should not be used as monotherapy, but only in combination with other methods of EH.[84-86]

The modern technology of combined EH of ulcerative GIB is the use of triple endoscopic therapy in the complex treatment of unstable-stopped gastroduodenal bleeding. Scientists of the Voronezh N.N. Burdenko State Medical University in randomized clinical trials applied an individual approach with combined methods of emergency and preventive EH, including first stopping bleeding by injection therapy with ε-aminocaproic acid, followed by APC and insufflation on the source of hemorrhage of granular sorbents (Aseptisorb-D, Aseptisorb-A) in combination with hemostatic agents Zhelplastan and PRP. The application of the developed technologies made it possible to ensure effective hemostasis of ongoing bleeding (FIA-FIB) in 95.2% of cases, to increase the reliability of preventing recurrence of hemorrhage (FIIA-FIIB) to 95.5%, with a total frequency of recurrence bleeding of 4.5% and activity involving operations of 1.5%.[87]

Promising technologies of EH

Some authors consider three important areas to be the latest achievement in the issues of EH of GIB: the use of Doppler scanning, modern large clips, and powdered hemostatic systems.[88]

Recently, there has been an increase in the interest of scientists in using the capabilities of ultrasound Doppler scanning in the issues of EH of GIB, which is due to the technological development of diagnostic equipment and increased availability of the Doppler probe in flexible endoscopy. The assessment of the source of UGIB using a Doppler probe is more accurate than the classical endoscopic assessment by Forrest, when predicting the risk of recurrence of bleeding, which can improve the quality of treatment of patients with GIB. The Doppler assessment allows establishment of the features of the blood supply to the source of gastroduodenal bleeding and to establish the rate of Doppler-positive arterial flow, which is an important predictor of the development of recurrent hemorrhage and determines the tactical tasks of EH. So, an interesting circumstance is that with the type of bleeding FIIC, which classically has a low risk of recurrence of hemorrhage, in 40.5% of cases, there is a positive arterial Doppler signal, which indicates a high risk of recurrence of hemorrhage and requires endoscopic intervention. The frequency of the positive Doppler signal in the FIA type is 100%, in FIB - 46.7%, FIIA - 90.7%, FIIB - 68.4%, and FIII - 8.3%, which must be taken into account in clinical practice. Repeated Doppler evaluation after primary EH also has prognostic value: maintaining a constant arterial flow in the area of the source of hemorrhage is associated with an increased risk of repeated bleeding. The Doppler scanning technique in GIB endoscopy looks very promising. The use of a Doppler probe makes it possible to more accurately determine the risk of repeated bleeding, facilitates the tracking of artery feeders, and allows evaluating the effectiveness of EH. The importance of Doppler scanning in modern therapeutic endoscopy requires further research and evaluation, but, apparently, this method has some advantages in certain clinical situations.[89-91]

In Japan, in 2012, a technique for hemostasis of UGIB by endoscopic hand suturing (EHS) was developed. In this technique, a bleeding defect is sutured with a continuous suture similar to the surgical stitching of a bleeding vessel. The rigid absorbable suture material is used, which excludes the spontaneous formation of nodes. Using a special flexible endoscopic needle holder (Olympus Co., Ltd., Tokyo, Japan), the endoscopist can securely grip and smoothly rotate the needle. The EHS technique was successfully carried out in experimental studies in vivo on a model of bleeding stomach defects in pigs and in 30 patients with bleeding defects of the gastroduodenal zone. The use of the EHS technique in 97% of cases showed positive results, hemostasis was reliable and final, there was no resumption of bleeding, regardless of the state of the blood clotting system. The EHS duration is 50 minutes with 8.0 stitches.[92]

An alternative to the EHS technique is the Overstitch™ technology (Apollo Endosurgery, Inc., Austin, Texas, USA). The Overstitch™ stitching system is designed to close the hole created for transluminal intervention (transgastric endoscopic appendectomy, transvaginal endoscopic cholecystectomy). In the 2010s, the use of the Overstitch™ system decreased due to the decline in the popularity of transluminal interventions, but Overstitch™ began to be used for intraluminal stitching of gastrointestinal tract tissues. Endoscopic suturing of the defects of the mucous membrane of the gastroduodenal region is useful for stopping GIB. Overstitch™ seems promising in the field of therapeutic endoscopy, since it is easy to use, requires a short suturing time (13 minutes per 1.6 stitches), and provides reliable, long-lasting closure of the defect for the entire wall thickness of the hollow organ. However, it is expensive and inaccessible in some parts of the world.[93]

It is expected that the development of endoscopic stitching techniques for bleeding defects will reduce the risk of bleeding recurrence in patients with high risk of needing an operation. Further studies of the use of EHS and Overstitch™ in hemostasis of GIB and the expansion of indications for the use of these methods are needed.

Conclusion

Thus, to date, there is no single universal method for arresting ulcerative gastroduodenal bleeding endoscopically. In this regard, the development of new, and the improvement of already used, methods of EH is an urgent task of modern emergency surgery.

Competing Interests

The authors declare that they have no competing interests.

***Corresponding author**: Prof. Evgeniy S. Ovsyannikov, PhD, ScD. Department of faculty therapy, Voronezh State Medical University named after N.N. Burdenko. Voronezh, Russia. E-mail: ovses@yandex.ru*

References

1. Gaiani F, De'Angelis N, Kayali S, Manfredi M, Di Mario F, Leandro G, Ghiselli A, Fornaroli F, De'Angelis GL. Clinical approach to the patient with acute gastrointestinal bleeding. Acta Biomed. 2018 Dec 17;89(8-S):12-19. doi: 10.23750/abm.v89i8-S.7861.
2. Jang JY. Recent Developments in the Endoscopic Treatment of Patients with Peptic Ulcer Bleeding. Clin Endosc. 2016;49(5):417-420. doi:10.5946/ce.2016.135
3. Abougergi MS, Travis AC, Saltzman JR. The in-hospital mortality rate for upper GI hemorrhage has decreased over 2 decades in the United States: a nationwide analysis. Gastrointest Endosc. 2015;81(4):882-8.e1. doi:10.1016/j.gie.2014.09.027
4. Cherednikov EF, Maleev YuV, Chernyh AV, Litovkina TE, Bondarenko AA, Cherednikov EE, Popov AV. [Current views on the diagnosis, treatment, and prevention of ruptured hemorrhagic syndrome (Mallory-Weiss syndrome)]. Journal of New Medical Technologies. 2016;23(4):161-172. [Article in Russian].
5. Cherednikov E F, Chernyh AV, Maleev YuV, Popov AV, Stekolnikov VV. [Topographical and anatomical prerequisites for the development of Mallory-Weiss syndrome]. Bulletin of the Russian Military Medical Academy.2015;(S2):153-154. [Article in Russian].
6. Laine L. CLINICAL PRACTICE. Upper Gastrointestinal Bleeding Due to a Peptic Ulcer. N Engl J Med. 2016;374(24):2367-2376. doi:10.1056/NEJMcp1514257
7. Tielleman T, Bujanda D, Cryer B. Epidemiology and Risk Factors for Upper Gastrointestinal Bleeding. Gastrointest Endosc Clin N Am. 2015;25(3):415-428. doi:10.1016/j.giec.2015.02.010
8. Budnevsky AV, Cherednikov EF, Popov AV, Ovsyannikov ES, Kravchenko AY, Fursov KO. A complex multidisciplinary approach to prevention gastro-duodenal bleeding in patients of general hospital. International Journal of Biomedicine. 2017;7(3):204-207. doi: 10.21103/Article7(3)_OA8
9. Cherednikov EF, Budnevsky AV, Popov AV, Fursov KO. A new opinion on gastroduodenal bleeding preventon in patients with somatic pathology. The EPMA Journal. 2017; 8(S1):46.
10. Iwamoto J, Murakami M, Monma T, et al. Current states of prevention of drug-induced gastroduodenal ulcer in real clinical practice: a cross-sectional study. J Clin Biochem Nutr. 2020;66(2):158-162. doi:10.3164/jcbn.19-66
11. Chu SJ, Yoon KT, Kim JS. Korean J Gastroenterol. 2020;76(5):232-237. doi:10.4166/kjg.2020.139
12. Joo MK, Park CH, Kim JS, Park JM, Ahn JY, Lee BE, Lee JH, Yang HJ, Cho YK, Bang CS, Kim BJ, Jung HK, Kim BW, Lee YC; Korean College of Helicobacter and Upper Gastrointestinal Research. [Clinical Guidelines for Drug-induced Peptic Ulcer, 2020 Revised Edition]. Korean J Gastroenterol. 2020 Sep 25;76(3):108-133. doi: 10.4166/kjg.2020.76.3.108. [Article in Korean].
13. Mujtaba S, Chawla S, Massaad JF. Diagnosis and Management of Non-Variceal Gastrointestinal Hemorrhage: A Review of Current Guidelines and Future Perspectives. J Clin Med. 2020;9(2):402. Published 2020 Feb 2. doi:10.3390/jcm9020402
14. Troland D, Stanley A. Endotherapy of Peptic Ulcer Bleeding. Gastrointest Endosc Clin N Am. 2018;28(3):277-289. doi:10.1016/j.giec.2018.02.002
15. Barannikov SV, Cherednikov EF, Yuzefovich IS, Banin IN, Polubkova GV, Vysotskaya AT, Maleev YuV, Ovsyannikov ES, Chernykh AV. Modern Clinical and Epidemiological Features and New Technological Possibilities in the Treatment of Bleeding Gastroduodenal Ulcers. International Journal of Biomedicine. 2021;11(4):428-434. doi:10.21103/Article11(4)_OA6
16. Kurniawan N, Keuchel M. Flexible Gastro-intestinal Endoscopy - Clinical Challenges and Technical Achievements. Comput Struct Biotechnol J. 2017 Jan 18;15:168-179. doi: 10.1016/j.csbj.2017.01.004.
17. Adianov VV, Cherednikov EF. [Optimizing treatment of gastroduodenal bleeding in patients with high surgical risk]. System Analysis and Management in Biomedical Systems. 2014;13(4):841-846. [Article in Russian].
18. Cherednikov EF, Barannikov SV, Glukhov AA, Banin IN, Maleev YuV, Adianov VV. [The use of Aseptisorb-A and platelet-rich plasma in the complex endoscopic treatment of patients with ulcerative gastroduodenal bleeding]. Bulletin of Experimental and Clinical Surgery.2017;10(2):116-122. doi: 10.18499/2070-478X-2017-10-2-116-122 [Article in Russian].
19. Baev VE. Experimental substantiation of the use of hydrogels for the treatment of bleeding stomach ulcers. Abstract for PhD Thesis. Voronezh. 1997. [in Russian].
20. Il'kanich AYa, Darvin VV, Ryzhikov MG, Oganyan AV. [Diagnosis and treatment of ulcerative gastroduodenal bleeding]. Yakutskij Medicinskij Zhurnal.2021;3(75):46-50. doi 10.25789/YMJ.2021.75.12. [Article in Russian].
21. Jung K, Moon W. Role of endoscopy in acute gastrointestinal bleeding in real clinical practice: An evidence-based review. World J Gastrointest Endosc. 2019;11(2):68-83. doi:10.4253/wjge.v11.i2.68
22. Wang TX, Zhang J, Cui LH, Tian JJ, Wei R. Efficacy of Therapeutic Endoscopy for Gastrointestinal Lesion (GI): A network meta-analysis. Pak J Med Sci. 2019;35(2):561-568. doi:10.12669/pjms.35.2.636
23. Barnert J, Messmann H. Diagnosis and management of lower gastrointestinal bleeding. Nat Rev Gastroenterol Hepatol. 2009;6(11):637-646. doi:10.1038/nrgastro.2009.167
24. Asge Technology Committee, Conway JD, Adler DG, Diehl DL, Farraye FA, Kantsevoy SV, Kaul V, Kethu SR, Kwon RS, Mamula P, Rodriguez SA, Tierney WM. Endoscopic hemostatic devices. Gastrointest Endosc. 2009 May;69(6):987-96. doi: 10.1016/j.gie.2008.12.251.
25. Biecker E. Diagnosis and therapy of non-variceal upper gastrointestinal bleeding. World J Gastrointest Pharmacol Ther. 2015;6(4):172-182. doi:10.4292/wjgpt.v6.i4.172
26. Mille M, Engelhardt T, Stier A. Bleeding Duodenal Ulcer: Strategies in High-Risk Ulcers. Visc Med. 2021;37(1):52-62. doi:10.1159/000513689
27. Laine L, McQuaid KR. Endoscopic therapy for bleeding ulcers: an evidence-based approach based on meta-analyses of randomized controlled trials. Clin Gastroenterol Hepatol. 2009;7(1):33-2. doi:10.1016/j.cgh.2008.08.016
28. Technology Assessment Committee, Croffie J, Somogyi L, Chuttani R, DiSario J, Liu J, Mishkin D, Shah RJ, Tierney W, Wong Kee Song LM, Petersen BT. Sclerosing agents for use in GI endoscopy. Gastrointest Endosc. 2007 Jul;66(1):1-6. doi: 10.1016/j.gie.2007.02.014.
29. ASGE Technology Committee, Bhat YM, Banerjee S, Barth BA, Chauhan SS, Gottlieb KT, Konda V, Maple JT, Murad FM, Pfau PR, Pleskow DK, Siddiqui UD, Tokar JL, Wang A, Rodriguez SA. Tissue adhesives: cyanoacrylate glue and fibrin sealant. Gastrointest Endosc. 2013 Aug;78(2):209-

15. doi: 10.1016/j.gie.2013.04.166.
30. Patent No. 2675996 C1 Russian Federation, MPK A61B 1/273, A61K 35/16, A61K 35/19. Method of endoscopic hemostasis in ulcerative gastroduodenal bleeding: No. 2017136682: application 17.10.2017: publ. 25.12.2018 / M.V. Podina, B. M. Belik, S. S. Keshchyan [et al.]. [In Russian].
31. Belik BM, Podina MV, Tenchurin RS, Skorlyakov BB, Usatkin AA, Baev OV, Keshchyan SS. [A differentiated approach to the use of endoscopic hemostasis methods in gastroduodenal ulcerative bleeding]. Bulletin of Surgical Gastroenterology. 2018;1:14. [Article in Russian].
32. Rey JW, Fischbach A, Teubner D, et al. Acute gastrointestinal bleeding - a new approach to clinical and endoscopic management. Eur J Gastroenterol Hepatol. 2015;27(5):483-491. doi:10.1097/MEG.0000000000000343
33. Potakhin SN. Risk factor analysis and method development for predicting the recurrence of gastroduodenal ulcer bleeding. Russian Open Medical Journal. 2020;9(4):419. doi 10.15275/rusomj.2020.0419.
34. Potahin SN, Shapkin YuG. [Comparative analysis of methods for predicting recurrence of ulcerative gastroduodenal]. Novosti Hirurgii. 2020;28(2):141-149. doi 10.18484/2305-0047.2020.2.141. [Article in Russian].
35. Barhatova NA. [The role of endoscopic photocoagulation hemostasis in gastrointestinal bleeding]. Vestnik Soveta Molodyh Uchyonyh i Specialistov CHelyabinskoj Oblasti. 2016; 2(13):7-9. [Article in Russian].
36. Shapkin YG, Potahin SN. [The dynamics of main indicators for the treatment of ulcerative gastroduodenal bleeding - the analysis of several years studies]. Saratov Journal of Scientific Research. 2014;10(3):456-460. [Article in Russian].
37. Grishaev VA, Shapkin YuG, Kapralov SV, Maslyakov VV. [Optimization of laser endoscopic hemostasis in gastrointestinal bleeding]. Vestnik Medicinskogo Instituta "REAVIZ": Reabilitatsiia, Vrach i Zdorov'e. 2018;2(32):26-31. [Article in Russian].
38. Shepet'ko EN, Efremov VV. [Modern methods of endoscopic hemostasis and its effectiveness in the treatment of acute ulcerative duodenal bleeding]. Hirurgiya. Vostochnaya Evropa. 2013;4(08): 65-74. [Article in Russian].
39. Petrov DYu, Fedorov ED, Yudin OI. [Comparative evaluation of endoscopic argonoplasmic coagulation and bipolar diathermocoagulation in ulcerative gastroduodenal bleeding]. Vestnik Rossijskogo Gosudarstvennogo Medicinskogo Universiteta. 2009; 6:19-22. [Article in Russian].
40. Cherednikov EF, Deryaeva OG, Adianov VV, Ovchinnikov IF, Popov AV. [Modern directions of prevention and treatment of patients with gastrointestinal bleeding in the center]. System Analysis and Management in Biomedical Systems. 2014; 13(2):426-433. [Article in Russian].
41. Bondarenko AA. Liquid diathermocoagulation in endoscopic arrest of profuse ulcerative gastroduodenal bleeding: experimental clinical study. Abstract for PhD Thesis. Voronezh. 2003: 22 pp. [In Russian].
42. Changela K, Papafragkakis H, Ofori E, Ona MA, Krishnaiah M, Duddempudi S, Anand S. Hemostatic powder spray: a new method for managing gastrointestinal bleeding. Therap Adv Gastroenterol. 2015 May;8(3):125-35. doi: 10.1177/1756283X15572587.
43. Nunoue T, Takenaka R, Hori K, Okazaki N, Hamada K, Baba Y, Yamasaki Y, Kono Y, Seki H, Inokuchi T, Takemoto K, Taira A, Tsugeno H, Fujiki S, Kawahara Y, Okada H. A Randomized Trial of Monopolar Soft-mode Coagulation Versus Heater Probe Thermocoagulation for Peptic Ulcer Bleeding. J Clin Gastroenterol. 2015 Jul;49(6):472-6. doi: 10.1097/MCG.0000000000000190.
44. Gonzales P, Klusewitz S, Marowske J, Gancayco J, Osswald MB, Setlik R. Everolimus Implicated in Case of Severe Gastrointestinal Hemorrhage. Case Rep Oncol Med. 2017;2017:3657812. doi:10.1155/2017/3657812
45. Kurosawa M, Takamatsu T, Kawano H, Hayashi Y, Miyahara H, Ota S, Okino A, Yoshida M. Endoscopic Hemostasis in Porcine Gastrointestinal Tract Using CO_2 Low-Temperature Plasma Jet. J Surg Res. 2019 Feb;234:334-342. doi: 10.1016/j.jss.2018.09.068.
46. Martins BC, Wodak S, Gusmon CC, Safatle-Ribeiro AV, Kawaguti FS, Baba ER, Pennacchi CM, Lima MS, Ribeiro U Jr, Maluf-Filho F. Argon plasma coagulation for the endoscopic treatment of gastrointestinal tumor bleeding: A retrospective comparison with a non-treated historical cohort. United European Gastroenterol J. 2016 Feb;4(1):49-54. doi: 10.1177/2050640615590303.
47. Chiu YC, Lu LS, Wu KL, Tam W, Hu ML, Tai WC, Chiu KW, Chuah SK. Comparison of argon plasma coagulation in management of upper gastrointestinal angiodysplasia and gastric antral vascular ectasia hemorrhage. BMC Gastroenterol. 2012 Jun 9;12:67. doi: 10.1186/1471-230X-12-67.
48. Schweizer U, Grund KE, Fundel J, Wichmann D, Königsrainer A. Therapie der nichtvariköse oberen gastrointestinalen Blutung: endoluminal – endovaskulär – chirurgisch [Treatment of nonvariceal upper gastrointestinal bleeding: endoluminal-endovascular-surgical]. Chirurg. 2019 Aug;90(8):607-613. doi: 10.1007/s00104-019-0948-7. [Article in German].
49. Ofosu A, Ramai D, Latson W, Adler DG. Endoscopic management of bleeding gastrointestinal tumors. Ann Gastroenterol. 2019;32(4):346-351. doi:10.20524/aog.2019.0391
50. Lebedev NV, Klimov AE, Barkhudarov AA. Gastroduodenal ulcerative bleeding. Pirogov Russian Journal of Surgery = Khirurgiya. Zurnal im. N.I. Pirogova. 2014;(8):23-27. [Article in Russian].
51. Ljubicic N, Budimir I, Biscanin A, Nikolic M, Supanc V, Hrabar D, Pavic T. Endoclips vs large or small-volume epinephrine in peptic ulcer recurrent bleeding. World J Gastroenterol. 2012 May 14;18(18):2219-24. doi: 10.3748/wjg.v18.i18.2219.
52. Ünal F, Çakır M, Baran M, Duygulu Ş, Aydoğdu S. Application of endoscopic hemoclips for nonvariceal upper gastrointestinal bleeding in children. Turk J Gastroenterol. 2014;25(2):147-151. doi:10.5152/tjg.2014.3419
53. Laine L, Jensen DM. Management of patients with ulcer bleeding. Am J Gastroenterol. 2012;107(3):345-361. doi:10.1038/ajg.2011.480
54. Schmidt A, Gölder S, Goetz M, et al. Over-the-Scope Clips Are More Effective Than Standard Endoscopic Therapy for Patients With Recurrent Bleeding of Peptic Ulcers. Gastroenterology. 2018;155(3):674-686.e6. doi:10.1053/j.gastro.2018.05.037
55. Weiland T, Rohrer S, Schmidt A, et al. Efficacy of the OTSC System in the treatment of GI bleeding and wall defects: a PMCF meta-analysis. Minim Invasive Ther Allied Technol. 2020;29(3):121-139. doi:10.1080/13645706.2019.1590418
56. Zhong C, Tan S, Ren Y, et al. Clinical outcomes of

over-the-scope-clip system for the treatment of acute upper non-variceal gastrointestinal bleeding: a systematic review and meta-analysis. BMC Gastroenterol. 2019;19(1):225. Published 2019 Dec 23. doi:10.1186/s12876-019-1144-4
57. Wedi E, Fischer A, Hochberger J, Jung C, Orkut S, Richter-Schrag HJ. Multicenter evaluation of first-line endoscopic treatment with the OTSC in acute non-variceal upper gastrointestinal bleeding and comparison with the Rockall cohort: the FLETRock study. Surg Endosc. 2018;32(1):307-314. doi:10.1007/s00464-017-5678-7
58. Rodriguez-Merchan EC. Fibrin glue for local haemostasis in haemophilia surgery. Hosp Pract (1995). 2017;45(5):187-191. doi:10.1080/21548331.2017.1384689
59. Olefir IA. The possibilities of using thrombin during diagnostic and therapeutic fibrogastroduodenoscopy for gastrointestinal bleeding. Spravochnik Vracha Obshchej Praktiki. 2021;(7):14-19. doi 10.33920/med-10-2107-02 [Article in Russian].
60. Chernousov AF, Horobryh TV, Urzhumceva GA, Urakova YaCh. [Endoscopic hemostasis using fibrin glue in ulcerative gastroduodenal bleeding in elderly and senile patients]. Annaly Hirurgii. 2006;(4):60-63. [Article in Russian].
61. Holster IL, van Beusekom HM, Kuipers EJ, Leebeek FW, de Maat MP, Tjwa ET. Effects of a hemostatic powder hemospray on coagulation and clot formation. Endoscopy. 2015;47(7):638-645. doi:10.1055/s-0034-1391353
62. Cherednikov EF, Kashurnikova MA, Romantsov MN, Barannikov SV, Bolkhovitinov A E, Gaponenkov DG, Lyubimov PYu. [Experimental study of new means of local hemostasis in the treatment of ulcerative bleeding]. Scientific and Medical Bulletin of the Central Chernozem Region. 2016;(65):27-33. [Article in Russian].
63. Bogopol'skij VE, Chernousov AF, Horobryh TV. Gastric and duodenal ulcer surgery. Moscow: "Prakticheskaya Meditsina"; 2016. [In Russian].
64. Barkun AN, Moosavi S, Martel M. Topical hemostatic agents: a systematic review with particular emphasis on endoscopic application in GI bleeding. Gastrointest Endosc. 2013;77(5):692-700. doi:10.1016/j.gie.2013.01.020
65. Ibrahim M, El-Mikkawy A, Mostafa I, Devière J. Endoscopic treatment of acute variceal hemorrhage by using hemostatic powder TC-325: a prospective pilot study. Gastrointest Endosc. 2013;78(5):769-773. doi:10.1016/j.gie.2013.07.037
66. Pittayanon R, Rerknimitr R, Barkun A. Prognostic factors affecting outcomes in patients with malignant GI bleeding treated with a novel endoscopically delivered hemostatic powder. Gastrointest Endosc. 2018;87(4):994-1002. doi:10.1016/j.gie.2017.11.013
67. Vitali F, Naegel A, Atreya R, Zopf S, Neufert C, Siebler J, Neurath MF, Rath T. Comparison of Hemospray® and Endoclot™ for the treatment of gastrointestinal bleeding. World J Gastroenterol. 2019 Apr 7;25(13):1592-1602. doi: 10.3748/wjg.v25.i13.1592.
68. Yau AH, Ou G, Galorport C, Amar J, Bressler B, Donnellan F, Ko HH, Lam E, Enns RA. Safety and efficacy of Hemospray® in upper gastrointestinal bleeding. Can J Gastroenterol Hepatol. 2014 Feb;28(2):72-6. doi: 10.1155/2014/759436.
69. Mutneja H, Bhurwal A, Go A, Sidhu GS, Arora S, Attar BM. Efficacy of Hemospray in Upper Gastrointestinal Bleeding: A Systematic Review and Meta-Analysis. J Gastrointestin Liver Dis. 2020;29(1):69-76. Published 2020 Mar 13. doi:10.15403/jgld-660
70. Cherednikov EF. Complex treatment of gastroduodenal ulcers using gel sorbents (clinical and experimental study). Abstract for ScD Thesis. Voronezh. 1998. [In Russian].
71. Cherednikov EF, Batkaev AR, Baev VE. [The Reparative regeneration of erosive-ulcerative lesions of the stomach and duodenum in the local treatment of hydrophilic granular sorbents]. System Analysis and Management in Biomedical Systems. 2005;4(2):224-225. [Article in Russian].
72. Cherednikov EF, Maleev YuV, Chernyh AV, Litovkina TE, Cherednikov EE, Shevtsov AN. [Modern views on the etiology and pathogenesis of ruptured hemorrhagic syndrome (Mallory-Weiss syndrome)]. Journal of anatomy and Histopathology. 2016;5(1):86-98. [Article in Russian].
73. Cherednikov EF, Barannikov SV, Romantsov MN, Popov AV. New aspects of preventive endoscopic hemostasis in the treatment of peptic ulcer bleeding in the experimental condition. The EPMA Journal. 2017; 8(S1):45.
74. Barannikov SV, Cherednikov EF, Yuzefovich IS; Mehantjeva LE, Filev IF, Maleev YuV, Ovsyannikov ES, Maslova VA. A Study of the Influence of New Generation Granulated Sorbents on the Processes Regulating the Aggregate State of the Blood with the Use of Piezoelectric Thromboelastography. International Journal of Biomedicine. 2021;11(3):286-290. doi:10.21103/ Article11(3)_OA6
75. Popov AV, Cherednikov EF, Deryaeva OG, Ovchinnikov IF, Cherednikov EE, Popov AV. [Investigation of the combined use of diotevin and diovine in the local treatment of simulated peptic ulcers]. Vestnik Novyh Medicinskih Tekhnologij. 2013;20(2):315-317. [Article in Russian].
76. Cherednikov EF, Glukhov AA, Romantsov MN, Maleev YuV, Barannikov SV, Shkurina IA, Vysotskaya AT, Ovsyannikov ES. Hemostatic agents in combination with diovine for local treatment of simulated bleeding gastric ulcers. International Journal of Biomedicine.2020;10(2):138-141. doi: 10.21103/Article10(2)_OA10
77. Cherednikov EF, Yuzefovich IS, Maleev YuV, Barannikov SV, Litovkina TE, Polubkova GV, Ovsyannikov ES.The Use of the Hemostatic Agent Zhelplastan in Combination with a Granulated Sorbent in the Treatment of Patients with Mallory Weiss Syndrome. International Journal of Biomedicine. 2021;11(2):160-163. doi:10.21103/Article11(2)_OA7
78. Romantsov MN, Cherednikov E F, Danilenko VI, Stepanov DS, Fursov K O, Deryaeva AG. [Morphological Characteristics of Processes of Simulated Bleeding Gastric Defects Reparation in Treatment with Gelplastan and Diovin]. Journal of Anatomy and Histopathology. 2017;6(1):81-86. [Article in Russian].
79. Cherednikov EF, Barannikov SV, Maleev YuV, Fursov KO, Litovkina TE, Zakurdaev EI, Ovsyannikov ES. Experimental justification of using Aseptisorb-A and platelet-rich plasma in endoscopic treatment of mold bleeding stomach defects. International Journal of Biomedicine.2017;7(4):298-301. doi:10.21103/Article7(4)_OA5
80. Cherednikov EF, Barannikov SV, Zhdanov AI, Moshurov IP, Polubkova GV, Maleev YuV, Ovsyannikov ES, Myachina DS. Combimed use of biologically active hemostatic and granulated sorbent in endoscopic cytoprotective hemostasis in patients with bleeding gastroduodenal ulcers. International Journal of Biomedicine. 2020;10(2):129-132. doi: 10.21103/ Article10(2)_OA8
81. Cherednikov EF, Barannikov SV, Fursov KO, Polubkova GV, Danilenko VI, Stepanov DS. [Healing of bleeding

experimental defects of the stomach with topical anilovin and platelet-rich plasma]. Journal of Volgograd State Medical University. 2017;2(62):130-133. doi: 10.19163/1994-9480-2017-2(62)-130-133 [Article in Russian]
82. Barkun AN, Almadi M, Kuipers EJ, Laine L, Sung J, Tse F, Leontiadis GI, Abraham NS, Calvet X, Chan FKL, Douketis J, Enns R, Gralnek IM, Jairath V, Jensen D, Lau J, Lip GYH, Loffroy R, Maluf-Filho F, Meltzer AC, Reddy N, Saltzman JR, Marshall JK, Bardou M. Management of Nonvariceal Upper Gastrointestinal Bleeding: Guideline Recommendations From the International Consensus Group. Ann Intern Med. 2019 Dec 3;171(11):805-822. doi: 10.7326/M19-1795. Epub 2019 Oct 22.
83. Gralnek IM, Dumonceau JM, Kuipers EJ, Lanas A, Sanders DS, Kurien M, Rotondano G, Hucl T, Dinis-Ribeiro M, Marmo R, Racz I, Arezzo A, Hoffmann RT, Lesur G, de Franchis R, Aabakken L, Veitch A, Radaelli F, Salgueiro P, Cardoso R, Maia L, Zullo A, Cipolletta L, Hassan C. Diagnosis and management of nonvariceal upper gastrointestinal hemorrhage: European Society of Gastrointestinal Endoscopy (ESGE) Guideline. Endoscopy. 2015 Oct;47(10):a1-46. doi: 10.1055/s-0034-1393172.
84. Vergara M, Bennett C, Calvet X, Gisbert JP. Epinephrine injection versus epinephrine injection and a second endoscopic method in high-risk bleeding ulcers. Cochrane Database Syst Rev. 2014;(10):CD005584. Published 2014 Oct 13. doi:10.1002/14651858.CD005584.pub3
85. Barkun AN, Martel M, Toubouti Y, Rahme E, Bardou M. Endoscopic hemostasis in peptic ulcer bleeding for patients with high-risk lesions: a series of meta-analyses. Gastrointest Endosc. 2009;69(4):786-799. doi:10.1016/j.gie.2008.05.031
86. Baracat F, Moura E, Bernardo W, et al. Endoscopic hemostasis for peptic ulcer bleeding: systematic review and meta-analyses of randomized controlled trials. Surg Endosc. 2016;30(6):2155-2168. doi:10.1007/s00464-015-4542-x
87. Cherednikov EF, Barannikov SV, Yuzefovich IS, Polubkova GV, Maleev YuV, Volkova IV, Vysotskaya AT, Strygin OV, Ovsyannikov ES. Innovative Endoscopic Technologies in the Complex Treatment of Patients with Unstable Stopped Gastroduodenal Bleeding. International Journal of Biomedicine. 2021;11(1):24-28. doi:10.21103/Article11(1)_OA4
88. Beales I. Recent advances in the management of peptic ulcer bleeding. F1000Res. 2017;6:1763. Published 2017 Sep 27. doi:10.12688/f1000research.11286.1
89. Jensen DM, Eklund S, Persson T, Ahlbom H, Stuart R, Barkun AN, et al. Reassessment of Rebleeding Risk of Forrest IB (Oozing) Peptic Ulcer Bleeding in a Large International Randomized Trial. Am J Gastroenterol. 2017 Mar;112(3):441-446. doi: 10.1038/ajg.2016.582.
90. Jensen DM, Kovacs TOG, Ohning GV, Ghassemi K, Machicado GA, Dulai GS, Sedarat A, Jutabha R, Gornbein J. Doppler Endoscopic Probe Monitoring of Blood Flow Improves Risk Stratification and Outcomes of Patients With Severe Nonvariceal Upper Gastrointestinal Hemorrhage. Gastroenterology. 2017 May;152(6):1310-1318.e1. doi: 10.1053/j.gastro.2017.01.042.
91. Jensen DM, Ohning GV, Kovacs TO, Ghassemi KA, Jutabha R, Dulai GS, Machicado GA. Doppler endoscopic probe as a guide to risk stratification and definitive hemostasis of peptic ulcer bleeding. Gastrointest Endosc. 2016 Jan;83(1):129-36. doi: 10.1016/j.gie.2015.07.012.
92. Goto O, Koizumi E, Higuchi K, Noda H, Onda T, Omori J, Kaise M, Iwakiri K. Cutting-Edge Technologies for Gastrointestinal Therapeutic Endoscopy. J Nippon Med Sch. 2021;88(1):17-24. doi: 10.1272/jnms.JNMS.2021_88-109.
93. Kantsevoy SV, Bitner M, Mitrakov AA, Thuluvath PJ. Endoscopic suturing closure of large mucosal defects after endoscopic submucosal dissection is technically feasible, fast, and eliminates the need for hospitalization (with videos). Gastrointest Endosc. 2014;79(3):503-507. doi:10.1016/j.gie.2013.10.051

International Journal of Biomedicine 12(1) (2022) 19-23
http://dx.doi.org/10.21103/Article12(1)_RA2

REVIEW ARTICLE

INTERNATIONAL JOURNAL OF BIOMEDICINE

Imaging of Neuropathic Pain

Mohamed A. Bedewi, MD, PhD

Department of Internal Medicine, College of Medicine, Prince Sattam Bin Abdulaziz University Al-Kharj, Kingdom of Saudi Arabia

Abstract

The International Association for the Study of Pain (IASP) defined neuropathic pain as "pain arising as a direct consequence of a lesion or disease affecting the somatosensory system." The origin of neuropathic pain (NP) could be from the brain, spinal cord, or peripheral nerves. NP represents a major neurological problem, with a prevalence of 1%-2% of the total population. It is disabling, rendering an urgent need for non-addictive, effective new therapies, and is characterized by resistance to treatment and poor patient satisfaction. We aim to review the role of modern imaging in the diagnosis of NP and the potential advantages and limitations of each modality. (**International Journal of Biomedicine. 2022;12(1):19-23.**)

Key Words: neuropathic pain • peripheral nerves • imaging

For citation: Bedewi MA. Imaging of Neuropathic Pain. International Journal of Biomedicine. 2022;12(1):19-23. doi:10.21103/Article12(1)_RA2

Abbreviations

MRI, magnetic resonance imaging; **NP**, neuropathic pain; **MI**, molecular imaging; **PET**, positron emission tomography

Pain is considered one of the most common reasons for patients to seek medical care. The attempt to understand pain represents one of the oldest challenges in the history of medicine.[1] Although research into the imaging of chronic neuropathic pain (NP) is promising, actual implementation remains a challenge. The International Association for the Study of Pain (IASP) defined neuropathic pain as "pain arising as a direct consequence of a lesion or disease affecting the somatosensory system."[2,3] The origin of NP could be from the brain, spinal cord, or peripheral nerves.[4] NP represents a major neurological problem,[5,6] with a prevalence of 1%-2% of the total population.[7,8] NP is less common than nociceptive pain; however, it is usually more severe and accompanied by emotional reactions.[9] NP is disabling, rendering an urgent need for non-addictive, effective new therapies.[4,5] NP is characterized by resistance to treatment and poor patient satisfaction.[10,11] Patient collaboration is needed to establish a proper history and physical examination. Several factors influence patients' experience of pain; some of them are emotional, others are educational. Because of this, objective tools are now demanded. Management of NP is often challenging and requires a multifaceted approach. Over the last two decades, several studies have been devoted to NP. Identifying the anatomical location of the pain is a must for definitive diagnosis, which is something that current neurophysiological tools can do so.[12-24] Understanding the pathophysiological mechanisms responsible for translating sensory signs into NP can lead to an effective and treatment-based approach.[17] Sensitization of the nociceptive pathways includes adaptive structural changes, molecular signaling, and cell-cell interactions. The main classes of therapeutics include sodium channels, calcium channels, and descending modulatory inhibitory pathways.[18] Currently, NP is believed to be caused by a change in the sensitivity of central and peripheral nervous system signaling. The central mechanism includes processing and integration of information in brain centers like the brainstem, cerebellum, and cerebral cortex. These centers are related to chronic pain and associated signs and symptoms. Peripheral mechanisms include sensitization of nociceptors,

***Corresponding Author:** Dr. Mohamed A. Bedewi, MD, PhD. Associate Professor of Radiology. College of medicine; Prince Sattam bin Abdulaziz University. Al-Kharj; Saudi Arabia. E-mail: mohamedbedewi@yahoo.com*

changes in ion channel expression, sympathetic neurons related to dorsal root ganglia, pseudo synaptic conduction, and ectopic and spontaneous discharges.[9] The pain matrix in the brain includes somatosensory cortices, anterior cingulate cortex, and insula. These centers undergo maladaptive changes like microglial activation, synaptic plasticity, and central sensitization resulting in hyperalgesia.[1] Advanced studies of this pain matrix could help in understanding the pathophysiological basis of different symptoms of NP.[19]

Imaging

Recent advances in machine learning have improved the understanding of NP, utilizing a larger scale of data related to neuroimaging. In cases of NP, it is sometimes difficult to determine if the degenerative or inflammatory changes seen on imaging are part of the aging process or part of the disease process causing the patients' symptoms. Degenerative changes can be seen in more than 60% of asymptomatic patients. Some abnormalities can also be seen in asymptomatic volunteers. The frequency of these abnormalities increases with age and is somewhat irrelevant to the patients' clinical condition. The presence of multiple abnormalities at the same time makes it difficult to determine which of them is the source of pain. Since treatment decisions are guided by imaging, the low specificity of radiological diagnosis leads to ineffective, delayed, or even inappropriate treatment.[1] The radiological diagnosis of NP remains challenging since findings seen on conventional CT and MRI imaging, with their low specificity and sensitivity, don't always match the clinical picture.[25] Challenges for peripheral nerve imaging include the complex nature of human pain and the subjective component. Combining the high sensitivity and specificity of molecular imaging (MI) with high contrast resolution of MRI and CT would improve the diagnosis of NP and produce better outcomes of guided therapy.[1] For some time, NP has lacked a suitable imaging modality, which has limited concomitant research on the pathogenesis and considerably affected the treatment of NP.[26] In the past, the role of imaging was limited to identifying anatomical sites that could be responsible for pain generation. Methods related to ion channels could involve toxic effects.[25]

Molecular imaging

One of the imaging options for NP is MI. An important feature of MI is the ability to identify abnormal biological processes despite virtually normal anatomical appearance. It takes advantage of inflammatory mediators and receptors involved in the pathogenesis of pain. New innovations of MI could also help in the development of unique aspects of treatment options. Identifying a single molecular pathway is difficult because of the complex nature of the biochemical routes for NP. Several factors limit the use of MI. A single marker cannot be used for all types of pain. Another problem with MI is technical limitations like volume averaging and patient motion artifact.[1] ^{18}F-fluorodeoxyglucose could be used in PET imaging as a marker, but the background activity could overshadow the area of interest, which could be sought as the source of pain. This could be decreased by combining CT with PET. The use of PET/MRI could even yield better results with excellent soft-tissue contrast resolution. One of the problems related to pain imaging is the subjective nature of pain, which could differ from patient to patient. Whole-body imaging was suggested to study both the peripheral and central nervous systems. This could be accomplished by biomarkers, which could estimate areas of increased activity, including both systems. NP could be thought of as pain resulting from the interaction between the peripheral immune system, neurons, and different types of glial cells (e.g., astrocytes, microglia, satellite cells). A nociceptive nerve can be excited by different types of mediators; some of them are neuroimmune, others are inflammatory, in addition to interaction with macrophages and ion channel dysregulation. Inflammatory mediators like prostaglandin E2, bradykinin, and chemokines are released at the site of tissue damage, activating inflammatory cells and the ends of peripheral neurons. These mediators interact with cell receptors, ending with intracellular kinase activation, which phosphorylate target proteins, changing activation thresholds and producing increased synaptic transmission efficiency between afferent neurons and dorsal horn neurons, resulting in pain. The current imaging tools to study nociceptive activity include functional, cellular-based, and molecular approaches detecting metabolic and mediator-related changes related to abnormal physiologic activity in the nervous system and allowing targeted therapy.[1] Macrophages have been found to be intimately related to the sites of nerve injury and inflammation, enhancing pain. Knowing the location of macrophage activity is easy because these cells express translocator proteins in pathologic activity. Radioligands to translocator proteins can define areas of macrophage activity. The sigma-1receptor is a transmembrane protein concentrated in macrophages and Schwann cells, which are involved in neural damage as well as neural inflammation and repair. In the case of active nerve inflammation, there is increased density of sigma-1receptor, which can be detected by radiolabeled ligands and can identify the site of neural damage in different conditions like regional pain syndrome, and inflammatory and non-inflammatory causes of NP.[1]

Other tracers

Cyclooxygenase (COX)-2 is the dominant source of prostaglandins, which mediate pain and inflammation. COX-2 converts arachidonic acid into prostaglandin H2, the precursor of all prostanoids. The role of COX-2 in the inflammatory process was enhanced after the success of COX-2 inhibitors in treating chronic pain. Radiolabeled COX-2 inhibitors could be used to image chronic pain.[27] Sodium and calcium channels show increased flux across the membrane in cases of NP with a change in the action potential of the excitation threshold, leading to the persistent firing of nerves. Manganese physiologically follows calcium, and in exciting cells, the rate of efflux of both of them is slow, resulting in the accumulation of manganese in the cell. This could enhance imaging through manganese-enhanced MRI and could act as an alternative for estimating calcium fluxes in nerve cells using manganese as a T1-shortening contrast agent.[28] In chronic pain syndromes, neuron cells utilize a considerable amount of metabolic activity, which makes them glucose avid with the associated increase in the uptake of glucose. FDG mimics glucose and could be entrapped inside cells during the glycolytic cycle. The combination of 18F-FDG PET with MRI could help

imaging and localization of neural metabolism. It is proposed that identification of the sites of increased metabolic activity of the neural tissues on imaging could be a useful strategy for tracing NP generators.[1] MMP-12- targeted magnetic iron oxide nanoparticle (IONP) was introduced as a potential biomarker for the management and diagnosis. The use of IONP MRI enhances the spin-spin relaxation time of related water protons, thus decreasing the T2 signal. IONP detects enzyme activity when conjugated to peptide sequences; when this sequence is cleaved by the target enzyme, the released IONP is taken up by surrounding tissues. MMPs are responsible for extracellular matrix degradation; they are a member of the family of calcium-dependent zinc endopeptidase. They could be targets for IONP-based MRI.[24]

MRI

For more than 20 years, MRI was used as a noninvasive imaging tool to diagnose neural disease and injuries. MRI is considered a promising imaging diagnostic tool due to its multiplanar capability and high contrast resolution.[24] MR neurography was introduced in the 1990s to describe the use of fat-suppressed pulse sequences and diffusion-weighted imaging to discriminate peripheral nerves from the surrounding tissues.[29] Commonly, peripheral nerves cannot be distinguished from surrounding tissues in T2-weighted images. As T2 relaxation time is prolonged, injured nerves appear either isointense or slightly hyperintense (bright) on T2-W1. Although these changes are clear, however, they are nonspecific, as chronically degenerating nerves cannot be differentiated from regenerating ones. Contrast agents manganese, like gadolinium, proved to be nonspecific.[24] The diagnosis of the cause of NP depends on identifying the main pathology in addition to the anatomical location. MRI abnormalities are found in a high percentage of asymptomatic patients. Besides, the prevalence of anatomical abnormalities in symptomatic and asymptomatic patients is similar. Because of this, a demand for a more accurate imaging modality is raised. [13,14,30-32]

Functional MRI

In the last two decades, the perception and transmission of pain in the brain were studied by functional MRI (fMRI). This type of MRI can be divided into structural and functional imaging. Structural imaging studies the anatomy of the brain and fiber connection between brain regions. The main techniques are conventional imaging, voxel-based morphometry (VBM), and diffuse tensor imaging (DTI).[26] VBM provides regions of interest for changes in brain function. DTI can analyze functional connectivity on an anatomical basis. fMRI studies brain functional activities via monitoring alterations in cerebral blood flow. There are two main subcategories for fMRI. The first and most widely available is called the blood oxygenation level-dependent (BOLD) technique. It reflects variations in the deoxyhemoglobin content and changes in the local cerebral blood flow.[26] To obtain normal neuron function, a stable level of oxygen supplied by hemoglobin is needed. In the magnetic field, deoxyhemoglobin exhibits paramagnetism while oxyhemoglobin exhibits diamagnetism. The difference in susceptibility between both types can be obtained by BOLD fMRI.[33] Upon neuron excitation, oxygen consumption increases with a concomitant decrease in blood oxygen content. This will be associated with a downward initial tilt angle of the BOLD signal. When blood flow increases, there will be a compensatory-associated increase in the oxygen level, and this will let the BOLD signal go up again. When neuron excitation stops and the need for oxygen is decreased, a negative signal will be recorded on BOLD and will eventually return to normal. Two types of fMRI exist; the first is task-state fMRI, which is the traditional way to study the activation of brain regions in NP. Task-state fMRI is a suitable tool for studying allodynia, where non-noxious stimuli can cause pain, causing misreading of somatosensory information. In allodynia, task-state studies BOLD activation/deactivation in the functionally related areas of the brain and can reveal functional connectivity of different brain regions by comparing the states of the pain stimulation of the ipsilateral part of the body to the contralateral part.[34] The second type is resting-state fMRI, which emerged in the past ten years as an alternative way to recognize regions of neuronal activity by estimating the functional connectivity in the brain. This type collects data in the relaxing state, with the exclusion of external stimuli. The obtained information reflects the baseline activities of the central nervous system in the resting state, which could use more than fifty percent of the total energy of the cerebrum with a spatial pattern called the resting brain functional network, which is based on the functional integration of several brain areas. This pattern is influenced by NP, and advances in understanding its influence could improve the management of NP.[35] Berger et al.[36] showed that resting-state fMRI proved the association of the components of the limbic system—amygdala, striatum, hippocampus, medial prefrontal cortex—with NP. Functional connectivity is a good estimate of signal correlations of activation of brain voxels. Changes in the activation-resting state could reveal a specific pattern for NP.[26]

VBM

VBM analyzes MR images at the voxel level. VBM accurately displays morphological changes of the brain through quantitative calculation of the volume and density changes in local gray and white matter. In NP, there is variation in the density of gray matter and change in the plasticity of the brain cortex. VBM can help estimate the length of disease and pain intensity in NP.[37] For example, it was found that in patients with postherpetic neuralgia, there was increased volume in the gray matter of the temporal lobe and cerebellum. In contrast, the parietal lobe, frontal lobe, and occipital lobes showed a reduction in their volume. [38]

DTI

DTI is based on estimating the direction of water diffusion. This is achieved by considering that diffusion of water is more restricted across axonal membranes than the long axis. Significant anatomical changes have been detected with DTI in different brain regions in patients with NP.[32] There is a current solid scientific belief that the human brain is composed of a complex and efficient network.[26] The white matter fiber bundle is responsible for the connection of the nodes of the network for transforming information in the brain. Damage to these bundles will affect information

transmission and cause pain/disease manifestations. DTI is the ideal noninvasive imaging tool for tracking white matter fiber bundles, thus reflecting the dispersion characteristics of water in white matter fibers and revealing the connection state of the brain network.[26]

fMRI in NP types

Primary trigeminal neuralgia occurs as a result of neurovascular compression. This can be studied by DTI, 3D TOF-MRA, and 3D FIESTA sequences, which show the anatomical relationship between arteries, veins, and nerves.[39,40] Task-state fMRI helped in studying cortical remodeling found in patients with phantom pain after amputation.[41] In diabetic peripheral neuropathy, functional-weakened connections were found between the medial dorsal nucleus, ventral posterior nucleus, and cerebral cortex.[42] In fibromyalgia, a weakened connection was found between the insula and thalamus.[43] Also, in patients with postherpetic neuralgia, there is a change in the microstructure integrity of the white matter in several brain regions.[44] Thus, advanced fMRI with the help of machine learning techniques could be used as imaging markers to diagnose NP.

Acknowledgments

The author would like to express his deep gratitude to the Deanship of Scientific Research at Prince Sattam Bin Abdulaziz University, Al-Kharj, Saudi Arabia.

References

1. Tung KW, Behera D, Biswal S. Neuropathic pain mechanisms and imaging. Semin Musculoskelet Radiol. 2015 Apr;19(2):103-11. doi: 10.1055/s-0035-1547371.
2. Meacham K, Shepherd A, Mohapatra DP, Haroutounian S. Neuropathic Pain: Central vs. Peripheral Mechanisms. Curr Pain Headache Rep. 2017 Jun;21(6):28. doi: 10.1007/s11916-017-0629-5.
3. Treede RD, Jensen TS, Campbell JN, Cruccu G, Dostrovsky JO, Griffin JW, Hansson P, Hughes R, Nurmikko T, Serra J. Neuropathic pain: redefinition and a grading system for clinical and research purposes. Neurology. 2008 Apr 29;70(18):1630-5. doi: 10.1212/01.wnl.0000282763.29778.59.
4. Geha PY, Apkarian AV. Brain imaging findings in neuropathic pain. Curr Pain Headache Rep. 2005 Jun;9(3):184-8. doi: 10.1007/s11916-005-0060-1.
5. Calvo M, Davies AJ, Hébert HL, Weir GA, Chesler EJ, Finnerup NB, Levitt RC, Smith BH, Neely GG, Costigan M, Bennett DL. The Genetics of Neuropathic Pain from Model Organisms to Clinical Application. Neuron. 2019 Nov 20;104(4):637-653. doi: 10.1016/j.neuron.2019.09.018.
6. Kushnarev M, Pirvulescu IP, Candido KD, Knezevic NN. Neuropathic pain: preclinical and early clinical progress with voltage-gated sodium channel blockers. Expert Opin Investig Drugs. 2020 Mar;29(3):259-271. doi: 10.1080/13543784.2020.1728254.
7. Chong MS, Bajwa ZH. Diagnosis and treatment of neuropathic pain. J Pain Symptom Manage. 2003 May;25(5 Suppl):S4-S11. doi: 10.1016/s0885-3924(03)00064-2.
8. Jensen TS, Gottrup H, Sindrup SH, Bach FW. The clinical picture of neuropathic pain. Eur J Pharmacol. 2001 Oct 19;429(1-3):1-11. doi: 10.1016/s0014-2999(01)01302-4.
9. Vranken JH. Elucidation of pathophysiology and treatment of neuropathic pain. Cent Nerv Syst Agents Med Chem. 2012 Dec;12(4):304-14. doi: 10.2174/187152412803760645.
10. Zilliox LA. Neuropathic Pain. Continuum (Minneap Minn). 2017 Apr;23(2, Selected Topics in Outpatient Neurology):512-532. doi: 10.1212/CON.0000000000000462.
11. Shkodra M, Brunelli C, Zecca E, Formaglio F, Bracchi P, Lo Dico S, Caputo M, Kaasa S, Caraceni A. Neuropathic pain: clinical classification and assessment in patients with pain due to cancer. Pain. 2021 Mar 1;162(3):866-874. doi: 10.1097/j.pain.0000000000002076.
12. Szok D, Tajti J, Nyári A, Vécsei L. Therapeutic Approaches for Peripheral and Central Neuropathic Pain. Behav Neurol. 2019 Nov 21;2019:8685954. doi: 10.1155/2019/8685954.
13. Murphy D, Lester D, Clay Smither F, Balakhanlou E. Peripheral neuropathic pain. NeuroRehabilitation. 2020;47(3):265-283. doi: 10.3233/NRE-208002.
14. Sasaki H, Takatsuna H, Inoue T, Matsui D, Sakoda H, Yokoyama M, Shiosakai K, Seki H, Uetake Y, Okuizumi K. A Cross-sectional Survey of Patients with Suspected Diabetic Peripheral Neuropathic Pain in Japan. Intern Med. 2021 Feb 1;60(3):357-365. doi: 10.2169/internalmedicine.5512-20.
15. Macone A, Otis JAD. Neuropathic Pain. Semin Neurol. 2018 Dec;38(6):644-653. doi: 10.1055/s-0038-1673679.
16. Attal N, Martinez V, Bouhassira D. Potential for increased prevalence of neuropathic pain after the COVID-19 pandemic. Pain Rep. 2021 Jan 27;6(1):e884. doi: 10.1097/PR9.0000000000000884.
17. Baron R, Binder A, Wasner G. Neuropathic pain: diagnosis, pathophysiological mechanisms, and treatment. Lancet Neurol. 2010 Aug;9(8):807-19. doi: 10.1016/S1474-4422(10)70143-5.
18. Finnerup NB, Kuner R, Jensen TS. Neuropathic Pain: From Mechanisms to Treatment. Physiol Rev. 2021 Jan 1;101(1):259-301. doi: 10.1152/physrev.00045.2019.
19. Thompson SJ, Bushnell MC. Rodent functional and anatomical imaging of pain. Neurosci Lett. 2012 Jun 29;520(2):131-9. doi: 10.1016/j.neulet.2012.03.015.
20. Bernetti A, Agostini F, de Sire A, Mangone M, Tognolo L, Di Cesare A, Ruiu P, Paolucci T, Invernizzi M, Paoloni M. Neuropathic Pain and Rehabilitation: A Systematic Review of International Guidelines. Diagnostics (Basel). 2021 Jan 5;11(1):74. doi: 10.3390/diagnostics11010074.
21. St John Smith E. Advances in understanding nociception and neuropathic pain. J Neurol. 2018 Feb;265(2):231-238. doi: 10.1007/s00415-017-8641-6.
22. Gilron I, Baron R, Jensen T. Neuropathic pain: principles of diagnosis and treatment. Mayo Clin Proc. 2015 Apr;90(4):532-45. doi: 10.1016/j.mayocp.2015.01.018.
23. Cruccu G, Truini A. A review of Neuropathic Pain: From Guidelines to Clinical Practice. Pain Ther. 2017 Dec;6(Suppl 1):35-42. doi: 10.1007/s40122-017-0087-0.
24. Husain SF, Lam RWM, Hu T, Ng MWF, Liau ZQG, Nagata K, Khanna S, Lam Y, Bhakoo K, Ho RCM, Wong HK. Locating the Site of Neuropathic Pain *In Vivo* Using MMP-12-Targeted Magnetic Nanoparticles. Pain Res Manag. 2019 Mar 6;2019:9394715. doi: 10.1155/2019/9394715.
25. Shen B, Behera D, James ML, Reyes ST, Andrews L, Cipriano PW, Klukinov M, Lutz AB, Mavlyutov T, Rosenberg J, Ruoho AE, McCurdy CR, Gambhir SS, Yeomans DC, Biswal S, Chin FT. Visualizing Nerve Injury in a Neuropathic Pain Model with [^{18}F]FTC-146 PET/MRI. Theranostics. 2017

Jul 8;7(11):2794-2805. doi: 10.7150/thno.19378.
26. Dou Z, Yang L. The application of functional magnetic resonance imaging in neuropathic pain. In: Medical imaging principles and applications. IntechOpen, 10/2019 UK. doi: 10.5772/intechopen.89200.
27. McCarthy TJ, Sheriff AU, Graneto MJ, Talley JJ, Welch MJ. Radiosynthesis, in vitro validation, and in vivo evaluation of 18F-labeled COX-1 and COX-2 inhibitors. J Nucl Med. 2002 Jan;43(1):117-24.
28. Jacobs KE, Behera D, Rosenberg J, Gold G, Moseley M, Yeomans D, Biswal S. Oral manganese as an MRI contrast agent for the detection of nociceptive activity. NMR Biomed. 2012 Apr;25(4):563-9. doi: 10.1002/nbm.1773.
29. Sneag DB, Queler S. Technological Advancements in Magnetic Resonance Neurography. Curr Neurol Neurosci Rep. 2019 Aug 24;19(10):75. doi: 10.1007/s11910-019-0996-x.
30. Agarwal A, Chandra A, Jaipal U, Bagarhatta M, Mendiratta K, Goyal A, Kumar R, Mangalhara N. Can imaging be the new yardstick for diagnosing peripheral neuropathy?-a comparison between high resolution ultrasound and MR neurography with an approach to diagnosis. Insights Imaging. 2019 Nov 1;10(1):104. doi: 10.1186/s13244-019-0787-6.
31. Ogon I, Takebayashi T, Takashima H, Morita T, Iesato N, Tanimoto K, Terashima Y, Yoshimoto M, Yamashita T. Analysis of Neuropathic Pain Using Magnetic Resonance Imaging T2 Mapping of Intervertebral Disc in Chronic Low Back Pain. Asian Spine J. 2019 Jun;13(3):403-409. doi: 10.31616/asj.2018.0147.
32. Alomar S, Bakhaidar M. Neuroimaging of neuropathic pain: review of current status and future directions. Neurosurg Rev. 2018 Jul;41(3):771-777. doi: 10.1007/s10143-016-0807-7.
33. Logothetis NK. The neural basis of the blood-oxygen-level-dependent functional magnetic resonance imaging signal. Philos Trans R Soc Lond B Biol Sci. 2002 Aug 29;357(1424):1003-37. doi: 10.1098/rstb.2002.1114.
34. Hubbard CS, Khan SA, Xu S, Cha M, Masri R, Seminowicz DA. Behavioral, metabolic and functional brain changes in a rat model of chronic neuropathic pain: a longitudinal MRI study. Neuroimage. 2015 Feb 15;107:333-344. doi: 10.1016/j.neuroimage.2014.12.024.
35. Lu H, Yuping N. When neuroscience meets network thinking: A new perspective on brain disorders. Chinese Journal of Neuromedicines. 2014;13(12):1292-1296
36. Berger SE, Baria AT, Baliki MN, Mansour A, Herrmann KM, Torbey S, Huang L, Parks EL, Schnizter TJ, Apkarian AV. Risky monetary behavior in chronic back pain is associated with altered modular connectivity of the nucleus accumbens. BMC Res Notes. 2014 Oct 20;7:739. doi: 10.1186/1756-0500-7-739.
37. Henry DE, Chiodo AE, Yang W. Central nervous system reorganization in a variety of chronic pain states: a review. PM R. 2011 Dec;3(12):1116-25. doi: 10.1016/j.pmrj.2011.05.018.
38. Cao S, Qin B, Zhang Y, Yuan J, Fu B, Xie P, Song G, Li Y, Yu T. Herpes zoster chronification to postherpetic neuralgia induces brain activity and grey matter volume change. Am J Transl Res. 2018 Jan 15;10(1):184-199.
39. Montano N, Conforti G, Di Bonaventura R, Meglio M, Fernandez E, Papacci F. Advances in diagnosis and treatment of trigeminal neuralgia. Ther Clin Risk Manag. 2015 Feb 24;11:289-99. doi: 10.2147/TCRM.S37592.
40. Chai W, You C, Zhang W, Peng W, Tan L, Guan Y, Chen K. Diffusion tensor imaging of microstructural alterations in the trigeminal nerve due to neurovascular contact/compression. Acta Neurochir (Wien). 2019 Jul;161(7):1407-1413. doi: 10.1007/s00701-019-03851-2.
41. Jutzeler CR, Curt A, Kramer JL. Relationship between chronic pain and brain reorganization after deafferentation: A systematic review of functional MRI findings. Neuroimage Clin. 2015 Oct 3;9:599-606. doi: 10.1016/j.nicl.2015.09.018.
42. Cauda F, Sacco K, D'Agata F, Duca S, Cocito D, Geminiani G, Migliorati F, Isoardo G. Low-frequency BOLD fluctuations demonstrate altered thalamocortical connectivity in diabetic neuropathic pain. BMC Neurosci. 2009 Nov 26;10:138. doi: 10.1186/1471-2202-10-138.
43. Cifre I, Sitges C, Fraiman D, Muñoz MÁ, Balenzuela P, González-Roldán A, Martínez-Jauand M, Birbaumer N, Chialvo DR, Montoya P. Disrupted functional connectivity of the pain network in fibromyalgia. Psychosom Med. 2012 Jan;74(1):55-62. doi: 10.1097/PSY.0b013e3182408f04.
44. Chen F, Chen F, Shang Z, Shui Y, Wu G, Liu C, Lin Z, Lin Y, Yu L, Kang D, Tao W, Li Y. White matter microstructure degenerates in patients with postherpetic neuralgia. Neurosci Lett. 2017 Aug 24;656:152-157. doi: 10.1016/j.neulet.2017.07.023.

International Journal of Biomedicine 12(1) (2022) 24-28
http://dx.doi.org/10.21103/Article12(1)_OA1

ORIGINAL ARTICLE

Radiology

INTERNATIONAL JOURNAL OF BIOMEDICINE

Standardization of a Non-Invasive MRI Assessment of Liver Iron Overload Using a Phantom Containing Superparamagnetic Iron Oxide Nanoparticles

Petr A. Bulanov[1*]; Evelina E. Manzhurtseva[1]; Petr E. Menshchikov[1,2], PhD; Dmitry A. Kupriyanov[1,2], PhD; Galina A. Novichkova[1], PhD, ScD; Galina V. Tereshchenko[1], PhD

[1]Dmitry Rogachev National Medical Research Center of Pediatric Hematology, Oncology and Immunology, Moscow, Russia
[2]Philips Healthcare, Moscow, Russia

Abstract

***Background*:** Liver iron overload is a common diagnosis in patients with frequent blood transfusions. MRI is a promising non-invasive method for assessing liver iron concentration. We have created an MR-compatible phantom to develop a method for the standardization of T2* mapping and following conversion of T2* values (ms) into iron concentration (mg/mL) for an assessment of overload grade.

***Methods and Results*:** The standardization process involved the development of an MR-compatible phantom with solutions of paramagnetic iron oxide nanoparticles of various concentrations mimicking various degrees of liver iron overload. Using this phantom, we assessed the repeatability of T2* values obtained on reference MRI scanners (3T and 1.5T) at the D. Rogachev NMRCPHOI on 6 MRI acquisitions with one-week intervals. To assess the reproducibility of the results obtained on other MRI scanners, we compared these measurements with the reference values.

***Conclusion*:** The method for the standardization of T2* mapping on various 1.5T and 3T MRI scanners was tested. This method is based on the use of our phantom to validate or calibrate (if necessary) the MRI study protocol. The standardization protocol provided an opportunity to use the empirical formula (revealed in our institute as well as in other studies) for converting T2* values from any MRI scanner into LIC (mg/mL). (**International Journal of Biomedicine. 2022;12(1):24-28.**)

Key Words: iron overload • MRI diagnosis • T2* mapping • MRI phantom • SPIO

For citation: Bulanov PA, Manzhurtseva EE, Menshchikov PE, Kupriyanov DA, Novichkova GA, Tereshchenko GV. Standardization of a Non-Invasive MRI Assessment of Liver Iron Overload Using a Phantom Containing Superparamagnetic Iron Oxide Nanoparticles. International Journal of Biomedicine. 2022;12(1):24-28. doi:10.21103/Article12(1)_OA1

Introduction

Iron overload is a condition in which extra iron builds up in organs and tissues, causing toxic damage and, consequently, organ dysfunction. Iron overload may occur due to hereditary hemochromatosis or result from anemia requiring regular transfusions of donor red blood cells.[1] Timely diagnosis of iron overload is essential for the prediction of target organ dysfunction as well as for the planning and monitoring of chelation therapy.[2] Until recently, the only accurate method of iron overload assessment was the analysis of liver samples by atomic absorption spectrometry. Serum ferritin concentration, widely used as an indirect measure of iron stores in patients with hemochromatosis, is not always a reliable indicator of iron status in patients suffering from post-transfusion iron overload. The applicability of liver biopsy is limited by such major negative factors as the invasiveness of the procedure and significant variability in iron concentration due to the small size of specimens and the heterogeneity of iron deposition in the liver.[3] New magnetic resonance imaging (MRI) technologies allow us to quantify iron concentration in the liver, heart, and pancreas using special pulse sequences.[4]

***Corresponding author**: Petr A. Bulanov. Dmitry Rogachev National Medical Research Center of Pediatric Hematology, Oncology and Immunology. Moscow, Russia. E-mail: petepeter@yandex.ru*

The most widely used quantification MRI method is T2* mapping.[5] Iron is stored in the liver parenchyma mainly in two forms: ferric hydroxide bound to ferritin and ferric hydroxide in hemosiderin. Because of the paramagnetic properties of iron, iron-containing substances also exhibit paramagnetic properties. Paramagnets are substances that, because of magnetization in the presence of an external magnetic field (for example, in MRI), generate large inhomogeneities in local magnetic fields and consequently affect T2* relaxation time, which is heavily dependent on such inhomogeneities.[3] T2* is measured by a gradient echo sequence (GRE) with multiple echo times (TEs). The obtained images are used to create a map of T2* value distribution (hereinafter referred to as a "T2* map") that is sensitive to ferritin and hemosiderin concentrations: the lower T2* values, the more iron is present in the area of interest, and the higher iron overload is.[6] This method is non-invasive and allows for a quick assessment of iron overload in the entire liver, thus solving the two major problems associated with liver biopsy at once. However, we cannot replace biopsy with T2* mapping because of the absence of standards for converting T2* values into liver iron concentration (LIC). The creation of the standard is crucially essential for further diagnosis and an accurate assessment of iron overload.

One of the main methods for T2* values to be converted into LIC is an experimental calibration based on T2* mapping and biopsy findings.[7] However, as seen from experience, such calibration curves may be specific to the cause of iron overload as well as to methods used in the experiment (T2* mapping parameters, biopsy techniques, scanners used, etc.).[7] In other words, these restrictions substantially limit using of the calibration curve anywhere except the place where the curve was obtained ("reference MRI scanner"). Nevertheless, using the calibration curves is possible if T2* values acquired on any MRI scanner will be matched with the values from the reference MRI scanner. FerriScan® (Australia) is the most successful attempt at standardization. It is a commercial product approved by the United States Food and Drug Administration (the FDA) to calculate LIC based on T2* values.[8] This technique has demonstrated high reproducibility in multicenter studies.[9] Nevertheless, its wide use is strongly limited by the high cost.

The aim of this study was to develop and validate an effective and simple algorithm that would help test the correspondence between T2* values obtained with various MRI scanners and those obtained with reference 1.5T and 3T MRI scanners at the National Medical Research Center of Pediatric Hematology, Oncology and Immunology named after Dmitry Rogachev by using an MR-compatible phantom containing paramagnetic iron oxide (Fe3O4) nanoparticles. Such an algorithm would allow healthcare facilities to easily start using T2* mapping to assess LIC (based on the conversion curve obtained by us previously[6]) without the necessity of laborious preliminary experimental creation of calibration curves.

Materials and Methods

The Development of a Phantom

The phantom consisted of 28 tubes, 50 ml each, filled with colloid solutions of various concentrations (Fig.1) containing paramagnetic iron oxide nanoparticles (Fe_3O_4). The nanoparticles were produced using the method proposed by Elmore[10]:

$$FeSO_4 7H2O + 2FeCl_3 6H_2O + 8NH_3 H_2O = Fe_3O_4 + 6NH_4Cl + (NH_4)2SO_4 + 23H_2O,$$

where iron(III) chloride hexahydrate and iron(II) sulfate heptahydrate were used as carriers of ferrous and ferric ions, ammonium hydrate was used to precipitate and synthesize the nanoparticles, and citric acid, a surfactant, was used for growth control and stabilization of the particles. The resulting solution was centrifuged at 1500 rpm for 5 minutes to precipitate large particles. The top layer of the solution filtered through standard filter paper with an average pore size of 3 - 5 µm was the colloidal suspension of iron oxide nanoparticles that we had aimed to obtain. The resulting solutions with high iron concentration were diluted to achieve T2* values similar to those seen in a healthy liver and in the four grades of iron overload.[6]

Fig. 1. A. An example of phantom positioning in an MRI scanner. B. The phantom containing superparamagnetic iron oxide nanoparticles (Fe_3O_4)

MRI Scanning and Post-processing

The phantom was scanned using four MRI scanners from different manufacturers and with different field strengths (Table 1).

Table 1.

MRI scanners used in the research

MRI scanner / Magnetic field strength	Maximum gradient strength /slew rate	Reference / Control	Receiver coil
Philips Achieva dStream (Best, The Netherlands) /3T	80 mT/m / 200 T/m/s	Reference 3T MRI scanner NMRCPHOI	dS Torso anterior coil combined with a coil integrated in the table, with 32 channels in total
Philips Achieva (Best, The Netherlands) /3T	80 mT/m / 200 T/m/s	Control 3T MRI scanner CRIEPST	dS Torso anterior coil combined with a coil integrated in the table, with 32 channels in total
Signa GE (Chicago, Illinois, USA)/1.5T	33 mT/m / 120 T/m/	Reference 1.5T MRI scanner NMRCPHOI	8-channel Body Array coil
Philips Ingenia (Best, The Netherlands) /1.5T	45 mT/m / 200 T/m/s	Control 1.5T MRI scanner NMRCTO	16-channel FlexCoverage Anterior coil

The phantom was scanned on the reference MRI scanners at the Dmitry Rogachev National Medical Research Center of Pediatric Hematology, Oncology and Immunology (NMRC PHOI) 6 times with one-week interval. T2* maps acquisition on control MRI scanners in Clinical and Research Institute of Emergency Pediatric Surgery and Traumatology (CRIEPST) and National Medical Research Center of Traumatology and Orthopedics named after N. N. Priorova (NMRCTO). Specifications of the reference and control MRI scanners are presented in Table 1. The MRI protocols included T2* mapping using multi-phase fast gradient echo (*mGRE*). For all the scanners, the main parameters were as follows: the flip angle (FA) - 45°, the echo time (TE) – 1.2 ms, the number of echoes – 20 with ΔTE = 1.5 ms, the repetition time (TR) – 350 ms; the resolution – 1.5×1.5 mm. For MRI scanners with field strengths of 1.5T and 3T, the slice thickness was 10 and 7 mm, respectively.

T2* values were calculated in two ways. One was automatic T2* mapping using integrated commercial software packages. Mean T2* values were measured within the marked regions of interest (ROI) on T2* maps. The other was manual data analysis using free-available conversional tables.[11] T2* values in ROI were computed by exponential approximation of decay curves via the maximum likelihood method.

Statistical Analysis. We calculated mean T2* values and standard deviations for each phantom tube. The statistical analysis was conducted using GraphPad Prism 8.0.1 software. The repeatability and reproducibility of T2* measurements were assessed. Repeatability was defined as the stability of data obtained during several scanning sessions on the same (reference) MRI scanner over a long period of time. To assess repeatability, we also calculated mean coefficients of variation with the following formula:

$$v_x = \frac{\sigma}{\bar{x}} * 100\%$$

Additionally, we evaluated linear correlations between the results obtained by automatic and manual processing (see MRI Scanning and Post-processing*)*.

Reproducibility was defined as the degree of agreement between T2* values obtained on the control MRI scanners and those obtained on the reference scanners using various methods of T2* calculation (see MRI Scanning and Post-processing). To test the reproducibility of the results across different MRI scanners, we estimated the correlation between measurements obtained on the reference and control MRI scanners. Additionally, Bland-Altman plots were created to assess the repeatability and reproducibility of the results visually.

Results

An example of a T2* map (calculated using commercial processing software for Philips 3T MRI scanner) is represented in Figure 2. The ranges of T2* values for 1.5 and 3T MRI scanners were as follows: from 18.4 to 0.7 ms and from 14.1 to 0.5 ms, respectively.

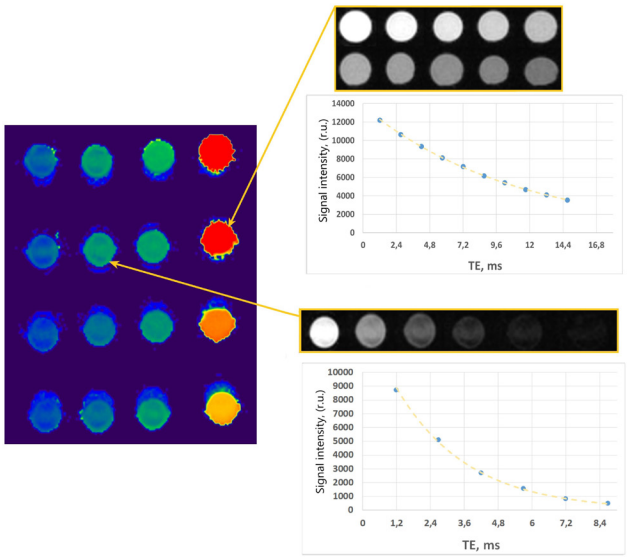

Fig. 2. *An example of a T2* map (on the left) obtained with commercial processing software on the Philips 3T scanner. For two tubes, the examples of T2* signal decay and the dependence of signal intensity (relative units) on TE, ms (TE_1 = 1.2 ms, ΔTE = 1.5 ms) are given. The upper plot was constructed for the tube with the real iron concentration of 0.21 mg/mL and the T2* time = 1.2±0.2 ms, the lower plot was constructed for the tube with the real iron concentration of 0.77 mg/mL and the T2* time = 9±0.2 ms.*

The mean coefficients of variation (C_v) for the reference 1.5 and 3T MRI scanners at our center were 4% and 5%, respectively. The analysis of the repeatability of the technique on the reference MRI scanners is presented in the form of Bland-Altman plots (Fig. 3 A, B). For both scanners, the 95% confidence intervals (CI) ranged from -0.4 to +0.4 ms. Standard deviations for 1.5T and 3T scanners lied in the range of 2% - 5% and 2% - 8%, respectively, whereas in the case of 3T MRI scanner, we observed an increase in the values of standard deviations and a decrease in T2* values.

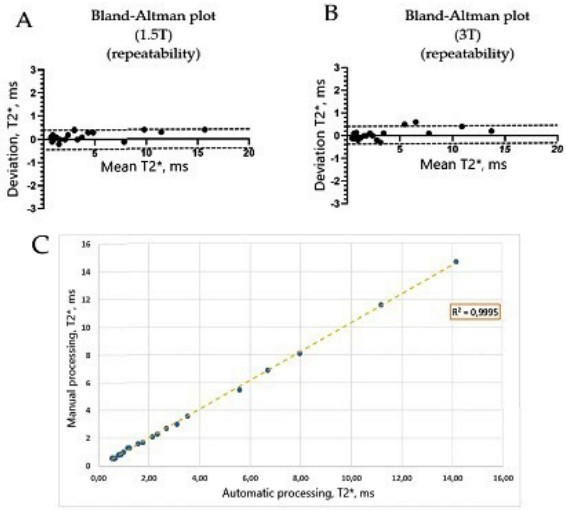

Fig. 3. *Testing the repeatability of the results: Bland-Altman plots for the repeatability of the results obtained on the reference scanners with field strengths of 1.5T (A) and 3T (B), showing the mean deviations of the T2* values (ms) from the average during 6 observations. The correlation between T2* values (ms) obtained by automatic mapping on a Philips 3T scanner and by manual processing of T2* values in ROI (B).*

Furthermore, we found a significant (R^2=0.99, P<0.01) correlation between the T2* values obtained using different calculation methods (Fig. 3B).

We found significant correlations between reference values and the values obtained on other scanners (Fig. 4 A, B): 1.5T - R2 = 0.99 (P<0.01); 3T - R2 = 0.99 (P<0.01). The analysis of the reproducibility of the technique using various MRI scanners is presented in the form of Bland-Altman plots (Fig. 4 C, D). For the scanners with field strengths of 1.5T and 3T, the 95% confidence intervals range from -0.4 to +0.4 ms, respectively.

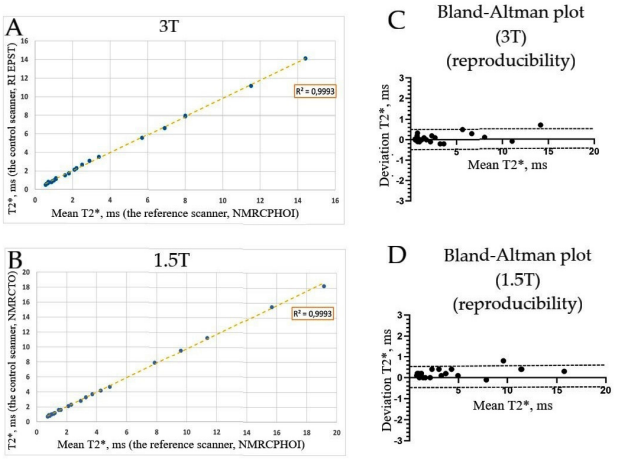

Fig. 4. *Testing the reproducibility of the results: A, B - correlations between the T2* values obtained on reference and other devices with field strengths of 3T and 1.5T, respectively. C, D - Bland-Altman plots for similar T2* values.*

Discussion

In this study, we analyzed the repeatability and reproducibility of an MRI technique for assessing iron overload in the liver based on the application of mGRE pulse sequence, the most available and frequently used technique for measuring iron overload. The coefficients of variation for 6 repeated measurements obtained over one and a half months from MRI scanners at the D. Rogachev NMRCPHOI were less than 5%, indicating excellent repeatability of T2* measurements on both scanners. These results are also confirmed by the statistical analysis and Bland-Altman plots. A significant correlation between T2* values calculated using different methods suggests that one is free to choose any way to process data obtained from the same MRI scanner.

The mean standard deviations show that relative errors of T2* increase proportionally to an increase in iron concentration in a tube due to faster signal decay at a higher iron concentration and, consequently, fewer points for the approximation used to determine T2* values. The lower the field strength is, the slower the T2* relaxation process occurs (which also explains the difference between T2* values). Therefore, T2* measurement errors turn out to be smaller at 1.5T field strength than at 3T. Still, this error associated with using 3T field strength scanners is not critical. It lies within confidence intervals (95%) for mean values obtained at 1.5T, which means that 3T MRI scanners can be successfully applied to detect iron overload. To reduce T2* measurement errors at 3T, ultra-short echo time (UTE) sequences can be used.[12] This technique provides the opportunity to reduce the initial TE value and thus to obtain more points for the approximation at high iron concentrations and to increase the accuracy of the approximation and the reliability of the results. Moreover, radial data collection used in the uTE sequence allows us to avoid respiratory motion artifacts,[13] providing the opportunity to use the free-breathing sequence,[14] which is undoubtedly essential when working with young children.

The results of reproducibility testing also suggest that the created phantom retains all necessary characteristics (homogeneity and the constancy of concentrations and its paramagnetic properties) during a long period of time and, thus, can be used for further evaluation of the reproducibility of T2* calculations on other scanners or with other scanning modes. In contrast to the previous attempts to create phantoms for T2* measurements,[15,16] in this study, we chose superparamagnetic iron oxide Fe3O4 (SPIO) nanoparticles as a paramagnetic material, since hemosiderin contains colloidal particles of ferric hydroxide.[17]

Using the phantom, we tested the reproducibility of the T2* values on MRI scanners from other institutions and compared them with the values obtained on the reference scanners. Based on the correlation and Bland-Altman analyses, T2* mapping techniques used on the 3T and 1.5T control MRI scanners demonstrated good reproducibility. As a result, the T2* measurements were consistent across various devices (lied within the 95% confidence interval). This result clearly indicates that the previously developed formulas for the conversion of T2* values into LIC can be used for these scanners as well. It should be considered that the mapping parameters were selected to be as similar as possible to those that we used on the reference scanner. The modification of the most parameters should not significantly change the calculated T2* values; however, the choice of TE values for the mGRE and uTE sequence should be very careful, since different sets of TE times can strongly affect the calculated T2* values due to the phase effects between fat and water signals.[5]

Thus, to use the previously obtained curves to convert T2* values into LIC, [4,6] it will be sufficient to test the correspondence of T2* values using the phantom we created. In case of any discrepancies, the scanning protocol should be modified until this concordance is obtained. Our experience gained in this study showed that good concordance could be obtained using scanners from different manufacturers, which was also confirmed by the previous studies.

The standardization protocol created in the following study provided an opportunity to use the empirical formula for converting T2* values into LICm that has been developed in our institute[4,6] as well as for other calibration curves [18,19] for any MRI scanners.

As a result of this study, the method for the standardization of T2* mapping on various 1.5T and 3T MRI scanners was tested. This method is based on the use of our MR-compatible phantom. Using this phantom allows for a quick and effective comparison of obtained T2* values against

the reference values and for calibration (if necessary). Liver iron overload can thus be measured without prior long-term validation of T2* mapping and conversion of T2* values (ms) into LIC (mg/mL).

Acknowledgments

We thank Prof. Akhadov T.A. from Clinical and Research Institute of Emergency Pediatric Surgery and Traumatology and Prof. Morozov A.K. from and National Medical Research Center of Traumatology and Orthopedics named after N.N. Priorova for the phantom acquisition sessions on MRI scanners.

Competing Interests

The authors declare that they have no competing interests.

References

1. Siah CW, Trinder D, Olynyk JK. Iron overload. Clin Chim Acta. 2005 Aug;358(1-2):24-36. doi: 10.1016/j.cccn.2005.02.022.
2. Smetanina NS. [Current possibilities of chelation therapy]. Russian Journal of Pediatric Hematology and Oncology. 2014;(1):51-61. doi: 10.17650/2311-1267-2014-0-1-51-61. [Article in Russian].
3. Labranche R, Gilbert G, Cerny M, Vu KN, Soulières D, Olivié D, Billiard JS, Yokoo T, Tang A. Liver Iron Quantification with MR Imaging: A Primer for Radiologists. Radiographics. 2018 Mar-Apr;38(2):392-412. doi: 10.1148/rg.2018170079.
4. Nazarova EE, Kupriyanov DA, Novichkova GA, Tereshchenko GV. [Noninvasive assessment of iron overload by magnetic resonance imaging]. Pediatric Hematology/Oncology and Immunopathology. 2020;19(3):158-163. doi: 10.24287/1726-1708-2020-19-3-158-163. [Article in Russian].
5. Hernando D, Levin YS, Sirlin CB, Reeder SB. Quantification of liver iron with MRI: state of the art and remaining challenges. J Magn Reson Imaging. 2014 Nov;40(5):1003-21. doi: 10.1002/jmri.24584.
6. Nazarova EE, Tereshchenko GV, Abakumov MA, Smantser VA, Kupriyanov DA, Smetanina NS. [MRI T2*-mapping for liver iron assessment in pediatric patients with secondary iron overload]. Pediatric Hematology/Oncology and Immunopathology. 2017;16(3):23-27. doi: 10.24287/1726-1708-2017-16-3-23-27.[Article in Russian].
7. Garbowski MW, Carpenter JP, Smith G, Roughton M, Alam MH, He T, Pennell DJ, Porter JB. Biopsy-based calibration of T2* magnetic resonance for estimation of liver iron concentration and comparison with R2 Ferriscan. J Cardiovasc Magn Reson. 2014 Jun 10;16(1):40. doi: 10.1186/1532-429X-16-40.
8. St Pierre TG, Clark PR, Chua-anusorn W, Fleming AJ, Jeffrey GP, Olynyk JK, Pootrakul P, Robins E, Lindeman R. Noninvasive measurement and imaging of liver iron concentrations using proton magnetic resonance. Blood. 2005 Jan 15;105(2):855-61. doi: 10.1182/blood-2004-01-0177.
9. St Pierre TG, El-Beshlawy A, Elalfy M, Al Jefri A, Al Zir K, Daar S, Habr D, Kriemler-Krahn U, Taher A. Multicenter validation of spin-density projection-assisted R2-MRI for the noninvasive measurement of liver iron concentration. Magn Reson Med. 2014 Jun;71(6):2215-23. doi: 10.1002/mrm.24854.
10. Gubin SP, Koksharov YuA, Khomutov GB, Yurkova GYu. Magnetic nanoparticles: preparation, structure and properties. Russ Chem Rev. 2005;74(6):489-520. doi: 10.1070/RC2005v074n06ABEH000897. [Article in Russian].
11. Fernandes JL, Fioravante LAB, Verissimo MP, Loggetto SR. A free software for the calculation of T2* values for iron overload assessment. Acta Radiol. 2017 Jun;58(6):698-701. doi: 10.1177/0284185116666416.
12. Doyle EK, Toy K, Valdez B, Chia JM, Coates T, Wood JC. Ultra-short echo time images quantify high liver iron. Magn Reson Med. 2018 Mar;79(3):1579-1585. doi: 10.1002/mrm.26791.
13. Haacke EM, Brown RF, Thompson M, Venkatesan R. Magnetic resonance imaging: Physical principles and sequence design. New York: J. Wiley & Sons. 1999.
14. Zhu X, Chan M, Lustig M, Johnson KM, Larson PEZ. Iterative motion-compensation reconstruction ultra-short TE (iMoCo UTE) for high-resolution free-breathing pulmonary MRI. Magn Reson Med. 2020 Apr;83(4):1208-1221. doi: 10.1002/mrm.27998.
15. Mobini N, Malekzadeh M, Haghighatkhah H, Saligheh Rad H. A hybrid (iron-fat-water) phantom for liver iron overload quantification in the presence of contaminating fat using magnetic resonance imaging. MAGMA. 2020 Jun;33(3):385-392. doi: 10.1007/s10334-019-00795-7.
16. Hines CD, Yu H, Shimakawa A, McKenzie CA, Brittain JH, Reeder SB. T1 independent, T2* corrected MRI with accurate spectral modeling for quantification of fat: validation in a fat-water-SPIO phantom. J Magn Reson Imaging. 2009 Nov;30(5):1215-22. doi: 10.1002/jmri.21957.
17. Saito H, Hayashi H. Transformation rate between ferritin and hemosiderin assayed by serum ferritin kinetics in patients with normal iron stores and iron overload. Nagoya J Med Sci. 2015 Nov;77(4):571-83.
18. Wood JC, Enriquez C, Ghugre N, Tyzka JM, Carson S, Nelson MD, Coates TD. MRI R2 and R2* mapping accurately estimates hepatic iron concentration in transfusion-dependent thalassemia and sickle cell disease patients. Blood. 2005 Aug 15;106(4):1460-5. doi: 10.1182/blood-2004-10-3982.
19. Storey P, Thompson AA, Carqueville CL, Wood JC, de Freitas RA, Rigsby CK. R2* imaging of transfusional iron burden at 3T and comparison with 1.5T. J Magn Reson Imaging. 2007 Mar;25(3):540-7. doi: 10.1002/jmri.20816.

International Journal of Biomedicine 12(2) (2022) 29-33
http://dx.doi.org/10.21103/Article12(1)_OA2

ORIGINAL ARTICLE

Radiology

INTERNATIONAL JOURNAL OF BIOMEDICINE

Ultrasonographic Measurement of Femoral Cartilage Thickness in Patients with Knee Osteoarthritis

Mohamed A. Bedewi[1]; Ayman A. Elsifey[1]; Moheyeldeen F. Naguib[1]; Ayman K. Saleh[2,3]; Sameer Al-Ghamdi[4]; Bader A. Alhariqi[1]; Nasser M. Aldossary[1]; Gehan Abdelwahab[5]; Naif Bin Nwihadh[2]; Amr A. Abd-Elghany[6,7]; Mahmoud H. El-Bidawy[8,9]

[1]Department of Internal Medicine, Prince Sattam Bin Abdulaziz University, College of Medicine, Al-Kharj, Saudi Arabia
[2]Department of Surgery, Prince Sattam Bin Abdulaziz University, College of Medicine, Al-Kharj, Saudi Arabia
[3]Orthopedic Department, Faculty of Medicine for Girls, Al-Azhar University, Cairo, Egypt
[4]Department of Family & Community Medicine, Prince Sattam Bin Abdulaziz University, College of Medicine, Al-Kharj, Saudi Arabia
[5]Department of Rheumatology and Rehabilitation, Faculty of Medicine, Minia University, Egypt
[6]Radiology and Medical Imaging Department, College of Applied Medical Sciences, Prince Sattam Bin Abdul-Aziz University, Al-Kharj, Saudi Arabia
[7]Biophysics Department, Faculty of Science, Cairo University, Giza, Egypt
[8]Department of Physiology, Kasr Al-Aini Faculty of Medicine, Cairo University, Cairo, Egypt
[9]Department of BMS, Division of Physiology, College of Medicine, Prince Sattam Bin Abdulaziz University, Al-Kharj, Saudi Arabia

Abstract

The aim of this study was to investigate the femoral cartilage thickness (FCT) by ultrasound in patients with knee osteoarthritis and compare them with those of healthy subjects.

Methods and Results: This cross-sectional study included 44 patients diagnosed with knee osteoarthritis (OA) and 49 healthy subjects. The FCT was measured using an L5-18 MHz linear probe. Measurements were taken from both knee joints in three regions: the medial condyle, lateral condyle, and intercondylar area. Our results showed thinner cartilage in OA patients than in the healthy subjects at the three examined locations bilaterally (medial condyle, lateral condyle, intercondylar area). In OA patients, FCT correlated positively with body mass index at the right lateral condyle, right intercondylar area, and left medial condyle (P<0.05).

***Conclusion*:** Our study revealed thinner FCT in patients with knee OA than in healthy subjects. Further studies considering the stratification of different stages of OA could yield better results.(**International Journal of Biomedicine. 2022;12(1):29-33.**)

Key Words: osteoarthritis • femoral cartilage thickness • ultrasound

For citation: Bedewi MA, Elsifey AA, Naguib MF, Saleh AK, Al-Ghamdi S, Alhariqi BA, Aldossary NM, Abdelwahab G, Nwihadh NB, Abd-Elghany AA, El-Bidawy MH. Ultrasonographic Measurement of Femoral Cartilage Thickness in Patients with Knee Osteoarthritis. International Journal of Biomedicine. 2022;12(1):29-33. doi:10.21103/Article12(1)_OA2

Abbreviations

BMI, body mass index; **FCT**, femoral cartilage thickness; **LIC**, left intercondylar area; **LLC**, left lateral condyle; **LMC**, left medial condyle; **MRI**, magnetic resonance imaging; **OA,** osteoarthritis; **RIC**, right intercondylar area; **RLC**, right lateral condyle; **RMC**, right medial condyle.

Introduction

Osteoarthritis (OA) of the knee is a common degenerative synovial joint disorder and is a significant cause of chronic pain and disability associated with structural and functional loss. It can result in morbidity and socioeconomic loss, particularly in the aging population.[1-4] OA of the knee is characterized by focal degeneration and progressive loss of the articular cartilage.[5] Femoral articular cartilage is hyaline type. It is composed of an extracellular matrix and chondrocytes.[4] The significance of correct assessment of the articular cartilage is increasing, especially with the development of new treatments for OA, like disease-modifying drugs, osteochondral autografting, and autologous chondrocyte implantation.[1,6] Successful assessment of disease progression and response to treatment that could control the course of the OA depend on finding a suitable method for assessing cartilage thickness.[5] The use of plain films was considered the main radiological tool for diagnosing knee OA. It reveals gross joint narrowing, including the meniscus as a proportion of the joint space. Conventional radiography does not directly visualize cartilage surface, and the correlation of the clinical symptoms with the width of the joint space could be misleading. CT can only determine surface defects of cartilage thickness, with the risk of high dose ionizing radiation and relatively high price.[1,4,6] MRI is a safe imaging modality that uses three-dimensional fat-suppressed spoiled gradient-recalled steady-state (3D SPGR), acquisition with high sensitivity to detect focal cartilage defects. However, MRI is an expensive modality, with limited accessibility, in addition to several problems with claustrophobic patients and patients with non-compatible metallic prostheses.[1]

Ultrasonography is also a safe technique, which is well tolerated by patients. It is thought to detect cartilage defects and bone erosions in the early phases of OA.[1] The aim of this study was to investigate the femoral cartilage thickness (FCT) by ultrasound in patients with knee osteoarthritis and compare them with those of healthy subjects.

Materials and Methods

Participants in the study were recruited between March 2020 and May 2020. This cross-sectional study included 44 patients diagnosed with knee OA, according to the American College of Rheumatology criteria. The study also involved 49 healthy subjects. Healthy subjects enrolled in the study had the following features: female or male, and no history of knee pain. For each participant, data including sex, age, weight, BMI, and height were acquired. Written informed consent was obtained from all participants.

Sonographic examination

The patients were investigated using an ultrasound machine equipped with an L5-18 MHz linear probe (Epic 5 Ultrasound system: Philips, Bothell, WA). Two radiologists with 7 years of experience in musculoskeletal ultrasound performed all studies. Three scans were performed for all participants. The probe was placed in the short axis above the patella. All participants were examined in a supine position with flexion of the knee joint. Measurements were taken from both knee joints in three regions: the medial condyle (RMC/LMC), lateral condyle (RLC/LLC), and intercondylar area (RIC/LIC) (Fig.1).

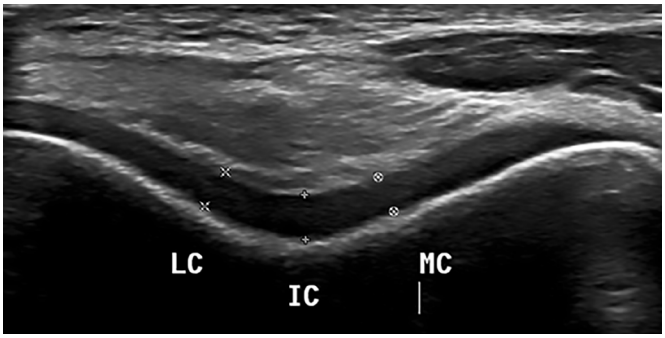

***Fig. 1. S**hort axis image of the femoral cartilage in a healthy subject. LC - lateral condyle, IC - intercondylar area, MC - medial condyle.*

Statistical analysis was performed using the standard Statistical Package for the Social Sciences (IBM SPSS Statistics for Windows, Version 21.0. Armonk, NY: IBM Corp). Continuous variables were presented as mean±standard deviation (SD). For data with normal distribution, inter-group comparisons were performed using Student's t-test. The frequencies of categorical variables were compared using Pearson's chi-squared test A probability value of $P<0.05$ was considered statistically significant.

Results

Measurements were taken from 88 knees of 44 OA patients (15 males, 29 females) with a mean age of 51.52±8.77 years [range 33-67], mean height of 160.45±10.03 cm [range 144-184], mean weight of 83.00±17.45 kg [range 56-123], and mean BMI of 32.28±5.50 kg/m^2 [range 24.2-49.9].

A total of 98 knees were included from 49 healthy subjects (30 males, 19 females) with the mean age of 31.73±7.80 years [range 17-62], mean height of 162.20±10.87 cm [range 135-195], mean weight of 65.99±16.54 kg [range 44-125], and mean BMI of 24.93±4.32 kg/m^2 [range 16.6-35.7]. The demographic features of OA patients and healthy subjects are shown in Table 1.

Table 1.

The demographic characteristics of OA patients and healthy subjects

Variable	Patients (n=44)	Control (n=49)	P-value
Age, years	51.52±8.77	31.73±7.80	<0.0001
Female, n (%)	29 (65.90)	19 (38.78)	
Male, n (%)	15 (34.10)	30 (61.22)	
Weight, kg	83.00±17.45	65.99±16.54	<0.0001
Height, cm	160.45±10.03	162.20±10.87	>0.05
BMI, kg/m^2	32.28±5.50	24.93±4.32	<0.0001

Table 2.

FCT (cm) in OA patients and healthy subjects

	Patients (n=44)		Control (n=49)		*P*-value
	Female (n=29) (1)	Male (n=15) (2)	Female (n=19) (3)	Male (n=30) (4)	
RIC	0.22±0.05	0.20±0.06	0.23±0.02	0.24±0.04	P_{1-3}>0.05 P_{2-4}=0.01
RMC	0.19±0.04	0.18±0.07	0.21±0.03	0.23±0.03	P_{1-3}>0.05 P_{2-4}=0.01
RLC	0.20±0.04	0.19±0.05	0.22±0.02	0.22±0.03	P_{1-3}<0.05 P_{2-4}=0.01
LIC	0.21±0.05	0.19±0.06	0.23±0.04	0.23±0.04	P_{1-3}>0.05 P_{2-4}=0.01
LMC	0.19±0.07	0.19±0.05	0.21±0.03	0.22±0.03	P_{1-3}>0.05 P_{2-4}=0.01
LLC	0.20±0.04	0.19±0.04	0.21±0.03	0.22±0.03	P_{1-3}>0.05 P_{2-4}<0.01

Table 3.

Correlations between demographic factors and FCT (cm) in OA patients

	RIC	RMC	RLC	LIC	LMC	LLC
Age	0.065	- 0.101	0.062	0.172	0.048	0.074
Sig	0.718	0.516	0.690	0.264	0.756	0.633
Weight	0.233	0.192	0.276	0.162	0.118	0.212
Sig	0.128	0.212	0.070	0.295	0.444	0.168
Height	0.008	0.024	0.024	0.010	0.009	0.03
Sig	0.959	0.878	0.877	0.950	0.955	0.780
BMI	**0.306**	0.227	**0.347**	0.212	0.155	0.246
Sig	**0.044**	0.138	**0.021**	0.168	0.314	0.107

Table 4.

Correlations between demographic factors and FCT in healthy subjects

	RIC	RMC	RLC	LIC	LMC	LLC
Age	0.064	- 0.013	0.063	0.112	0.074	- 0.080
Sig	0.662	0.928	0.669	0.445	0.612	0.583
Weight	0.270	0.225	0.112	0.046	0.244	0.168
Sig	0.060	0.121	0.444	0.754	0.092	0.248
Height	**0.336**	0.265	0.290	0.005	**0.319**	0.194
Sig	**0.018**	0.066	0.043	0.974	**0.025**	0.181
BMI	0.131	0.164	- 0.048	0.126	0.175	0.114
Sig	0.370	0.261	0.745	0.390	0.230	0.435

The intra-observer reliability was 0.80. Measurements of the mean FCT showed statistically significant lower values in patients with knee OA than in healthy subjects in the six parameters. In OA patients, FCT correlated positively with BMI at the RLC, RIC, and LMC (P<0.05). Other demographic factors showed no significant correlation with FCT in OA patients. In healthy subjects, the FCT correlated positively with height at the RLC, RIC, and LMC (P<0.05). Other demographic factors showed no significant correlation with the FCT in healthy subjects (Tables 2-6).

Table 5.

Independent t-test comparing FCT (cm) in OA patients

	Gender	n	Mean	SD	t-statistic	Sig
RIC	Female	29	0.22	0.05	1.175	0.2468
	Male	15	0.20	0.06		
RMC	Female	29	0.19	0.04	0.605	0.5484
	Male	15	0.18	0.07		
RLC	Female	29	0.20	0.04	0.721	0.4747
	Male	15	0.19	0.05		
LIC	Female	29	0.21	0.05	1.175	0.2468
	Male	15	0.19	0.06		
LMC	Female	29	0.19	0.07	0.000	1.0000
	Male	15	0.19	0.05		
LLC	Female	29	0.20	0.04	0.786	0.4382
	Male	15	0.19	0.04		

Table 6.

Independent t-test comparing FCT (cm) in healthy subjects

	Gender	n	Mean	SD	t-statistic	Sig
RIC	Female	19	0.23	0.02	1.010	0.3177
	Male	30	0.24	0.04		
RMC	Female	19	0.21	0.03	2.274	0.0276
	Male	30	0.23	0.03		
RLC	Female	19	0.22	0.02	0.000	1.0000
	Male	30	0.22	0.03		
LIC	Female	19	0.23	0.04	0.000	1.0000
	Male	30	0.23	0.04		
LMC	Female	19	0.21	0.03	1.137	0.2613
	Male	30	0.22	0.03		
LLC	Female	19	0.21	0.03	1.137	0.2631
	Male	30	0.22	0.03		

Discussion

In this study, we evaluated FCT by ultrasound in knees of OA patients and whether the result is related to any of the demographic factors. Ultrasonography is a cheap, non-invasive diagnostic tool for examining the knee joint. Cartilage appears in ultrasound as homogenously anechoic with a distinct bone margin. Ultrasound can also assess the collateral ligaments and patellar tendon, in addition to effusion and bursitis.[5] The importance of ultrasound in the diagnosis of knee OA has increased over the last twenty years.[1] The knee joint is usually involved by OA, ending with injury of the articular cartilage. Articular cartilage consists of two phases: a fluid phase, and a solid phase. The interactions of the components of these two phases support articular cartilage to resist compressive forces.[7] Several studies reported the FCT assessment in healthy adults and in different sets of diseases.[8-13] Our study focuses on OA as one of the most prevalent disorders affecting the knee joint with significant morbidity and socioeconomic loss. Assessment of cartilage thickness is essential for early detection of OA, follow-up of disease progression, and evaluation of treatment. Cartilage thickness may increase in the earlier cases of OA; however, well-established OA is characterized by narrowed tibiofemoral cartilage, erosions, and cartilage loss in late disease. Accurate measurement of cartilage thickness can be very useful clinically for detecting focal cartilage defects.[6,14] During the course of knee OA, as mentioned in previous studies, cartilage loss starts in the medial tibiofemoral compartment and then progresses to the lateral tibiofemoral compartment.[15] In our study, FCT was thinner in patients with knee OA than in healthy subjects at the medial condyle, lateral condyle, and intercondylar region. Our results showed thinner cartilage in OA patients than in the healthy subjects at the three examined locations bilaterally (medial condyle, lateral condyle, intercondylar area) (Figure 2). BMI showed a correlation with three out of six measurements in OA in our study. Compared to Ozgonenel et al.,[14] our measurements were lower at both condyles together with the intercondylar area. This is likely attributed to the recruitment of early cases of knee OA in that study.

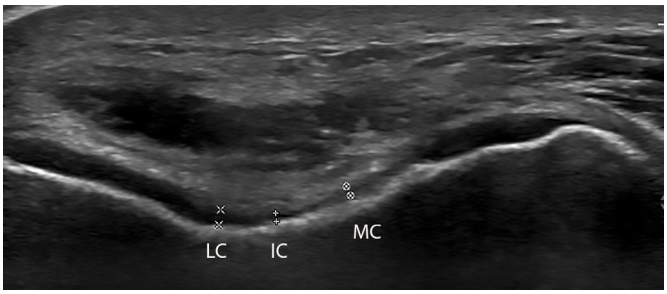

Fig. 2. *Long axis image of the femoral cartilage in an osteoarthritic patient. LC- lateral condyle, IC - intercondylar area, MC - medial condyle.*

The present study has limitations. First, the sample population is heterogeneous, which limits the generalization of the results. Second, the sample size is relatively small.

Conclusion

Our study revealed thinner FCT in patients with knee OA than in healthy subjects. Further studies considering the stratification of different stages of OA could yield better results.

Competing Interests

The authors declare that they have no competing interests.

Acknowledgments

The authors would like to express their sincere gratitude to the Deanship of Scientific Research at Prince Sattam Bin Abdulaziz University, Al-Kharj, Saudi Arabia.

References

1. Yoon CH, Kim HS, Ju JH, Jee WH, Park SH, Kim HY. Validity of the sonographic longitudinal sagittal image for assessment of the cartilage thickness in the knee osteoarthritis. Clin Rheumatol. 2008 Dec;27(12):1507-16. doi: 10.1007/s10067-008-0956-3.
2. Özçakar L, Tunç H, Öken Ö, Ünlü Z, Durmuş B, Baysal Ö, Altay Z, Tok F, Akkaya N, Doğu B, Çapkın E, Bardak A, Çarlı AB, Buğdaycı D, Toktaş H, Dıraçoğlu D, Gündüz B, Erhan B, Kocabaş H, Erden G, Günendi Z, Kesikburun S, Omaç ÖK, Taşkaynatan MA, Şenel K, Uğur M, Yalçınkaya EY, Öneş K, Atan Ç, Akgün K, Bilgici A, Kuru Ö, Özgöçmen S. Femoral cartilage thickness measurements in healthy individuals: learning, practicing and publishing with TURK-MUSCULUS. J Back Musculoskelet Rehabil. 2014;27(2):117-24. doi: 10.3233/BMR-130441.
3. Mesci N, Mesci E, Külcü DG. Association of neuropathic pain with ultrasonographic measurements of femoral cartilage thickness and clinical parameters in patients with knee osteoarthritis. J Phys Ther Sci. 2016 Aug;28(8):2190-5. doi: 10.1589/jpts.28.2190.
4. Wang Z, Liang L. Research on quantitative measurement method of articular cartilage thickness change based on MR image. J Infect Public Health. 2020 Dec;13(12):1993-1996. doi: 10.1016/j.jiph.2019.08.020.
5. Naredo E, Acebes C, Möller I, Canillas F, de Agustín JJ, de Miguel E, Filippucci E, Iagnocco A, Moragues C, Tuneu R, Uson J, Garrido J, Delgado-Baeza E, Sáenz-Navarro I. Ultrasound validity in the measurement of knee cartilage thickness. Ann Rheum Dis. 2009 Aug;68(8):1322-7. doi: 10.1136/ard.2008.090738.
6. Schmitz RJ, Wang HM, Polprasert DR, Kraft RA, Pietrosimone BG. Evaluation of knee cartilage thickness: A comparison between ultrasound and magnetic resonance imaging methods. Knee. 2017 Mar;24(2):217-223. doi: 10.1016/j.knee.2016.10.004.
7. Kilic G, Kilic E, Akgul O, Ozgocmen S. Ultrasonographic

***Corresponding author:** Dr. Mohamed A. Bedewi, MD, PhD. Associate Professor of Radiology. College of medicine; Prince Sattam bin Abdulaziz University. Al-Kharj; Saudi Arabia. E-mail: mohamedbedewi@yahoo.com*

assessment of diurnal variation in the femoral condylar cartilage thickness in healthy young adults. Am J Phys Med Rehabil. 2015 Apr;94(4):297-303. doi: 10.1097/PHM.0000000000000179.
8. Roberts HM, Moore JP, Thom JM. The Reliability of Suprapatellar Transverse Sonographic Assessment of Femoral Trochlear Cartilage Thickness in Healthy Adults. J Ultrasound Med. 2019 Apr;38(4):935-946. doi: 10.1002/jum.14775.
9. Kazam JK, Nazarian LN, Miller TT, Sofka CM, Parker L, Adler RS. Sonographic evaluation of femoral trochlear cartilage in patients with knee pain. J Ultrasound Med. 2011 Jun;30(6):797-802. doi: 10.7863/jum.2011.30.6.797.
10. Karkucak M, Batmaz İ, Civan N, Kilinc F, Capkin E, Sariyildiz MA, Garipoğlu MA, Onder MA, Ozcakar L. Ultrasonographic measurement of femoral cartilage thickness in acromegalic patients. Clin Rheumatol. 2015 Jan;34(1):157-61. doi: 10.1007/s10067-014-2543-0.
11. Harkey MS, Blackburn JT, Nissman D, Davis H, Durrington I, Rizk C, Kuismanen A, Pietrosimone B. Ultrasonographic Assessment of Femoral Cartilage in Individuals With Anterior Cruciate Ligament Reconstruction: A Case-Control Study. J Athl Train. 2018 Nov;53(11):1082-1088. doi: 10.4085/1062-6050-376-17.
12. Ünal HU, Tok F, Adıgüzel E, Gezer M, Aydın İ, Yılmaz B, Oğuz Y. Ultrasonographic evaluation of the femoral cartilage thickness in patients with chronic renal failure. Ren Fail. 2016;38(4):600-4. doi: 10.3109/0886022X.2016.1149685.
13. Adiguzel E, Tok F, Ata E, Yaşar E, Yılmaz B. Ultrasonographic Assessment of Femoral Cartilage Thickness in Patients With Cerebral Palsy. PM R. 2018 Feb;10(2):154-159. doi: 10.1016/j.pmrj.2017.07.002.
14. Özgönenel L, Okur SÇ, Dogan YP, Çaglar NS. Effectiveness of Therapeutic Ultrasound on Clinical Parameters and Ultrasonographic Cartilage Thickness in Knee Osteoarthritis: A Double-Blind Trial. J Med Ultrasound. 2018 Oct-Dec;26(4):194-199. doi: 10.4103/JMU.JMU_21_18.
15. Favre J, Scanlan SF, Erhart-Hledik JC, Blazek K, Andriacchi TP. Patterns of femoral cartilage thickness are different in asymptomatic and osteoarthritic knees and can be used to detect disease-related differences between samples. J Biomech Eng. 2013 Oct 1;135(10):101002-10. doi: 10.1115/1.4024629.

International Journal of Biomedicine 12(1) (2022) 34-37
http://dx.doi.org/10.21103/Article12(1)_OA3

ORIGINAL ARTICLE

Radiology

INTERNATIONAL JOURNAL OF BIOMEDICINE

Shear Wave Elastography of the Sural Nerve in Healthy Subjects: A Pilot Study

Mohamed A. Bedewi[1*]; Mamdouh A. Kotb[2,3]; Bader A. Alhariqi[1]; Nasser M. Aldossary[1]; Mohamed Sherif El-sharkawy[4]; Ezzat M. Awad[5]

[1]Department of Internal Medicine, Prince Sattam Bin Abdulaziz University, College of Medicine, Al-Kharj, Saudi Arabia
[2]Neurology Department, College of Medicine, Prince Sattam Bin Abdulaziz University, Al-Kharj, Kingdom of Saudi Arabia
[3]Neurology Department, Faculty of Medicine, Minia University, Minia, Egypt
[4]Department of Radiology and Medical Imaging, King Saud University, King Saud University Medical City, Riyadh, Saudi Arabia
[5]Department of Vascular Biology and Thrombosis Research, Center for Physiology and Pharmacology, Institute for Specific Prophylaxis and Tropical Medicine [ISPTM], Center for Pathophysiology, Infectiology and Immunology (CePII), Medical University of Vienna, Vienna, Austria

Abstract

The goal of this study is to evaluate the potential ability of shear wave elastography (SWE) to evaluate the sural nerve (SN) in healthy subjects.

***Methods and Results*:** Thirty-six SNs were evaluated in 18 healthy adult subjects. Subjects were examined in the prone position with the ankle in the neutral position, and the knees fully extended; a linear transducer was used [L18-4, MHZ] (EPIQ Elite SW 5.0.1, Philips). Nerve conduction studies were performed with the Nihon-Cohden Neuropack device. The mean cross sectional area of the SN at both sides was 4.03±1.16 mm^2. The mean shear elastic modulus of the right SN in the short axis was 24.92±6.08 kPa, while in the long axis it was 26.45±5.66 kPa. The mean shear elastic modulus of the left SN in the short axis was 24.1±4.1 kPa [range 19-33.13], while in the long axis it was 23.9±4.9 kPa [range 16.4-30.77]. The cross sectional area of the SN correlated positively with height ($P<0.05$), weight ($P<0.001$), and body mass index ($P<0.01$).

Conclusion: SWE could play a complementary role in future evaluation of SN pathologies. (**International Journal of Biomedicine. 2022;12(1):34-37.**)

Key Words: sural nerve • shear wave elastography • body mass index

For citation: Bedewi MA, Kotb MA, Alhariqi BA, Aldossary NM, El-Sharkawy MSh, Awad EM. Shear Wave Elastography of the Sural Nerve in Healthy Subjects: A Pilot Study. International Journal of Biomedicine. 2022;12(1):34-37. doi:10.21103/Article12(1)_OA3

Abbreviations

BMI, body mass index; **CSA**, cross sectional area; **LA**, long axis; **SA**, short axis; **SN**, sural nerve; **SWE**, shear wave elastography.

Introduction

The sural nerve (SN) is a small sensory nerve, which is formed by a branch of the common fibular nerve (lateral sural cutaneous nerve) and a branch of the tibial nerve (medial sural cutaneous nerve). It supplies the skin of the lateral side of the foot and the lateral and posterior part of the inferior third of the leg.[1-3] Anatomical and topographical variations are common. Union of the SN roots can occur at the proximal part of the calf, although occasionally, more distal fusion can be seen.

During its course, the SN has a close relationship with the short saphenous vein and the Achilles tendon.[1-5] The SN is essential in several clinical situations. In nerve conduction studies, it is used to diagnose polyneuropathies like sciatic and tibial neuropathies, as well as lumbosacral plexopathies.[6-11] Also, the SN biopsy represents the mainstay in the diagnostic workup of some other types of peripheral nerve diseases.[12,13] Nerve graft procedures are another important use of the SN.[1] Ultrasound was used for more than two decades to assess the musculoskeletal system. It is a non-invasive, fast, and dynamic diagnostic technique. These features favor its use over magnetic resonance imaging for a small nerve like the SN. Sonoelastography was first described in the 1990s to detect tissue stiffness. Two main types of elastography are present at the moment. The first is strain elastography, where mild pressure is applied by a probe to estimate the tissue stiffness, resulting in qualitative and semi-quantitative values. The other type is SWE, where the probe induces a pulse that propagates waves in a transverse manner with resultant attenuation by the different target tissues. The amount of stiffness is related to the velocity of wave propagation. SWE is now widely used in evaluating many organs, such as the liver, breast, and thyroid gland. Recently it has been introduced to assess the musculoskeletal and peripheral nervous systems.[14-24] The goal of this study is to evaluate the potential ability of SWE to evaluate the SN in healthy subjects.

Materials and Methods

Thirty-six SNs were evaluated in 18 healthy adult subjects. After obtaining institutional review board approval, subjects were recruited between September 2019 and December 2019, and written consent was obtained. Our inclusion criteria were healthy male or female, age range of 24-46. The following were excluded in each subject: the presence of pain due to neuropathy, limb weakness, trauma to the lower limb. Demographic data were obtained for all subjects.

Subjects were examined in the prone position with the ankle in the neutral position, and the knees fully extended; a linear transducer was used [L18-4, MHZ] (EPIQ Elite SW 5.0.1, Philips). An experienced radiologist performed all studies; images were reviewed by a neurologist. The SN was first scanned in the axial scan above the level of the lateral malleolus and lateral to the lesser saphenous vein, and then the CSA was measured. For the SWE measurements, each subject was scanned three separate times. A confidence map was used to increase the reliability of the study. After axial scanning and the SWE measurements were taken, the transducer was rotated 90º for longitudinal SWE measurements. When the nerve was identified, the transducer was held stationary for 4 seconds with the region of interest diameter measuring 2mm and placed within the hyperechoic epineurium. Average, median, and maximum elasticity were recorded in kPa. The color scale was set at a 0 to 200 kPa. The blue color was set for soft tissues and red for stiff tissues (Figures 1 and 2).

Nerve conduction studies were performed with the Nihon-Cohden Neuropack device. An expert neurologist performed electrodiagnostic studies. All studies were performed at optimal room temperature.

Statistical analysis was performed using the standard Statistical Package for the Social Sciences (IBM SPSS Statistics for Windows, Version 21.0. Armonk, NY: IBM Corp). Inter-observer agreement was measured using Cohen's kappa (k) statistic. Continuous variables were presented as mean±standard deviation (SD). For data with normal distribution, inter-group comparisons were performed using Student's t-test. The frequencies of categorical variables were compared using Pearson's chi-squared test A probability value of $P<0.05$ was considered statistically significant.

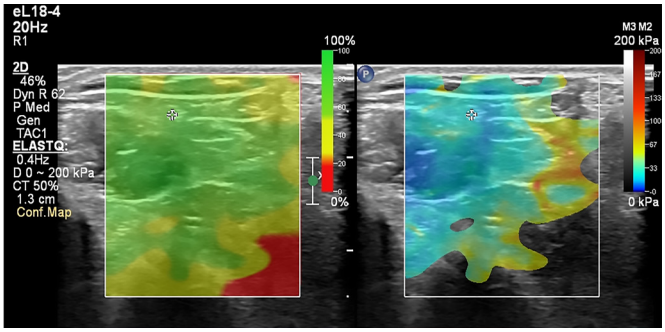

Fig. 1. *Axial scan view of the sural nerve shear wave elastography with stiffness measurement in kPa.*

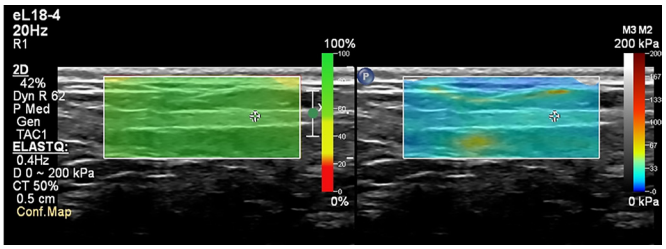

Fig. 2. *Longitudinal view of the sural nerve shear wave elastography with stiffness measurement in kPa.*

Results

Our study included 18 healthy adult subjects, with a mean age of 32.67±7.07 years [range 24-46], mean height - 157.89±8.29 cm [range 144-177], mean weight - 60.67±9.15 kg [range 43-84], mean BMI - 4.27±2.58 kg/m^2 [range 20.7-30.9]. Table 1 shows CSA and stiffness estimates of the SN. Table 2 shows descriptive statistics used in our study. The intra-observer reliability calculations resulted in an overall intra-class correlation coefficient of 0.80. The mean CSA of the SN at both sides was 4.03±1.16 mm^2 [range 2-7]. The mean CSA area of the right SN was 4±1.3 mm^2 [range 2-7]. The mean shear elastic modulus of the right SN in the SA was 24.92±6.08 kPa [range 14.3-34.9], while in the LA it was 26.45±5.66 kPa [range 11-34.5]. The mean CSA of the left SN was 4.04±1.03 mm^2 [range 2.3-6.1]. The mean shear elastic modulus of the left SN in the SA was 24.1±4.1 kPa [range 19-33.13], while in the LA it was 23.9±4.9 kPa [range 16.4-30.77]. No statistical differences were noted between the right

and left sides regarding the CSA (P=0.955), shear wave elastic modulus of the SN in the SA (P=0.635), and shear wave elastic modulus of the SN in the LA (P=0.152). The CSA of the SN correlated positively with height (P<0.05), weight (P<0.001), and BMI (P<0.01). No correlation was noted between CSA and age in our study. No statistical relation could be noted between elasticity measurements in long and short axes. The SN elastic modulus also showed no correlation with CSA in the LA nor SA. Height, weight, and BMI showed no correlation with SN elastic modulus in short or long axes. Only age showed a negative correlation with LA measurements.

Table 1.

CSA and shear elastic modulus of the sural nerve

	Right	Left	P-value
CSA Mean ±SD Minimum / Maximum	4±1.3 2 / 7	4±1.0 2.3 / 6.1	0.955
SA Mean ±SD Minimum / Maximum	24.9± 6.08 14.3 / 34.9	24.1±4.1 19 / 33.1	0.635
LA Mean ±SD Minimum / Maximum	26.5±5.66 11 / 34.5	23.9±4.9 16.4 / 30.8	0.152

CSA in mm^2; LA- Long axis stiffness in kPa; SA- Short axis stiffness in kPa

Table 2.

Correlations between age, weight, height, and BMI, with CSA, and elastic modulus of the SN in long and short axis

		Sural CSA	Sural SA	Sural LA
Age	Pearson Correlation	.127	-.216	-.402
	Sig. (2-tailed)	.460	.205	.015
	n	36	36	36
Height	Pearson Correlation	.331	.171	.095
	Sig. (2-tailed)	.049	.318	.581
	n	36	36	36
Weight	Pearson Correlation	.573	.268	.197
	Sig. (2-tailed)	.000	.114	.248
	n	36	36	36
BMI	Pearson Correlation	.491	.201	.179
	Sig. (2-tailed)	.002	.240	.297
	n	36	36	36
Sural CSA	Pearson Correlation	1	.196	.186
	Sig. (2-tailed)		.252	.277
	n	36	36	36
Sural SA	Pearson Correlation	.196	1	.192
	Sig. (2-tailed)	.252		.263
	n	36	36	36
Sural LA	Pearson Correlation	.186	.192	1
	Sig. (2-tailed)	.277	.263	
	n	36	36	36

Discussion

In the last decade, several studies considered major peripheral nerves by SWE. Kantraci et al. [25] studied the median nerve SWE proximal to the carpal tunnel and revealed a mean stiffness of 32 kPa. Paluch et al. studied the ulnar nerve at different levels of the arm and forearm, with mean stiffness of 33 kPa [range 19-52].[26,27] He et al.[28] studied the median nerve at the forearm with a mean stiffness of 35 kPa, as well as the tibial nerve, which showed a mean stiffness value of 36.5 kPa. These values are comparable to the mean stiffness of the SN in our study [SA=24.5 kPa, LA=25.2 kPa], especially when we consider the small size of the SN. Several obstacles were reported when scanning the peripheral nerves with SWE. For example, nerve stiffness can vary substantially with different limb positions and different magnitudes in the upper or lower limb.[29] Another important factor is the position of the nerve and proximity to the bone, with the possibility of repetitive compression.[30] Some authors reported the importance of probe orientation, whether it is only in SA or both long and short axes. In the study done by Aslan et al.,[31] the elastography values were higher when taken on LA than on SA. No difference in the stiffness values between long and short axes was noted in our study. We believe that we cannot generalize this fact and apply it to other nerves that are in close proximity to bone, like the radial nerve in the spiral groove or the common fibular nerve in relation to the fibular neck. In these sites, we expect higher values on LA views. Limitations of this study include the following: First, small sample size limits generalization of our results; second, the female gender dominated and the age range was narrow; third, the SN was scanned at a single location; fourth, the study included healthy subjects. Further larger caliber studies, including variable pathologies of the SN, including mononeuropathy and polyneuropathies, are encouraged.

In conclusion, we believe that SWE could play a complementary role in future evaluation of SN pathologies.

Acknowledgments

The authors would like to express their sincere gratitude to the Deanship of Scientific Research at Prince Sattam Bin Abdulaziz University, Al-Kharj, Saudi Arabia.

Competing Interests

The authors declare that they have no competing interests.

References

1. Choi H, Chung SY, Kang S, Son SH, Yoon JS. Could Ultrasound-Guided Stimulation of Sural Nerve Affect Nerve

***Corresponding Author:** Dr. Mohamed A. Bedewi, MD, PhD. Associate Professor of Radiology. College of medicine; Prince Sattam bin Abdulaziz University. Al-Kharj; Saudi Arabia. E-mail: mohamedbedewi@yahoo.com*

Conduction Study? Ann Rehabil Med. 2019 Feb;43(1):74-80. doi: 10.5535/arm.2019.43.1.74.
2. Bianchi S, Droz L, Lups Deplaine C, Dubois-Ferriere V, Delmi M. Ultrasonography of the Sural Nerve: Normal and Pathologic Appearances. J Ultrasound Med. 2018 May;37(5):1257-1265. doi: 10.1002/jum.14444.
3. Belsack D, Jager T, Scafoglieri A, Vanderdood K, Van Hedent E, Vanhoenacker F, Marcelis S, De Maeseneer M. Ultrasound of the sural nerve: normal anatomy on cadaveric dissection and case series. Eur J Radiol. 2013 Nov;82(11):1953-8. doi: 10.1016/j.ejrad.2013.05.014.
4. Garagozlo C, Kadri O, Atalla M, Polanco F, Massaband A, Coey J, Sulaiman S. The anatomical relationship between the sural nerve and small saphenous vein: An ultrasound study of healthy participants. Clin Anat. 2019 Mar;32(2):277-281. doi: 10.1002/ca.23302.
5. Kerasnoudis A, Ntasiou P, Barmpalios G. Prognostic value of nerve ultrasound and electrophysiological findings in traumatic sural neuropathy. J Electromyogr Kinesiol. 2018 Oct;42:20-23. doi: 10.1016/j.jelekin.2018.06.004.
6. Kim Y, Kim DH, Kim NH, Kim BH, Park BK. Dorsal sural neuropathy: electrophysiological, ultrasonographic, and magnetic resonance imaging findings. Muscle Nerve. 2012 Oct;46(4):597-600. doi: 10.1002/mus.23428.
7. Pazzaglia C, Minciotti I, Coraci D, Briani C, Padua L. Ultrasound assessment of sural nerve in Charcot-Marie-Tooth 1A neuropathy. Clin Neurophysiol. 2013 Aug;124(8):1695-9. doi: 10.1016/j.clinph.2013.02.020.
8. Coraci D, Giovannini S, Bernetti A, Cordenonssi JT, Erra C, Piccinini G, Padua L. Nerve ultrasound to prevent and treat iatrogenic sural nerve injury. J Electromyogr Kinesiol. 2019 Feb;44:173-174. doi: 10.1016/j.jelekin.2018.08.007.
9. Chang HP, Wu CH, Özçakar L. Ultrasonographic Imaging for Sural Nerve Injury after Achilles Tendon Repair. Med Ultrason. 2018 May 2;20(2):254-255. doi: 10.11152/mu-1436.
10. Kim KH, Yoo JY, You BC. Ultrasonographic evaluation of sural nerve for nerve conduction study. Ann Rehabil Med. 2014 Feb;38(1):46-51. doi: 10.5535/arm.2014.38.1.46.
11. Üçeyler N, Schäfer KA, Mackenrodt D, Sommer C, Müllges W. High-Resolution Ultrasonography of the Superficial Peroneal Motor and Sural Sensory Nerves May Be a Non-invasive Approach to the Diagnosis of Vasculitic Neuropathy. Front Neurol. 2016 Mar 30;7:48. doi: 10.3389/fneur.2016.00048.
12. Sommer C. Nerve and skin biopsy in neuropathies. Curr Opin Neurol. 2018 Oct;31(5):534-540. doi: 10.1097/WCO.0000000000000601.
13. Prada V, Massucco S, Venturi C, Geroldi A, Bellone E, Mandich P, et al. Diagnostic Value of Sural Nerve Biopsy: Retrospective Analysis of Clinical Cases From 1981 to 2017. Front Neurol. 2019 Nov 22;10:1218. doi: 10.3389/fneur.2019.01218.
14. Sigrist RMS, Liau J, Kaffas AE, Chammas MC, Willmann JK. Ultrasound Elastography: Review of Techniques and Clinical Applications. Theranostics. 2017 Mar 7;7(5):1303-1329. doi: 10.7150/thno.18650.
15. Winn N, Lalam R, Cassar-Pullicino V. Sonoelastography in the musculoskeletal system: Current role and future directions. World J Radiol. 2016 Nov 28;8(11):868-879. doi: 10.4329/wjr.v8.i11.868. P
16. Garra BS. Elastography: history, principles, and technique comparison. Abdom Imaging. 2015 Apr;40(4):680-97. doi: 10.1007/s00261-014-0305-8.
17. Shiina T, Nightingale KR, Palmeri ML, Hall TJ, Bamber JC, Barr RG, et al. WFUMB guidelines and recommendations for clinical use of ultrasound elastography: Part 1: basic principles and terminology. Ultrasound Med Biol. 2015 May;41(5):1126-47. doi: 10.1016/j.ultrasmedbio.2015.03.009.
18. Doyley MM, Parker KJ. Elastography: general principles and clincial applications. Ultrasound Clin. 2014 Jan;9(1):1-11. doi: 10.1016/j.cult.2013.09.006.
19. Wee TC, Simon NG. Ultrasound elastography for the evaluation of peripheral nerves: A systematic review. Muscle Nerve. 2019 Nov;60(5):501-512. doi: 10.1002/mus.26624.
20. Davis LC, Baumer TG, Bey MJ, Holsbeeck MV. Clinical utilization of shear wave elastography in the musculoskeletal system. Ultrasonography. 2019 Jan;38(1):2-12. doi: 10.14366/usg.18039.
21. Klauser AS, Miyamoto H, Bellmann-Weiler R, Feuchtner GM, Wick MC, Jaschke WR. Sonoelastography: musculoskeletal applications. Radiology. 2014 Sep;272(3):622-33. doi: 10.1148/radiol.14121765.
22. Taljanovic MS, Gimber LH, Becker GW, Latt LD, Klauser AS, Melville DM, Gao L, Witte RS. Shear-Wave Elastography: Basic Physics and Musculoskeletal Applications. Radiographics. 2017 May-Jun;37(3):855-870. doi: 10.1148/rg.2017160116.
23. Ryu J, Jeong WK. Current status of musculoskeletal application of shear wave elastography. Ultrasonography. 2017 Jul;36(3):185-197. doi: 10.14366/usg.16053.
24. Paluch Ł, Nawrocka-Laskus E, Wieczorek J, Mruk B, Frel M, Walecki J. Use of Ultrasound Elastography in the Assessment of the Musculoskeletal System. Pol J Radiol. 2016 May 20;81:240-6. doi: 10.12659/PJR.896099.
25. Kantarci F, Ustabasioglu FE, Delil S, Olgun DC, Korkmazer B, Dikici AS, Tutar O, Nalbantoglu M, Uzun N, Mihmanli I. Median nerve stiffness measurement by shear wave elastography: a potential sonographic method in the diagnosis of carpal tunnel syndrome. Eur Radiol. 2014 Feb;24(2):434-40. doi: 10.1007/s00330-013-3023-7.
26. Paluch Ł, Noszczyk B, Nitek Ż, Walecki J, Osiak K, Pietruski P. Shear-wave elastography: a new potential method to diagnose ulnar neuropathy at the elbow. Eur Radiol. 2018 Dec;28(12):4932-4939. doi: 10.1007/s00330-018-5517-9.
27. Paluch Ł, Noszczyk BH, Walecki J, Osiak K, Kiciński M, Pietruski P. Shear-wave elastography in the diagnosis of ulnar tunnel syndrome. J Plast Reconstr Aesthet Surg. 2018 Nov;71(11):1593-1599. doi: 10.1016/j.bjps.2018.08.018.
28. He Y, Xiang X, Zhu BH, Qiu L. Shear wave elastography evaluation of the median and tibial nerve in diabetic peripheral neuropathy. Quant Imaging Med Surg. 2019 Feb;9(2):273-282. doi: 10.21037/qims.2019.02.05.
29. Simon NG, Walker S. The role of limb position in the interpretation of nerve conduction studies. Muscle Nerve. 2017 Sep;56(3):353-354. doi: 10.1002/mus.25657.
30. Bortolotto C, Turpini E, Felisaz P, Fresilli D, Fiorina I, Raciti MV, Belloni E, Bottinelli O, Cantisani V, Calliada F. Median nerve evaluation by shear wave elastosonography: impact of "bone-proximity" hardening artifacts and inter-observer agreement. J Ultrasound. 2017 Nov 17;20(4):293-299. doi: 10.1007/s40477-017-0267-0.
31. Aslan M, Aslan A, Emeksiz HC, Candan F, Erdemli S, Tombul T, et al. Assessment of Peripheral Nerves With Shear Wave Elastography in Type 1 Diabetic Adolescents Without Diabetic Peripheral Neuropathy. J Ultrasound Med. 2019 Jun;38(6):1583-1596. doi: 10.1002/jum.14848.

International Journal of Biomedicine 12(1) (2022) 38-42
http://dx.doi.org/10.21103/Article12(1)_OA4

ORIGINAL ARTICLE

Obstetrics and Gynecology

INTERNATIONAL JOURNAL OF BIOMEDICINE

Cardiac Phenotypes of Pregnant Women with Hypertensive Disorders in Different Ethnic Groups

Bakhtykei M. Gasanova[1], PhD; Victor E. Radzinsky[1], PhD, ScD; Miroslava L. Polina, PhD[2]; Natalya I. Douglas, PhD, ScD[3]; Tatiana E. Burtseva, PhD, ScD[3]; Praskovya N. Zakharova[3]; Tatyana V. Dedy, PhD[4]

[1]*Peoples' Friendship University of Russia (RUDN University), Moscow, Russia*
[2]*Women's Health Medical Center, Moscow, Russia*
[3]*M. K. Ammosov North-Eastern Federal University, Yakutsk, Yakutia*
[4]*Federal Medical-Biological Agency, Moscow, Russia*

Abstract

The objective of this study was to conduct a comparative analysis of the features of LV myocardial remodeling in pregnant women with chronic arterial hypertension (CAH) and preeclampsia (PE) on the background of CAH.

Methods and Results: The study cohort included pregnant women (n=547) with hypertensive disorders. All women were divided into two groups: Group 1 included 376 Caucasian patients living in the Republic of Dagestan; Group 2 included 171 patients living in the Republic of Sakha (Yakutia) (indigenous residents [Yakuts and Evenks). Later on, all patients were divided into the following subgroups: Sub1A (n=134), and Sub2A (n=69) – pregnant women with CAH; Sub1B (n=242) and Sub2B (n=102) – pregnant women with PE on the background of CAH. The diagnosis of pregnant women with CAH was made on the basis of existing national and foreign recommendations that an increase in SBP ≥140 mmHg and/or DBP ≥90 mmHg indicates CAH. Different patterns of left ventricular (LV) geometry were defined based on left ventricular mass index (LVMI) and relative wall thickness (RWT), as recommended by the American Society of Echocardiography. The observed/predicted LVM ratio was calculated as 100×(oLVM/pLVM). Participants with an oLVM/pLVM ratio of >128% were categorized as having "inappropriate" LVM (iLVM).

iLVM was found in Subgroups 1B and 2B in the third trimester. The frequency of LV remodeling in pregnant women of Subgroups 1 A and 2A in the second and third trimesters did not differ significantly. In Subgroup 1B, the frequency of concentric left ventricular hypertrophy (cLVH) was higher in the third trimester (42.6%) than in the second trimester (26.9%) (P=0.000). Moreover, in the third trimester, the frequency of cLVH was significantly higher in Subgroup 1B than in Subgroup 2B (42.6% and 29.4%, respectively, P=0.022). At the same time, in the third trimester, the frequency of left ventricular concentric remodeling (LVCR) was significantly higher in Subgroup 2B than in Subgroup 1B (56.9% and 44.2%, respectively, P=0.032). In the second trimester in Subgroup 1B, the frequency of LVCR was higher than in Subgroup 1A (50% and 38.1%, respectively, P=0.026). By the third trimester, the severity of LV remodeling has increased significantly in Subgroup 1B. Thus, in Subgroup 1B, the frequency of c LVH reached 42.6% compared to 31.3% in Subgroup 1A (P=0.03). In Subgroup 2B, in the third trimester, the frequency of LVCR was slightly higher than in Subgroup 2A (56.9% and 43.5%. respectively, P=0.08).

Conclusion: Living conditions predetermine the prevalence of iLVM and LVCR in pregnant northerners with CAH. A more common type of LV remodeling in pregnant women with CAH in conditions of high-altitude hypoxia is also LVCR, which transforms into cLVH by the third trimester in pregnant women with PE on the background of CAH. The study of the type of LV geometry and the appropriateness of LVM allows us to clarify the degree of LV damage in hypertension-related pregnancy. iLVM in pregnant women with CAH appears to be a predictor of the development of PE. The revealed changes in the LV structure—LVCR and cLVH—are more significant in PE on the background of CAH. (**International Journal of Biomedicine. 2022;12(1):38-42.**)

Key Words*:* chronic arterial hypertension • preeclampsia • left ventricular remodeling • inappropriate left ventricular mass

For citation: Gasanova BM, Radzinsky VE, Polina ML, Douglas NI, Burtseva TE, Zakharova PN, Dedy TV. Cardiac Phenotypes of Pregnant Women with Hypertensive Disorders in Different Ethnic Groups. International Journal of Biomedicine. 2022;12(1):38-42. doi:10.21103/Article12(1)_OA4

Abbreviations

BMI, body mass index; **CAH**, chronic arterial hypertension; **DBP**, diastolic BP; **EF**, ejection fraction; **IVST**, interventricular septal thickness; **LVPWT**, left ventricular posterior wall thickness; **LVM**, left ventricular mass; **LVMI**, left ventricular mass index; **LVH**, left ventricular hypertrophy; **LVEDV**, left ventricular end-diastolic volume; **LVESV,** left ventricular end-systolic volume; **LVEDD**, left ventricular end-diastolic dimension; **LVESD**, left ventricular end-systolic dimension; **LVCR**, left ventricular concentric remodeling; **cLVH**, concentric left ventricular hypertrophy; **eLVH**, eccentric left ventricular hypertrophy; **iLVM**, inappropriate LVM; **PE**, preeclampsia; **RWT**, relative wall thickness; **SBP**, systolic BP; **SV**, stroke volume.

Introduction

Hypertensive conditions complicate up to 10% of pregnancies worldwide and are a leading cause of maternal, fetal, and neonatal morbidity and mortality.[1] The frequency of adverse outcomes in these women has doubled over the past 10–20 years.[2,3] There is evidence of the relationship between chronic arterial hypertension (CAH), which existed before pregnancy, and the risk of developing severe hypertension and preeclampsia.[4]

Chronic arterial hypertension (CAH), defined by clinical practice guidelines as SBP (≥140 mmHg) and or DBP ((≥90 mmHg) before pregnancy or up to 20 weeks, complicates or use of antihypertensive medication before pregnancy. Preeclampsia (PE), a pregnancy-specific disorder characterized by hypertension (≥140/90 mmHg) and proteinuria (≥300 mg in 24-hour urine), occurs de novo or may be superimposed on CAH.

Human health can be affected by various factors, including environmental, social, climatic, demographic, and economic factors.[5,6] The Republic of Dagestan, one of the largest republics of the North Caucasus, is located on the northeastern slope of the Great Caucasus Range and in the southwest of the Caspian Lowland. In the structure of general morbidity and mortality of the population, the pathology of the cardiovascular system occupies the leading place.[7] Most Dagestan people are residents of the mountainous and high-mountainous parts. It creates an unsolvable problem of ensuring the population's access to medical care, increasing complications of pregnancy and childbirth.[9] The Republic of Sakha (Yakutia) occupies one-fifth of Russia. Yakutia is one of the coldest regions in the world. Extreme climatic factors of Yakutia have a depleting effect on the functional reserves of the human body. The tension of the adaptive mechanisms often manifests itself in the form of an increase in blood pressure.[9,10]

Cardiac remodeling during pregnancy is considered a physiological adaptation to an increased volumetric load and increased body needs.[11]

Hypertrophy is understood as an increase in heart mass above normal value with an increase in hemodynamic load: afterload (pressure load), or preload (volume load), or both at the same time.

Left ventricular hypertrophy (LVH) is defined as increased left ventricular mass in response to volume overload and/or pressure overload.[12] Pressure overload typically leads to concentric LVH, volume overload (anemia and hypervolemic states) – to eccentric LVH. According to the concept of "hypertensive" LV remodeling, concentric hypertrophy in CAH is regarded as an adaptive response to normalize tension in the heart wall.[13] There is also a possibility of developing eccentric LVH.[14]

The impact of LV remodeling patterns, especially concentric LVH, on the risk of developing PE has not been definitively resolved. It is necessary to study the predictive value of cardiac "phenotypes" of pregnant women with CAH, considering ethnic characteristics to individualize treatment and reduce the risk of developing severe forms of the disease.

The objective of this study was to conduct a comparative analysis of the features of LV myocardial remodeling in pregnant women with CAH and PE on the background of CAH.

Materials and Methods

The study cohort included pregnant women (n=547) with hypertensive disorders. All women were divided into two groups: Group 1 included 376 Caucasian patients living in the Republic of Dagestan; Group 2 included 171 patients living in the Republic of Sakha (Yakutia) (indigenous residents [Yakuts and Evenks]).

Later on, all patients were divided into the following subgroups: Sub1A (n=134), and Sub2A (n=69) – pregnant women with CAH; Sub1B (n=242) and Sub2B (n=102) – pregnant women with PE on the background of CAD. Control group 1 (CG1) consisted of healthy pregnant women (n=34) living in the Republic of Dagestan. Control group 2 (CG2) consisted of healthy pregnant women (n=40) living in the Republic of Dagestan.

Inclusion criteria: single-child progressing pregnancy, the presence of CAH confirmed before pregnancy, the woman's informed consent for participation in research.

The diagnosis of pregnant women with CAH was made based on existing national and foreign recommendations that an increase in SBP ≥140 mmHg and/or DBP ≥90 mmHg indicates CAH. The program of a patient's examination included a survey on a special questionnaire, anthropometric examination using a standard technique, office blood pressure (BP) measurement, echocardiography.

BMI was calculated as weight in kilograms divided by squared height in meters (kg/m^2). A BMI of less than 18.5 kg/m^2 is considered underweight; normal weight – a BMI of 18.5 kg/m^2 to 24.9 kg/m^2; overweight – a BMI of 25 kg/m^2 to 29.9 kg/m^2; obesity – BMI of≥30 kg/m^2.

Office BP was measured using a mercury sphygmomanometer, according to Korotkov's method. BP was measured three times, and the means of these measurements were used in the analyses.

Echocardiography was carried out according to the recommendations of the American Society of Echocardiography[15] in M- and B-modes. The following

parameters were measured and calculated: IVST, LVPWT, LVEDD, LVESD, EF, LVEDV, LVESV, SV, EF. LVM was calculated using the formula of R. Devereux and Reichek.[16] LVMI was calculated as LVM indexed to height$^{2.7}$, and LVH was defined as LVMI ≥ 45 g/m$^{2.7}$ [17] RWT was calculated as 2 times PWT divided by the LV diastolic diameter. Normal RWT was defined as RWT ≤0.42, and increased RWT was defined as RWT>0.42.[17] Patterns of the left ventricular structure were defined as follows: normal (normal LVMI and RWT≤0.42); concentric remodeling (normal LVMI and RWT>0.42); eccentric hypertrophy (LVH and RWT≤0.42); and concentric hypertrophy (LVH and RWT>0.42).[17]

Predicted LVM was calculated using the following formula: pLVM=55.37+[(6.64×height(m$^{2.7}$)+(0.64×SW (g-m/beat)]–(18.07×gender), where SW (stroke work) in gram-meters/beat [g-m/beat]) was computed as follows: cuff SBP×stroke volume×0.0144; female gender coefficient = 2.[18]

The observed/predicted LVM ratio was calculated as 100×(oLVM/pLVM). Participants with an oLVM/pLVM ratio of >128% were categorized as having "inappropriate" LVM (iLVM).[19]

*S*tatistical analysis was performed using the statistical software package SPSS version 19.0 (Armonk, NY: IBM Corp.). The normality of the distribution of continuous variables was tested by the one-sample Kolmogorov-Smirnov test. Baseline characteristics were summarized as frequencies and percentages for categorical variables and as mean (M) and standard error of the mean (SEM) for continuous variables. The Student unpaired t-test was used to compare average values for data with normal distribution. Mann-Whitney U test was used to compare means of 2 groups of variables not normally distributed. Group comparisons with respect to categorical variables are performed using chi-square test. A probability value of $P \leq 0.05$ was considered statistically significant.

Results and Discussion

The average age of pregnant women in Croups 1 and 2 did not differ – 33.4±4.6 years and 34.6±5.2 years, respectively (Table 1). The BMI of pregnant women in Group 2 was slightly higher than in Group 1. The average height of pregnant women in Group 2 was slightly lower than in Group 1. The number of pregnant women with BMI > 30 kg/m^2 in Groups 1 and 2 did not differ, as well as the number of births.

Table 1.

Main characteristics of pregnant women with CAH

Variable	Group 1 (n=376)	Group 2 (n=171)	*P*-value
Age, yrs	34.6±5.2	33.4±4.6	0.85
BMI, kg/m^2	25.1±6.1	26.7±4.8	0.84
Height, cm	165.4±5.8	156.68±6.2	0.27
Parity (number of births)	2.4±1.1	2.2±1.2	0.86
BMI >30 kg/m^2	27(7.2%)	14 (8.2%)	0.68

The oLVM/pLVM values in pregnant women of Group 1 are presented in Table 2. In the second and third trimesters, in Subgroup 1B, the oLVM/pLVM ratio was significantly higher than in Control group 1 and Subgroup 1A (P<0.05). iLVM was found in Subgroup 1B in the third trimester.

Table 2.

oLVM/pLVM ratio (%) in pregnant women of Group 1 according to stages of pregnancy

Trimester	Subgroup 1A (n=134) [1]	Subgroup 1B (n=242) [2]	CG1 (n=34)[3]	Statistics
2nd trimester	114.8±2.6	124.8±4.3	100.4±4.5	P_{1-2}=0.047 P_{1-3}=0.006 P_{2-3}=0.00
3rd trimester	118.7±4.3	130.5±3.8	107.3±3.6	P_{1-2}=0.04 P_{1-3}=0.04 P_{2-3}=0.00

The oLVM/pLVM values in pregnant women of Group 2 are presented in Table 3. In the second trimester and the third trimester, in Subgroup 2B, the oLVM/pLVM ratio was significantly higher than in Control group 2 and Subgroup 2A (P<0.05). iLVM was found in Subgroup 2B in the third trimester.

Table 3.

oLVM/pLVM ratio (%) in pregnant women of Group 2 according to stages of pregnancy

Trimester	Subgroup 2A (n=69) [1]	Subgroup 2B (n=102) [2]	CG2 (n=40) [3]	Statistics
2nd trimester	116.2±2.2	126.7±4.6	107.3±3.8	P_{1-2}=0.02 P_{1-3}=0.04 P_{2-3}=0.001
3rd trimester	122.7±2.2	135.3±4.2	110.4±3.8	P_{1-2}=0.00 P_{1-3}=0.006 P_{2-3}=0.00

In the meta-analysis performed by De Haas et al.,[20] forty-eight studies were included, with publication dates ranging from 1977 to 2016. The authors found that during normotensive pregnancy, most cardiac geometric indices change from the second trimester onwards (LVM and RWT increase by 20% and 10%, respectively, that consistent with concentric rather than eccentric remodeling). A more remarkable change in LVM (95% increase from reference) and RWT (56% increase from reference data) occurs during hypertensive pregnancy.

The introduction of the oLVM/pLVM ratio, which allows us to differentiate the risk group for severe hypertension and PE with an indicator ">128%," showing the presence of iLVM, regardless of the LVH type, seems optimal when examining women with CAH. Patterns of the left ventricular structure in pregnant women with hypertensive disorders in various ethnic populations are presented in Table 4.

The frequency of LV remodeling in pregnant women of Subgroups 1 A and 2A in the second and third trimesters did

not differ significantly. In Subgroup 1B, the frequency of cLVH was higher in the third trimester (42.6%) than in the second trimester (26.9%) (*P*=0.000). Moreover, in the third trimester, the frequency of cLVH was significantly higher in Subgroup 1B than in Subgroup 2B (42.6% and 29.4%, respectively, *P*=0.022). At the same time, in the third trimester, the frequency of LVCR was significantly higher in Subgroup 2B than in Subgroup 1B (56.9% and 44.2%, respectively, *P*=0.032). It is important to note that in the second trimester in Subgroup 1B, the frequency of LVCR was higher than in Subgroup 1A: 50% and 38.1%, respectively, *P*=0.026). By the third trimester, the severity of LV remodeling has increased significantly in Subgroup 1B. Thus, in Subgroup 1B, the frequency of c LVH reached 42.6% compared to 31.3% in Subgroup 1A (*P*=0.03). In Subgroup 2B, in the third trimester, the frequency of LVCR was slightly higher than in Subgroup 2A (56.9% and 43.5%, respectively, *P*=0.08).

Table 4.

Patterns of the left ventricular structure in pregnant women with hypertensive disorders in various ethnic groups

Group		n	2nd trimester				3rd trimester			
			Normal geometry	CRLV	eLVH	cLVH	Normal geometry	CRLV	eLVH	cLVH
Subgroup 2A	abs	69	13	31	5	20	13	30	0	26
	%		18.8	44.9	7.2	29.0	18.8	43.5	0.0	37.7
Subgroup 1A	abs	134	33	51	9	41	23	62	7	42
	%		24.6	38.1	6.7	30.6	17.2	46.3	5.2	31.3
P-value			NS	NS	NS	NS	NS	NS	NS	NS
Subgroup 2B	abs	102	20	49	0	33	14	58	0	30
	%		19.6	48.0	0.0	32.4	13.7	56.9	0.0	29.4
Subgroup 1B	abs	242	56	121	0	65	32	107	0	103
	%		23.1	50.0	0.0	26.9	13.2	44.2	0.0	42.6
P-value			NS	NS	-	NS	NS	0.032	-	0.022
CG2	abs	40	31	4	5	0	26	0	14	0
	%		77.5	10.0	12.5	0.0	65.0	0.0	35.0	0.0
CG1	abs	34	28	0	6	0	26	0	8	0
	%		82.4	0.0	17.6	0.0	76.5	0.0	23.5	0.0

It should be noted that the incidence of cLVH in both ethnic samples was higher than that of other authors in foreign sources.[14] probably due to late seeking medical care and delayed hypertensive therapy. This fact is probably due to the high frequency of delayed hypotensive therapy in our samples.

Variants of LV geometric types in Control groups 1 and 2 did not practically differ. Conclusions about the adverse effect of abnormal LV geometry on the prognosis of arterial hypertension and hypertension-related pregnancy prevail in cLVH.[21-24]

According to Mureddu et al.,[25] iLVM is associated with concentric geometry, high peripheral resistance, and depressed wall mechanics. Several studies have shown that the deviation of LVM from the value appropriate for stroke work, body size, and sex correlates with measures of myocardial function better than LVM.[25-29] iLVM in the indigenous women of the Yakutia population indicated a better informative value of this parameter than the type of LV geometry in assessing the nature of adaptation of the heart muscle to stress. These differences might be related to the anthropometric measurement between the Caucasian and Mongoloid populations.[30,31]

The indigenous women of Yakutia are characterized by typical features inherent in the northern adaptive type – a short body length with a relatively high body density, a stocky physique with well-developed musculoskeletal mass, increased waist and hip circumference.[5] Such characteristics represent the result of adaptation to the harsh climatic and geographical conditions of living in the North.[32] These living conditions predetermine the prevalence of iLVM and LVCR in pregnant northerners with CAH.

The peculiarities in LV remodeling of pregnant women living in different regions of the Republic of Dagestan consist in adaptation to hypoxia conditions of women living in the mountainous areas.[33] A more common type of LV remodeling in pregnant women with CAH in conditions of high-altitude hypoxia is also LVCR, which transforms into cLVH by the third trimester in pregnant women with PE on the background of CAH.

Conclusion

The study of the type of LV geometry and the appropriateness of LVM allows us to clarify the degree of LV damage in hypertension-related pregnancy. iLVM in pregnant women with CAH appears to be a predictor of the development of PE. The revealed changes in the LV structure—LVCR and cLVH—are more significant in PE on the background of CAH.

Competing Interests

The authors declare that they have no competing interests.

References

1. Pinheiro TV, Brunetto S, Ramos JG, Bernardi JR, Goldani MZ. Hypertensive disorders during pregnancy and health outcomes in the offspring: a systematic review. J Dev Orig Health Dis. 2016;7(4):391-407. doi: 10.1017/S2040174416000209.
2. Panova IA, Malyshkina AI, Rokotyanskaya EA, Smirnova EV. [Risk factors for the addition of preeclampsia in women with chronic arterial hypertension]. Russian Bulletin of Obstetrician-Gynecologist. 2014;(6):37-42. [Article in Russian]
3. Ananth CV, Peltier MR, Kinzler WL, Smulian JC, Vintzileos AM. Chronic hypertension and risk of placental abruption: is the association modified by ischemic placental disease? Am J Obstet Gynecol. 2007 Sep;197(3):273.e1-7. doi: 10.1016/j.ajog.2007.05.047.
4. Nzelu D, Dumitrascu-Biris D, Nicolaides KH, Kametas NA. Chronic hypertension: first-trimester blood pressure control and likelihood of severe hypertension, preeclampsia, and small for gestational age. Am J Obstet Gynecol. 2018;218(3):337.e1-337.e7. doi: 10.1016/j.ajog.2017.12.235.
5. Alekseeva TI. Human adaptation in various ecological niches of the Earth (biological aspects): lecture course.

Moscow: Publishing House of MNEPU; 1998. [in Russian]
6. Nikolaev VG, Medvedev NN, Nikolenko VN, Petrova MM, Sindeeva LV, Nikolaev NN, et al. Essays on integrative anthropology: monograph. Krasnoyarsk: KrasGMU; 2015. [in Russian]
7. Gasangadzhieva AG, Gabibova PI, Daudova MG, Galkina IV, Giraev KM, Magomedova ZYa. [Medical-Environmental Assessment and Forecasting of Socially Significant Pathology of the Population of the Republic of Dagestan]. South of Russia: ecology, development. 2019;14(4):147-164. [Article in Russian]
8. Gabibova PI. Monitoring the health of the population of the Republic of Dagestan. Topical issues of modern science. 2013;7-15. [in Russian]
9. Petrova PG. Ecological-physiological aspects of human adaptation to the conditions of the North. Yakutsk: Dani AlmaS; 2011. [in Russian]
10. Sofronova SI, Klimova TM, Kirillina MP, Nikolaev VM, Kononova IV, Kuzmina AA, Romanova AN. Association of the AGTR1 Gene A1166C (rs5186) Polymorphism with Essential Hypertension in the Indigenous Population of the Arctic. International Journal of Biomedicine. 2021;11(3):361-366. doi:10.21103/Article11(3)_OA14
11. Papadopoulou E, Kaladaridou A, Agrios J, Matthaiou J, Pamboukas C, Toumanidis S. Factors influencing the twisting and untwisting properties of the left ventricle during normal pregnancy. Echocardiography. 2014;31:155–163.
12. Cuspidi C, Sala C, Negri F, Mancia G, Morganti A., Italian Society of Hypertension. Prevalence of left-ventricular hypertrophy in hypertension: an updated review of echocardiographic studies. J Hum Hypertens. 2012 Jun;26(6):343-9.
13. Nadruz W. Myocardial remodeling in hypertension. J Hum Hypertens. 2015;29(1):1-6. doi: 10.1038/jhh.2014.36.
14. Ambia AM, Morgan JL, Wells CE, Roberts SW, Sanghavi M, Nelson DB, Cunningham FG. Perinatal outcomes associated with abnormal cardiac remodeling in women with treated chronic hypertension. Am J Obstet Gynecol. 2018;218(5):519.e1-519.e7. doi: 10.1016/j.ajog.2018.02.015.
15. Voigt JU, Pedrizzetti G, Lysyansky P, Marwick TH, Houle H, Baumann R, et al. Definitions for a common standard for 2D speckle tracking echocardiography: consensus document of the EACVI/ASE/Industry Task Force to standardize deformation imaging. Eur Heart J Cardiovasc Imaging. 2015;16(1):1-11. doi: 10.1093/ehjci/jeu184.
16. Devereux RB, Reichek N. Echocardiographic determination of left ventricular mass in man. Anatomic validation of the method. Circulation. 1977 Apr;55(4):613-8. doi: 10.1161/01.cir.55.4.613.
17. Lang RM, Badano LP, Mor-Avi V, Afilalo J, Armstrong A, Ernande L, et al. Recommendations for cardiac chamber quantification by echocardiography in adults: an update from the American Society of Echocardiography and the European Association of Cardiovascular Imaging. Eur Heart J Cardiovasc Imaging. 2015 Mar;16(3):233-70. doi: 10.1093/ehjci/jev014. Erratum in: Eur Heart J Cardiovasc Imaging. 2016 Apr;17(4):412.
18. de Simone G, Devereux RB, Kimball TR, Mureddu GF, Roman MJ, Contaldo F, Daniels SR. Interaction between body size and cardiac workload: influence on left ventricular mass during body growth and adulthood. Hypertension. 1998 May;31(5):1077-82. doi: 10.1161/01.hyp.31.5.1077.
19. de Simone G, Verdecchia P, Pede S, Gorini M, Maggioni AP. Prognosis of inappropriate left ventricular mass in hypertension: the MAVI Study. Hypertension. 2002 Oct;40(4):470-6. doi: 10.1161/01.hyp.0000034740.99323.8a.
20. De Haas S, Ghossein-Doha C, Geerts L, van Kuijk SMJ, van Drongelen J, Spaanderman MEA. Cardiac remodeling in normotensive pregnancy and in pregnancy complicated by hypertension: systematic review and meta-analysis. Ultrasound Obstet Gynecol. 2017;50(6):683-696.
21. Paoletti E, De Nicola L, Gabbai FB, Chiodini P, Ravera M, Pieracci L, et al. Associations of Left Ventricular Hypertrophy and Geometry with Adverse Outcomes in Patients with CKD and Hypertension. Clin J Am Soc Nephrol. 2016;5;11(2):271-9.
22. Gerdts E, Cramariuc D, de Simone G, Wachtell K, Dahlöf B, Devereux RB: Impact of left ventricular geometry on prognosis in hypertensive patients with left ventricular hypertrophy (the LIFE study). Eur J Echocardiogr. 2008; 9: 809–815. doi: 10.1093/ejechocard/jen155.
23. Lieb W, Gona P, Larson MG, Aragam J, Zile MR, Cheng S, Benjamin EJ, Vasan RS: The natural history of left ventricular geometry in the community: Clinical correlates and prognostic significance of change in LV geometric pattern. JACC Cardiovasc Imaging 2014;7:870–878.
24. Kim MJ, Seo J, Cho KI, Yoon SJ, Choi JH, Shin MS. Echocardiographic Assessment of Structural and Hemodynamic Changes in Hypertension-Related Pregnancy. J Cardiovasc Ultrasound. 2016 Mar;24(1):28-34.
25. Mureddu GF, Pasanisi F, Palmieri V, Celentano A, Contaldo F, de Simone G. Appropriate or inappropriate left ventricular mass in the presence or absence of prognostically adverse left ventricular hypertrophy. J Hypertens. 2001 Jun;19(6):1113-9.
26. Anstey DE, Tanner RM, Booth JN 3rd, Bress AP, Diaz KM, Sims M, et al. Inappropriate Left Ventricular Mass and Cardiovascular Disease Events and Mortality in Blacks: The Jackson Heart Study. J Am Heart Assoc. 2019 Aug 20;8(16):e011897. doi: 10.1161/JAHA.118.011897.
27. Devereux RB, Lutas EM, Casale PN, Kligfield P, Eisenberg RR, Hammond IW, et al. Standardization of M-mode echocardiographic left ventricular anatomic measurements. J Am Coll Cardiol. 1984 Dec;4(6):1222-30.
28. Muiesan ML, Salvetti M, Paini A, Monteduro C, Galbassini G, Bonzi B, et al. Inappropriate left ventricular mass changes during treatment adversely affects cardiovascular prognosis in hypertensive patients. Hypertension. 2007;49:1077–1083.
29. Cioffi G, Rossi A, Zoppini G, Targher G, de Simone G, Devereux RB, et al. Inappropriate left ventricular mass independently predicts cardiovascular mortality in patients with type 2 diabetes. Int J Cardiol. 2013;168:4953–4956.
30. Yusupov RD, Nikolaev VG, Sindeeva LV, Alyamovsky VV, Kazakova GN, Anisimov MM. [Ethnic particularities of somatometric and cephalometric parameters in women of Eastern Siberia]. Fundamental'nye Issledovaniia. 2013;7-1: 207-212. [Article in Russian]
31. Koynosov PG, Chiryatyeva TV, Orlov SA, Koynosov AP. [Anatomical and anthropological features of the physical development of the inhabitants of the Middle Priobye]. Medical Science and Education of the Urals. 2016; 1:46–49. [Article in Russian]
32. Guryeva AB, Alekseyeva VA, Petrova PG. Characteristics of the anthropometric measures and biological age of girls of Yakut ethnicity depending on tanner's index. Wiad Lek. 2016;69(3 pt 2):471-474.
33. Pronina LV. [Features of Physical Development and Functional Condition of the Cardiovascular System of Girls Living in Various Regions of the Republic of Dagestan]. Izvestia of the Dagestan State Pedagogical University. Natural and exact sciences. 2017; 11 (1): 77-81. [Article in Russian].

International Journal of Biomedicine 12(1) (2022) 43-48
http://dx.doi.org/10.21103/Article12(1)_OA5

ORIGINAL ARTICLE

Obstetrics and Gynecology

INTERNATIONAL JOURNAL OF BIOMEDICINE

Predicting Fetal Weight by Ultrasonography Using Hadlock Formula 1

Mohamed Adam*

Department of Radiological Sciences, College of Applied Medical Sciences, King Khalid University, Abha, Kingdom of Saudi Arabia

Abstract

Background: Accurate fetal weight estimations by ultrasound are essential in determining the method and time of delivery. Hadlock formulas have been proposed for providing fetal weight estimations, including Hadlock 1, Hadlock 2, Hadlock 3, and Hadlock 4. Because none of the formulas have been verified, it is unknown which one can be best applied to the Saudi population. This study aims to determine the validity of the Hadlock formula 1 for EFW by using ultrasonography.

Methods and Results: The study sample was 198 women with singleton pregnancies with gestational ages between 37 and 41 weeks, admitted for ultrasound evaluation. The FW was estimated by ultrasound using the Hadlock formula 1. After the ultrasound EFW, we followed up with the pregnant women within three days (from ultrasound scan to delivery date) and measured actual BW. The study found that the mean BW was 3179±387 g, ranging from 2500 g to 4290 g. The mean ultrasound EFW was 3055±378 g, ranging from 2500 g to 4100 g. The difference between the mean ultrasound EFW and actual BW (123.81±107.95 g) was significant (P=0.0014).The formula for prediction of birth weight is BW=0.9831EFW by ultrasound±175.55g. In addition, a significantly positive correlation was found between ultrasound EFW and BW (r=0.961, P=0.000).

Conclusion: The significantly positive correlation between EFW by ultrasound and BW indicates that the Hadlock formula 1 for predicting FW is accurate, valid, and effective in the research environment.(**International Journal of Biomedicine. 2022;12(1):43-48.**)

Key Words: birth weight • Hadlock formula • estimated fetal weight • ultrasonography

For citation: Adam M. Predicting Fetal Weight by Ultrasonography Using Hadlock Formula 1. International Journal of Biomedicine. 2022;12(1):43-48. doi:10.21103/Article12(1)_OA5

Abbreviations

AC, abdominal circumference; **BW**, birth weight; **BPD**, biparietal diameter; **EFW**, estimated fetal weight; **FL**, femur length; **FW**, fetal weight; **HC**, head circumference.

Introduction

Birth weight (BW) is an important determinant of newborn survival.[1,2] Therefore, weight assessment is an essential aspect of antenatal care utilized in labor, delivery, growth monitoring, and managing high-risk pregnancies.[1] An accurate estimation of fetal weight (FW) is beneficial in late pregnancy because it helps obstetricians with providing labor management and determining the mode of delivery. Because of the possible difficulties from low and high fetal BW during labor and the puerperium, it is often necessary to accurately evaluate prenatal FW. Intrauterine growth restriction, preterm delivery or both are responsible for the increased perinatal morbidity and mortality associated with low BW. Shoulder dystocia, bone injuries, brachial plexus injury, and intrapartum hypoxia are among the potential problems of vaginal delivery for overly large fetuses. Thus, there is a significant concern for the mother's health, including her birth canal and pelvic floor.[3,4]

Leopold techniques and ultrasonography are the most common methods for predicting FW.[5,6] However, clinical EFW has been demonstrated to predict BW accurately. Baum et al.[7] found no significant difference between clinical and

***Corresponding Author:** Dr. Mohamed Adam. College of Applied Medical Sciences, King Khalid University, Abha, Aseer Region, Kingdom of Saudi Arabia. E-mail: o_maurie2006@yahoo.com*

sonographic EFW; 64% and 62.5% of the estimates were within 10% of the actual BW, respectively. In both term and postdate newborns, the clinical and ultrasound estimations of maternal EFW were the same. Clinical EFW, according to some experts, is more accurate than ultrasound EFW.[8] However, the accuracy of using several ultrasound parameters to estimate FW is receiving more attention; Shepard, Hadlock, Campbell S, and Nahum GG, among others, have developed several formulas and equations for predicting FW.[9-12] Ultrasound EFW is relatively accurate, with a 1%–5% margin of error. Although some researchers believe sonographic estimations are superior to clinical estimates, others have found that the two procedures provide equivalent levels of accuracy. This study aims to determine the validity of the Hadlock formula 1 for EFW by using ultrasonography.

Materials and Methods

This prospective, cross-sectional, nonintervention, comparative descriptive study was carried out over 36 months from June 2019 to June 2021 at the Obstetrics and Gynecology Hospital, El-mahala Aseer region, Abha.

The study sample was 198 women with singleton pregnancies with gestational ages between 37 and 41 weeks, admitted for ultrasound evaluation. The participants were randomly selected from a group of antenatal care with accurate menstrual dates. Pregnant women with medical conditions that might affect FW, multiple pregnancies or fetal chromosomal or congenital anomalies were excluded. The FW was estimated by ultrasound using the Hadlock formula 1, which was set into the ultrasound equipment by the radiology unit. After the ultrasound EFW, we followed up with the pregnant women within three days (from ultrasound scan to delivery date) and measured actual BW.

Index Tests

We approached women with singleton pregnancies and sought and received their informed consent to participate in this study. After that, the participants were initially given a routine sonographic evaluation, performed following the practice guidelines for the performance of obstetric ultrasound examinations of the American Institute of Ultrasound in Medicine (AIUM).[13] The scan was performed in a dimly lit room to minimize the screen's reflected artifact, with the participants in a supine position and a sonic coupling agent applied to their abdomen. Next, a simple sweep of the transducer was conducted up, down, and across their abdomen to get a rough sense of the uterine contents before focusing on specific areas of interest. The participants were closely observed to catch any agitation, shortness of breath or dizziness due to inferior vena cava compression by the gravid uterus. Participants who exhibited these symptoms were rolled onto their sides until these symptoms disappeared, after which they were moved back to the supine position, and the scan was completed. A based scan of gross anatomic abnormalities and maternal pelvis for masses was conducted after getting a rough sense of the fetus' position within the uterus, fetal heartbeat, placenta localization, liquor, and gestational age. After evaluating the pregnancy, the EFW was identified by measuring the femur length (FL), head circumference (HC), and abdominal circumference (AC) using internal electronic calibers. The results were presented in centimeters (cm).

Femur Length Measurement

FL was obtained from the longest longitudinal and coronal section of the femoral diaphysis. In the coronal plane, the lateral surface of the near side femur and the medial surface of the far side femur were imaged, while in a sagittal scan, the anterior or posterior surfaces of the femur were imaged depending on the direction of the sound beam with respect to the femur. In most cases, the iliac bone was used as a reference point, rotating the transducer until the longest FL was recognized. Next, the calipers were positioned, and the end-to-end length of the diaphysis was measured, excluding any ossified portion of the femoral neck, head, and distal or proximal epiphyses.

Abdominal Circumference Measurement

AC was obtained after determining the lie of the fetus and the orientation of the fetal spine's long axis. Next, the transducer was quickly rotated, and the image was frozen for AC measurement. From the true axial section of the fetus' upper abdomen at the level of the umbilical vein, left portal vein, and portal sinus confluence, the AC was measured using electronic calibers by tracing the outer edge of the fetal abdomen (skin/amniotic fluid interface).

Head Circumference Measurement

HC was measured on the same plane as biparietal diameter (BPD)—axial plane—that traverses the thalami and cavum septum pellucidum. The transducer must be perpendicular to the central axis of the head, and the hemispheres and calvaria should appear symmetric. In addition, the cerebellar hemispheres should not be in the image plane, or the probe will be too cauda and give an inaccurate size of the fetal head.

Statistical analysis was performed using the standard Statistical Package for the Social Sciences (IBM SPSS Statistics for Windows, Version 21.0. Armonk, NY: IBM Corp). Continuous variables were presented as mean±standard deviation (SD). A probability value of $P<0.05$ was considered statistically significant.

Results

A total of 198 women with singleton pregnancies aged 15 to 56 years were studied over six months. Their average age was 32.6 years; height range was 146–158 cm; weight range was 45–132 kg; BMI was 17.63–9.08 kg/cm^2, and fetal age was 37–41 weeks with a mean of 38 weeks and four days. The interval between ultrasound scanning and delivery date was 0–3 days. The study found that the mean BW was 3179±387g, ranging from 2500g to 4290g. The mean ultrasound EFW was 3055±378g, ranging from 2500g to 4100g (Table 1). The difference between the mean ultrasound EFW and actual BW (123.81±107.95g) was significant (P=0.0014) in a paired-test, with a significantly positive correlation between BW and EFW (r=0.961, *P=0.000*) (Tables 1 and 2).

The study predicts the BW depending on EFW and found that actual BW=0.9831EFW±175.55g, with strong power for prediction (R^2=0.923) (Table 3, Figure 1).

Table 1.

Mean and standard deviation, range and correlation between maternal factors and EFW, BW

Variables	n	Mean ± SD	Range	*P*-value for *r*	
				EFW by US	BW
Maternal age, yrs	198	32.63±8.609	15-56	0.013	0.026
Height, cm		159.64±7.092	146-185	0.000	0.001
Weight, kg		73.05±13.469	45-132	0.760	0.904
BMI, kg/cm^2		28.77±5.62	17.63-49.08	0.057	0.10
Fetal age, weeks		38.51±1.12	37-41	0.000	0.000
EFW at US, g		3055.99±378.80	2500-4100	--	0.000
BW, g		3179.80±387.67	2500-4290	0.000	--

Table 2.

Pair sample t-test for compare the mean difference between actual BW and US EFW

Variables	Paired Differences					t	df	r	Sig. (2-tailed)
	Mean	SD	Std. Error Mean	95% CI of the Difference					
				Lower	Upper				
BW – EFW	123.81	107.95	7.67225	108.68	138.94	16.138	197	0.961	.000

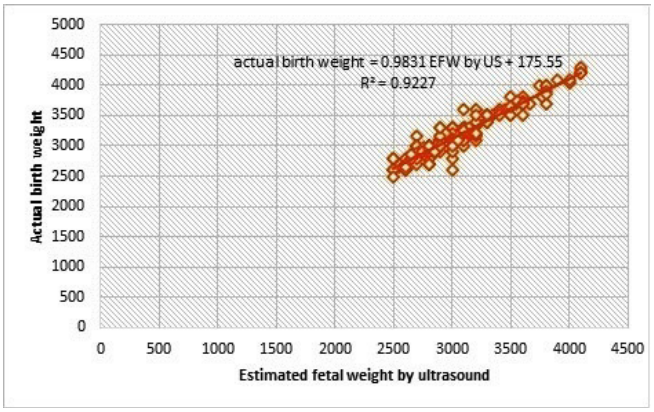

Fig.1

Table 3.

Prediction of BW depending on ultrasound EFW (regression analysis)

		Unstandardized coefficients		Standardized coefficients	t	Sig.	r	R^2	Std. Error of the Estimate
		B	Std. Error	Beta					
1	(Constant)	175.554	62.573		2.806	.006	0.961	0.923	108.04205
	EFW	.983	.020	.961	48.377	.000			
a. Dependent Variable: BW									

Furthermore, the Wilcoxon signed-ranked test showed that in the 50th percentile, the ultrasound EFW was 3000g, while BW was 3100g, with a z-score of -10.73 based on negative rank (P<0.001) (Table 4).

Table 4.

Wilcoxon Signed-Ranks Test to assess the correlation between BW and EFW by US

Variables	n	Minimum	Maximum	Percentiles			Z score	Sig. (2-tailed)
				25th	50th (Median)	75th		
EFW	198	2500.00	4100.00	2800.00	3000.00	3212.500	-10.730b	0.000
BW	198	2500.00	4290.00	2900.00	3100.00	3425.00		

For the comparison study, three accuracy measures were used to analyze the number of estimates within ±10% of BW, the results showed that the overall mean percentage error was -3.85%, and the overall mean absolute error was 123.81 g (Table 5, Figures 2 and 3).

Table 5.

Mean absolute and percentage errors between ultrasound and birth weight

Birth weight Stratum	Ultrasound EFW
overall	
Mean absolute error	123.81±107.95 (Std. Error 7.76)
Mean percentage error	-3.85±3.45 (Std. Error 0.24)
Error of estimation	26.92 for US EFW, 27.55 for BW
Correlation	0.961*
Fetal weight grouping depending on ultrasound	
2500 ≤ 3000 g (112 fetus)	
Mean absolute error	127.94±114.61(Std. Error 10.83)
Mean percentage error	-4.26±3.85 (Std. Error 0.36)
Error of estimation	13.18 for US EFW, 16.11 for BW
3001≤ 3500 g (57 fetus)	
Mean absolute error	123.33±107.81(Std. Error 14.27)
Mean percentage error	-3.58±3.06 (Std. Error 0.40)
Error of estimation	18.04 for US EFW, 24.67 for BW
3501≥4000 g (24 fetus)	
Mean absolute error	104.79±85.83(Std. Error 17.52)
Mean percentage error	-2.71±2.23 (Std. Error 0.45)
Error of estimation	27.99 for US EFW, 32.40 for BW
More than 4000 g (5 fetus)	
Mean absolute error	128.00±40.86(Std. Error 18.27)
Mean percentage error	-3.02±0.93 (Std. Error 0.41)
Error of estimation	0.00 for US EFW, 18.27 for BW

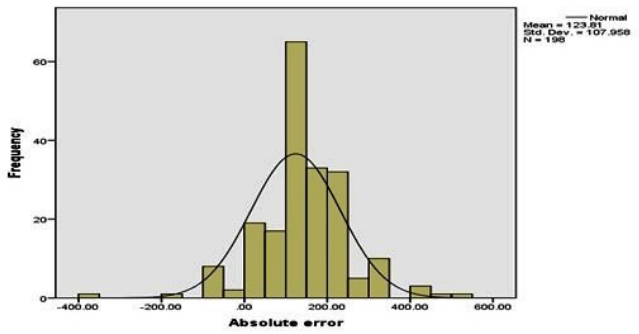

Fig.2.

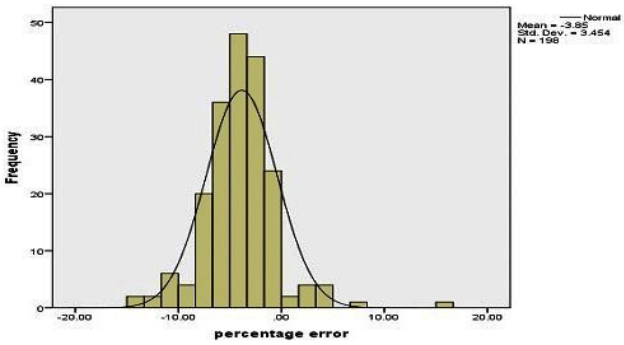

Fig.3.

Table 6.

Bland–Altman plots test to assess the level of agreement between EFW by ultrasound and BW

Bland-Altman			
		95% Confidence Interval	
	Estimate	Lower	Upper
Bias (n = 198)	123.8	109	138.9
Lower limit of agreement	-87.8	-114	-61.9

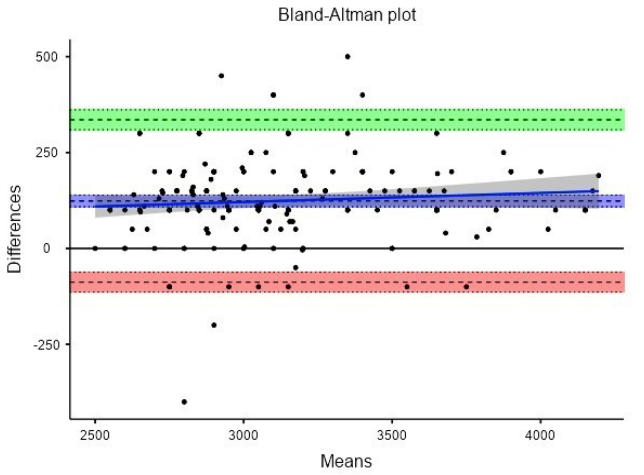

Fig.4.

The Bland-Altman plot showed a strong level of agreement between EFW and BW. The lower limit of the estimate was -87.8, and the upper limit was 335.4. Only a minimal number of estimated cases lie outside the upper and lower agreement limits, showing that ultrasound EFW is a strong predictor of BW (Table 6, Figure 4)

Discussion

Low and excessive FW and intrauterine growth restriction during labor and the puerperium can result in perinatal morbidity, mortality, and long-term neurologic developmental disorders. Therefore, an accurate prediction of antenatal FW is essential to reducing the risk of perinatal morbidity, mortality, and long-term neurologic developmental disorders. In obstetrics, accurate FW prediction is of great concern. Because FW cannot be directly measured, it is calculated based on the fetus and its mother‘s physical features. Ultrasonographic methods are the most widely used of the various techniques, but only a few studies have examined the accuracy of ultrasonic measures in predicting FW to determine the optimum formula. The accuracy of ultrasound EFW has increased in the past decade, with recent studies consistently producing random errors below 10%. The accuracy of these measurements is attributable to the incorporated parameters. The Hadlock formula 1 is still the most reliable regression method and produces the fewest random errors.[13] We found a significantly positive correlation between ultrasound EFW and BW (r=0 .961, P<0.001). The study also found a significant linear relationship between ultrasound EFW and BW (R^2=0.923). This is consistent with the data of Njoku et al.,[14] who found a positive linear correlation between ultrasound EFW and BW (R^2=0.7646). The results showed that the overall mean percentage error was -3.85%, and the overall mean absolute error was 123.81 g. In Njoku et al.,[14] the mean percentage error was -3.1% and the overall mean absolute error was 123.61 g. Our study results differ slightly from Okafor et al.,[15] who studied 170 Nigerian pregnant women, with 0–2 days’ time intervals between ultrasound scan and delivery by using the Hadlock formula 3 to estimate FW. They found that the mean BW was 3.47±0.47 kg, while the mean EFW was 3.43±0.8 kg. A positive correlation was found between the ultrasound EFW and the actual BW (r=0.75, P=0.04), with a mean error of 41.17 g and a mean absolute error of 258.22 g.

Our findings are consistent with those by Basha et al.,[16] who used the Hadlock formula 1 for EFW for pregnant Jordanian women. They yielded acceptable results in terms of actual neonatal weight at birth; additionally, Donma et al.[17] found that Hadlock’s ultrasound estimations are superior to Shepard and Nahum’s equation.

Furthermore, there is a significant association between the ultrasound EFW and BW with maternal age and height but no significant link between maternal weight and BMI in ultrasound EFW and BW. Many studies have independently confirmed the relationship between an offspring’s BW and their adult weight. There is an agreement between this study and a previous one [18] that used the fetal development charts from the World Health Organization for which maternal

height and age had a significant effect on fetal growth. In contrast, we found that BMI and maternal weight have no significant effect on EFW and BW.[13,14,19] The Bland-Altman plot showed a strong level of agreement between EFW and BW. The lower limit of the estimate was -87.8, and the upper limit was 335.4 (95% agreement limit). Another study found that the bias was -85.06g. Eze et al.[20] also found strong agreement between EFW by ultrasound and BW. Consistently, our findings agree with a study conducted in Nigeria in which EFW was measured in 282 women with singleton pregnancies by using Hadlock formula 3 in the Bland-Altman plot.[20,21] In that study, a Wilcoxon signed-ranked test showed that in the 50th percentile, the ultrasound EFW was 3000g, while the BW was 3100 g, with a z-score of -10.73 based on a negative rank (P<0.001).

Except for sharing nutrition and access to private health care, there are differences in the habits and lifestyles of different groups in Saudi Arabia. Yet nearly all Saudi Arabian women in the Aseer region do not smoke, drink alcohol, or use hazardous chemicals. Despite multiple studies that have found a correlation between social factors and BW, there are differing perspectives on why this is true. Other factors could include differences in the quality and amount of medical treatment, food, housing conditions, social support and unemployment, and some women may have greater exposure to dangerous chemicals or increased risk of infectious disease. However, more research is needed to improve FW accuracy, ascertain if EFW near delivery improves outcomes, and determine how applicable these methods are to situations that affect BW, such as premature rupture of membranes and obesity, which were not included in the current study.

Conclusion

The significantly positive correlation between EFW by ultrasound and BW indicates that the Hadlock formula 1 for predicting FW is accurate, valid, and effective in the research environment.

Institutional Review Board Statement

The study was conducted according to the guidelines of the Declaration of Helsinki and approved by the Ethical Committee of Scientific Research, King Khalid University Faculty of Medicine with approval number (ECM#89000), (HAPO-06-B-001).

Informed Consent Statement

Written informed consent to publish this paper was obtained from the study participants.

Data Availability Statement

The study protocol can be accessed upon demand by interested researchers if justified. This study is not registered in any repository. The TMMR-RS is registered on ClinicalTrials.gov (NCT01819077).

Competing Interests

The authors declare that they have no competing interests.

Acknowledgments

The authors would like to thank the Deanship of Scientific Research at King Khalid University for their technical support. We also thank the staff of Abha Mahala Hospital for their contributions, cooperation, and support during the survey.

References

1. Bajracharya J, Shrestha NS, Karki C. Accuracy of prediction of birth weight by fetal ultrasound. Kathmandu Univ Med J (KUMJ). 2012 Apr-Jun;10(38):74-6.
2. Ekele B, Otubu JAM. Maternal and perinatal mortality. Textb Obstet Gynecol Med Student Agboola A, Ed 2nd ed Ibadan, Niger Heinemann Educ Books. Published online 2006:526-531.
3. Jahanfar S, Lim K, Ovideo-Joekes E. Birth weight discordance and adverse perinatal outcomes. J Perinat Med. 2017 Jul 26;45(5):603-611. doi: 10.1515/jpm-2016-0089.
4. Kehinde OA, Njokanma OF, Olanrewaju DM. Parental socioeconomic status and birth weight distribution of Nigerian term newborn babies. Niger J Paediatr. 2013 Mar;40(3):299-302. doi: 10.4314/njp.v40i3,20.
5. Westerway SC. Estimating fetal weight for best clinical outcome. Australas J Ultrasound Med. 2012 Feb;15(1):13-17. doi: 10.1002/j.2205-0140.2012.tb00136.x.
6. Ashrafganjooei T, Naderi T, Eshrati B, Babapoor N. Accuracy of ultrasound, clinical and maternal estimates of birth weight in term women. East Mediterr Health J. 2010 Mar;16(3):313-7.
7. Baum JD, Gussman D, Wirth JC 3rd. Clinical and patient estimation of fetal weight vs. ultrasound estimation. J Reprod Med. 2002 Mar;47(3):194-8.
8. Shittu AS, Kuti O, Orji EO, Makinde NO, Ogunniy SO, Ayoola OO, Sule SS. Clinical versus sonographic estimation of foetal weight in southwest Nigeria. J Health Popul Nutr. 2007 Mar;25(1):14-23.
9. Shepard MJ, Richards VA, Berkowitz RL, Warsof SL, Hobbins JC. An evaluation of two equations for predicting fetal weight by ultrasound. Am J Obstet Gynecol. 1982 Jan 1;142(1):47-54. doi: 10.1016/s0002-9378(16)32283-9.
10. Hadlock FP, Harrist RB, Martinez-Poyer J. In utero analysis of fetal growth: a sonographic weight standard. Radiology. 1991 Oct;181(1):129-33. doi: 10.1148/radiology.181.1.1887021.
11. Campbell S, Warsof SL, Little D, Cooper DJ. Routine ultrasound screening for the prediction of gestational age. Obstet Gynecol. 1985 May;65(5):613-20.
12. Nahum GG, Pham KQ, McHugh JP. Ultrasonic prediction of term birth weight in Hispanic women. Accuracy in an outpatient clinic. J Reprod Med. 2003 Jan;48(1):13-22.
13. American Institute of Ultrasound in Medicine. AIUM practice guideline for the performance of obstetric ultrasound examinations. J Ultrasound Med. 2010 Jan;29(1):157-66. doi: 10.7863/jum.2010.29.1.157.
14. Njoku C, Emechebe C, Odusolu P, Abeshi S, Chukwu

C, Ekabua J. Determination of Accuracy of Fetal Weight Using Ultrasound and Clinical Fetal Weight Estimations in Calabar South, South Nigeria. Int Sch Res Notices. 2014 Nov 10;2014:970973. doi: 10.1155/2014/970973.
15. Okafor CO, Okafor CI, Mbachu II, Obionwu IC, Aronu ME. Correlation of Ultrasonographic Estimation of Fetal Weight with Actual Birth Weight as Seen in a Private Specialist Hospital in South East Nigeria. Int J Reprod Med. 2019 Oct 27; 2019:3693797. doi: 10.1155/2019/3693797.
16. Basha AS, Abu-Khader IB, Qutishat RM, Amarin ZO. Accuracy of sonographic fetal weight estimation within 14 days of delivery in a Jordanian population using Hadlock formula 1. Med Princ Pract. 2012;21(4):366-9. doi: 10.1159/000335539.
17. Donma MM, Donma O, Sonmez S. Prediction of birth weight by ultrasound in Turkish population. Which formula should be used in Turkey to estimate fetal weight? Ultrasound Med Biol. 2005 Dec;31(12):1577-81. doi: 10.1016/j.ultrasmedbio.2005.07.017.
18. Stein AD, Lumey LH. The relationship between maternal and offspring birth weights after maternal prenatal famine exposure: the Dutch Famine Birth Cohort Study. Hum Biol. 2000 Aug;72(4):641-54.
19. Kiserud T, Piaggio G, Carroli G, Widmer M, Carvalho J, Neerup Jensen L, Giordano D, Cecatti JG, Abdel Aleem H, Talegawkar SA, Benachi A, Diemert A, Tshefu Kitoto A, Thinkhamrop J, Lumbiganon P, Tabor A, Kriplani A, Gonzalez Perez R, Hecher K, Hanson MA, Gülmezoglu AM, Platt LD. The World Health Organization Fetal Growth Charts: A Multinational Longitudinal Study of Ultrasound Biometric Measurements and Estimated Fetal Weight. PLoS Med. 2017 Jan 24;14(1):e1002220. doi: 10.1371/journal.pmed.1002220. Erratum in: PLoS Med. 2017 Mar 24;14 (3):e1002284. Erratum in: PLoS Med. 2017 Apr 20;14 (4):e1002301. Erratum in: PLoS Med. 2021 Jan 7;18(1):e1003526. PMID: 28118360; PMCID: PMC5261648.
20. Eze CU, Abonyi LC, Njoku J, Okorie U, Owonifari O. Correlation of ultrasonographic estimated fetal weight with actual birth weight in a tertiary hospital in Lagos, Nigeria. Afr Health Sci. 2015 Dec;15(4):1112-22. doi: 10.4314/ahs.v15i4.9.
21. Dimassi K, Douik F, Ajroudi M, Triki A, Gara MF. Ultrasound Fetal Weight Estimation: How Accurate Are We Now Under Emergency Conditions? Ultrasound Med Biol. 2015 Oct;41(10):2562-6. doi: 10.1016/j.ultrasmedbio.2015.05.020.

International Journal of Biomedicine 12(1) (2022) 49-54
http://dx.doi.org/10.21103/Article12(1)_OA6

ORIGINAL ARTICLE

Experimental Surgery

INTERNATIONAL JOURNAL OF BIOMEDICINE

Flow Sorption Debridement of Aseptic and Purulent Soft Tissue Wounds

Anton P. Ostroushko[1*], PhD; Alexandr A. Glukhov[1], PhD, ScD; Alexandr A. Andreev[1], PhD, ScD; Vladimir A. Vecherkin[1], PhD, ScD; Viktoriya V. Shishkina[2], PhD; Anastasiya Yu. Laptiyova[1]; Sergey V. Lobas[1]; Dmitriy I. Sazhnev[1]; Alexandr A. Shmarin[3]; Elena V. Mikulich[1], PhD; Sergey N. Boyev[1], PhD

[1]Voronezh State Medical University named after N. N. Burdenko
[2]Research Institute of Experimental Biology and Medicine, Voronezh State Medical University named after N. N. Burdenko
[3]Clinical Hospital "Russian Railways-Medicine"
Voronezh, the Russian Federation

Abstract

***Background*:** Treatment of isolated and combined open soft tissue wounds remains relevant due to the growth of severe injuries, comorbid pathologies, and immunosuppressive conditions, along with a decrease in antibiotic sensitivity of microorganisms. The aim of this study was to compare the effectiveness of the jet oxygen-sorption treatment (JOST) and flow sorption debridement techniques (FSDT) in the therapy of experimental soft tissue wounds.

***Methods and Results*:** The effectiveness of the JOST and FSDT was compared in 2 series of experiments on 288 laboratory Wistar rats with simulated soft tissue wounds. Series 1 (S1) involved 144 animals divided into 2 control groups (CG) and 2 experimental groups (EG); the effectiveness of the developed techniques for the aseptic wound treatment was studied in these groups of animals. Series 2 (S2) involved 144 animals divided into 2 CGs and 2 EGs; in S2, purulent soft tissue wounds were studied. The effectiveness of the developed techniques in the complex treatment of experimental wounds was assessed immediately, on Days 1, 3, 5, 7 and 10 after simulating the pathological process. The assessment included the animals' condition, the dynamics of the course of reparative processes (local symptoms of inflammation; granulation; epithelialization of wounds; and size and dynamics of the area of the defect), and histological research methods.

The use of the JOST has practically no benefits in aseptic wound treatment, compared to FSDT. The use of the JOST and FSDT contributed to a significant acceleration of healing process in aseptic wounds that was expressed in the decreased local inflammatory reactions, higher activity of metabolic processes based on the dynamics of RNA and SH-groups. The most pronounced positive dynamics in the treatment of purulent wounds was observed when applying FSDT. Compared with the findings obtained in CG1-S2, FSDT contributed to a reduction in necrolysis termination by 25.7%, fibrinolysis - by 25.5%, granulation - by 20.0%, epithelization - by 18.9%, wound discharge - by 27.8%.

Conclusion: The developed technique of FSDT in the complex treatment of soft tissue wounds provides the most pronounced positive dynamics, accelerates reparative tissue processes, and reduces the duration of wound cleansing and healing for both aseptic and purulent wounds.(**International Journal of Biomedicine. 2022;12(1):49-54.**)

Key Words: soft tissue wounds • jet oxygen-sorption treatment • flow sorption debridement techniques

For citation: Ostroushko AP, Glukhov AA, Andreev AA, Vecherkin VA, Shishkina VV, Laptiyova AYu, Lobas SV, Sazhnev DI, Shmarin AA, Mikulich EV, Boyev SN. Flow Sorption Debridement of Aseptic and Purulent Soft Tissue Wounds. International Journal of Biomedicine. 2022;12(1):49-54. doi:10.21103/Article12(1)_OA6

Introduction

Treatment of isolated and combined open soft tissue wounds remains relevant due to the growth of severe injuries, comorbid pathologies, and immunosuppressive conditions, along with a decrease in antibiotic sensitivity of microorganisms.[1-4] The development of surgical wound infection significantly aggravates the course of pathology;

its complications account for one-third of deaths in the postoperative period. Suppression of inflammation, prevention or reduction of bacterial contamination and oxidative stress are of great importance in local wound treatment. In this regard, the use of sorbents has proved to be highly effective.

Novel materials, techniques and devices are constantly being introduced into surgical practice to advance clinical outcomes of this group of patients, but their effectiveness is still not adequate. Effects based on the use of oxygen therapy and sorbents that potentiate the repair of tissue defects have proven appropriate in various areas of medicine.[5-9]

The aim of the study was to compare the effectiveness of the jet oxygen-sorption treatment (JOST) and flow sorption debridement techniques (FSDT) in the therapy of experimental soft tissue wounds.

Materials and Methods

The JOST and FSDT were applied using an original device consisting of a nozzle, mixing chambers in series, containers for powdered drugs, a gas flow switch and a gas pressure regulator, and a system of silicone tubes (Fig.1). Sources of oxygen, carbon dioxide or sterile air can be used to create a sorption-gas suspension.

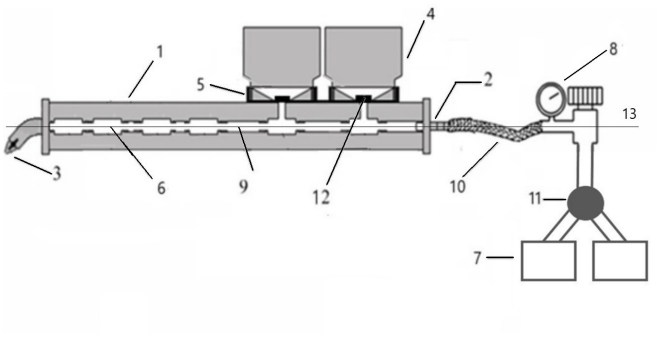

Fig. 1. *Scheme of the device for FSDT*

1 – Body frame of the device, 2 – Adapter, 3 – Nozzle for directing the outgoing flow, 4 - Containers for powdered drugs, 5 – Connecting collar, 6 - Mixing chambers, 7 – Gas sources, 8 – Gas pressure regulator, 9 – System of silicone tubes, 10 - Hose, 11 - Gas flow switch, 12 - Valves that regulate the supply of drugs, 13 - Imaginary horizontal axis around which the body of the device (1) is rotated by 180^0.

The JOST technique included 3 successive stages of wound surface therapy by using:

(a) a dispersed flow of physiological solution - a special device UGOR-1M;

(b) an oxygen flow (a pressure of 6 atm) - a special device for the flow sorption debridement technique;

(c) a suspension of atoxyl in oxygen until a uniform layer covering the wound was formed - a special device for the flow sorption debridement technique.

The FSDT was also performed in 3 successive stages, but instead of oxygen, carbon dioxide was used (a pressure of 6 atm); this was due to the absence of signs of anaerobic infection in purulent wounds (simulation of the wound process was performed using *St. aureus*), higher safety of the technique applied. The FSDT is crucially different from the JOST technique by the possibility of using a gas sorption mixture depending on the nature of the microflora(anaerobes or aerobes), i.e., the possibility of using oxygen, carbon dioxide, or air.

The effectiveness of the JOST and FSDT was compared in 2 series of experiments on 288 laboratory Wistar rats with simulated soft tissue wounds. Series 1 (S1) involved 144 animals divided into 2 control groups (CG) and 2 experimental groups (EG); the effectiveness of the developed techniques for the aseptic wound treatment was studied in these groups of animals. Series 2 (S2) involved 144 animals divided into 2 CGs and 2 EGs; in S2, purulent soft tissue wounds were studied (Table 1).

Table 1.

Characteristics of the subgroups in Series 1 and 2 of experiments

Subgroup	Number of animals	Brief description of the study groups
Series 1 / aseptic wounds		
CG1-S1	36	No treatment
CG2-S1	36	Applications of atoxyl on the wound surface
EG1-S1	36	JOST using atoxyl
EG2-S1	36	FSDT using atoxyl
Series 2 / purulent wounds		
CG1-S2	36	No treatment
CG2-S2	36	Applications of atoxyl on the wound surface
EG1-S2	36	JOST using atoxyl
EG2-S2	36	FSDT using atoxyl

In animals of CG1-S1 and CG1-S2, no wound treatment was performed, the natural course of the wound process was studied. In the remaining groups, wound dressings were performed daily. In animals of CG2-S1 and CG2-S2, atoxyl was additionally applied on the wound surface. In animals of EG1-S1 and EG1-S2, the JOST using atoxyl was performed. In animals of EG2-S1 and EG2-S2, the FSDT using atoxyl was performed. The described procedures were performed in both series of experiments daily until the wound closed.

The atoxyl preparation applied in the study is a super-finely dispersed enterosorbent of the fourth generation with wound healing, antimicrobial, bacteriostatic, and detoxifying effects, recommended for external use in the complex treatment of purulent wounds, trophic ulcers, and burns. The preparation has no effect of reverse sorption.

All procedures with animals were performed under general anesthesia (Zoletil-100) in compliance with sterility.

In the S1, wound simulation included skin shaving in the wither area followed by its excision with a superficial fascia 1.5cm in diameter, according to the established pattern. After meticulous hemostasis, the resulting defect was abundantly washed with a sterile solution. The aseptic wound was formed.

In S2, a suspension of *St. aureus* (109 microns/ml) was introduced into the wound after simulation, and the wound was closed. Three days after wound contamination, the sutures were removed, the wound edges were separated. In all animals, there were signs of a pronounced inflammatory reaction and the purulent wound was formed.

The effectiveness of the developed techniques in the complex treatment of experimental wounds was assessed immediately, on Days 1, 3, 5, 7 and 10 after simulating the pathological process. The assessment included the animals' condition, the dynamics of the course of reparative processes (local symptoms of inflammation; granulation; epithelialization of wounds; and size and dynamics of the area of the defect), and histological research methods.

Statistical analysis was performed using the Statistica 6.1 software package (Stat-Soft Inc., USA). The normality of distribution of continuous variables was tested by the Kolmogorov-Smirnov test with the Lilliefors correction and Shapiro-Wilk test. For descriptive analysis, results are presented as mean±standard deviation (SD). For data with normal distribution, inter-group comparisons were performed using Student's t-test. Mann-Whitney U test and Wilcoxon criterion were used to compare means of variables not normally distributed. Spearman's rank correlation coefficient was calculated to measure the strength and direction of the relationship between two variables. A probability value of $P<0.05$ was considered statistically significant.

Work on the animals was done in compliance with the principles of the Helsinki Declaration on the humane treatment of animals, stated in normative documents of the European community(86/609/EU), Manual on Experimental (Preclinical) Study of New Pharmacological Substances, and "Good laboratory practice" (MHRF Order No. 708н dated 23.08.2010).

Results

The peri-wound edema was arrested most rapidly in CG2-S1, compared to CG1-S1, by 13.6% (Table 2). In EG1-S1 and EG2-S1, the elimination of peri-wound edema was found in 2.48±0.41 and 2.48±0.32 days after injury, respectively. In CG1-S2 and CG2-S2, peri-wound edema was eliminated in 3.91±0.20 and 3.50±0.20 days, respectively; in EG1-S2 and EG2-S2 – 3.43±0.20 and 3.41±0.20 days, respectively.

Experimental hyperemia of the paravual area was eliminated faster in CG2-S1 than in CG1-S1 by 5.6%. The use of the JOST in the complex treatment of aseptic wounds resulted in the relief of experiments hyperemia in 2.31±0.55 days after injury in EG1-S1 and in 2.37± 0.30 days after injury in EG2-S1. In CG1-S2, experiments hyperemia was eliminated in 3.88±0.21 days. In CG2-S2, EG1-S2, EG2-S2, hyperemia was reduced most rapidly, more than in CG1-S2 – by 14.5%, 18.9%, and 19.1%, respectively.

Wound exudate decreased in 3.50±0.36 days in CG1-S1. In CG2-S1, EG1-S1, EG2-S1, wound exudate decreased most rapidly in CG1-S1 – by 22.3%, 71.1%, and 70.9%, respectively.

Table 2.

Terms for relief of local signs of inflammation in the study subgroups, days

Sign	Series 1				Series 2			
	CG1	CG2	EG1	EG2	CG1	CG2	EG1	EG2
Edema	3.25±0.27	2.81±0.32	2.48±0.41*	2.48±0.32*	3.91±0.20	3.50±0.20*	3.43±0.20*	3.41±0.20*
Hyperemia	2.87±0.46	2.71±0.30	2.31±0.55	2.37±0.30	3.88±0.21	3.32±0.20*	3.15±0.20*	3.14±0.20*
Wound exudates/ discharge [1]	3.50±0.36	2.72±0.34	2.45±0.31*	2.48±0.31*	6.28±0.32	5.46±0.43	4.73±0.39*	4.54±0.38*

*[1]– Reduction of the amount to scant discharge; * P<0.05 - compared with CG1*

In the S2, the amount of wound discharge decreased in 6.28±0.32 days in CG1-S2. In CG2-S2, EG1-S2, EG2-S2, wound discharge decreased most rapidly in CG1-S2 – by 13.1%, 24.7%, and 27.8%, respectively.

Table 3.

Detection of the signs of the wound process in Series 2 of experiments, days

Sign	CG1-S2	CG2-S2	EG1-S2	EG2-S2
Necrolysis	3.5±0.2	3.3±0.2	2.7±0.2*	2.6±0.2*
Fibrinolysis	5.1±0.3	4.8±0.3	3.9±0.2*	3.8±0.2*
Granulation	3.5±0.3	3.3±0.2	3.0±0.2*	2.8±0.2*
Epithelialization	5.3±0.3	5.0±0.3	4.5±0.3*	4.3±0.3*

**– P<0.05 compared with CG1*

Necrolysis duration of 3.5±0.2 days was found in CG2-S2 and was shorter by 5.8% in CG2-S2, 22.9% in EG1-S2, and 25.7% in EC2-S2 (Table 3).

Fibrinolysis was observed in 5.1±0.3 days in CG1-S1 and was found earlier by 5.9% in CG2-S2, 23.2% in EG1-S2, and 25.5% in EG2-S2.

Granulations appeared within 3.5±0.3 days in CG1-S2, faster by 5.8% in CG2-S2, 14.3% in EG1-S2, and 20.0% in EG2-S2.

Epithelialization was noted in 5.3±0.3 days in CG1-S2 and was faster by 5.7% in CG2-S2, 15.1% in EG1-S2, and 18.9% in EG2-S2.

Table 4.

Dynamics of RNA and SH-groups in Series 1 of experiments, relative units (U)

Subgroup	Day 1	Day 3	Day 7	Day 10
RNA level				
CG1-S1	0.23±0.01	0.27±0.01*	0.30±0.02*	0.30±0.02*
CG2-S1	0.24±0.01	0.26±0.01*	0.32±0.02*^	0.33±0.02*^
EG1-S1	0.26±0.01	0.28±0.01	0.32±0.02	0.34±0.02
EG2-S1	0.26±0.01	0.27±0.01	0.33±0.02	0.35±0.02
SH-group level				
CG1-S1	0.26±0.01	0.27±0.01	0.28±0.02	0.27±0.01
CG2-S1	0.27±0.02	0.27±0.02	0.29±0.01	0.28±0.02
EG1-S1	0.28±0.02	0.28±0.02	0.34±0.02	0.30±0.02
EG2-S1	0.26±0.02	0.28±0.02	0.33±0.02	0.29±0.01

**P<0.05 - compared to Day 1; ^P<0.05 - compared to CG1-S1.*

In the S1, the highest RNA level (0.23±0.01U) was detected in the growth plate in CG1-S1 on Day 1, demonstrating the severity of metabolic processes in this area (Table 4).

The level of SH-groups on Day 1 prevailed in the more superficial layers and was more pronounced in the intact epithelium. The level of SH-groups in the germ layer was 0.26±0.01U. On Day 3, the RNA level increased in deeper layers of the epidermis in CG1-S1; the perinuclear accumulation of RNA was rarely observed. On Day 5, the distribution of SH-groups in the epidermis was practically equal to findings obtained on Day 3. In CG1-S1, on Days 7 and 10, a further increase in the intensity of metabolic processes was observed in the damage zone in GC1-S1; this was supported by an increase in the levels of RNA and SH-group up to 0.30±0.02U and 0.28±0.02U by Day 7 and 0.30±0.02U and 0.27±0.01U by Day 10, respectively.

In CG2-S1, on Day 1, moderate basophilia with a pronounced reaction was revealed in the growth plate. The levels of RNA and SH-groups were 0.24±0.01U and 0.27±0.02U, respectively. On Day 3, we found an increase in the RNA level up to 0.26±0.01U and stabilization of SH-group parameters (0.27±0.02U). On Day 7, the RNA level increased up to 0.32±0.02U in CG2-S1. SH-groups were determined mainly in the surface layers of the defect (0.29±0.01U), which could be evidence of epithelium keratinization. On Day10, the levels of RNA and SH-groups were 0.33±0.02U and 0.28±0.02U, respectively.

In EG1-S1, on Day 1, the levels of RNA and SH-groups were 0.26±0.01U and 0.28±0.02U, respectively. On Day 3, the RNA level increased to 0.28±0.01U, and the level of SH-groups was stabilized. On Days 7 and 10, we found a further increase in the RNA level up to 0.32±0.02U and 0.34±0.02U, SH-groups up to 0.29±0.01U and 0.28±0.02U, respectively.

In EG2-S1, on Day 1, the levels of RNA and SH-groups were 0.26±0.01U and 0.26±0.02U, respectively. The growth of SH-groups demonstrated progression in the processes of epithelial cell regeneration. On Day 3, the levels of RNA and SH-groups increased up to 0.27±0.01U and 0.28±0.02U, respectively, being accompanied by regeneration of the skin surface. On Days 7 and 10, at the end of the defect epithelialization, the RNA levels reached 0.33±0.02U and 0.35±0.02U, respectively, SH-groups – 0.33±0.02U and 0.29±0.02U, respectively.

In the S2**,** we analyzed values of alkaline phosphatase (ALP) as a marker of the duration of wound process and the maturation of granulation tissue (Table 5). In CG1-S2, on Day 1 of the experiment, the ALP level was 27.3±2.3U and increased up to 42.5±2.5U by Day 7. Similar dynamics was noted in CG2-S2; however, on Days 1, 3, 5, and 7, the ALP was higher than in CG1-S2 by 34.5%, 25.1%, 26.4%, and 21.5%, respectively. The most pronounced dynamics in the ALP level was observed in animals of EG1-S2 and EG2-S2 (Day 1 - 50.3±2.6U and 52.5±2.6U, respectively; Day 3 - 57.7±2.7U and 58.1±3.1U, respectively; Day 5 - 65.0±2.7U and 66.9±2.9U, respectively; Day 7 - 75.6±3.1U and 77.6±3.2Us, respectively). On Day 7 after the experiment, the lowest ALP value (46.5±2.5U) was found in CG1-S2, most likely associated with the minimum activity of metabolic processes in the injured tissues.

Table 5.

Dynamics of ALP in purulent wounds of the soft tissues, relative units (U)

Day	CG1-S2	CG2-S2	EG1-S2	EG2-S2
1	27.3±2.3	41.7±2.5^	50.3±2.6^	52.5±2.6
3	37.7±2.3*	50.3±2.6*^	57.7±2.7*^	58.1±3.1*
5	42.5±2.5*	57.7±2.8*^	65.0±2.7*^	66.9±2.9*
7	46.5±2.5*	59.2±2.9*^	75.6±3.1*^	77.6±3.2*^

**P<0.05- compared to Day 1; ^P<0.05 - compared to CG1-S2.*

In EG1-S2 and EG2-S2, the microbial contamination of the purulent wound discharge (microbial bodies per ml) was significantly lower than in CG1-S2 at all stages of observation (Table 6).

There were no significant differences between groups in the wound area after simulation (Table 7). In CG1-S1, the wound area steadily decreased during the entire observation period, compared to the initial size, by 34.8%, 61.5%, 82.5, and 99.9% on Days 1, 3, 7, and 10 after wound simulation, respectively.

In EG1-S1 and EG2-S1, the wound area decreased by 39.1% and 38.6% on Day 1, 74.3% and 73.5% on Day 3,

91.8% and 91.0% on Day 7, 99.99% and 99.98% on Day 10, respectively, compared with the initial findings.

In CG2-S1, we found a reduction in size of the defect by 36.7%, 67.2%, 86.5%, and 99.95% on Days 1, 3, 7, and 10, respectively, compared with the sizes obtained immediately after wound simulation.

In CG1-S2, the wound area steadily decreased during the entire observation period, compared to the initial size, by 27.9%, 55.1%, 72.2%, and 85.4% on Days 1, 3, 7, and 10 after wound simulation, respectively.

In CG2-S2, we found a reduction in size of the defect by 32.7%, 60.9%, 80.1%, and 93.1% on Days 1, 3, 7, and 10, respectively, compared with the sizes obtained immediately after wound simulation.

Table 6.

Dynamics of microbial contamination of the purulent wound discharge (microbial bodies per ml)

Day	CG1-S2	CG2-S2	EG1-S2	EG2-S2
1	10^9-10^{10}	10^8-10^9	10^7-10^9	10^7-10^9
3	10^5-10^8	10^3-10^5	10^2-10^3	10^2-10^3
5	10^3-10^5	10^2-10^3	10^2-10^3	10^2-10^4
7	10^3-10^6	10^1-10^2	10^1-10^2	10^1-10^3

Table 7.

Dynamics of the wound area in animals, mm²

Subgroup	Day after wound simulation				
	Immediately	Day 1	Day 3	Day 7	Day 10
Series 1 / aseptic wounds					
CC1-S1	131.9±13.5	86.1±8.6*	50.8 ±5.5*	23.1±2.7*	11.5±1.3*^
CG2-S1	131.8±13.1	83.8±8.6	43.7±5.3*	17.8±2.7*	6.1±1.3*^
EG1-S1	133.8±10.8	81.0±6.1*	35.2±3.1*^	11.9±0.9*^	1.1±0.1*^
EG2-S1	132.9±14.0	81.1±8.3*^	35.7±3.9*^	12.0±2.0*^	1.4±0.6*^
Series 2 / purulent wounds					
CG1-S2	116.3±10.7	83.9±7.6*	52.3±5.6*	32.4±3.6*	17.0±1.5*^
CG2-S2	118.4±10.5	79.7±7.8*	46.4±5.0*	23.6±2.9*^	8.3±1.4*^
EG1-S2	118.9±10.1	78.6±6.1*	35.1±3.7*^	12.3±1.7*^	1.4±0.7*^
EG2-S2	117.3±13.3	79.8±8.0*	32.9±4.0*^	10.7±2.2*^	1.0±0.6*^

**P<0.05 - compared to the initial wound size in the group, ^P<0.05 – compared to CG1*

In EG1-S2 and EG2-S2, the wound area decreased by 33.9% and 32.0% on Day 1, 70.1% and 71.9% on Day 3, 89.7% and 90.9% on Day 7, 99.99% and 99.99% on Day 10, respectively, with the sizes obtained immediately after wound simulation.

Conclusion

The use of the the jet oxygen-sorption treatment has practically no benefits in aseptic wound treatment, compared to the flow sorption debridement techniques. The use of the the jet oxygen-sorption treatment and flow sorption debridement techniques contributed to a significant acceleration of healing process in aseptic wounds that was expressed in the decreased local inflammatory reactions, higher activity of metabolic processes based on the dynamics of RNA and SH-groups. The most pronounced positive dynamics in the treatment of purulent wounds was observed when applying flow sorption debridement techniques. Compared with the findings obtained in CG1-S2, flow sorption debridement techniques contributed to a reduction in necrolysis termination by 25.7%, fibrinolysis - by 25.5%, granulation - by 20.0%, epithelialization - by 18.9%, wound discharge - by 27.8%. The developed of flow sorption debridement techniques in the complex treatment of soft tissue wounds provides the most pronounced positive dynamics, accelerates reparative tissue processes, and reduces the duration of wound cleansing and healing for both aseptic and purulent wounds.

Competing Interests

The authors declare that they have no competing interests.

References

1. Shishmanyan DB. [Characteristics of emergency patients' admission at the maxillofacial department. Bulletin of Medical Internet Conferences]. 2015;5:10:1166. [Article in Russian].
2. Akers KS, Mende K, Cheatle KA, Zera WC, Yu X, Beckius ML, et al.; Infectious Disease Clinical Research Program Trauma Infectious Disease Outcomes Study Group. Biofilms and persistent wound infections in United States military trauma patients: a case-control analysis. BMC Infect Dis. 2014;14:190. Published 2014 Apr 8. doi:10.1186/1471-2334-14-190
3. Murphy-Lavoie HM, Bhimji SS. Diabetic, Foot infections. Treasure Island (FL): StatPearls Publishing; 2017 Jun. Available from http://www.ncbi.nlm.nih.gov/books/NBK441914/PubMed PMID: 28722943.
4. Gatiatullin IZ, Shevlyuk NN, Tretyakov AA, Fadeev SB, Shchuplova EA. [Features of reparative histogenesis in the treatment of extensive purulent wounds of the soft tissues

***Corresponding author**: Anton P. Ostroushko, PhD. Voronezh State Medical University named after N.N. Burdenko. Voronezh, Russia. E-mail: antonostroushko@yandex.ru*

using biodegradable hydroxoapatite-collagen material]. Bulletin of New Medical Technologies. Electronic Edition. 2018; 6: 304-309. [Article in Russian].
5. Arkhipov DV, Andreev AA, Atyakshin DA, Glukhov AA, Ostroushko AP. [Oxygen sorption jet treatment in the therapy of purulent soft tissue wounds]. Journal of Experimental and Clinical Surgery. 2020;13:1(46):41-45.[Article in Russian].
6. Fedyanin SD, Kosinets VA, Khrustalev BM, Minchenya VT, Alekseev YuG, Niss VS, Yatsko AS. [Impulse KM-1 VAC therapy apparatus in the complex treatment of surgical infections of the skin and soft tissue]. Bulletin of Pirogov National Medical and Surgical Center. 2021;16:2:72-76. [Article in Russian].
7. Vinnik YuS, Salmina AB, Teplyakova OV, Drobushevskaya AI, Pozhilenkova EA, Morgun AV, Shapran MV, Kovalenko AO. [The results of combined ozone therapy using in complex treatment of soft tissues infections in patients with diabetes mellitus type II]. Chirurgiia. 2015;2:63-69. [Article in Russian].
8. Vinnik YS, Plakhotnikova AM, Kirichenko AK. [The use of a directed flow of ozone-oxygen gas mixture to sanitize a purulent wound in the experiment]. Novosti Khirurgii. 2015;23(4): 372-378. [Article in Russian].
9. Girev EA, Zarivchatskii MF, Orlov OA, Shavkunov SP. [Investigation of the concentration of oxygen in soft tissues of an operative wound edge in stomach cancer surgery]. Family Health — the 21 Century. 2015;1(1):57-67. [Article in Russian].

International Journal of Biomedicine 12(1) (2022) 55-57
http://dx.doi.org/10.21103/Article12(1)_OA7

ORIGINAL ARTICLE

Experimental Surgery

INTERNATIONAL JOURNAL OF BIOMEDICINE

Experimental Evaluation of the Effectiveness of the Laparoscopic Method for Suturing a Perforated Ulcer of the Anterior Wall of the Stomach by Forming a "Covered Perforation" with a Fold-Duplicator

Evgeny V. Borzov[1], PhD, ScD; Ilya V. Sazhin[2,3], PhD; Sergey N. Shurygin[3,2], PhD, ScD; Leonid V. Safonov[4*], PhD; Archil S. Tsulaya[2]; Sarkis A. Asratyan[2], PhD; Alexander V. Kutenev[3], PhD; Aleksandr N. Alimov[5,1], PhD, ScD

[1]*Ivanovo State Medical Academy, Ivanovo, Russia*
[2]*Moscow City Clinical Hospital after V.M. Buyanov, Moscow, Russia*
[3]*Peoples' Friendship University of Russia (RUDN University), Moscow, Russia*
[4]*Federal Science Center of Physical Culture and Sport (VNIIFK), Moscow, Russia*
[5]*Pirogov Russian National Research Medical University, Moscow, Russia*

Abstract

Improvement of existing methods and development of new techniques for performing videoendoscopic operations in emergency surgical pathology allows increasing the efficiency and safety of surgical interventions, which is especially important in emergency surgery. The aim of the study was to experimentally evaluate the effectiveness of the laparoscopic method of suturing a perforated ulcer of the anterior wall of the body of the stomach by forming a "covered perforation" with a fold-duplicator. The article presents the results of a comparative study of the course of recovery in laboratory animals after suturing a perforated ulcer of the anterior wall of the stomach by the traditional method of applying a double-row, interrupted suture and a new method based on forming a covered perforation by creating a fold-duplicator.(**International Journal of Biomedicine. 2022;12(1):55-57.**)

Key Words: perforated gastric ulcer • covered perforation • fold-duplicator

For citation: Borzov EV, Sazhin IV, Shurygin SN, Safonov LV, Tsulaya AS, Asratyan SA, Kutenev AV, Alimov AN. Experimental Evaluation of the Effectiveness of the Laparoscopic Method for Suturing a Perforated Ulcer of the Anterior Wall of the Stomach by Forming a "Covered Perforation" with a Fold-Duplicator. International Journal of Biomedicine. 2022;12(1):55-57. doi:10.21103/Article12(1)_OA7

Abbreviation

PGU, perforated gastric ulcer.

Introduction

A new method has been developed for laparoscopic suturing of a perforated ulcer of the anterior wall of the gastric body and the gastric antrum with the formation of a covered perforation in the form of a fold-duplicator.[1,2] The article presents a morphological substantiation for the effectiveness of the method, based on the results of experimental studies on laboratory animals. Prior to the start of this study, we carried out extensive preparatory experimental work on modeling the technique of the proposed method on the cadaveric material of the stomach of sexually mature Urzhum pigs along with a study of the deformation of the gastric lumen in the operation area using the plaster modeling method (Fig.1). Comparing the method proposed by us and the classical suturing of the

***Corresponding author**: Leonid V. Safonov, PhD. Federal Science Center of Physical Culture and Sport (VNIIFK), Moscow, Russia. E-mail: lsaf@mail.ru*

perforation zone with interrupted sutures, we did not find significant differences that would adversely affect the passage of gastric contents.

Fig. 1. *Plaster models of the inner wall of the stomach using various methods of suturing a perforated gastric ulcer.*

1.1. Closing the perforation with a fold-duplicator.

1.2. Closing the perforation with a double-row interrupted suture

Materials and Methods

The study was carried out on 12 Chinchilla rabbits, weighing 3100-4200g. The morphological reaction of tissues in the operation area was studied in the experimental group (EG, n=6) with the classical suturing of a perforated gastric ulcer (PGU) and the control group (CG, n=6) with PGU suturing using the developed method. The size defect of PGU was 10 mm.

Median laparotomy was performed under ether anesthesia. A perforated hole about 10×10mm in size was formed on the anterior wall of the gastric body of the animals, using surgical, sharp-pointed scissors. Then it was sutured with an absorbable poly-filament thread with a conditional diameter of 2/0 on a piercing needle (26 mm), ½ of the circumference.

In EG, the suturing of PGU was carried out by the proposed method of forming a covered perforation with the imposition of 2 main and 2 additional sutures. In CG, PGU was sutured in the traditional way by applying a double-row interrupted suture through the edges of the defect using a similar thread.

For the morphological study, 2 rabbits from each study group were withdrawn from the experiment on Days 7, 14 and 21. The animals underwent excision of the stomach wall in the area of the sutured perforation. The preparation was fixed in a solution of 10% neutral formalin for 2 hours. Morphological features of the course of the tissue healing process in the area of the closed perforation were studied in 2 groups of animals. The course of pathohistological changes in macropreparations and micropreparations of tissues was studied using a Leica DM-1000 microscope.

Results and Discussion

Macropreparations

On Day 7 of the postoperative period, the morphological features in the stomach wall of rabbits in both groups showed a more pronounced deformity of the stomach in the surgical area in rabbits of EG than in CG. At the same time, in the bulk of all macropreparations, a pronounced fold was determined from the side of the gastric mucosa, protruding into the gastric lumen by an average of 4 mm, which did not affect the passage of gastric contents.

Morphologically, the most pronounced deformation of the stomach in rabbits of the EG, compared with the CG, was found on Day 14 after the operation. In particular, the size of the fold from the side of the serous membrane reached the largest size, up to 20×40mm, while the mucosal fold decreased several times.

On Day 21 after the operation, there were no morphological differences in the nature of the deformation of the stomach wall in the area of operation in rabbits of 2 groups.

Micropreparations

On Day 7 after the operation, similar phenomena were observed in histological preparations obtained from animals of the studied groups. In both groups, a zone of transmural necrosis was identified with early epithelialization phenomena in the form of "crawling" of the integumentary epithelium, somewhat more pronounced in EG. In the projection of the epithelialization zone, the growth of the "young" connective tissue with the phenomena of neoangiogenesis was noted. At the same time, in both groups, a similar pattern of lymphocyte-leukocyte perifocal inflammatory infiltration was noted in the proper layer of the mucous membrane. A similar focal lymphoid infiltration and edema with thickening of the submucosal layer were observed outside the necrosis zone.

By Day 14 after the operation, in both groups, we found a similar narrowing of the necrosis zone with an expansion of the zone of active epithelialization, and a decrease in the inflammatory response due to a reduction of edema and infiltration of the mucous membrane; the appearance of a muscle membrane was noted in the area of surgical intervention.

On Day 21 of the postoperative period, the structure of the gastric mucosa was restored; the inflammation signs persisted only in the form of small fields of lympho-leukocyte infiltration. Growth of "mature" connective tissue was noted, more pronounced in the submucosal layer and somewhat less in the remaining layers of the stomach wall. In rabbits of CG, a slightly more pronounced lymphoid infiltration was noted at the level of the mucosal lamina propria. In histological preparations of animals of both groups, particles of suture material with a scanty macrophage-lymphoplasmacytic reaction were determined.

In the animals of EG, with the closure of the gastric wall defect by creating a covered perforation with a fold-duplicator, there were no microscopic signs of abscessing in the operation area or leakage of the gastric lumen.

The morphological study of the stomach wall macropreparions of animals on Day 21 after the operation indicates that the developed method for suturing the anterior wall of the stomach by creating a covered perforation does not differ morphologically and histologically from the traditional method of suturing with a double-row interrupted

suture. The microscopic picture, comparable in animals of the experimental and control groups, reflects the similarity of the course of inflammatory and reparative processes in the area of perforation suturing. Pathohistological differences in the healing process in the operation area between the animals of the experimental and control groups are insignificant, which allows us to consider both methods of closing the perforation hole almost equivalent.

The described method of suturing PGU with a fold-duplicator of its anterior wall was developed as a technical option for surgeons in cases of perforations of the anterior wall of the gastric body and the gastric antrum. In such cases, it is possible to suture a perforated hole more than 10mm with rigid, inflamed edges of the perforation zone in conditions of local peritonitis.

Conclusions

1. The developed method of laparoscopic suturing of a perforated ulcer of the anterior wall of the gastric body and the gastric antrum by forming a covered perforation and the classical method of suturing with a double-row interrupted suture are characterized by a similar course of the inflammatory reaction and reparative processes.

2. The presented method of laparoscopic suturing of a perforated ulcer of the anterior wall of the stomach by forming a covered perforation with a fold-duplicator is consistent, functional and morphologically identical to the traditional method of suturing the perforation with a double-row interrupted suture; therefore, it can be considered as a variant of a surgical technique for closing perforated ulcers of the anterior wall of the gastric body and the gastric antrum.

Competing Interests

The authors declare that they have no competing interests.

References

1. Sazhin IV. Method for laparoscopic suturing of perforated gastric ulcer with formation of covered perforation. Available from: https://patenton.ru/patent/RU2748880C1.pdf
2. Khripun AI, Sazhin IV, Tsulaya AS, Shurygin SN, Safonov LV, Vaganov AG, Asratyan SA, Alimov AN. Laparoscopic repair of perforated gastric ulcer by forming a “covered perforation.” International Journal of Biomedicine. 2021;1(11):29-31.

International Journal of Biomedicine 12(1) (2022) 58-62
http://dx.doi.org/10.21103/Article12(1)_OA8

ORIGINAL ARTICLE

Experimental Medicine

INTERNATIONAL JOURNAL OF BIOMEDICINE

Activity of Hepatic Enzymes of Isolated Hepatocytes under the Influence of Copper Acetate

Natalia N. Dremina, PhD; Irina S. Trukhan, PhD; Olesya V. Say; Irina A. Shurygina, PhD, ScD

Irkutsk Scientific Center of Surgery and Traumatology
Irkutsk, the Russian Federation

Abstract

The article describes a biochemical method for characterizing the hepatocyte culture under the action of copper acetate (CA). Isolated primary hepatocyte culture was exposed to CA in different concentrations, and then the activity of alanine aminotransferase (ALT), aspartate aminotransferase (AST), alkaline phosphatase (ALP), and the amount of glucose, in the culture medium was determined. The result showed that the level of cell membrane damage and the release of ALT and AST into the extracellular space depend on the concentration of the acting substance, and, in addition, AST was found to be more sensitive to the toxic effects of CA. However, the activity of ALP proved to be an indicator of the copper ions' action on the enzyme but not of destructive processes in the hepatocyte culture. At the same time, a decrease in the glucose level may be used as a characteristic of the cell metabolic activity. Based on the results obtained, we can conclude that proposed analysis methods allow us to comprehensively characterize the processes occurring with cultured hepatocytes under the influence of CA.(**International Journal of Biomedicine. 2022;12(1):58-62.**)

Key Words: hepatocytes • alanine aminotransferase • aspartate aminotransferase • alkaline phosphatase

For citation: Dremina NN, Trukhan IS, Say OV, Shurygina IA. Activity of Hepatic Enzymes of Isolated Hepatocytes under the Influence of Copper Acetate. International Journal of Biomedicine. 2022;12(1):58-62. doi:10.21103/Article12(1)_OA8

Abbreviations

ALT, alanine aminotransferase; **AST**, aspartate aminotransferase; **ALP**, alkaline phosphatase; **CA**, copper acetate

Introduction

The mammalian liver is the essential center in which numerous metabolic, regulatory, homeostatic, and detoxification processes are concentrated, making normal organism development possible. It is known that the functional features of this organ are provided by hepatocytes, highly differentiated cells that make up about 90% of the volume of the liver parenchyma.[1-4] Hepatocytes ensure the metabolism of endogenous compounds and xenobiotics by forming highly water-soluble metabolites that are subsequently excreted from the organism and they are also responsible for the synthesis and secretion of various proteins (albumin, fibrinogen, coagulation factors) and bile acids. Hepatocytes are also involved in maintaining the homeostasis of carbohydrates, lipids, and amino acids, and in the formation of urea. Because of their morphological and functional characteristics, these cells are of particular interest for cell technologies. Currently, the application areas of the human and animal hepatocyte cultures are quite extensive; however, the most popular uses of these cultures remain in the screening of pharmaceuticals, including for the so-called ADME/Tox (absorption, distribution, metabolism, excretion, and toxicity) studies of new compounds.[5] That is because the metabolism of liver cells is the main removal route of about 75% of drugs from the body and is mediated by the functioning of the hepatocyte enzymatic systems, which provide the reactions of functionalization and conjugation of xenobiotic compounds.[6] In this regard, hepatocyte cultures are still considered the most

**Corresponding author:* *Natalya N. Dremina, PhD. Irkutsk Scientific Center of Surgery and Traumatology. Irkutsk, the Russian Federation, E-mail: drema76@mail.ru*

suitable model for analyzing the absorption kinetics of drugs and test compounds, assessing hepatic clearance, recognizing metabolites, and predicting drug interactions with each other.

Analysis of the transcriptome, proteome, and metabolome of cells exposed to the compounds under study makes it possible to predict the risks associated with the occurrence of hepatocellular affections; however, these methods are expensive, difficult to perform and require high-accuracy equipment. Therefore, the search for techniques characterized by high sensitivity, low expenses, and easy realization is still topical. That is why the possibility of using clinical diagnostic methods in biotechnological practice attracts attention. In particular, clinical analyses reflecting pathological changes in the liver functioning and hepatocyte damage of varying severity are of special interest. Such methods include tests widely used in medical practice for diagnosing liver disease and based on the determination of the activity of ALT, AST, and ALP in the blood serum.[7,8]

The purpose of this investigation was to estimate the suitability of biochemical methods to determine the activity of AST, ALT, ALP, and the amount of glucose in the culture medium for toxicity analysis when exposed to different concentrations of CA on hepatocytes.

The choice of the preparation was determined by the properties of this metal. On the one hand, copper is an essential element for organism development and takes part in many physiological processes that include metabolism, tissue respiration, and the synthesis of collagen and elastin; it is also responsible for the activity of enzymes, hormones, and vitamins. However, in excess, copper is an extremely toxic element. In the case of metabolic disorders, copper can accumulate in the organism, in particular in the liver, which results in severe diseases of the central nervous system and internal organs.[9]

Materials and Methods

Isolation of the primary culture of rat hepatocytes

An acute experiment was carried out to isolate the primary culture of hepatocytes of Wistar rats weighing 200g. Animals were housed in accordance with the Good Laboratory Practice (GLP) rules. The experiments were performed in accordance with the norms for the humane treatment of animals regulated by the International Guidelines of the Association for the Assessment and Accreditation of Laboratory Animal Care in accordance with the protocol approved by the Institutional Animal Care and Use Committee of the Irkutsk Scientific Center of Surgery and Traumatology. All surgical interventions were performed under aseptic conditions. The surgery was performed under general intravenous anesthesia using 0.7 ml of a 5% solution of telazol in phosphate-buffered saline intramuscularly and subsequent chloroform inhalation until the loss of locomotor activity but with the maintenance of the cardiac muscle contractile activity.

The primary culture of hepatocytes was obtained by perfusion of the liver through the portal vein. Heparin sodium 5000 IU/ml solution (1ml) in 0.9% sodium chloride was injected, followed by a solution of Krebs-Ringer's buffer with EDTA without calcium (pH 7.2–7.4, 37 °C) (5) with a volume of 210ml and with a perfusion rate of 30ml/min. Then the buffer was replaced with a 0.07% collagenase solution (Sigma-Aldrich) in Hank's Balanced Salt with calcium and magnesium (HBSS, Sigma-Aldrich) of 120ml at the temperature of 37°C. The liver was transferred into pre-cooled Hank's buffer (T=4°C), the liver capsule was dissected, the cells were filtered through a cell filter with a pore size of 70 μm (Corning, BioCoat) and washed with Hank's buffer followed by centrifugation at 50 g for 5 minutes at 4°C. Cells were resuspended in William's E medium (Gibco) with the addition of 10% fetal bovine serum (FBS, Sigma-Aldrich) and Primary Hepatocyte Maintenance Supplement (Gibco) that consist of dexamethasone and a cocktail solution containing GlutaMAX™, HEPES, penicillin-streptomycin, insulin, transferrin, selenium complex, BSA and linoleic acid introduced to the medium according to the manufacturer's instructions. The obtained hepatocyte culture was incubated at 37°C, 90% humidity, and 5% CO_2 in Biostation CT (Nikon). To investigate the toxicity of the chosen preparation, the cells were used for the experiment within 24 hours after isolation because we did not observe changes in the functioning of the enzymatic systems of hepatocytes during this period.[5,10]

Two hours after isolation, the nutrient medium was replaced, and a CuAc2 solution was added to the medium to a final concentration of 50 μg/ml or 200 μg/ml. After 6h and 24h, the nutrient medium was taken to determine the ALT, AST, ALP activity, and glucose concentration. The culture medium of hepatocytes without the addition of CuAc2 served as a control (the corresponding amount of the water was introduced to the culture).

Biochemical research

A biochemical study was carried out on a biochemical analyzer Mindray BS-380 (Mindray, China). The activity of ALT and AST and the amount glucose were determined by a standard method using a Vector Best kit (Russia, series 12, 14); the ALP activity was analyzed using a Mindray kit (China, series 140319007).

Statistical analysis was carried out in the R software environment. A non-parametric Kruskal-Wallis test was used for comparisons of median values among groups, followed by post-hoc analysis using Tukey test. Mann–Whitney–Wilcoxon test was used for pairwise comparison. A value of $P<0.05$ was considered significant.

Results and Discussion

At the first stage, we obtained a primary culture of Wistar rat hepatocytes. After 2 hours, the culture medium was replaced with a fresh one, and the hepatocyte culture was introduced into the experiment.

The analysis of ALT activity 6 and 24 hours after the introduction of CuAc2 into the culture medium showed that incubation with both low (50 μg/ml) and high (200 μg/ml) concentrations of this metal salt led to no significant increase in enzyme activity in the medium, in comparison with the control group (data not demonstrated).

A similar result was obtained when analyzing the AST activity after 6 hours of exposure with CA in two experimental

groups (CuAc2 50 μg/ml and CuAc2 200 μg/ml) (Fig. 1A). However, a significant increase was observed 24 hours after exposure to the CuAc2 in the concentration of 200 μg/ml on hepatocytes (Fig. 1B).

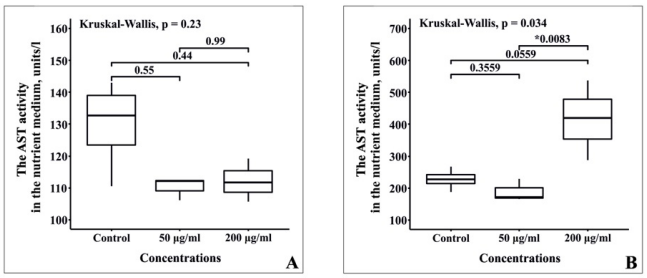

Fig. 1. *Changes in AST activity after exposure to CuAc2 at concentrations of 50 μg/ml and 200 μg/ml on hepatocyte culture for 6 hours (A) and 24 hours (B) compared with the control group. Medians, first and third quartiles are shown.*

When comparing enzyme activity 6 hours and 24 hours after the addition of CA, an increase in the AST activity was found in two experimental groups and the control group (Fig. 2B), whereas significant ALT activity growth was observed only after incubation with CuAc2 at a concentration of 200 μg/ml (Fig. 2A). In this case, a rising enzyme activity may be associated with destructive processes attended by a breach of membrane integrity and the release of enzymes into the extracellular space.

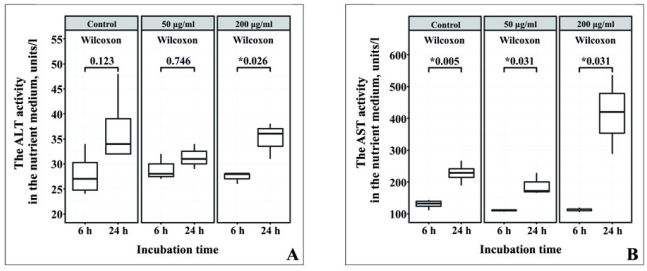

Fig. 2. *Comparison of the ALT (A) and AST (B) activity in the control group and groups with adding CuAc2 at the concentrations of 50 μg/ml and 200 μg/ml after incubation for 6 or 24 hours. Medians, first and third quartiles are shown.*

Interesting results were obtained in the analysis of the ALP enzyme. It was found after 6 hours of incubation with CuAc2 at both tested concentrations, the enzyme activity was significantly lower than in the control group (Fig. 3A). A similar picture was observed after 24 hours of incubation with CuAc2 in different concentrations (Fig. 3B). This effect is probably caused by the replacement of zinc ions included in the structure of the enzyme with copper ions, as a result of which there is a decrease in the ALP activity.

When comparing glucose levels with the control group, a significant decrease of its amount was noted in both experimental groups 6 hours and 24 hours after the addition of CA solution (Fig. 4). The described change is associated with the high hepatocyte metabolic activity, which increases even more under the action of copper ions. In particular, it is known that copper is a cofactor of cytochrome c oxidase, one of the mitochondrial respiratory chain enzymes involved in the aerobic oxidation of various metabolites, including glucose. At the same time, during the following 18 hours of incubation with CA, no further decrease in the amount of glucose in the medium was observed, which may be associated with the accumulation of excess amounts of copper in the cells and the related toxic effect. In this case, the heterogeneity of the obtained primary culture can contribute to the maintenance of relatively constant glucose content as a result of balancing the intake of this carbohydrate by actively metabolizing hepatocytes and the death of cells that accumulate excess amounts of this element.

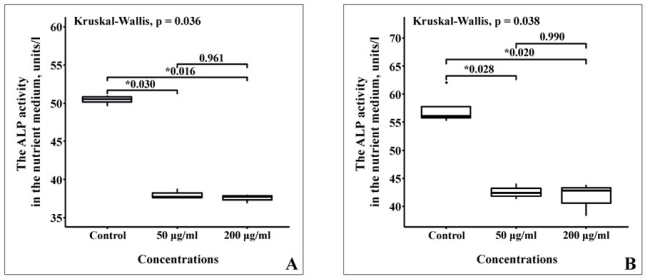

Fig. 3. *Changes in ALP activity after exposure to CuAc2 at concentrations of 50 μg/ml and 200 μg/ml on hepatocyte culture for 6 hours (A) and 24 hours (B) compared with the control group. Medians, first and third quartiles are shown.*

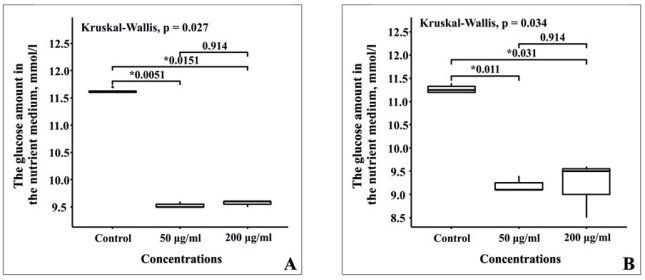

Fig. 4. *Changes in glucose level after exposure to CuAc2 at concentrations of 50 μg/ml and 200 μg/ml on hepatocyte culture for 6 hours (A) and 24 hours (B) compared with the control group. Medians, first and third quartiles are shown.*

Discussion

The ALT and AST enzymes are considered as specific markers of liver cell damage. The level of increased enzyme activity allows us to come to a conclusion about the degree of cytolysis processes, and it is generally recognized that the elevated ALT and AST activities are a consequence of damage to the hepatocyte cytoplasmic membranes, followed by the release of intracellular enzymes into the extracellular space. ALT activity can increase during the late phase of cellular damage when cytolysis occurs as a result of direct damage to hepatocytes. Although plasma membrane injury and protein leakage are considered the most common causes of elevated ALT levels, there is evidence that other

mechanisms may be involved.[11] Unlike ALT, the main part (over 80%) of AST is concentrated in the mitochondria, and the hepatic AST fraction primarily reflects the damage to the hepatocyte mitochondrial membrane.[7] It is also known that some substances exhibit a higher affinity for the inner mitochondrial membrane, entering the matrix region, promoting the release of AST, the mitochondrial function, and disruption of energy metabolism, which eventually leads to initiating apoptotic pathways.[12]

Another factor contributing to the increase in the level of aminotransferases in some cases is not cell damage but the induction of their expression. It is assumed that some substances are capable of increasing enzyme activities.[13] For example, in an experiment on mice, the growth of ALT and AST activity was noted after exposure to tetrachloromethane, and it was canceled after the use of protein synthesis inhibitors.

ALT and AST expression can also be regulated through IRE1α/c-Jun pathway signaling. It has been shown that inhibition of microsomal triglyceride transfer protein (MTP) leads to GPT/GOT1 (ALT and AST genes) transcription enhancement by increasing the regulation of the IRE1α/cJun pathway, which results in intensification of ALT and AST synthesis and release. Thus, the transcriptional regulation of the GPT/GOT1 genes is the main stress response mechanism leading to an increase in the level of transaminases, which may represent a normal reaction to stress for survival.[14] In general, although elevated levels of aminotransferase activity may be due to a number of reasons, prevalent causes, apparently, are damage to plasma membranes and cell death. This is evidenced by the dependence of the increased level of enzyme activity on the concentration of copper ions in the culture medium and the higher sensitivity of AST in comparison with ALT. The latter is explained by the fact that AST is presented in hepatocytes predominantly by the mitochondrial isoenzyme and respectively makes a greater contribution to the rise in activity caused by destructive processes in the culture especially affecting mitochondria.

ALP, which catalyzes the removal of phosphoric acid from its organic compounds, has optimal activity at pH of 8.6–10.1 and is located on the external surface of the cell membrane where it takes part in the transport of phosphorus. The enzyme is found in almost all organs, but its maximum amount is detected in the hepatobiliary system, bone tissue, intestines, placenta, and lactating mammary gland. For diagnostic purposes, the identification of bone and hepatic isoforms of ALP is most often carried out.[15] The activity of the hepatic phosphatase form is commonly enhanced due to damage or destruction of hepatocytes, as well as breaching of bile transport. The hepatocellular mechanism of increasing the ALP activity plays a crucial role in viral and autoimmune hepatitis, and toxic and medicinal damage to the liver. Along with pathological conditions, there is also a growth of physiological ALP activity in blood serum, which is noted during intensive development or pregnancy. Low ALP levels are observed in hypothyroidism, pernicious anemia, congenital hypophosphatasia, and zinc deficiency, as well as in the chronic form of Wilson–Konovalov disease.[16]

Zinc and magnesium are essential cofactors of the ALP enzyme. It has been demonstrated that when high concentrations of copper solution were added to the nutrient medium of hepatocytes, zinc was replaced by copper in the structure of ALP and the enzyme activity decreased.[15] Apparently, in our study, high concentrations of CA solution also influenced ALP activity.

Conclusion

The results of the biochemical analysis of the culture medium reflect both the physiological and pathological state of hepatocytes under the action of a CA solution. Therefore, this method can be used in cell technologies to analyze the enzymatic activity of hepatocyte cultures. In particular, the determination of ALT and AST activity levels can be utilized to assess the degree of toxic effect, though AST, due to its features, was found to be more sensitive when exposed to a copper preparation. At the same time, the ALP activity level in this study did not serve as an indicator of the destructive processes in the hepatocyte culture, reflecting to a greater extent the interaction of the enzyme with copper ions. The analysis of the glucose content in the medium is applicable to estimating the metabolic activity of cells under the influence of the tested substance. In general, it can be concluded that the methods used allow us to assess the change in the balance between the death of hepatocytes and an increase in the energy metabolism, depending on the amount of copper ions in the medium.

Competing Interests

The authors declare that they have no competing interests.

References

1. Chow-Shi-Yée M, Grondin M, Ouellet F, Averill-Bates DA. Control of stress-induced apoptosis by freezing tolerance-associated wheat proteins during cryopreservation of rat hepatocytes. Cell Stress Chaperones. 2020 Nov;25(6):869-886. doi: 10.1007/s12192-020-01115-y.
2. Nahmias Y, Berthiaume F, Yarmush ML. Integration of technologies for hepatic tissue engineering. Adv Biochem Eng Biotechnol. 2007;103:309-29. doi: 10.1007/10_029.
3. Stanger BZ. Cellular homeostasis and repair in the mammalian liver. Annu Rev Physiol. 2015;77:179-200. doi: 10.1146/annurev-physiol-021113-170255.
4. Beckwitt CH, Clark AM, Wheeler S, Taylor DL, Stolz DB, Griffith L, Wells A. Liver 'organ on a chip'. Exp Cell Res. 2018 Feb 1;363(1):15-25. doi: 10.1016/j.yexcr.2017.12.023.
5. Shulman M, Nahmias Y. Long-term culture and coculture of primary rat and human hepatocytes. Methods Mol Biol. 2013;945:287-302. doi: 10.1007/978-1-62703-125-7_17.
6. Jeong H, Stika CS. Methods to study mechanisms underlying altered hepatic drug elimination during pregnancy. Semin Perinatol. 2020 Apr;44(3):151228. doi: 10.1016/j.semperi.2020.151228.
7. Sookoian S, Pirola CJ. Liver enzymes, metabolomics and genome-wide association studies: from systems biology to

the personalized medicine. World J Gastroenterol. 2015 Jan 21;21(3):711-25. doi: 10.3748/wjg.v21.i3.711.
8. Chesnokova NP, Ponukalina EV, Polutova NV. [Etiology, pathogenesis and metabolic signs of carbohydrate metabolism insufficiency in the liver]. Nauchnoe Obozrenie. Medicinskie Nauki. 2019;1:76-8. [Article in Russian].
9. Parahonskij AP. [The role of copper in the body and the significance of its imbalance]. Estestvenno-Gumanitarnye Issledovaniya. 2015;10(4):73-84. [Article in Russian].
10. Hewitt NJ, Lechón MJ, Houston JB, Hallifax D, Brown HS, Maurel P, Kenna JG, Gustavsson L, Lohmann C, Skonberg C, Guillouzo A, Tuschl G, Li AP, LeCluyse E, Groothuis GM, Hengstler JG. Primary hepatocytes: current understanding of the regulation of metabolic enzymes and transporter proteins, and pharmaceutical practice for the use of hepatocytes in metabolism, enzyme induction, transporter, clearance, and hepatotoxicity studies. Drug Metab Rev. 2007;39(1):159-234. doi: 10.1080/03602530601093489.
11. McGill MR. The past and present of serum aminotransferases and the future of liver injury biomarkers. EXCLI J. 2016 Dec 15;15:817-828. doi: 10.17179/excli2016-800.
12. Prasanna PL, Renu K, Valsala Gopalakrishnan A. New molecular and biochemical insights of doxorubicin-induced hepatotoxicity. Life Sci. 2020 Jun 1;250:117599. doi: 10.1016/j.lfs.2020.117599.
13. Khan HA, Ahmad MZ, Khan JA, Arshad MI. Crosstalk of liver immune cells and cell death mechanisms in different murine models of liver injury and its clinical relevance. Hepatobiliary Pancreat Dis Int. 2017 Jun;16(3):245-256. doi: 10.1016/s1499-3872(17)60014-6.
14. Josekutty J, Iqbal J, Iwawaki T, Kohno K, Hussain MM. Microsomal triglyceride transfer protein inhibition induces endoplasmic reticulum stress and increases gene transcription via Ire1α/cJun to enhance plasma ALT/AST. J Biol Chem. 2013 May 17;288(20):14372-14383. doi: 10.1074/jbc.M113.459602.
15. Lowe D, Sanvictores T, John S. Alkaline Phosphatase. 2021 Aug 11. In: StatPearls [Internet]. Treasure Island (FL): StatPearls Publishing; 2022 Jan–. PMID: 29083622.
16. Shaver WA, Bhatt H, Combes B. Low serum alkaline phosphatase activity in Wilson's disease. Hepatology. 1986 Sep-Oct;6(5):859-63. doi: 10.1002/hep.1840060509.

International Journal of Biomedicine 12(1) (2022) 63-66
http://dx.doi.org/10.21103/Article12(1)_ShC1

SHORT COMMUNICATION

INTERNATIONAL JOURNAL OF BIOMEDICINE

Leukocyte Shift Index and Subtypes of Acute Otitis Media in Children

Nadezhda E. Kuznetsova[1,2], PhD; Maria N. Ponomareva[1], PhD, ScD; Tatiana B. Kuznetsova[1]

[1]Tyumen State Medical University; [2]Tyumen Region Clinical Hospital №2
Tyumen, Russian Federation

Abstract

The aim of this research was to study the features of clinical and laboratory parameters of acute otitis media **(**AOM), taking into account the value of the leukocyte shift index (LSI) in pediatric patients with the demonstration of clinical cases.

***Methods and Results*:** This study included 100 children (55 boys and 45 girls) with AOM. The mean age of all patients was 4.32±0.31 years. Group 1 included 50 patients (30 boys and 20 girls) with acute suppurative otitis media (SupAOM). Group 2 included 50 patients (25 boys and 25 girls) with acute serous otitis media (SerAOM). As a marker for determining the activity of the inflammatory process and the disorders of the immunological reactivity of the body, we chose LSI, calculated taking into account the parameters of the general blood test. Our results show the diagnostic significance of LSI in predicting the clinical course of AOM in patients in the age group of 2-16 years. The development of SerAOM is predicted when the LSI is 1.05±0.08; SupAOM - 2.08±0.23

Conclusion:The results obtained can be useful in providing specialized medical care for children of this age group, for optimizing the algorithms for preventive examinations and therapeutic interventions, and for offering the possibility of predicting the severity of the disease and timely treatment of SupAOM requiring a surgical intervention followed by systemic antibiotic therapy in order to prevent otogenic complications and hearing.(**International Journal of Biomedicine. 2022;12(1):63-66.**)

Key Words: acute otitis media • leukocyte shift index • children

For citation: Kuznetsova NE, Ponomareva MN, Kuznetsova TB. Leukocyte Shift Index and Subtypes of Acute Otitis Media in Children. International Journal of Biomedicine. 2022;12(1):63-66. doi:10.21103/Article12(1)_ShC1

Abbreviations

AOM, acute otitis media; **LSI**, leukocyte shift index; **SerAOM**, acute serous otitis media; **SupAOM**, acute suppurative otitis media; **ICC**, intracranial complication.

Introduction

In recent years, the number of patients with acute otitis media (AOM) has increased, accounting for 75.1% - 80% of all diseases of the middle ear.[1] A study has shown that in the Russian Federation, acute serous otitis media (SerAOM) (ICD-10-CM Code H65.07) and acute suppurative otitis media (SupAOM) (ICD-10-CM Code H66.019) are the main causes of hearing loss in children aged 2-5 years.[2] The growth of otogenic complications in children amounts to one case of intracranial complication (ICC) per 350-450 cases of inflammatory diseases of the middle ear. The mortality rate for ICC ranges from 5% to 50%.[3,4] Despite the achievements of modern medicine, the otogenic ICC in purulent-inflammatory diseases of the ear in children remain relevant subjects for research.[5]

The aim of this research was to study the features of clinical and laboratory parameters of AOM, taking into

***Corresponding author:** Nadezhda E. Kuznetsova, PhD. Tyumen State Medical University. Tyumen, the Russian Federation. E-mail: e-mail: kne61@mail.ru*

account the value of the leukocyte shift index (LSI) in pediatric patients with the demonstration of clinical cases.

Materials and Methods

This study included 100 children (55 boys and 45 girls) with AOM. The mean age of all patients was 4.32±0.31 years. All patients were treated in the department of pediatric otolaryngology at the Regional Clinical Hospital No.2 of Tyumen in the period from 2018 to 2020. Group 1 included 50 patients (30 boys and 20 girls) with SupAOM. Group 2 included 50 patients (25 boys and 25 girls) with SerAOM.

As a marker for determining the activity of the inflammatory process and the disorders of the immunological reactivity of the body, we chose LSI, calculated taking into account the parameters of the general blood test.[6,7] LSI = (eosinophils + basophils + myelocytes + metamyelocytes + stabs + segmented neutrophils) / (monocytes + lymphocytes). The LSI value of 1.96±0.56 is considered normal.[6]

All children were admitted on an emergency basis with complaints of earache, headaches, unilateral or bilateral hearing loss, hyperthermia, anxiety, sleep disturbance, and speech development disorders. All children were examined by an otorhinolaryngologist, pediatrician, as well as by a neurologist, anesthesiologist, neurosurgeon, and audiologist according to the indications.

Upon admission, patients underwent clinical and laboratory diagnostics, radiography, and CT of the temporal bones and paranasal sinuses. CT or MRI with contrast was performed for diagnostic purposes to exclude ICI. Children of Group 1 underwent surgical treatment (myringotomy), which was supplemented with antromastoidotomy, according to the indications. All received a course of antibiotic therapy and local therapy.

Statistical analysis was performed using the statistical software STATISTICA (v10.0, StatSoft, USA). The normality of distribution of continuous variables was tested by one-sample Kolmogorov-Smirnov test. Continuous variables were presented as mean±SEM. Means of 2 continuous normally distributed variables were compared by independent samples Student's t test. A value of $P<0.05$ was considered significant.

The study was conducted in accordance with ethical principles of the WMA Declaration of Helsinki (1964, ed. 2013) and approved by the Tyumen State Medical University Ethics Committee. Written informed consent was obtained from the parent/guardian of each patient.

Results

A comparative analysis of LSI in the studied groups revealed significant fluctuations in this indicator from 0.77 to 3.8 in Group 1 and from 0.33 to 2.56 in Group 2. In the age subgroup of 13-16 years, SupAOM was detected in one patient and SerAOM in 4 cases. LSI levels in the patients (n=41) from 2 to 16 years of Group 1 were 2.08±0.23, and of Group 2 (n=47), 1.05±0.08 ($P=0.0001$). In Groups 1 and 2, LSI values in the age groups of 2-5 years were 2.19±0.28 and 1.00±0.07 ($P=0.0001$), respectively; in the age groups of 6-12 years, 2.98±0.82 and 1.07±0.17 ($P=0.0435$), respectively (Table 1).

Table 1.
LSI values in Croups 1 and 2 according to the age subgroups

Age subgroups (yrs)	Mean age		LSI		*P*-value
	Group 1 n=50	Group 2 n=50	Group 1 n=50	Group 2 n=50	-
0-1	0.83±0.09 n=9	0.83±0.20 n=3	1.20±0.43 n=9	0.77±0.44 n=3	0.5022
2-5	3.29±0.17 n=34	3.69±0.20 n=35	2.19±0.28 n=34	1.00±0.07 n=35	0.0001
6-12	6.50±0.37 n=6	8.63±0.86 n=8	2.98±0.82 n=6	1.07±0.17 n=8	0.0435
13-16	13.0 n=1	14.50±0.75 n=4	1.04 n=1	1.64±0.92 n=4	-

P-value between LSI (Group1 and Group 2)

LSI levels are affected by the characteristics of the physiological state of neutrophils and lymphocytes, depending on age (the first cross at 5 days and the second at 5 years); obviously, this circumstance explains the absence of statistically significant differences between Groups 1 and 2 in children aged between 0 and 2 years ($P>0.05$).

Currently, the use of LSI for predicting SupAOM in children has enough grounds for clinical use in practical healthcare, and widespread implementation in the algorithms of preventive examinations. Domestic scientists have shown the role of LSI in assessing the body's immunological reactivity, the severity of endogenous intoxication, and its complications.[7,8] The results obtained in our study indicate that in children aged between 2 and 16 years, the LSI levels of 1.05±0.08 and 2.08±0.23 can suggest the formation of SerAOM and SupAOM, respectively.

In addition, the possibility of early diagnosis of the purulent process in the middle ear, both at the outpatient stage of diagnosis and upon admission to the ENT department of a children's hospital, is very important. The availability of the LSI assessment, its information content in the absence of expensive diagnostic methods (multispiral CT, tympanometry, otomicroscopy) allows performing timely diagnosis, surgical treatment, and the necessary antibiotic therapy to prevent otogenic complications.

Case Presentation 1

An 11-year-old boy was admitted on 07.18.2019 to the department of pediatric otolaryngology for emergency indications. Complaints: pain in the left ear, fever up to 38.0°C.

Anamnesis morbid

The child fell ill on 07.15.19. Outpatient treatment (amoxicillin, otipax) was prescribed by an ENT doctor.

Anamnesis vitae

Child from second full-term pregnancy, body weight at birth – 4200g. The patient grew and developed according to his age. Scheduled vaccinations. Past diseases: acute respiratory infections, chickenpox, bronchitis, tonsillitis, pneumonia. History of allergies is not burdened. History of allergies is not burdened.

Clinical Findings, Diagnostic Assessment, and Treatment

General condition of moderate severity. Consciousness is clear. Body temperature - 38.0°C. The respiratory rate – 21 breaths per minute. The heart rate is 84 bpm. The abdomen is soft; the liver and spleen are not palpable. Urination is not disturbed. The stool is normal.

Local status

Nose: without features.

Oropharynx: mucous membranes are pink and edematous; the pharynx is symmetrical; the soft palate is mobile, with no plaque.

Larynx: sonorous voice, free breathing.

Ears: Tympanic membrane of AD is grey, the cone of light is preserved; tympanic membrane of AS is hyperemic, infiltrated, the cone of light is not preserved.

Standard laboratory diagnostic methods are performed. General blood test (07.18.2019): Segmented Neutrophils – 67%, Stabs - 5%; Basophils - 1%; Lymphocytes - 20%; Monocytes - 7%; Eosinophils -1%, Platelets 126×10^9/L, Hemoglobin 137 g/L; Erythrocytes 5.13×10^{12}/L, Leukocytes 8.71×10^9/l. LSI=2.7.

LSI=2.7.

Ophthalmologist's examination, "Acute suppurative left-sided non-perforated otitis media."

Treatment: Paracentesis of the left tympanic membrane (of 07.18.2019) followed by conservative therapy.

Local status at discharge (07.26.2019).

Otoscopy: AS - the ear canal is free, the tympanic membrane is gray, the identification marks are distinguishable; AD - the ear canal is free, the tympanic membrane is gray, the identification marks are distinguishable.

This clinical case indicates that the value of LSI of 2.08 is associated with the development of an acute purulent process, requiring a surgical intervention followed by systemic antibiotic therapy.

Case Presentation 2

A 12-year-old girl was admitted on 08.17.2020 to the department of pediatric otolaryngology for emergency indications. Complaints: hearing loss.

Anamnesis morbid

The child was sick for 3 months; against the background of frequent colds, hearing loss appeared. Conservative treatment without effect. Tympanogram (07.28.2020): type C/ type B.

Anamnesis vitae

The patient grew and developed according to his age. Scheduled vaccinations. Past diseases: acute respiratory infections, otitis media, chickenpox, bronchitis, tonsillitis, paracentesis of the eardrums on both sides (07.03.2020). History of allergies is not burdened.

Clinical Findings, Diagnostic Assessment, and Treatment

General condition of moderate severity. Consciousness is clear. Body weight - 53 kg, height - 158 cm. The respiratory rate – 22 breaths per minute, saturation - 100%. The heart rate is 98 bpm. The abdomen is soft; the liver and spleen are not palpable. Urination is not disturbed. The stool is loose.

Local status

Nose: without features. Oropharynx: mucous membranes are moist and pink; the pharynx is symmetrical; the soft palate is mobile, with no plaque.

Larynx: sonorous voice, free breathing.

Ears: Tympanic membrane of AD is gray-cloudy, retracted, the contours are poorly distinguishable; tympanic membrane of AS gray-cloudy, retracted, the contours are poorly distinguishable. Whispered speech: AD/AS - 6 m /4 m.

Standard laboratory diagnostic methods are performed. General blood test (08.17.2020): Basophils - 1%; Neutrophils - 46.8%; Lymphocytes - 40.2%; Monocytes - 8.9%; Eosinophils -3.1%.

LSI=1.04.

Ophthalmologist's examination, "Acute left-sided serous otitis media."

Treatment: Conservative therapy.

Local status at discharge (08.20.2020).

Otoscopy: AS - the ear canal is free, the tympanic membrane is gray, the identification marks are distinguishable; AD - the ear canal is free, the tympanic membrane is gray, the identification marks are distinguishable. Whispered speech: AD/AS - 6 m / 6 m.

This clinical case indicates that the value of LSI of 1.04 is associated with the development of an acute serous otitis media.

Conclusion

This study demonstrates the diagnostic significance of LSI in predicting the clinical course of acute otitis media in patients in the age group of 2-16 years. The development of acute serous otitis media is predicted when the LSI is 1.05±0.08; acute suppurative otitis media - 2.08±0.23

The results obtained can be useful in providing specialized medical care for children of this age group, for optimizing the algorithms for preventive examinations and therapeutic interventions, and for offering the possibility of predicting the severity of the disease and timely treatment of acute suppurative otitis media requiring a surgical intervention followed by systemic antibiotic therapy in order to prevent otogenic complications and hearing loss.

Competing Interests

The authors declare that they have no competing interests.

References

1. Garashchenko TI, Kozlova RS. [Acute otitis media in children. Prejudices of pharmacotherapy]. Detskaya Otorinolaringologiya. 2013;(3):31-36. [Article in Russian].
2. Yablonsky SV. [Modern approaches to the diagnosis and treatment of middle ear diseases in children]. Rossiyskaya Otorinolaringologiya. 2004;(4):91-99. [Article in Russian].
3. Yakovlev VN, Kunelskaya NL, Yanyushkina ES. [Exudative otitis media]. Vestnik Otorinolaringologii. 2010;(6):77-80. [Article in Russian].
4. Kuznetsova NE, Sinyakov AYu, Veshkurtseva IM, Kuznetsova TB. [The nature of intracranial complications in purulent-inflammatory pathology of the ear in children]. Scientific-Practical Conference "Modern aspects of head and neck surgery." 2019:17-18. [Article in Russian].
5. Kuznetsova NE, Mamedov RR, Shcherbakova AF. Prevalence of otitis media with effusion in children. International Journal of Biomedicine. 2020;10(1):86-88. doi: 10.21103/Article10(1)_ShC1
6. Ivanov DO, Shabalov NP, Shabalova NN, Kurzina EA, Kostyuchek IN. [Leukocyte indices of cellular reactivity as an indicator of the presence of hypo- and hyperergic variants of neonatal sepsis]. Available from: http://www.medlinks.ru/article.php?sid=22330.[Article in Russian].
7. Mustafina ZhG, Kramorenko IuS, Kobtseva VIu. [Integral hematological indices in assessing body immunological reactivity in patients with ophthalmic pathology]. Klin Lab Diagn. 1999 May;(5):47-9. [Article in Russian].
8. Speransky II, Samoilenko GE, Lobacheva MV. [Complete blood count - are all of its possibilities exhausted? Integral indices of intoxication as criteria for assessing the severity of endogenous intoxication, its complications, and the effectiveness of treatment]. Acute and Emergency Conditions in the Practice of a Doctor. 2009.19(6):5. [Article in Russian].

International Journal of Biomedicine 12(1) (2022) 67-69
http://dx.doi.org/10.21103/Article12(1)_ShC2

SHORT
COMMUNICATION

INTERNATIONAL
JOURNAL
OF BIOMEDICINE

Efficiency of High-Resolution MRI at Different Stages of Subchondral Insufficiency Fracture of the Knee

Akeksandr Ivankov*; Pavel Seliverstov, PhD, ScD

Irkutsk Scientific Center of Surgery and Traumatology
Irkutsk, the Russian Federation

Abstract

The history of subchondral insufficiency fracture is closely related to a pre-existing diagnosis of spontaneous osteonecrosis of the knee (SONK). Previously, it was thought that subchondral linear or lunate pathological changes on magnetic resonance imaging (MRI) scans in elderly patients with a history of osteoporosis are the result of spontaneous osteonecrosis, but in the 2000s, studies by T. Yamamoto showed that a small proportion of patients with osteonecrosis of the femoral head initially have a fracture of insufficiency that gets complicated by secondary osteonecrosis. Subsequent studies of SONK also showed that the subchondral insufficiency fracture is precisely the initial process, osteonecrosis is secondary and it is a complication of the fracture. The aim of our study was to evaluate the effectiveness of high-resolution MRI at different stages of this disease.(**International Journal of Biomedicine. 2022;12(1):67-69.**)

Key Words: high-resolution MRI • osteoporosis • knee

For citation: Ivankov A, Seliverstov P. Efficiency of high-resolution MRI at different stages of subchondral insufficiency fracture of the knee. International Journal of Biomedicine. 2022;12(1):67-69. doi:10.21103/Article12(1)_ShC2

Introduction

Insufficiency fracture is a type of stress fracture that usually occurs in individuals over 50-55 years of age with normal joint stress. The reason for this fracture is the weakening of the trabeculae of the subchondral bone marrow of any condyle of the knee joint, more often the medial one.[1-4] The history of the diagnosis of insufficiency fracture is associated with the fact that in a number of cases, researchers led by T. Yamamoto[5] found a non-classical diagnostic picture when osteonecrosis of the femoral head was suspected, which later turned out to be an insufficiency fracture. And subsequent studies by T. Yamamoto et al.[5-7] showed that in the knee joint, in patients with a presumed diagnosis of spontaneous osteonecrosis, the insufficiency fracture was the initial process resulting from the weakening of trabeculae in the subchondral bone, and osteonecrosis was a secondary and optional process. It should be noted that at the initial stages of insufficiency fracture, the process is not complicated with early treatment of the patient, and osteonecrosis and subchondral collapse (flattening of the articular surface) are secondary and, in fact, they are a complication of the insufficiency fracture itself.[8] The main methods for diagnosing subchondral insufficiency fracture are primary radiography and MRI.[9] X-ray of the knee joint has limited capabilities since it does not allow visualization of the edema and the area of subchondral fracture at the early and advanced stages of the process.[9] In this case, the MRI is the method of choice since it has more possibilities for assessing the state of the bone and soft tissues of the joint.[9]

MRI-semiotics

Diagnostic MRI criteria for subchondral insufficiency fracture include diffuse bone marrow edema of the affected articular condyle[8,10] (Fig.1), hypointense fracture line on T1-WI and fluid-sensitive modes (T2- and PD with fat suppression – FS) (Fig.2), hypointense "thickening" on T1- and PD-FS (T2-FS) in the area of the cortical bone layer (Fig.3). In the presence of complications in the form of secondary osteonecrosis in the area of subchondral fracture, there is a risk of collapse (flattening) of the articular surface of the affected condyle of the joint. The area of secondary osteonecrosis on liquid-sensitive tomograms PD-FS (T2-FS) is visualized as an

***Corresponding author:** Aleksandr Ivankov, Irkutsk Scientific Center of Surgery and Traumatology. Irkutsk, Russia. E-mail:ivankovap16@gmail.com*

area of increased signal in the area between the fracture line and the subchondral cortical bone layer[10] (Fig.4). Subchondral collapse (flattening) of the affected articular surface is shown in Figure 5.

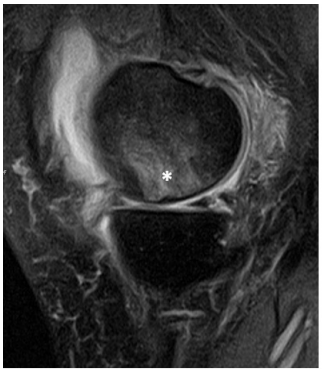

Fig. 1. *MRI (PD-FS). Subchondral edema in the fracture zone (asterisk).*

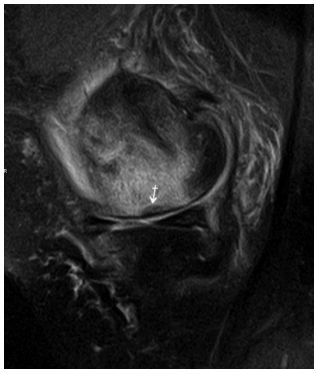

Fig. 2. *MRI (PD-FS). Insufficiency fracture. Fracture line (arrow)*

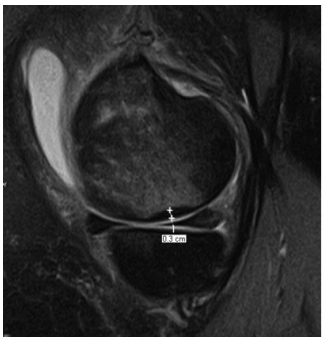

Fig. 3. *MRI (PD-FS). Insufficiency fracture. Hypointense "thickening" (measured).*

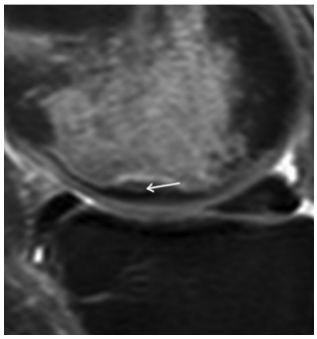

Fig. 4. *MRI (PD-FS). The area of increased signal (zone of secondary osteonecrosis).*

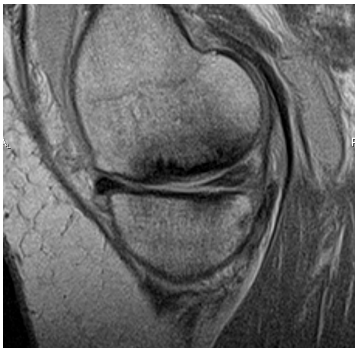

Fig. 5. *MRI (PD-WI). Insufficiency fracture. Subchondral collapse of the weight-bearing aspect femoral condyle.*

Materials and Methods

We studied 150 patients with subchondral insufficiency fracture at different stages of the process. For the purpose of clinical control of the diagnosis, the patients underwent control MRI after 3 months with a second consultation with an orthopedist. MRI was performed on a 1.5T MRI machine (Toshiba) using a 4-channel knee coil. Scanning parameters: PD-, PD-FS, T1-WI, coronal, sagittal, and axial plane, matrix 288x384, FOV 15 cm. An early stage of subchondral fracture was found in 39 patients (up to 3-4 days from the onset of the disease), 82 patients had an advanced stage of the disease, and 29 patients had a stage of complications. The ratio of men to women was almost equal - 48% men and 52% women. The average age of the studied patients was 63.1 (range 51-89 years) years. The standard formulas were used to calculate the sensitivity, specificity, and accuracy of the MRI method at an early stage, an advanced stage, and a stage of complications.

Results

The most common localization of insufficiency fracture in the knee was the medial condyle of the femur (79,3%), the second most frequent was the lateral condyle of the femur - 12%; 8,0% of lesions were localized in the medial parts of the tibial plateau and only 0,6% in the lateral parts of the tibial plateau. Localization of insufficiency fractures was predominantly central (coronary scans) - 76.5%, in the peripheral regions in 23.5% of patients. On sagittal tomograms, the fracture zone was also localized mainly centrally (middle third of the condyle) - 81.4%, in 17.6% of patients in the posterior parts of the condyle, and only 1% in the anterior third of the condyle. Synovitis was also found in 100% of cases in patients with insufficiency fracture and perifocal edema of the surrounding soft tissues in 91% of cases. Quite often, a fracture of insufficiency was combined with a rupture of the meniscus; in our survey, 91.3% of patients had a rupture of the adjacent meniscus, more often the medial one (78.2%). The chondromalacia zone (Noyes) of the adjacent articular surface was found in 96.7% of patients.

The information content of the MRI study consisted of the calculation of the sensitivity, specificity, and accuracy of the method at three stages: early stage, advanced stage, and at the stage of complications. The survey gave the following results (Table 1).

Table 1.

The informativeness of MRI at different stages of subchondral insufficiency fracture

Criteria	Early stage	Advanced stage	Stage of complications
Sensitivity	97.2%	100%	96.0%
Specificity	66.6%	75.0%	75.0%
Accuracy	94.8%	98.7%	93.1%

Thus, at an early stage in the presence of subchondral edema and the formation of a fracture line, there is some risk of an erroneous diagnosis since posttraumatic condyle contusion and transient osteoporosis of the knee condyle have a similar MRI picture; therefore, the sensitivity of MRI at this stage is very high, but the specificity does not show such high numbers.

At the stage of complications, there is a risk of a false-positive result because subchondral collapse of the affected condyle can be the outcome of osteoarthritis or acute impression fracture. Therefore, the specificity of the MRI method at the stage of complications is not so high.

In general, as shown in the table, the informativeness of the MRI method is rather high at different stages of subchondral insufficiency fracture.

In conclusion, subchondral insufficiency fracture of the knee is an urgent medical problem that requires high-quality early diagnosis. The method of choice for subchondral insufficiency fracture is a high-resolution MRI of the knee joint, which demonstrates high sensitivity, specificity, and accuracy.

Competing Interests

The authors declare that they have no competing interests.

References

1. Allam E, Boychev G, Aiyedipe S, Morrison W, Roedl J, Singer A, et al. Subchondral insufficiency fracture of the knee: unicompartmental correlation to meniscal pathology and degree of chondrosis by MRI. Skeletal Radiol. 2021 Nov;50(11):2185-2194. doi: 10.1007/s00256-021-03777-w.
2. Barras LA, Pareek A, Parkes CW, Song BM, Camp CL, Saris DBF, Stuart MJ, Krych AJ. Post-arthroscopic Subchondral Insufficiency Fractures of the Knee Yield High Rate of Conversion to Arthroplasty. Arthroscopy. 2021 Aug;37(8):2545-2553. doi: 10.1016/j.arthro.2021.03.029.
3. Saber M. Subchondral insufficiency fracture of the knee. Radiopaedia. 2021. Available from: https://radiopaedia.org/articles/subchondral-insufficiency-fracture-of-the-knee?lang=us
4. Nicoletti D. Subchondral insufficiency fracture - knee. Radiopaedia. 2021. Available from: https://radiopaedia.org/cases/subchondral-insufficiency-fracture-knee?lang=us
5. Yamamoto T, Bullough PG. Spontaneous osteonecrosis of the knee: the result of subchondral insufficiency fracture. J Bone Joint Surg Am. 2000 Jun;82(6):858-66. doi: 10.2106/00004623-200006000-00013.
6. Yamamoto T, Schneider R, Bullough PG. Insufficiency subchondral fracture of the femoral head. Am J Surg Pathol. 2000 Mar;24(3):464-8. doi: 10.1097/00000478-200003000-00017.
7. Yamamoto T, Iwamoto Y, Schneider R, Bullough PG. Histopathological prevalence of subchondral insufficiency fracture of the femoral head. Ann Rheum Dis. 2008 Feb;67(2):150-3. doi: 10.1136/ard.2006.066878.
8. Lee S, Saifuddin A. Magnetic resonance imaging of subchondral insufficiency fractures of the lower limb. Skeletal Radiol. 2019 Jul;48(7):1011-1021. doi: 10.1007/s00256-019-3160-4.
9. Expert Panel on Musculoskeletal Imaging:, Bencardino JT, Stone TJ, Roberts CC, Appel M, Baccei SJ, Cassidy RC, et al. ACR Appropriateness Criteria® Stress (Fatigue/Insufficiency) Fracture, Including Sacrum, Excluding Other Vertebrae. J Am Coll Radiol. 2017 May;14(5S):S293-S306. doi: 10.1016/j.jacr.2017.02.035.
10. Gorbachova T, Melenevsky Y, Cohen M, Cerniglia BW. Osteochondral Lesions of the Knee: Differentiating the Most Common Entities at MRI. Radiographics. 2018 Sep-Oct;38(5):1478-1495. doi: 10.1148/rg.2018180044.

Online-Only Articles

International Journal of Biomedicine 12(1) (2022) 70-81
http://dx.doi.org/10.21103/Article12(1)_GE

Guest Editorial

INTERNATIONAL JOURNAL OF BIOMEDICINE

Role of Biomolecules and Biologics in Precision Medicine, Personalized Medicine, and Emerging Therapies

Gundu H. R. Rao*, Emeritus Professor

Laboratory Medicine and Pathology
Director of Thrombosis Research, Lillehei Heart Institute
University of Minnesota, Minneapolis, USA

Abstract

In the 1990s, DNA sequencing technologies could only read bite-sized pieces of DNA. Then came the human genome project (HGP), a thirteen-year international effort, 1990-2003, with the primary goal of discovering the complete set of human genes, sequencing nucleotides, and making the information accessible worldwide for further biological studies. We have come a long way since that time in terms of sequencing the genes of the human genome. Now the researchers can sequence the DNA and analyze gene-expressed proteins in individual cells, allowing them to dissect the complexities of genetic diseases with exceptional details. Currently, technologies are available for single-cell or multi-omics platforms to analyze genotype and phenotype. The completion of this one-of-a-kind project created public expectations for immediate, better health care delivery and possible cures for 'so called' incurable diseases. The HGP was the single most influential investment made in modern basic science research. A monumental breakthrough in medicine has given us the ability to sequence the DNA in cancer cells to identify possible errors in mutations. The impact of the HGP's success was so significant that President Barack Obama initiated a very ambitious new 'precision medicine' research initiative and announced the launch of this project during his State of the Union Address in 2015. The benefits of precision and personalized medicine include predicting susceptibility to diseases, improving disease diagnostics, preempting disease progression, customizing disease prevention strategies, and developing personalized drugs and therapies. As examples of emerging therapies, we have discussed the role of biomolecules and biologics in precision medicine applications like 'The All of Us,' personalized medicine approaches for monogenic diseases like hemophilia, sickle cell disease, and other rare genetic disorders, and CRISPR gene-editing technologies. Biomolecules play an essential role in all life processes, a variety of signaling processes, which are vital for normal functioning of physiological responses, in the early diagnosis of risk factors for various diseases, in the development of diseases and their progress. Furthermore, biomolecules, RNAs, DNAs, molecular and cellular engineering, genetic engineering of biologics, cells, tissues, and organs, play an important role in emerging therapeutic applications. The majority of the therapies discussed in this review are regulated as biologics under the Public Health Services Act of the USA. There is great interest in developing targeted therapy or precision medicine therapy for monogenic diseases, organ transplant applications, and tumor management, designed to interfere with targeted molecules for cancer-causing genes to slow the spread of cancer cells. Because molecular engineering, the development of biologics, gene-editing applications, and biomanufacturing are key components of emerging therapies, a keynote series was organized at INTERPHEX in November of 2021. INTEPHEX is the premier event that offers the latest intelligence, cutting-edge technologies, and state-of-the-art innovation for product development for pharmaceutical and biotechnology platforms. In an earlier article in this journal, we described drug discovery and development in the COVID Age; this overview provides a birds-eye view of the salient findings in each emerging area of medicine—precision medicine, personalized medicine, and emerging therapies.(**International Journal of Biomedicine. 2022;12(1):70-81.**)

Key Words: biomolecules • precision medicine • personalized medicine • emerging therapies

For citation: Rao GHR. Role of Biomolecules and Biologics in Precision Medicine, Personalized Medicine, and Emerging Therapies. International Journal of Biomedicine. 2022;12(1):70-81. doi:10.21103/Article12(1)_GE

Abbreviations

3BP, 3-bromopyruvate; **ADAR1**, RNA-specific adenosine deaminase 1; **AT**, ataxia-telangiectasia; **ATTR**, Transthyretin amyloidosis; **BRCA**, BReast CAncer genes; **Cop 1**, constitutive photomorphogenesis protein 1; **CAD,** chronic allograft damage; **CAR-T cells,** chimeric antigen receptor T cells; **CSD2**, superoxide dismutase; **CTGF**, connective tissue growth factor; **CAFs,** cancer associated

fibroblasts; **CRISPR**, clustered regularly interspersed sort palindromic repeats; **COPD**, chronic obstructive pulmonary disease; **CPFE**, combined pulmonary fibrosis and emphysema; **DNA**, deoxyribonucleic acid; **DYRKIA**, dual specificity tyrosine-(Y)-phosphorylation regulated kinase 1A; **EMT**, epithelial-mesenchymal transition; **EGF**, epidermal growth factor; **FGF**, fibroblast growth factor; **FAM13A**, family with sequence similarity 13 member A; **GFP**, green fluorescent protein; **GRIN2B**, glutamate ionotropic receptor NMDA type subunit 2B; **HGP**, Human Genome Project; **HGF**, hepatocyte growth factor; **HER2**, human epidermal growth factor receptor 2; **HIF**, hypoxia-inducible factor; **HDR**, homology-directed repair; **IRF4**, interferon regulatory factor 4; **IGF**, insulin-like growth factor; **IL6**, interleukin 6; **IPF**, idiopathic pulmonary fibrosis; **Kras**, Kirsten rat sarcoma viral oncogene homolog; **mRNA**, messenger RNA; **miRNA**, microRNA; **MAPK**, mitogen-activated protein kinase; **MLL**, mixed lineage leukemia; **NF-kB**, nuclear factor kappa B; **NHEJ**, non-homologous end joining; **NCI**, national cancer institute; **PDGF,** platelet-derived growth factor; **PTPN2**, protein tyrosine phosphatase non-receptor type 2; **PML-RARa,** promyelocytic leukemia-retinoic acid receptor α; **PD-1**, programmed cell death protein-1; **PDL1,** programmed death ligand-1; **PI3K**. phosphoinositide 3-kinase; **Pou2af**, POU class 2 homeobox associating factor coding gene; **RNA**, ribonucleic acid; **RRM2**, ribonucleotide reductase regulatory subunit M2; **RAS-MAPK,** Ras/mitogen activated protein kinase; **SNPs,** single nucleotide polymorphisms; **Sc4mol**, gene encoding a methyl sterol oxidase; **STAT**, signal transducer and activator of transcription; **sgRNA**, single-guide RNA; **TME**, tumor microenvironment; **TFs**, transcription factors; **TOLLIP**, toll-interacting protein; **VEGF**, vascular endothelial growth factor; **XBP1**, X-box binding protein 1.

Introduction

The unprecedented pandemic of coronavirus disease has created unfathomable healthcare and economic crisis worldwide.[1-4] According to healthcare experts, over 1400 pathogens are capable of infecting humans, of which 500 are capable of human-to-human transmission of pathogens.[5] Just over two decades ago, the Nobel Laureate Joshua Lederberg wrote, "The future of humanity and microbes likely will unfold as episodes of a suspense thriller,"- that could be titled 'Our Wits and Their Genes.'[6] We did not have to wait for a distant future. It looks like the SARS-CoV-2 genes have done it. They have evolved from a simple respiratory virus to a highly transmissible killer virus. The 1918 Influenza virus epidemic was considered the 'Mother of All Pandemics,' as it caused greater than 50 million deaths.[7] Since that time, a major question has been lurking in the minds of researchers. What makes some viruses so fatal? Have some critical viral genetic events produced a virus of remarkable pathogenicity? For instance, of the various variants of coronavirus that have appeared, the delta variant so far seems to be more virulent than the others. On the other hand, the new variant Omicron with over 50 mutations seems to be more infectious than delta and relatively less dangerous. Maybe natural selection prefers the survival of the species better than the severity of the disease. The authors of a seminal article on Spanish Influenza concluded, "Even with modern antiviral and antibacterial drugs, vaccines, and prevention knowledge, the return of a pandemic virus equivalent in the pathogenicity to the virus of 1918 would likely kill >100 million people worldwide."[7] Luckily for us, this prediction has not come true so far, despite the high transmissibility and pathogenicity of the coronavirus (nCoV-2).

SARS-CoV-2 (COVID-19) pandemic is an unusual, singular disaster - it made the world realize the seriousness of this public health crisis. Since it was identified in Wuhan, China (December 2019), SARS-CoV-2 is continuously evolving into different strains and spread worldwide. Global public health experts were totally unprepared for this magnitude of spread and destruction. However, it also helped the Governments, philanthropies, academicians, pharma companies to channel huge sums of money and efforts toward COVID-19 research. The unprecedented coronavirus pandemic also gave tremendous opportunities for drug discovery and development. Professor Cody Meissner at Tufts University School of Medicine in Boston says, "It is absolutely astonishing that this happened (Operation Warp Speed; development of Covid vaccines) in such a short time—to me, it is equivalent to putting a person on the Moon." "This is going to change vaccinology forever."[8,9] In the early days of the outbreak of this virus, Chinese researchers revealed the genomic information of the virus implicated in the Wuhan pneumonia outbreak. Scientists at Moderna Biotech, specializing in messenger RNA (mRNA) research, were able to design a vaccine on paper in 48 hours, 11 days before the US even had its first recorded Covid case. Within six weeks, Moderna had doses of vaccine ready for testing in animals. It is worth mentioning here the significant contributions of the US National Institutes of Health; Dr. Graham and Dr. McLellan of Vaccine Research Center, Bethesda, Maryland; Dr. Drew Weismann of Perelman School of Medicine, University of Pennsylvania; and Dr. Katalin Kariko of BioNTech, Germany, for the eventual success of mRNA vaccine development. COVID-19 pandemic and the discovery of mRNA vaccines, to a great extent, have eclipsed the news about all other current innovative research and innovations. In this overview, we will briefly review some milestones in the development of bioactive molecules, biologics, cellular and molecular therapeutics, genetically modified molecules, cells, tissues, organs, and the use of gene-editing tools in precision medicine, personalized medicine, and emerging therapies.

RNA Therapies

Among biomolecules, nucleic acids, namely DNA and RNA, have the unique function of storing an organism's genetic code, which is critical for the sustenance of life. Researchers from the Houston Methodist Research Institute, Texas, have reviewed the limitless future of RNA therapeutics.[9] According to them, RNA therapeutics comprise a rapidly expanding category of drugs (biologics) that will change the standard care for many diseases and actualized personalized medicine. They further emphasize that the drugs are cost-effective, relatively

simple to manufacture, and can target undruggable pathways. There are several cell-based therapies, which use mRNAs for the expression of desired proteins, and have reached clinical trials. The RNAs can also be designed to serve as gene-editing tools to achieve the expression of desired proteins. RNA therapy involves the use of coding RNA such as mRNA or RNAs such as noncoding small interfering RNAs (siRNA), antisense oligonucleotides (ASO), to target mRNA and clustered short palindromic repeats (CRISPR/Cas) endonuclease to target DNA and proteins. Rapid development in this technology has resulted in the approval, in both the USA and Europe, of two RNA-based therapies, for the treatment of hereditary ATTR amyloidosis, a progressive, potentially fatal disorder. Several miRNAs have recently been found to regulate adipose tissue biology, to promote metabolic diseases, muscle biology, insulin secretion, and action. Their altered expression may play a role in the development of obesity, metabolic disorders, and their clinical complications.[10] We are interested in exploring the role of miRNAs in the development of metabolic risks, such as oxidative stress (miR34a, miR638, miR150-3p), inflammation (miR27a, miR146a, miR155), endothelial dysfunction (miR29, miR126a-3p), subclinical atherosclerosis (miR121), diabetes-related clinical complications such as peripheral neuropathy (miR146a), retinopathy (miR21, miR124, miR200), nephropathy (miR29c), various vasculopathies (miR200b, miR200c, miR503), as well as fetal reprogramming of adipose tissue biology. We and others hope that this emerging technology will rapidly develop innovations in RNA therapies, facilitate the cost-effective manufacture of therapeutic products, validate them for clinical effectiveness, and provide safe and effective therapeutics to the clinic. The ability to rapidly develop or alter the sequence of the mRNA construct for personalized treatments or to adapt to an evolving pathogen (COVID) makes them unique therapeutics of the future.

Precision Medicine

President Obama announced a research initiative that aims to accelerate progress toward a new era of precision medicine in January of 2015, with the following announcement: "Tonight, I am launching a new Precision Medicine Initiative to bring us closer to curing diseases like cancer and diabetes — and to give all of us access to the personalized information we need to keep ourselves and our families healthier." The proposed initiative has two main components: a near-term focus on cancers and a longer-term aim to generate knowledge applicable to the whole range of health and disease. The initiative is supposed to tap into converging trends of increased connectivity, through social media and mobile devices, and Americans' growing desire to be active partners in medical research.[11,12] Authors describe, "The convergence of genetics, informatics, and imaging, along with other technologies such as cell sorting, epigenetics, proteomics, and metabolomics, is rapidly expanding the scope of precision medicine by refining the classification of disease, often with important prognostic and treatment implications." Despite the growing knowledge in a variety of related areas, our ability to harness the vast amounts of new knowledge and treatment options with the framework of everyday clinical practice poses a huge challenge. The accumulation of huge amounts of data, which is collected and shared through machines and machine learning applications, must be processed by data analysts, in a way, that brings value and accuracy. There is a great need to build a multidisciplinary team to process such massive research and clinical data.

What are some concerns about such 'Top-Down" approaches? The All of Us Research Program plans to enroll a diverse group of at least 1 million persons in the United States to accelerate biomedical research and improve health.[13] The program aims to make the research accessible to all participants, and it is developing new approaches to generate, access, and make data broadly available to approved researchers. As of 2019, more than 175,000 participants have contributed biospecimens. The All of Us data repository should permit researchers to consider individual differences in lifestyle, socioeconomic factors, environment, and biological characteristics, to advance the precision diagnosis, prevention, and treatment. The major weakness of The All of Us program is it does not focus on any particular set of diseases or health status. Whereas, the investigators of this study cited in support of their approach, the success of international studies such as the U.K. Biobank, the Million Veteran Program, the China Kadoorie Biobank, and other research groups, which have shown the power of very large cohorts for biomedical discovery. The investigators accept the general concern that the translation of biological and environmental discoveries into improved health is unlikely to occur quickly. Since 2015, Congress has allocated 1.02 billion to the All of Us program. The 21st Century Cures Act has authorized an additional 1.14 billion through 2026.

A WHITE HOUSE blog dated January 30, 2015, claims that Precision Medicine is already working to cure Americans. It lists six personal stories of how precision medicine has allowed cutting-edge treatment to further individuals' health and affects the lives of everyday Americans, their families, and generations to come. Although not related to The All of Us project, the stories include that of William Elder Jr., who has been diagnosed with cystic fibrosis; Emily Whitehead, who was the first pediatric patient to be treated with a new kind of cancer immunotherapy; Melanie Nix diagnosed with breast cancer (Positive for BRCA gene mutations); Hugh and Beatrice Rienhoff, who had a defect resembling Marfan Syndrome; Kareem Abdul-Jabbar, the famous basketball legend, who was diagnosed with a form of leukemia, and also mentions the name of Professor Keith Yamamoto, University of California, one of the pioneers of precision medicine. Some of the known successes of precision medicine are the treatment of BRCA with Olaparib (86% success), EGFR with Erlotinib Osimertinib (70% success), HER2 with Lapatinib Pertuzumab (50-70% success), and KIT with Imatinib (50-80% success). An emerging trend in precision medicine is the use of artificial intelligence and machine learning approaches to improve the traditional symptom-driven practice of medicine. Precision medicine, from a clinician's perspective, is about matching the right drugs to the right needs of the patient. Personalized medicine is still in its infancy—the future holds great potential. The current understanding of precision medicine can be best summarized by the statement of Dr. Nikhil Wagle, a cancer

specialist at Dana-Faber Cancer Institute in Boston, "There are very few instances in which we can look at a genomic test and pick up a drug off the shelf and say, 'That will work.' That's our goal in the long run, but in 2018 we are not there yet." One emerging trend in precision medicine is the use of artificial intelligence and machine learning to improve the traditional symptom-driven practice of medicine.

Personalized Medicine

Human Genome Project, which began in the 1990s, developed a complete sequence of the human genome (20,500 genes) in 2003. This historic milestone had a great impact on how one studies and treats diseases. Since that time, researchers have been able to identify the genetic basis of genomic variation of thousands of diseases. Emmanuelle di Tomaso, Head of Oncology, Precision Medicine, at Bayer, says, "Advancement in genomics and the advancement of related precision therapies, that pinpoint the genomic alteration driving specific disease, are transforming clinicians' approach to treatment." A prime example would be the success story of the personalized therapy of Mila Makovec—a hyper-personalized, first individually tailored treatment of its kind. Mila was diagnosed with a devastating genetic disorder called Batten disease. Clinicians in Boston, including Dr. Timothy Yu of Children's Hospital Boston, developed a personalized medicine, 'milasen', a one-of-a-kind drug, which has been named after her. Gina Kolata of the New York Times writes, "A new drug, created to treat just one patient, has pushed the bounds of personalized medicine." Milasen is a 22-nucleotide antisense oligonucleotide with the same backbone and sugar chemistry as nusinersen.[14] Nusinersen marketed as Spinraza has been used to treat spinal muscular atrophy. Since 2016, more than 10,000 people have been treated with this drug worldwide. The rapid advance made in this case was the result of prior knowledge that antisense oligonucleotides can be customized in a sequence-specific fashion—the precedent of nusinersen, being safe and effective, against spinal muscular atrophy, and relative simplicity of manufacturing.

Ipek Kuzu became the first handful of patients to receive a hyper-personalized gene-medicine tailored to treat a unique mutation. Ipek, a three-year-old, has ataxia-telangiectasia (A-T), a disease caused by an error in her DNA. It causes the loss of brain cells and could lead to infection and cancer. The one-person drug, designed by her doctor in Boston, Dr. Timothy Yu, is named 'atipeksen' for A-T and Ipek. Most of such diseases are caused by 'genetic typos.' The clinicians change the code, reprogram the drug, and treat many genetic diseases.[15] There are several challenges facing the development of personalized gene-modulating drugs. The first and the foremost is the cost of the development of such unique drugs. The second obstacle is that insurance companies do not cover such experimental drug development and treatments. Unless such treatments become cost-effective, they will be orphan drugs. There are some moves to convince funding agencies such as the National Institutes of Health, the need to fund such projects. According to a news report in the MIT Technology Reviews (2020), the FDA is considering giving doctors leeway to modify genetic drugs to try new patients without securing permission each time. Yet another serious challenge is, that short of a true healing, it may be impossible to be sure that they really work.

Transfusion-dependent β-thalassemia (TDT), and sickle cell disease (SCD), are monogenic diseases with severe and potentially life-threatening manifestations (NEJM 2021;384:252-260). A study sponsored by CRISPR Therapeutics and Vertex Pharmaceuticals describes the first two patients, one with TDT, and the other with SCD, who were infused with CTX001(autologous CRISPR.Cas9-edited CD34+HSPCs that were genetically edited to reactivate the production of fetal hemoglobin) and enrolled in CLIMB THAL-111 and CLIMB SCD-121 clinical trials. The authors of this multi-country study concluded, "Initial results from the follow-up of the first two patients who were treated with CTX001 have shown the intended CRISPR-Cas9 editing of BCL11A in long-term hematopoietic stem cells, with durable engraftment, high levels of fetal hemoglobin expression and the elimination of vaso-occlusive episodes or need for transfusion." Gene therapy is currently treating diseases ranging from neuromuscular disorders, hematological disorders, cancer, and blindness. Even though such therapies are available, health insurance companies will not cover the cost, ranging from 400,000 to 2 million. "Completely curing patients is obviously going to be a huge success, but it is not yet an achievable aim in a lot of situations." Says Julie Cruddle, a neurologist, and gene therapy researcher, at the University of Washington. There is no field in medicine that stands to benefit more from personalized medicine than organ transplantation.[16]

In 1954, the kidney was the first human organ to be transplanted successfully at the Brigham Hospital, Boston MA. Dr. Joseph Murray was honored with the Nobel Prize in medicine in 1990 for his efforts in the development of Kidney transplantation. In first-of-a-kind kidney transplantation, the University of Alabama surgical team transplanted gene-edited kidneys of a pig into a man who was brain dead. The transplanted kidneys made urine within 23 minutes. However, these kidneys did not remove creatinine from his system. Liver, heart, and pancreas transplants were successfully performed by the late 1960s. In 1967, both heart and liver transplantation was done successfully. Almost 107,000 people in the USA are currently waiting for life-saving organ transplantation. The major reason for late allograft loss is chronic allograft damage (CAD). The underlying mechanisms of CAD are poorly understood and need to be unraveled if graft function and treatment are to be successful.[16] According to the experts, the definition and identification of valid pre-and post-transplantation biomarkers will facilitate personalized medicine, leading to long-term graft survival. Emerging therapies integrate information from multiple platforms, like genotype analyses, single nucleotide polymorphisms (SNPs), epigenetic studies, analyses of mRNA, miRNA, proteins, peptides, and metabolite profiling. This massive information must be processed by using artificial intelligence and machine learning software analytics to develop appropriate risk analysis and prediction of success rates.

We mentioned in the previous paragraph that thousands of patients are waiting for organ transplantation. To overcome chronic allograft damage of the transplanted organ, Dr. Bartley Griffith, a distinguished Professor at the University of Maryland,

performed the first-ever gene-edited pig heart transplantation to Mr. David Bennett, who was waiting for a heart transplant for several months. The genetically modified pig was created by Revivicor, a biotech company. US/FDA had authorized the surgery on December 31, 2021, under 'expanded access' or sometimes referred to as "compassionate use." To genetically modify the heart, three genes were 'knocked out' for enzymes that enable pig cells to synthesize sugars (alpha-gal) that are responsible for causing an 'antibody-mediated' rejection of pig organs in humans. Six tweaks were made in the DNA for additions of human genes; two anti-inflammatory genes, two genes that promote normal coagulation and prevent blood vessel damage, and two other regulatory proteins that help tamp down antibody response. Another one was also 'knocked out' to prevent excessive growth of the pig heart tissue. Six human genes were inserted to encourage immune acceptance of the pig heart. Xenotransplantation has seen significant advances with the advent of CRISPR-Cas9 genome editing, which has made it easier to create pig organs that are less likely to be rejected by human immune systems.

Dr. Bert W. O'Malley, President and CEO of the University of Maryland Medical Center, called the surgery a "historic, monumental step forward." For decades, we have been at the forefront of research, driving progress toward the promise of xenotransplantation, as a viable solution to the organ crisis; many believed that this breakthrough would be well into the future. I remember my days at the University of Minnesota, decades ago, when the University established a new center of excellence for "Xenotransplant Research." The University of Maryland, School of Medicine, with the help of Revivicor, Blacksburg, Virginia (United Therapeutics), has achieved a major milestone in xenotransplantation. Revivicor was also behind the successful transplantation of a kidney into a human patient last October 2021, which was the first milestone in proving the viability of xenotransplantation. Harvard scientist George Church cofounded a company, eGenesis, which is working on using CRISPR gene editing to make animal organs viable for human organ transplantation. A company in Auckland, New Zealand (NZeno), is breeding miniature pigs whose kidneys remain human-sized, without growth-hormone modifications. As in any innovation, there is always a gap between the research findings, recognition of the importance of such discoveries by the regulatory agencies, and application of such findings at clinical trials. This procedure is new highly experimental, but the technique could help reduce transplant waiting lists in the future.

In the early 80s, we at the University of Minnesota were interested in pancreatic islet cell transplantation for restoring functionalities in a diabetic animal model. We used the streptozotocin-induced diabetic rat model for these studies. The diabetic animals showed an altered arachidonic acid metabolism. They produced more of proaggregatory thromboxanes and less of vasodilatory prostacyclins (Fig 1). Thromboxanes mobilize cytosolic calcium and induce platelet activation. Whereas prostacyclins, via the action of cAMP, lower cytosolic calcium and induce normalization of platelet activity. Once the pancreatic islet cells were successfully transplanted to these diabetic animals, the rats produced normal levels of thromboxane and prostacyclin levels, suggesting that this drug-induced diabetic state could be reversed and altered physiology could be normalized.[17]

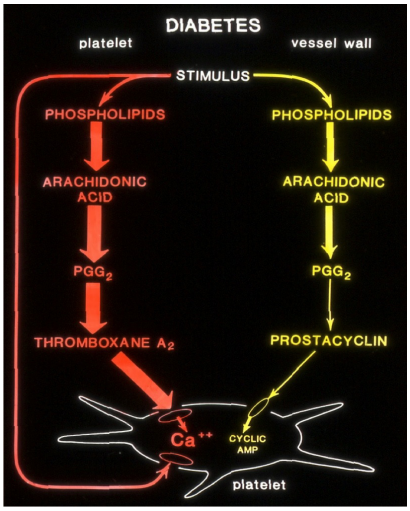

Fig 1. *Altered arachidonic acid metabolism in diabetic rats.*
(Courtesy. Dr. Jon Gerrard, Winnipeg, Canada)

Four decades after we demonstrated the beneficial effects of islet cell transplantation, Vertex Pharmaceuticals of Boston, MA, have reported the results of a trial, which infused cells grown from stem cells, like the insulin-producing pancreatic islet cells, in the first-ever human studies of this kind. Mr. Shelton was the first recipient who received the cell infusion on June 29 of this year (2021). The New York Times (November 27, 2021) published an article titled, "A Cure for Type-1 Diabetes? For One Man, It Seems to Have Worked." The challenge these researchers faced was to find out what sequence of chemical messages would turn stem cells into insulin-secreting islet-like cells.[18] The major concern that clinicians still have is "the trade-off between the burdens of diabetes and potential complications from immunosuppressive medications."

Emerging Innovative Anti-Cancer Therapies

Target specific delivery of therapeutics is a challenge when toxic drugs must be delivered to tumors. As early as in the early 80s, researchers experimented with the idea of coupling one of the most toxic biomolecules (Ricin), a glycoprotein from castor seeds to cell-specific monoclonal antibodies, for use in targeted delivery of anticancer drugs.[19] They demonstrated that a monoclonal antibody, rat IgG2b directed against Thy 1.2 antigen, provides a new binding site for the murine thymus cell surface. The authors concluded that "Ricin-monoclonal antibody hybrids of this type (could be considered a biologics or a device), combine a high degree of cell-type selectivity and toxicity, and may have pharmacological utility as antitumor agents. Viruses have been used as novel vectors for the cell-specific delivery of macromolecules, including toxins. UK researchers have shown that Ricin, a known toxin, could be encapsulated in a bacteriophage and delivered in a cell-specific

manner to the targeted tissue.[20] Yet another toxic, small biomolecule of therapeutic importance is 3-Bromo pyruvate (3BP), a potent and specific anticancer drug, which targets cancer cells' energy metabolism, both its high glycolysis and mitochondrial oxidative phosphorylation.

Professor Pederson and associates at the Johns Hopkins University, School of Medicine, report a bench side discovery that led to the effective bedside treatment of a cancer patient.[21] Targeted delivery of anticancer drugs is made difficult by a series of biological barriers that impede the drugs from reaching the target. Researchers from the University of Sciences and Technology, China, report a stimuli-responsive clustered nanoparticle to systematically overcome multiple barriers by sequentially responding to the endogenous attributes of the tumor microenvironment. They have shown that, once the cluster accumulates on the tumor cells, the intrinsic tumor extracellular acidity would trigger the discharge of platinum prodrug-conjugated poly (amidoamine) dendrimers. They claim that such structural alteration in size greatly facilitates tumor penetration and cell internalization of the therapeutics.

Tumor Microenvironment (TME)

Pancreatic cancer is a devastating disease, the 5-year survival is less than 5%, and most deaths are due to metastatic disease.[22] The pancreatic tumor environment comprises of tumor cells and a variety of stromal or non-malignant cells, including stellate cells, inflammatory and immune cells, blood vessels, extracellular matrix proteins, cytokines, growth factors, and tumor-derived exosomes.

A study of 52,728 patients with pancreatic cancer (Surveillance, Epidemiology and End Results; SEER) revealed that the rate of distant metastasis increased in a linear fashion with the increasing size of the tumor. Cancer stem cell theory proposes that solid tumors contain a small population of tumor-initiating cells or cancer stem cells that are responsible for tumor initiation. Epithelial-mesenchymal transition (EMT) involves the expression of adhesion molecules, acquisition of an invasive phenotype, which promotes cellular disassociation, degradation of the basement membrane, and acquiring drug resistance. Several transcription factors (Snail, Slug, and Twist 1) promote the activation of EMT, whereas EMT is characterized by downregulation of epithelial markers (E-cadherin, Vimentin, and Fibronectin). Inflammation seems to be a major driver of EMT in pancreatic cancer cells. Inflammation also seems to modulate Kras (one of the genes involved in the epidermal growth factor receptor pathway) and drive tumorigenesis. Furthermore, the fibroinflammatory response seems to influence the epigenome and metabolome, including Kras targets (Csf2, Rrm2, and Sc4mol). Some of the potential growth factors include connective tissue growth factor (CTGF), hepatocyte growth factor (HGF), insulin-like growth factor (IGFs), and interleukin-6 (IL-6), involved in Ras-MAPK, MYC, and STAT signaling.[22] Exosomes are vesicles that are released from the cells to provide intercellular communication, containing DNA fragments, mRNAs, and miRNAs.

Tumor Suppression

There is emerging interest in metabolic pathways to tumorigenesis. The tumor cell and tissue metabolism seem to be far greater than normal cell and tissue metabolism. Therefore, the importance of altering tumor tissue metabolism has emerged as a crucial part of the current cancer research. Many tumors can adopt a low-glucose consumption strategy by utilizing alternative energy sources such as fatty acids, amino acids, and lactate. Most cancers (90%) exhibit the "Warburg effect," showing a significant increase in glycolysis, even in the presence of oxygen. Professor Peter L. Pederson and associates at Johns Hopkins School of Medicine have demonstrated that 3-Bromo-pyruvate (3BP), a small molecule, can "trick" the cancer cells and enter like a trojan horse and deplete their energy metabolism.[23] Cancer cells that exhibit the "Warburg effect" pump out lactic acid through a transporter. The number of these transporters in cancer cells is much greater than in normal cells. Therefore, 3BP, which mimics the lactic acid in its chemical structure, enters the cancer cells preferably via this transporter and destroys them. It can be delivered to cancerous tumors via various routes. We have been exploring opportunities to test the efficacy of this therapy in India as a US-India bilateral research project.

An active tumor needs plenty of energy and nutrition to maintain accelerated growth, which is common in tumor progression. Neoangiogenesis is a key process to attain the needed vasculature in the tumor environment. Therefore, researchers are focusing their efforts on developing angiogenesis inhibitors as a desirable anti-cancer strategy.[24] Because of this focus, several regulatory and signaling molecules modulating angiogenesis are of interest, including growth factors (VEGF, PDGF, FGF, EGF), receptor tyrosine kinases, transcription factors such as HIF, as well as signaling molecules like MAPK and P13K. The ability of a tumor to induce neoangiogenesis is termed "angiogenic switch", which happens when the tumor needs extra vascularization to meet the nutritional demands of the rapidly growing tissues. During that time, pro-angiogenic growth factors bind to receptors on endothelial cells, stimulate vasodilation, permeability, and secrete matrix metalloproteinases. Once these cells are detached, they migrate and proliferate, and form new branches from the existing vasculature. Combination of angiostatin and endostatin gene transfer seems to induce synergistic antiangiogenic activity in vitro and antitumor efficacy in leukemia and solid tumors in mice. There is a great demand for pro-/anti-angiogenesis medicines to treat ischemic strokes, brain tumors, and neurodegenerative diseases. Researchers from the National Cancer Institute of NIH conclude, "Initial trials of putative anti-angiogenesis inhibitors have shown some promise in cancer, although this has not always translated to the clinic."

Personalized Cancer Therapy

Personalized, Chimeric Antigen Receptor (CAR) T-cell gene immunotherapy for aggressive pediatric blood cancers has been hailed as transformative in Pediatric Medicine. CAR-T cell therapy approach was first developed by Dr. Carl June, a Professor of Pathology and Laboratory Medicine, Perelman School of Medicine at the University of Pennsylvania. CAR-T

cell therapy genetically modifies patient's immune cells to make them seek out and kill leukemia cells. Physician-scientists of Children's Hospital, of Philadelphia (CHOP) presented their work on Kymriah ® (tisagenlecleucel, formerly CTL019)- the first-ever U. S. FDA approved personalized CAR-T cell gene therapy for aggressive blood cancers at the 60th American Society of Hematology meetings in 2018. An updated, longer-term analysis of ELIANA, the first global CAR-T cell therapy trial of Kymriah in children and young patients, showed an 82% remission rate within three months and 62% survival at 24 months. "Our unrivaled immunotherapy program treated the first, and now more patients than any other pediatric institution in the world, with this immunotherapy," says Stephen Hunger, Chief of the Division of Oncology and Director of the Center of Childhood Cancer Research at CHOP. Immunotherapy has shown success in 15 different types of cancers, including lung cancer, head and neck cancer, bladder cancer, kidney cancer, and Hodgkin lymphoma. More than 1,000 immunotherapy clinical trials are underway across the country.

Suzanne Topalian, associate director of the Bloomberg-Kimmel Institute for Cancer Immunotherapy at Johns Hopkins School of Medicine, led a team that contributed to the discovery that many cancers "put the brakes" on the body's immune cells, that would normally attack a tumor and destroy it. Dr. Topalian and associates developed a class of drugs called immune checkpoint (ICP) inhibitors that take the brakes off the immune system and give a second chance for the immune system to fight cancer. Immunotherapy helps a person's own cells to attack their cancer. Therefore, it is personal medicine approach therapy at its best. However, the real challenge is to find out why the majority of people with cancer do not respond to immunotherapy drugs. There is a great effort to find out who will and who won't respond to immunotherapy treatments. The team at Johns Hopkins has identified biomarkers in a small group of patients, which will indicate who will respond well to checkpoint blockers. Currently, we know very little about the various actors that modulate the tumor microenvironment and the pathways that modulate various immune reactions. However, cancer researchers say that the pace of immunotherapy development is' truly breathtaking', and this momentum needs to maintain in order to achieve success soon. Three decades ago, researchers at the National Cancer Institute (NCI) of NIH started working on CAR-T cell treatments painstakingly and demonstrated the benefits of this approach in the treatment of a variety of cancers. What started three decades ago as a speculative idea in these laboratories is now common practice in hospitals around the world. In a short overview like this, it is difficult to discuss all aspects of Immuno-oncology. Readers are urged to refer to original articles on this topic as well as to the extensive review articles.[25]

Despite the advances made in cancer immunotherapy, a great many challenges still exist. First and foremost is the inability to predict treatment efficacy and patient response to various customized treatments. We need to develop knowledge about additional biomarkers for risk assessment and prediction of success rates. We also need to develop clinical protocols based on the information available from large databases, to optimize the therapies and efficacy of such personalized therapies.

The fact that to date immunotherapies have demonstrated efficacy in a minority of patients indicates that we do not fully understand the multiple molecular mechanisms that modulate tumor biology, growth, and metastasis. The observed variability in patient response to immunotherapies may be attributed to a lack of information on a variety of biomarkers that modulate the tumor biology, tumor heterogeneity, tumor metastasis, variability in tumor type and stage of development, treatment history, and underlying immunosuppressive biology of the tumor.[26] Personalized drug combinations seem to be the futuristic approach to cancer immunotherapy. To achieve such a degree of success, the clinicians need information on mutation profile, genetic signature, epigenetic modifications of immune and tumor cells, antibody response, biomarker profile, immune cell characterization, and predictive genetic markers and the ability to analyze such massive data and come up with appropriate treatment protocols to enhance the success rates.

Gene Expression and Tumor Progression or Regression

When considering gene expression and tumor biology, two types of mutations modulate cancer cells; tumor suppression genes, which inhibit cell growth and division, and proto-oncogenes, which accelerate cell growth and division. Gene expression is regulated during transcription and RNA processing. The transcription control regions of protein-encoding genes include the core promoter, where RNA polymerase-11 binds the proximal and distal promoter, responsible for gene expression regulation, and the enhancers and silencers.[27] Transcription factors transduce the proliferation signals elicited by growth factors. It is well established that human oncogenes encode transcription factors, which are prevalent in neoplasias (MYC, MLL, PML-RARa). The most prominent tumor suppressors (p53) are transcription factors. Studies with carcinogens have demonstrated that changes in DNA methylation, histone acetylation and methylation, non-coding RNAs, post-translational modifications are all epigenetic promoters of tumor progression.[28] In order to use the high-throughput data available on tumor promoters, suppressors,-resulting gene expressions, modulation of transcription factors, growth factors, and various signaling mechanisms, appropriate software analytics and integrative algorithms are needed. This brings the need for a multidisciplinary approach to cancer management.

Cells become cancerous after mutations accumulate in various genes that modulate cell proliferation. In normal cells, hundreds of genes control the process of cell division and normal growth. Studies by researchers at Cancer Genome Project, Wellcome Trust Sanger Institute, UK, have demonstrated that most cancer cells possess 60 or more mutations. Growth-promoting genes like signaling protein Ras, are among the most mutated in cancer cells, promoting the formation of cells that will be strongly stimulated by growth receptors. Some anticancer drugs, for instance, work to counteract these effects by blocking the action of growth-promoting signals. The well-known breast cancer drug, Herceptin, blocks receptor tyrosine kinase (RTKs). At the same time, mutations that lead to the

suppression of cell proliferation are known as tumor suppressor genes. Many cancer cells have two copies of the gene that codes for p53, a multifunctional protein that senses DNA damage and acts as a transcription factor for checkpoint control of genes. If the checkpoints are missed, or repair genes are damaged, then the rate of damage increases in the tumor microenvironment. Tumor molecular profiling and analysis of the mutational landscape seems to have become a fundamental component of precision oncology.[29] Genomically-guided clinical trials have begun to evaluate the efficacy of approved investigational molecularly targeted therapies, for distinct tumor types with shared genetic features.

Several studies have demonstrated the role of the tumor microenvironment in the modulation of tumor progression and resistance to therapies. According to Dr. Yu Sun of Shanghai Institute of Biological Sciences, China, the TME decreases drug penetration confers genetic mutations and epigenetic changes, collectively modifying disease mortality and disturbing clinical indexes.[30-33] Intrinsic mechanisms that are responsible for this tumor resistance are enhanced drug efflux, blunted apoptotic signaling, increased metabolic activity, loss of specific oncogenes, a gain of stem cell plasticity, strengthened DNA damage machinery -promoted by mutation-selective and tumor heterogeneity. The TME comprises carcinogenetic cells, cancer-associated fibroblasts (CAFs), cancer-associated DNA (cDNAs), immune cells [T and B lymphocytes, tumor-associated macrophages (TAMs), and natural killer cells], the vascular system, and the extracellular matrix (ECM, including secreted cytokines, chemokines, metabolites, and exosomes). The transformed cancer cells seem to interact with stromal cells in the TME and promote tumor resistance. There are many signaling pathways responsible for therapeutic resistance by tumors. A well-thought-out therapy protocol should consider the multiple mechanisms involved in tumor resistance to therapy and optimize the therapies accordingly.

Gene Editing Tools and Emerging Therapies

The discovery of gene-editing tools has extended our ability to modulate genetic defects, treat diseases, and develop more accurate cellular and molecular therapies.[33] Since the discovery of CRISPR-Cas endonuclease as a programmable-guide nuclease, gene editing with engineered nucleases has rapidly developed into emerging therapies.[34] Clustered regularly interspaced short palindromic repeats (CRISPR), 'acts as molecular scissor', to find specific bits of DNA inside the cell (Fig 2). When CRISPR Cas9 protein is added to a cell, along with a piece of guide RNA (gRNA), the Cas9 proteins bind to the gRNA and move along the strands of DNA until it finds a 20 -DNA-letter sequence that matches the part of the gRNA sequence. The gRNA is made up of two units: crisprRNA (crRNA), a 17-20 nucleotide sequence complementary to the target DNA, and a tracrRNA, which serves as a binding scaffold for the Cas nuclease. Customized Cas proteins also have been developed, which do not cut the DNA, but merely turn on (CRISPRa) or off (CRISPRi). Some of the salient ongoing studies using this gene-editing tool include treating hemoglobinopathies (aiming to treat β-thalassemia and sickle cell disease with gene-edited hematopoietic stem cells), editing cells inside the body to treat genetically defined diseases, creating next-generation cell therapies for cancer, improving stem cell use for tissue engineering, transplantation, and other therapies through gene editing. The three main categories of genetic editing that can be performed with CRISPR include disruption of an unwanted segment of DNA (CAR-T Therapies), deletion of an unwanted section of DNA (treatment of hemoglobinopathies), or addition of a fragment of a DNA. Opportunities are abundant as more than 10,000 monogenic diseases are caused by single mutations in individual genes.

Precision medicine, personalized medicine, and genetic engineering are emerging new fields that have gained a lot of popularity, encouragement, and funding in recent years. CRISPR editing technology may be used in combination with Cas9 endonucleases for the development of new diagnostic and treatment strategies. The most used CRISPR system is the Type11 CRISPR-Cas system, which is made up of three main components, including the trans-activating crRNA (tracrRNA), the crisprRNA, and an endonuclease. Since the time the cancer researchers realized that changes in the DNA cause cancer, they have been exploring ways to correct those cancer-inducing mutations by manipulating the DNA. A game-changer occurred with the realization that a gene-editing tool could alter the DNA in human cells like a very precise, 'easy-to-use' pair of molecular scissors. As shown in Figure 2, the gene-editing tool consists of a gRNA and DNA-cutting enzyme (Cas9). The researchers design the guide RNA to mirror the DNA of the gene to be edited (Target). The gRNA pairs with the Cas endonuclease and leads the Cas to the target gene's DNA. When the gRNA matches up with the target gene's DNA, Cas cuts the DNA. There exist some concerns that this tool may cut DNA out of the target area (off-target). Yet another concern is, what if it starts cutting random parts of the genome? Finally, getting the gene-editing tool into the cells itself could be a challenge at times.

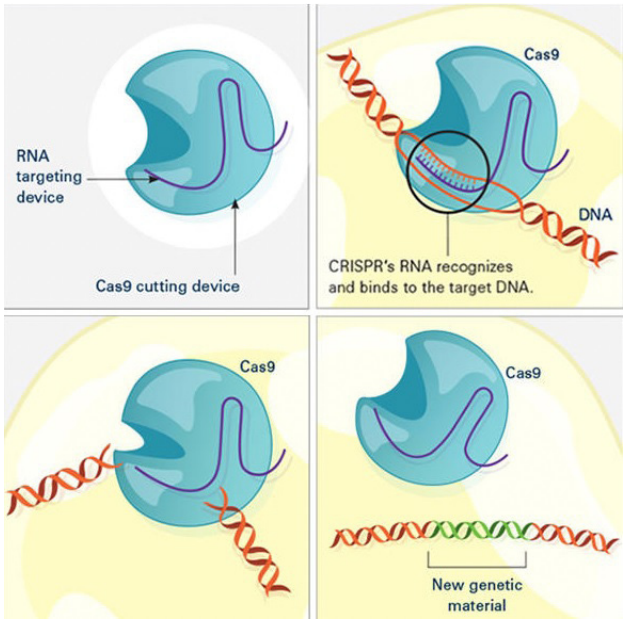

Fig. 2. *Schematic Diagram of How CRISPR Gene-Editing Tool works.*

(Credit: National Institute of General Medical Sciences, the US National Institutes of Health)

An especially exciting area of innovation in cancer therapy is cell-based therapy, a treatment that uses a patient's own immune cells, or the immune cells from another individual, to engineer potent killer cells and help fight the disease. According to Tamas Oravecz, Vice President, Cell Therapy Platform and Discovery, Janssen R & D, "Cell therapy has the potential to be a one-time, singular treatment that provides benefits throughout a patient's entire lifetime." Because "cell therapy provides the body with 'immunological memory,' which means that a person's immune system stores information about a certain stimulus, like a cancer cell, so it destroys it when encountered again." In brief, the technology involves procuring immune cells from the patients adding laboratory engineered (genetically engineered/ molecular engineering) chimeric antigen receptor (CAR) to the T cells. This modification turns T cells into CAR- T cells that attack the patient's cancer cells. A large number of CAR-T cells are produced in the laboratory and are given to the patients by infusions a few weeks after therapeutic protocols are initiated. Another area of great interest is to use immune cells from healthy donors. This approach is faster and less expensive to manufacture than CAR-T using patients' own cells. Fate Therapeutics, in partnership with Janssen R&D, uses induced pluripotent stem cells (iPSCs) to mass-produce therapeutic cells for cancer therapy. Cellular therapy is considered the therapy of the future

To discover gene targets in cancer cells whose loss enhances anti-tumor immunity, the researchers at the Dana-Farber Cancer Institute, Boston, constructed a murine lentiviral CRISPR-Cas9 knockout (MusCK) library.[35] This library included 5 sgRNAs for each of the over 4500 genes implicated in tumor initiation progression and immune modulation, which contains both custom-designed short crRNA sequences fused to the scaffold tracrRNA sequence. The principal component analyzed in these studies was an abundance of expression of sgRNA under each condition in 4T 1 cells. T cell-deficient hosts had the biggest tumors, and immune-competent hosts had the smallest. Functional Genomic screening using CRISPR-Cas9 resulted in the discovery of a novel cancer target. CRISPR screens in cancer cells co-cultured with T cells have identified genes that are; modulators of tumor immunity, novel immune-oncology targets, multiple regulators of PD-L1, Loss of Ptpn 2, and Adar1as an enhancer of tumor sensitivity to immunotherapy. These studies have demonstrated that E3 ligase Cop1 is a modulator of macrophage infiltration, secretion of chemokines, and enhancer of anti-tumor immunity. Furthermore, such studies demonstrate the effectiveness of in vivo CRISPR screens in identifying cancer-cell-intrinsic TME regulators.

To successfully apply gene-editing tools for in vivo studies, one needs an efficient and robust screening method with high levels of CAS9 and reliable single guide RNAs (sgRNA). In a recent study, German and French collaborators provide a sgRNA design tool that selects high-fidelity sgRNAs and Cas9 that expresses high levels of Cas9 in transgenic mouse lines.[36] The researchers were able to achieve average knockout efficiency of 80% in primary B Cells. The authors developed a Cas9-transgenic mouse with ubiquitous expression of Cas9 by crossing Rosa 26-with Cre-deleter mice and evaluated the expression of Cas9, in the resulting R-26-Cas9iGFP/+animals. All hematopoietic populations exhibited high GFP levels, including hematopoietic cells in the bone marrow and various lineages, such as T, B, and myeloid cells. They also studied the inactivation of transcription factors (TFs), known to be important for B cell differentiation. Expressing of sgRNA targeting for TFs, led to a strong survival disadvantage of Cas9-expressing cells, showing the decreased percentage of GFP+cells. These studies further demonstrated that the following TFs: Prdm 1, Xbp1, Irf4, Pou2af 1, and Myc are important for B-cell survival, proliferation, and terminal differentiation. To identify genes of importance for B-cell activation, they selected 83 candidate genes upregulated during plasma cell differentiation, designed sgRNA for each gene, and studied using GFP+ and CD138+ cells as readouts. Take-home lessons from these studies are that the screening system developed by these researchers leads to clear and consistent functional results, permitting the use of small-scale screens in primary mouse cells without the need for high numbers of sgRNA genes or deep sequencing.

Despite the fact the targeted nucleases are powerful tools for modulating gene alterations, there are some concerns that researchers have about the editing tool cutting 'off target' regions of the DNA. Researchers from the Massachusetts Institute of Technology (MIT) have described a set of tools for Cas9-mediated genome editing via nonhomologous end joining (NHEJ), or homology-directed repair (HDR), in mammalian cells.[37] To minimize off-target cleavage, they describe a double-nicking strategy, using Cas9 nickase mutant with paired guide RNAs. They have shown that by fusing the crRNA with tracrRNA one can develop a chimeric, single-guide RNA (sgRNA) Cas9 and can be directed toward any target of interest. They predict that by directly injecting sgRNA and mRNA encoding Cas9 into embryos, one can enable rapid generation of transgenic mice with modified alleles. In this study, they have demonstrated simultaneous targeting of two human DYRK1A and GRIN2B loci at efficiencies of 65-58% for each locus. The authors provide extensive details of the protocols used for each of their experiments, also address concerns, questions, which are frequently asked (discuss.genome-engineering.org), and answers to some of the questions from their personal experience.

The first clinical trial in the United States to test a CRISPR-made cancer therapy was launched in 2019 at the University of Pennsylvania. The study, funded by the National Cancer Institute (NCI) of NIH, is testing a type of immunotherapy in which patients' own immune cells are genetically modified to better 'see' and kill their cancer. According to NCI news of July 27, 2020, therapy involves making four genetic modifications to T cells, immune cells that can kill cancer. First, the addition of a synthetic gene gives the T cells a claw-like protein (called a receptor) that 'sees' NY-ESO-1, a molecule on some cancer cells. Then the CRISPR is used to remove three genes; two that can interfere with the NY-ESO-1 receptor and another that limits the cancer-killing abilities. The product that was developed to achieve these desired features was grown in large quantities and infused into patients. This procedure was tested in two patients (multiple myeloma and sarcoma) and found safe for use. The tumors stopped growing for a while but resumed growing later. Other clinical studies of CRISPR-made cancer treatments are underway. A few trials are testing CRISPR-engineered VAR-T cell therapies, another type of immunotherapy. One company is

testing CRISPR-engineered CAR -T Cells in people with B cell cancers and people with myeloma.

Cancer immunotherapy has started to undermine melanoma, non-small cell lung cancer, kidney cancer, head and neck cancers, and Hodgkin's lymphoma. There are tremendous opportunities in this field of research. In this overview, we have just discussed a few examples of emerging therapies. Readers are urged to consult original articles and monographs on this subject.[38-43]

There is a false belief that the availability of vast amounts of multi-omics data generated from large cohorts of the population represents a unique opportunity for the development of precision medicine. Researchers from Harvard Medical School rightly point out that it is the algorithms encoding causal reasoning domain (e.g., clinical and biological) knowledge that will facilitate the transformation of medicine to precision medicine.[43,44] In their review of this topic, they discuss principles of data science and suggest three defining tasks: 1) Association prediction, 2) Intervention, 3) Counterfactual causal interference. They conclude, "As machine learning algorithms become ubiquitous tools to handle quantitatively "big data," their integration with causal reasoning and domain knowledge is instrumental to qualitatively transform medicine, which will, in turn, improve health outcomes of patients." Mexican researchers have studied the association between genetic variants (SNPs), previously associated with COPD and IPF (FAM13A), rs2736100 (TERT), rs2076295 (DSP), 128 rs5743890, and rs111521887 (TOLLIP), and the risk of CPFE in a mestizo Mexican population.[45] They point out a differential genomic profile between COPD patients with emphysema, IPF, and CPFE that could represent different underlying mechanisms involved in the pathogenesis of the three diseases.

Like the ideas that exist about the role of precision medicine, there is a widespread belief that the underlying heterogeneity of many diseases suggests strategies for treating an individual with a disease, alternately a possibility for monitoring or preventing a disease. Because of such a belief, there is an increased expectation that treatments should be tailored or 'personalized' to that individual's unique biochemical and physiological profile.[46] We have discussed a few successful cases where drugs were developed to treat individuals with incurable conditions. The ubiquity of smartphones and smartphones 'apps' has created a concept of 'digital therapeutic' or digital healthcare.[47] Many digital 'apps' have undergone evaluation for their ability to engage users and provide benefits.[48] The US/FDA has created guidelines for registering digital therapeutics as insurance-reimbursable, approved health technologies. Dr. Kevin Dozo of Integrative Biomedical Sciences, Faculty of Health Sciences, University of Cape Town, South Africa, summarizes the progress in emerging cancer therapies in his recent review, "Although there may be successful stories to tell, evidence/data showing that cancer treatment (chemotherapy, radiotherapy, immunotherapy) itself and the involvement of tumor stromal components can result in resistance is discouraging. This is akin to unsuccessful attempts at removing rogue regimes and can cause the hardening of such regimes."[49] Researchers from the Center for Open Science University of Virginia attempted to replicate 193 experiments from 53 papers, but experienced reproducibility challenges at every phase of the research lifecycle. They also indicate none of the 193 experiments were described completely enough to design a replication protocol, without requesting clarifying details from the original authors. [50]

Conclusions

The first therapeutic protein molecule, other than antibodies (1986), is insulin (discovered in 1921), the first recombinant biopharmaceutical, approved in the USA in 1982 as an interchangeable biosimilar. Emerging innovations and advances in molecular biology, genomics, cellular and molecular engineering have dramatically increased the discovery and development of new and novel biopharmaceuticals. Big Pharma companies now have the capability to develop both small molecules as well as blockbuster biologics. Advances in biotechnology, genomics, progress made in decoding of the RNAs and DNAs, availability to gene-editing tools, stem cell, and gene therapy applications have given researchers a great opportunity to develop precision medicine as well as personalized medicine. Having said that, we must inform the readers that the development of mRNA vaccines from the time the data on the SARS-CoV-2 genome was made available to a working vaccine was nothing short of a modern miracle. Success made in the rapid development of these technologies has given researchers, pharma companies, and clinicians limitless opportunities for RNA therapeutics for use as the standard care for many diseases, especially for the development and progress of personalized medicine. Scientists have used the word 'limitless' to describe the future of these emerging therapeutics.

High-throughput analytical technologies, 'big data,' artificial intelligence, and machine learning applications have revolutionized medical research. At the time of this writing, the largest application of genetic testing in medicine occurs in newborn screening. There are suggestions and speculations that genomic sequencing could become a standard component of newborn care. Currently, we still have a limited understanding of strategies and protocols for managing genomic data, and analyzing the massive amounts of data available for developing useful information for clinical applications. This is true for other emerging areas such as genomics, epigenomics, genome-association study (GWAS), as well as for studies on microbiomes, proteomics, metabolomics, transcriptomics, and multi-Omic platforms. Despite the advances made in these areas, routine implementations of data on a population scale require advances in data acquisition, analysis, and cost-effectiveness. Clinicians would like to see the progress made in these areas to a level when they can just look at big-data banks and find specific causes for a disease (clinical decision support system), or a cluster of diseases, pick up a drug or a combination of drugs, off the shelf or find an approved safe efficacious therapy for such a disease that will work. We are not there yet.

In a Lancet Editorial (May 15, 2021) titled, '20 Years of precision medicine in oncology' the editor concludes, "But the past 20 years have been colored by advanced scientific conceptual breakthroughs, without adequate focus on the basic building blocks of implementation, and the practicalities of patient

care." In a way, this editorial stresses the need for a solution that is formulated on evidence-based observations, rather than depending upon sporadic discoveries and innovations. A century ago, the discovery of a biomolecule, 'insulin,' played an important role in understanding the role of hyperglycemia and how to control this altered glucose metabolism. The discovery of another set of biomolecules, 'antibiotics' gave us the ability to control to a great extent infectious diseases. Then came the discovery of the structure of a macromolecule of great importance to life itself, DNA. Knowledge gained over the years gave us an opportunity to reconstruct and reprogram a messenger RNA, to use as a therapeutic agent at the shortest possible time. This technology of mRNA therapy used not only a biomolecule but an 'entire cargo' of biologics to achieve safe delivery of a therapeutic messenger. The ability to decipher the biological code of the nucleotide sequence and reconstruct the desired protein/peptide messengers has increased our capabilities to develop a host of novel emerging therapeutics. The discovery of a novel 'molecular scissor,' CRISPR-Cas9, - a simpler, faster, precise, gene-editing tool, will change the way we perform cancer research as well as gene therapies.

References

1. Pak A, Adegboye OA, Adekunle AI, Rahman KM, McBryde ES, Eisen DP. Economic Consequences of the COVID-19 Outbreak: the Need for Epidemic Preparedness. Front Public Health. 2020 May 29;8:241. doi: 10.3389/fpubh.2020.00241.
2. Blumenthal D, Fowler EJ, Abrams M, Collins SR. Covid-19 - Implications for the Health Care System. N Engl J Med. 2020 Oct 8;383(15):1483-1488. doi: 10.1056/NEJMsb2021088. Epub 2020 Jul 22. Erratum in: N Engl J Med. 2020 Jul 23;: PMID: 32706956.
3. Rao GHR. SARS-CoV-2 biochemistry, Transmission, Clinical Manifestations and Prevention. International Journal of Biomedicine. 2020;10(4):303-311. *doi:* 10.21103/Article10(4)_GE
4. Rao GHR: Biomedicine in the COVID Age: Opportunities, Responses, and Challenges. International Journal of Biomedicine. 2021;11(3):241-249. doi: 10.21103/Article11(3)_RA1
5. Institute of Medicine (US) Forum on Microbial Threats. Microbial Evolution and Co-Adaptation: A Tribute to the Life and Scientific Legacies of Joshua Lederberg: Workshop Summary. Washington (DC): National Academies Press (US); 2009. PMID: 20945572.
6. Lederberg J. Infectious history. Science. 2000 Apr 14;288(5464):287-93. doi: 10.1126/science.288.5464.287.
7. Taubenberger JK, Morens DM. 1918 Influenza: the mother of all pandemics. Emerg Infect Dis. 2006 Jan;12(1):15-22. doi: 10.3201/eid1201.050979.
8. Pardi N, Hogan MJ, Porter FW, Weissman D. mRNA vaccines - a new era in vaccinology. Nat Rev Drug Discov. 2018 Apr;17(4):261-279. doi: 10.1038/nrd.2017.243.
9. Damase TR, Sukhovershin R, Boada C, Taraballi F, Pettigrew RI, Cooke JP. The Limitless Future of RNA Therapeutics. Front Bioeng Biotechnol. 2021 Mar 18;9:628137. doi: 10.3389/fbioe.2021.628137.
10. Landrier JF, Derghal A, Mounien L. MicroRNAs in Obesity and Related Metabolic Disorders. Cells. 2019 Aug 9;8(8):859. doi: 10.3390/cells8080859.
11. Collins FS, Varmus H. A new initiative on precision medicine. N Engl J Med. 2015 Feb 26;372(9):793-5. doi: 10.1056/NEJMp1500523.
12. Jameson JL, Longo DL. Precision medicine--personalized, problematic, and promising. N Engl J Med. 2015 Jun 4;372(23):2229-34. doi: 10.1056/NEJMsb1503104.
13. All of Us Research Program Investigators, Denny JC, Rutter JL, Goldstein DB, Philippakis A, Smoller JW, Jenkins G, Dishman E. The "All of Us" Research Program. N Engl J Med. 2019 Aug 15;381(7):668-676. doi: 10.1056/NEJMsr1809937.
14. Kim J, Hu C, Moufawad El Achkar C, Black LE, Douville J, et al. Patient-Customized Oligonucleotide Therapy for a Rare Genetic Disease. N Engl J Med. 2019 Oct 24;381(17):1644-1652. doi: 10.1056/NEJMoa1813279.
15. Hayden EC. If DNA is Like a Software, Can We Fix the Code? MIT Technology Reviews. 123 (2):47-49, 2020.
16. Roedder S, Vitalone M, Khatri P, Sarwal MM. Biomarkers in solid organ transplantation: establishing personalized transplantation medicine. Genome Med. 2011 Jun 8;3(6):37. doi: 10.1186/gm253.
17. Gerrard JM, Stuart MJ, Rao GH, Steffes MW, Mauer SM, Brown DM, White JG. Alteration in the balance of prostaglandin and thromboxane synthesis in diabetic rats. J Lab Clin Med. 1980 Jun;95(6):950-8.
18. Drew L. How stem cells could fix type-1 diabetes. Nature. 2021;595:s64-s66. doi: 10.1038/d41586-021-01842-x
19. Youle RJ, Neville DM Jr. Anti-Thy 1.2 monoclonal antibody linked to ricin is a potent cell-type-specific toxin. Proc Natl Acad Sci U S A. 1980 Sep;77(9):5483-6. doi: 10.1073/pnas.77.9.5483.
20. Wu M, Brown WL, Stockley PG. Cell-specific delivery of bacteriophage-encapsidated ricin A chain. Bioconjug Chem. 1995 Sep-Oct;6(5):587-95. doi: 10.1021/bc00035a013.
21. Ko YH, Verhoeven HA, Lee MJ, Corbin DJ, Vogl TJ, Pedersen PL. A translational study "case report" on the small molecule "energy blocker" 3-bromopyruvate (3BP) as a potent anticancer agent: from bench side to bedside. J Bioenerg Biomembr. 2012 Feb;44(1):163-70. doi: 10.1007/s10863-012-9417-4.
22. Li HJ, Du JZ, Du XJ, Xu CF, Sun CY, Wang HX, et al. Stimuli-responsive clustered nanoparticles for improved tumor penetration and therapeutic efficacy. Proc Natl Acad Sci U S A. 2016 Apr 12;113(15):4164-9. doi: 10.1073/pnas.1522080113.
23. Ansari D, Friess H, Bauden M, Samnegård J, Andersson R. Pancreatic cancer: disease dynamics, tumor biology and the role of the microenvironment. Oncotarget. 2018 Jan 6;9(5):6644-6651. doi: 10.18632/oncotarget.24019.
24. Cook KM, Figg WD. Angiogenesis inhibitors: current strategies and future prospects. CA Cancer J Clin. 2010 Jul-Aug;60(4):222-43. doi: 10.3322/caac.20075.
25. Marshall HT, Djamgoz MBA. Immuno-Oncology: Emerging Targets and Combination Therapies. Front Oncol. 2018 Aug 23;8:315. doi: 10.3389/fonc.2018.00315.
26. Ventola CL. Cancer Immunotherapy, Part 3: Challenges and Future Trends. P T. 2017 Aug;42(8):514-521.

***Contact Information:** Emeritus Professor Gundu H. R. Rao, Laboratory Medicine and Pathology, Director, Thrombosis Research, Lillehei Heart Institute, University of Minnesota. E-mail: gundurao9@gmail.com*

27. Delgado MD, León J. Gene expression regulation and cancer. Clin Transl Oncol. 2006 Nov;8(11):780-7. doi: 10.1007/s12094-006-0132-7.
28. Kagohara LT, Stein-O'Brien GL, Kelley D, Flam E, Wick HC, Danilova LV, et al. Epigenetic regulation of gene expression in cancer: techniques, resources and analysis. Brief Funct Genomics. 2018 Jan 1;17(1):49-63. doi: 10.1093/bfgp/elx018.
29. Zehir A, Benayed R, Shah RH, Syed A, Middha S, Kim HR, et al. Mutational landscape of metastatic cancer revealed from prospective clinical sequencing of 10,000 patients. Nat Med. 2017 Jun;23(6):703-713. doi: 10.1038/nm.4333. Epub 2017 May 8. Erratum in: Nat Med. 2017 Aug 4;23 (8):1004.
30. Sun Y. Tumor microenvironment and cancer therapy resistance. Cancer Lett. 2016 Sep 28;380(1):205-15. doi: 10.1016/j.canlet.2015.07.044.
31. Lasfar A, Balan M, Cohen-Solal KA, Zloza A. Editorial: Tumor Microenvironment and Resistance to Current Therapies. Front Oncol. 2019 Nov 14;9:1131. doi: 10.3389/fonc.2019.01131.
32. Wu P, Gao W, Su M, Nice EC, Zhang W, Lin J, Xie N. Adaptive Mechanisms of Tumor Therapy Resistance Driven by Tumor Microenvironment. Front Cell Dev Biol. 2021 Mar 1;9:641469. doi: 10.3389/fcell.2021.641469.
33. Li H, Yang Y, Hong W, Huang M, Wu M, Zhao X. Applications of genome editing technology in the targeted therapy of human diseases: mechanisms, advances and prospects. Signal Transduct Target Ther. 2020 Jan 3;5(1):1. doi: 10.1038/s41392-019-0089-y.
34. Cornu TI, Mussolino C, Cathomen T. Refining strategies to translate genome editing to the clinic. Nat Med. 2017 Apr 3;23(4):415-423. doi: 10.1038/nm.4313.
35. Wang X, Tokheim C, Gu SS, Wang B, Tang Q, Li Y, et al. In vivo CRISPR screens identify the E3 ligase Cop1 as a modulator of macrophage infiltration and cancer immunotherapy target. Cell. 2021 Oct 14;184(21):5357-5374.e22. doi: 10.1016/j.cell.2021.09.006.
36. Chu VT, Graf R, Wirtz T, Weber T, Favret J, Li X, et al. Efficient CRISPR-mediated mutagenesis in primary immune cells using CrispRGold and a C57BL/6 Cas9 transgenic mouse line. Proc Natl Acad Sci U S A. 2016 Nov 1;113(44):12514-12519. doi: 10.1073/pnas.1613884113.
37. Ran FA, Hsu PD, Wright J, Agarwala V, Scott DA, Zhang F. Genome engineering using the CRISPR-Cas9 system. Nat Protoc. 2013 Nov;8(11):2281-2308. doi: 10.1038/nprot.2013.143.
38. Azangou-Khyavy M, Ghasemi M, Khanali J, Boroomand-Saboor M, Jamalkhah M, Soleimani M, Kiani J. CRISPR/Cas: From Tumor Gene Editing to T Cell-Based Immunotherapy of Cancer. Front Immunol. 2020 Sep 29;11:2062. doi: 10.3389/fimmu.2020.02062.
39. Chira S, Gulei D, Hajitou A, Berindan-Neagoe I. Restoring the p53 'Guardian' Phenotype in p53-Deficient Tumor Cells with CRISPR/Cas9. Trends Biotechnol. 2018 Jul;36(7):653-660. doi: 10.1016/j.tibtech.2018.01.014.
40. Joung J, Konermann S, Gootenberg JS, Abudayyeh OO, Platt RJ, Brigham MD, Sanjana NE, Zhang F. Genome-scale CRISPR-Cas9 knockout and transcriptional activation screening. Nat Protoc. 2017 Apr;12(4):828-863. doi: 10.1038/nprot.2017.016.
41. Chen S, Sanjana NE, Zheng K, Shalem O, Lee K, Shi X, Scott DA, Song J, Pan JQ, Weissleder R, Lee H, Zhang F, Sharp PA. Genome-wide CRISPR screen in a mouse model of tumor growth and metastasis. Cell. 2015 Mar 12;160(6):1246-60. doi: 10.1016/j.cell.2015.02.038.
42. Raper V. To Root Out Cancer Immunotherapies Dig Deeper. Gen Eng. & Biotech News. 2017;38(1) December 26.
43. Raita Y, Camargo CA Jr, Liang L, Hasegawa K. Big Data, Data Science, and Causal Inference: A Primer for Clinicians. Front Med (Lausanne). 2021 Jul 6;8:678047. doi: 10.3389/fmed.2021.678047.
44. Tejera P, Jardim J, Laucho-Contreras ME. Editorial: Precision Medicine in Pulmonary Diseases-Same Principles, New Approach. Front Med (Lausanne). 2021 Dec 20;8:821013. doi: 10.3389/fmed.2021.821013.
45. Guzmán-Vargas J, Ambrocio-Ortiz E, Pérez-Rubio G, Ponce-Gallegos MA, Hernández-Zenteno RJ, Mejía M, Ramírez-Venegas A, Buendia-Roldan I, Falfán-Valencia R. Differential Genomic Profile in *TERT, DSP*, and *FAM13A* Between COPD Patients With Emphysema, IPF, and CPFE Syndrome. Front Med (Lausanne). 2021 Aug 19;8:725144. doi: 10.3389/fmed.2021.725144.
46. Goetz LH, Schork NJ. Personalized medicine: motivation, challenges, and progress. Fertil Steril. 2018 Jun;109(6):952-963. doi: 10.1016/j.fertnstert.2018.05.006.
47. Sverdlov O, van Dam J, Hannesdottir K, Thornton-Wells T. Digital Therapeutics: An Integral Component of Digital Innovation in Drug Development. Clin Pharmacol Ther. 2018 Jul;104(1):72-80. doi: 10.1002/cpt.1036.
48. Tate, AR, Rao GHR. Activity Trackers, Wearables, Noninvasive Technologies for Early Detection, and Management of Cardiometabolic Risks. International Journal of Biomedicine. 2020;10(3):189-197. doi: 10.21103/Article10(3)_RA2
49. Dzobo K. Taking a Full Snapshot of Cancer Biology: Deciphering the Tumor Microenvironment for Effective Cancer Therapy in the Oncology Clinic. OMICS. 2020 Apr;24(4):175-179. doi: 10.1089/omi.2020.0019.
50. Errington TM, Denis A, Perfito N, Iorns E, Nosek BA. Challenges for assessing replicability in preclinical cancer biology. Elife. 2021 Dec 7;10:e67995. doi: 10.7554/eLife.67995.

International Journal of Biomedicine 12(1) (2022) 82-88
http://dx.doi.org/10.21103/Article12(1)_RA3

REVIEW ARTICLE

INTERNATIONAL JOURNAL OF BIOMEDICINE

The Ability of Contrast-Enhanced Ultrasound, Conventional Ultrasound, and ^{99m}Tc-MIBI Scintigraphy for the Detection of Parathyroid Lesion in Patients with Primary Hyperparathyroidism

Maryam M. Alramadhan[1]; A. Alsolai[2]; Rana A. Eisa[3*]; Awadia Gareeballah[4]

[1]*King Saud Medical City, Riyadh, Saudi Arabia*
[2]*Diagnostic Radiology Department, College of Applied Medical Sciences, King Saud University, Riyadh, Saudi Arabia*
[3]*Health Sciences Department, Colleges of Applied Studies and Community Services, King Saud University, Riyadh, Saudi Arabia*
[4]*Department of Diagnostic Radiologic Technology, Faculty of Applied Medical Sciences, Taibah University, Al-Madinah Al-Munawara, Saudi Arabia*

Abstract

The aim of this review was to compare the efficiency of conventional ultrasound (CUS), contrast-enhanced ultrasound (CEUS), and ^{99m}Tc-MIBI scintigraphy in imaging parathyroid gland lesions in patients with primary hyperparathyroidism (PHPT).

In this review, we attempted to present a clear view of the most reliable or precise technique for detecting parathyroid gland (PG) pathology in PHPT. Our study relied on secondary data based on the review of the extant literature on PHPT imaging. The research retrieved articles from the scholarly databases Google Scholar, Web of Science, and PUBMED/MEDLINE that examine the efficiency of CUS, CEUS, and ^{99m}Tc-MIBI scintigraphy in imaging PGs in PHPT patients. The study retrieved secondary data from past research identified using keyword and medical subject heading terms like "Ultrasound," "Contrast-Enhanced Ultrasound," "Sonography in parathyroid," "Primary hyperthyroidism," "Scintigraphy," and "Contrast-enhanced ultrasound in parathyroid disease." This study only relied on original contribution papers presented in English and published between 2011 and 2021. We found that CEUS has a comparable sensitivity to ^{99m}Tc-MIBI scintigraphy so that it can be used in patients who have a contraindication to scintigraphy or in a hospital without nuclear medicine facility. CEUS is able to detect very small size adenomas, whereas the detection using scintigraphy depends on the size of the diseased glands and the cytology.(**International Journal of Biomedicine. 2022;12(1):82-88.**)

Key Words: contrast-enhanced ultrasound • conventional ultrasound • primary hyperparathyroidism • scintigraphy

For citation: Alramadhan MM, Alsolai A, Eisa RA, Gareeballah A. The Ability of Contrast-Enhanced Ultrasound, Conventional Ultrasound, and 99mTc-MIBI Scintigraphy for the Detection of Parathyroid Lesion in Patients with Primary Hyperparathyroidism. International Journal of Biomedicine. 2022;12(1):82-88. doi:10.21103/Article12(1)_RA3

Abbreviations

CEUS, contrast-enhanced ultrasound; **CUS**, conventional ultrasound; **CT**, computed tomography; **PTA**, parathyroid adenoma; **PG**, parathyroid gland; **PHPT**, primary hyperparathyroidism; **SA**, single adenoma; **SPECT,** singlephoton emission computed tomography.

Primary hyperparathyroidism (PHPT) is characterized by elevated serum calcium concentration and elevated or inappropriately normal parathyroid hormone levels. Silverberg describes the skeletal hallmark of PHPT as osteitis fibrosa cystica, radiographically characterized by brown tumors of the long bones, subperiosteal bone resorption, distal tapering of the clavicles, and phalanges, and "salt-and-pepper" erosions of the skull. Nephrocalcinosis and nephrolithiasis, as

well as neuromuscular symptoms (proximal muscle weakness, atrophy, hyperreflexia, and gait disturbances), are present in the majority of patients.[1]

PHPT results from excessive secretion of parathyroid hormone from one or more of PGs. The underlying cause of sporadic PHPT is unknown in most cases. Long-term lithium therapy, a history of radioactive iodine therapy for thyroid disease, or external neck radiation are risk factors for sporadic PHPT. Other risk factors recently described are chronically low calcium intake and higher body weight.[2,3]

The most common pathological finding in patients with PHPT is a solitary PTA, occurring in 80% of patients.[4] All 4 PGs are involved in approximately 15% of patients. Golden SH parathyroid carcinoma has been found in <1% of all cases of PHPT.[5]

CUS and ^{99m}Tc-MIBI scintigraphy (^{99m}Tc sestamibi, also known as hexakis 2-methoxyisobutyl isonitrile) are the imaging techniques for the preoperative location of PTAs. Numerous studies comparing these techniques suggest similar sensitivities and specificities for detecting solitary adenoma. Localization accuracy is also improved when both studies are obtained preoperatively. Contrast-enhanced CT and MRI can also effectively locate PTAs but are less commonly used for preoperative location.[6]

Currently, CEUS has been used to help distinguish PTAs from thyroid nodules and lymph nodes. One study revealed CEUS had a sensitivity of 66.7% for detection of SAs compared to 77.8% for ^{99m}Tc-MIBI SPECT scintigraphy and 51.8% for a high-resolution ultrasound.[7] The sensitivity increased to 82.7% when ^{99m}Tc-MIBI scintigraphy and CEUS results were paired together. CEUS may be superior to high-resolution ultrasound because the ultrasound contrast agent allows for amplification of vascular signals in the lesions, providing additional diagnostic value.[7-9] One study showed that the CEUS had a sensitivity of 98.4% and specificity of 98.4% for detecting pathology in PGs.[8] CEUS is a highly sensitive, quick, and cost-efficient method for localization of pathological PGs and is reliable even in the presence of concomitant goiter, after previous neck surgery, and with the multigland disease.[9,10] The CEUS features of the intrathyroidal adenoma include intense, homogeneous, and very early arterial enhancement, which is often apparent as quickly as 4–5 seconds after injection. Further, enhancement tends to persist in the adenoma after the adjacent thyroid has begun to clear the contrast agent. CEUS has localized a PTA in the setting of multiple background thyroid nodules in Hashimoto's disease.[11]

In this review, we attempted to present a clear view of the most reliable or precise technique for detecting PG pathology in PHPT. Our study relied on secondary data based on the review of the extant literature on PHPT imaging. The research retrieved articles from the scholarly databases Google Scholar, Web of Science, and PUBMED/MEDLINE that examine the efficiency of CUS, CEUS, and ^{99m}Tc-MIBI scintigraphy in imaging PGs in PHPT patients. The study retrieved secondary data from past research identified using keyword and medical subject heading terms like "Ultrasound," "Contrast-Enhanced Ultrasound," "Sonography in parathyroid," "Primary hyperthyroidism," "Scintigraphy," and "Contrast-enhanced ultrasound in parathyroid disease." This study only relied on original contribution papers presented in English and published between 2011 and 2021. The study focused on pre-surgical detection and localization of pathologic PGs using CUS, CEUS, and scintigraphy. However, systematic reviews, literature reviews, case reports, and studies undertaken before this period were considered inadequate, or the data was too old, and therefore excluded. The papers provide varying perspectives on PHPT and the treatment approaches. Each of these approaches is individually important towards understanding the collective gains made and existing gaps in the treatment of the disease.

The data needed for the cross-document comparisons included the journal name, date of publication, number of times cited, and the study design. Additional considerations had inclusion and exclusion criteria, population and period, and the accuracy, specificity, and sensitivity of the result. This paper compares and analyzes the efficiency of the 3 discussed techniques (CUS, ^{99m}Tc-MIBI scintigraphy, and CEUS) per the sensitivity, specificity, and ability to detect ectopic glands, thyroid concomitant goiter, and multiglandular disease. The paper considered additional factors influencing efficiencies, including cost, invasiveness, treatment side effects, anatomical resolution, radiology expertise, and availability. These factors are critical to early detection, proper diagnosis, effective treatment of the disease, and potential prevention.

We reviewed a total of 64 articles; 49 studies met exclusion criteria. Results in 15 studies were selected for review: the included studies reported various imaging modalities for pre-surgical localization: CEUS, CUS, and ^{99m}Tc-MIBI scintigraphy. Seven papers compared CEUS with CUS, 2 compared CEUS with ^{99m}Tc-MIBI scintigraphy, and 5 compared ^{99m}Tc-MIBI scintigraphy with CUS. CEUS and ^{99m}Tc-MIBI scintigraphy. Half of the studies included were retrospective studies. All the studies included patients with PHPT, which indicates surgery, diagnosed clinically and by biomedical results. The patients with recurrent, persistent, or secondary hyperparathyroidism or with a history of allergy to contrast media were excluded. The included articles that use CEUS as an imaging modality for localization are summarized in Table 1, and those that use CUS and scintigraphy are summarized in Table 2.

CEUS

Nine articles included had publication periods from 2011 to 2019. All studies used SonoVue (Bracco S.p.A., Milan, Italy) as the contrast agent and were performed by expert operators. The use of CEUS has the advantage of identifying the pathological PGs from the adjacent isoechoic thyroid nodules and the cervical lymphadenopathy, where they may have the same echogenicity. Several studies have demonstrated higher sensitivity of CEUS in detecting single PTA. CEUS alone had a sensitivity of 66.7%-100%. Summarization of 9 published articles can be found in Table 1. Thus, the sensitivity and specificity of CEUS and CUS for detecting SAs are presented. The statistical *P*-value in the sensitivity between the 2 modalities was reported in 7 of the 9 articles included.

Table 1.

Studies that compare the use of CEUS with CUS or/and ^{99m}Tc-MIBI scintigraphy

	STUDY	Imaging Modality	n	SA	MGD/ surgical result	CG	Ectopic	Sensitivity,%	Specificity,%	Sensitivity *P*- value
1	Hornung et al.[12]	CUS CEUS	60 60	22 59	NR NR	8 NR	0/0 0/0	70% 98.3%	NR NR	0.001
2	Uller et al. [8]	CEUS	26	23	2/2	14	0/0	98.4%	98.4%	<0.05
3	Agha et al. [9]	CUS CEUS	30 30	25 29	0/1 1 /1	NR NR	0/0 0/0	80% 100%	NR NR	0.015
4	Karakas et al. [15]	CUS CEUS	25 25	18 18	1/5 1/5	1/1 1/1	0/0 0/0	86% 86%	NR NR	NR
5	Agha et al.[10]	CUS CEUS	75 75	48 68	1/5 5 /5	16 25	NR NR	68.5% 97.1%	NR NR	<0.006
6	Aghaa et al. [24]	Sci CEUS	75 143	45 139	NR NR	NR NR	NR NR	60.8% 97.2%	NR NR	0.019
7	Para Ramírez et al. [7]	CUS Sci CEUS	27 27 27	14 21 18	0/2 0/2 2 /2	NR NR NR	NR NR NR	51.8% 77.8% 66.7%	NR NR NR	NR
8	Da Silva et al. [13]	CUS CEUS	42 42	NR 42	NR NR	NR NR	NR NR	100%	NR NR	0.356
9	Piccin et al. [14]	CUS CEUS	336 198	NR NR	NR NR	99	NR NR	76.2% 72.8%	97.3% 97.3%	0.337

n - number of patients; Sci- ^{99m}Tc-MIBI scintigraphy; SA - single adenoma; MGD - multiglandular disease; CG - concomitant goiter; NR - not reported; Ectopic - ectopic parathyroid gland; 0/0 - none of patients has ectopic glands.

Table 2.

Studies that compare the use of ^{99m}Tc-MIBI scintigraphy (Sci) with CUS

	Study	Imaging modality	n.	SA	MGD	CG	Ectopic	Sensitivity%	Specificity	Sensitivity P- value
10	Elsayed and Ali.[17]	CUS Sci CUS +Sci	45 45 45	NR NR NR	NR NR NR	NR NR NR	NR NR NR	94.4% 97.4% 97.4%	44.4% 71.4% 83.3%	NR
11	Argirò et al.[18]	CUS Sci CUS+ Sci	46 46 46	41 38 43	0 0 0	NR NR NR	0/1 0/1 0/1	89.1% 83.6% 93.4%	97.5% 98.3% 98.3%	NR
12	Scattergood et al.[19]	CUS Sci CUS+ Sci	184 184 184	NR NR/ NR	NR NR NR	NR NR NR	0/0 0/0 00	70% 64% 81%	57% 57% 71%	0.34 <0.001
13	Vitetta et al.[20]	CUS Sci	108 108	NR NR	NR/9	NR NR	14/18 16/18	84% 71%	94% 90%	<0.05 <0.05
14	Ibrahim and Elsadawy [21]	CUS Sci US+ Sci	40 40 40	35 34 37	0 0 (Multidrug)	0/1 NR NR	NR NR NR	87.5% 85% 92.5%	66.6% 100% 100%	NR
15	Akbaba et al.[22]	US Sci US+ Sci	98 98 98	82 66 93	NR/2 NR/2	0/7 NR NR	0/2 2/2 2/2	87.2% 70.2% 94.9%	25% 50% NR	NR

n - number of patients; Sci- ^{99m}Tc-MIBI scintigraphy; SA - single adenoma; MGD - multiglandular disease; CG - concomitant goiter; NR - not reported; Ectopic - ectopic parathyroid gland; 0/0 - none of patients has ectopic glands.

In a study by Agha et al.,[9] which included 30 patients, 3 imaging modalities were used for pre-surgical mapping; the sensitivity of CUS, ^{99m}Tc-MIBI scintigraphy, and CEUS were 80%, 80%, and 100%, respectively. CEUS was superior in detecting PGs in a patient with concomitant thyroid goiter or in the presence of lymphadenopathy, where it is known that the ability of CUS in such cases is limited. However, none of the patients presented with ectopic PG, which is known as one of the CUS limitations that would affect the sensitivity of CEUS.

Hornung et al.[12] concluded that CEUS is a highly sensitive diagnostic tool for localizing pathology in PGs in PHPT patients. Nevertheless, it can only be recommended as a first-line diagnostic procedure in specialized clinical centers with experienced investigators, as its sensitivity is 98.3%, compared to 70% in CUS.

In a study by Silva et al.,[13] a review of 42 patients showed that the sensitivity of CEUS reached 100%. None of the included patients presented with ectopic parathyroid locations. However, that study revealed a new method to quantify the contrast in PGs by using Vuebox Perfusion Analysis software, where the dynamic CEUS analyzed 42 patients with symptoms of PHPT. According to the results, qualitative measurement of contrast perfusion is more accurate than quantitative analysis by Vuebox. However, the latter seems a promising method in the quantification measurement of CEUS, where 25 of 28 cases were successfully diagnosed with PTAs (sensitivity of 89.3%). This result makes the diagnoses more accurate and less expensive but requires slight improvements to the software to prevent potential human-induced errors.

Piccin et al.[14] found that the sensitivity of color Doppler US was significantly higher than SPECT, while the sensitivity of 4D-CT was significantly better than US and SPECT for the preoperative localization of abnormal parathyroid gland/s. The authors concluded that in patients with concomitant thyroid pathology, the combination of US and 4D-CT represents a reliable localization technique.

The sensitivity of CEUS for detecting single adenomas was 97.1%, and double adenomas reached 100% in 70 patients diagnosed with PHPT in a study by Agha et al.[10] Also, CEUS showed the sensitivity of detecting concomitant thyroid goiter as 100%, while that of CUS was 64%. In a study performed by Ramírez et al.,[7] CEUS revealed a sensitivity of 66.7% for detecting SAs, in comparison with 77.8% for ^{99m}Tc-MIBI SPECT scintigraphy and 51.8% for high-resolution US in 29 patients with PHPT. With CEUS, DAs could be detected in both cases.

In a study by Karakas et al.,[15] 25 patients with biochemically proven PHPT underwent preoperative US, MIBI/SPECT, and CEUS. In 17(68%) patients, US and MIBI/SPECT raised suspicion of parathyroid lesions and all suspected lesions were reassessed by CEUS. However, additional information was not obtained about using CEUS compared to results of US and MIBI/SPECT.

The sensitivity of CEUS in detecting small size adenoma (0.5cm -1.5cm) was significantly higher than the CUS. The sensitivity achieved by CEUS and CUS from each study included in this review is represented in a column chart (Fig.1).

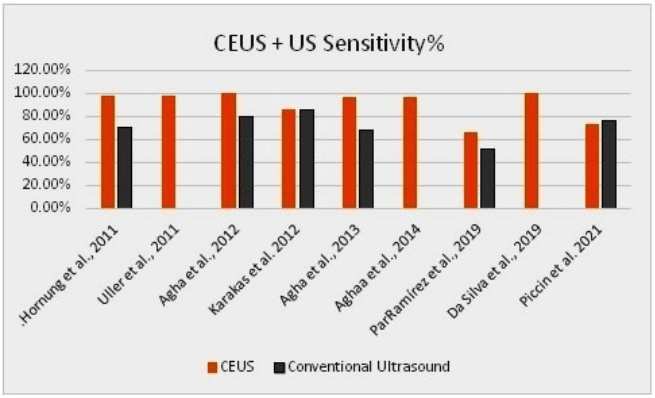

Fig. 1. *The sensitivity achieved by CEUS and CUS.*

CUS and ^{99m}Tc-MIBI Scintigraphy

In a systematic review and meta-analysis, the pooled sensitivity of CUS was reported to reach 80% and scintigraphy 83% among 12 studies. Ruda et al.,[16] analyzing 20,225 cases of PHPT, stated that the sensitivity for ^{99m}Tc-MIBI scintigraphy and CUS were 88.44% and 78.55%, respectively for single adenoma, 44.46% and 34.86% for multiple gland hyperplasia disease, and 29.95% and 16.20% for double adenoma, respectively.

The comparison between 6 studies using CUS and ^{99m}Tc-MIBI scintigraphy and combining the 2 methods is summarized in Table 2. The sensitivity and specificity of each study are included. The numerical values for an single adenoma detected by CUS or ^{99m}Tc-MIBI scintigraphy were not reported in 3 papers, and the *P*-value of the sensitivity between the 2 imaging procedures was calculated only in 2 studies.

Elsayed and Ali [17] compared the efficacy of CUS and ^{99m}Tc-MIBI scintigraphy and a combination of these methods in preoperative detection and localization of PHPT. The study, which included 45 patients, revealed that the sensitivity and specificity for ^{99m}Tc-MIBI scintigraphy were 97.4% and 71.4%, and the values for CUS were 94.4% and 44.4%, respectively. However, the combined approach values were higher, returning 97.4% for sensitivity, 83.3% for specificity, and 95.6% for accuracy. The study recommends a combined approach that uses CUS and ^{99m}Tc-MIBI scintigraphy for PHPT localizing. This approach would result in higher efficiency with a reduced chance of missing parathyroid due to the presence of concomitant thyroid pathology.

Argirò et al.[18] examined the diagnostic accuracy of ^{99m}Tc-MIBI scintigraphy in preoperative localization of PTAs as compared to CUS. The study included 46 PHPT patients who underwent CUS, ^{99m}Tc-MIBI scintigraphy, and MRI. The researchers found that ultrasound was effective, correctly localizing 41 out of the 46 PTA cases. CUS had 89.1% sensitivity and 97.5% specificity. In comparison, ^{99m}Tc-MIBI scintigraphy was accurate for 38 of the 46 cases, with a sensitivity score of 83.6% and a specificity score of 98.3%; the combined method yielded a sensitivity of 93.4% and specificity of 98.3%.

Scattergood et al.[19] analyzed the patients with a histological diagnosis of a PTA. The authors determined that CUS had a higher sensitivity than ^{99m}Tc-MIBI scintigraphy: the sensitivity of CUS was 70%, specificity - 57%, while the sensitivity of ^{99m}Tc-MIBI scintigraphy was 64% and specificity - 57%. There was enhanced sensitivity and specificity when CUS and ^{99m}Tc-MIBI scintigraphy were combined in preoperative localization for PHPT patients - 81% and 71%, respectively.

Vitetta et al.[20] conducted a retrospective comparative study to determine the prospective functions of parathyroid scintigraphy and ultrasonography localization of the neck. The study also measured the intra-operator reliability, and the agreement between the 2 ultrasound sonographers was high.

Ibrahim and Elsadawy[21] stated that the combined use of CUS and ^{99m}Tc-MIBI scintigraphy improved the pre-surgical localization of PTAs.

The study by Akbaba et al.[22] compared various preoperative imaging methods used for PHPT patients. Specifically, the study compared CUS, ^{99m}Tc-MIBI scintigraphy, SPECT, and MRI. The accuracy rates for these preoperative approaches were assessed in 98 patients with known PHPT. Each patient was taken through parathyroidectomy. In that study, a preoperative localization approach was used in 82 cases of patients with abnormal PGs, while ^{99m}Tc-MIBI scintigraphy was done in 66 of the cases. The study determined that CUS has the highest values for sensitivity, specificity, and diagnostic accuracy, compared to other methods. The sensitivity, specificity and diagnostic accuracy values were 87.2%, 25.0%, and 83.0% for CUS, 70.2%, 50.0%, and 69.4% for ^{99m}Tc-MIBI scintigraphy, 75.5%, 50.0%, and 74.5% for SPECT, and 63.8%, 50.0%, and 63.3% for MRI, respectively. Therefore, CUS was found to be the most effective preoperative approach. The combination of CUS with ^{99m}Tc-MIBI scintigraphy yielded more sensitivity, and diagnostic accuracy was 94.9% and 91.1%, respectively.

The sensitivity achieved by ^{99m}Tc-MIBI scintigraphy and CUS from each study included in this review are represented in a column chart (Fig.2).

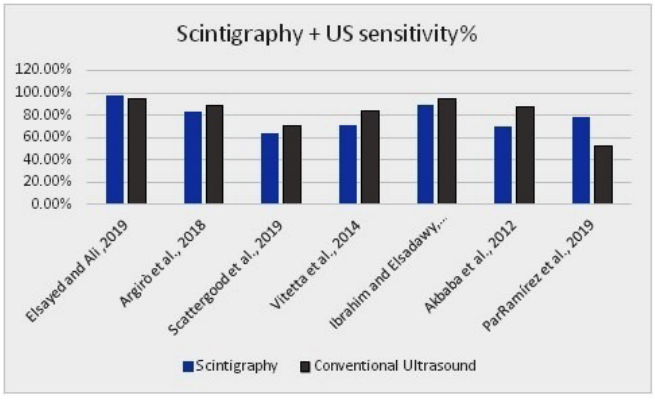

Fig. 2. *The sensitivity achieved by ^{99m}Tc-MIBI scintigraphy and CUS*

It is essential for all patients diagnosed with PHPT to undergo preoperative imaging. Wilhelm et al.[23] recommended that cervical ultrasonography performed by an experienced parathyroid sonographer is the least costly imaging modality and, when combined with ^{99m}Tc-MIBI scintigraphy or 4-dimensional CT, is the most cost-effective strategy. Preoperative, ultrasound-directed, fine-needle aspiration biopsy of parathyroid lesions is highly specific but is rarely necessary and can have undesirable consequences. Cervical ultrasonography is recommended to localize parathyroid disease and assess for concomitant thyroid disease. ^{99m}Tc-MIBI scintigraphy is the dominant radioisotope in parathyroid scintigraphy.

Each sestamibi protocol (dual-phase, iodine 131 subtraction, SPECT) has individual strengths and weaknesses. Combined CUS and ^{99}mTc-MIBI scintigraphy imaging increases localization accuracy and improves sensitivity.[23]

Our review shows that CEUS has a sensitivity of 66.7%-100%, CUS – 51.8%-94.6%, and ^{99m}Tc-MIBI scintigraphy – 61.8%-97.4%. These values place CEUS as one of the imaging procedures that could be selected for pre-surgical mapping. CEUS has a sensitivity slightly higher than CUS and comparable to ^{99m}Tc-MIBI scintigraphy in localization. We found that CEUS does not limit the size of the gland; the ability to detect very small size (6mm) has been proved in 4 studies.

Agha et al.[24] concluded that CEUS represents a high sensitivity method for the localization of PTAs independent of findings in ^{99m}Tc-MIBI scintigraphy, and that in the presence of appropriate expertise in CEUS, no further diagnostic procedures are required. However, Scattergood et al.[19] recommended using CEUS as second-line imaging when the lesions cannot be localized by CUS or ^{99m}Tc-MIBI scintigraphy.

The time required and the cost for the 3 imaging modalities was analyzed by Agha et al.[9] The authors noted that imaging by ^{99m}Tc-MIBI scintigraphy requires the longest time to complete the exam and attracts the highest price. The procedure entails injecting contrast and waiting after the injection until patients leave the exam room. It requires approximately 3h and costs an average of $443. On the other hand, CUS and CEUS need less time and have a lower cost. The differences in the time required and the cost is beneficial for the healthcare provider and the patient's situation. However, the need for sonographers and radiologists to perform the exam limits the prevalent use of CEUS in some countries as this exam is highly operator-dependent, as opposed to scintigraphy, which is less operator-dependent. The early enhancement of the contrast in PTA and early washout (3-5 min after injection) are the imaging characteristics that confirm the presence of PTA. Also, in patients with cervical lymph nodes that are sometimes indistinguishable from parathyroid disease, lymph nodes showed an early enhancement of the contrast at the hilum and a late enhancement of the parenchyma.[9]

Study Limitations

In this literature review, we analyzed only studies that used CEUS and papers that used the first-line methods for pre-surgical localization of parathyroid adenomas. The specificity and accuracy for CEUS could not be achieved in some studies because only non-healthy participants were included in the

analysis. Also, the positive predictive value was not mentioned in most of the papers and the sensitivity confidence intervals were reported in 4 studies only; thererfore, this review cannot achieve a meta-analysis. Difficulties have been found in communications with some affiliation authors, maybe because none used email addresses or for other unknown reasons. Moreover, some studies did not provide the ultrasound grey-scale findings as it was done for all the patients, especially if the patient had concomitant goiter or thyroid nodular, which is known to limit the ultrasound efficiency in detecting parathyroid glands.

Conclusion

CUES represented a safe, cost-efficient, highly sensitive method for detecting the disease in parathyroid glands for PHPT patients, even if the concomitant goiter is present or if patients have multigland disease. CEUS has a comparable sensitivity to ^{99m}Tc-MIBI scintigraphy, so that it can be used in patients who have a contraindication to scintigraphy or in a hospital without nuclear medicine facility. However, further studies are recommended to determine whether CUES can be used as a standard diagnostic procedure for pre-surgical localization. Ultrasound had a higher sensitivity and lower specificity than ^{99m}Tc-MIBI scintigraphy. A combined approach enhances the performance of either method used independently.

Competing Interests

The authors declare that they have no competing interests.

References

1. Walker MD, Bilezikian JP. Primary Hyperparathyroidism. 2021 Apr 19. In: Feingold KR, Anawalt B, Boyce A, Chrousos G, de Herder WW, Dhatariya K, Dungan K, Hershman JM, Hofland J, Kalra S, Kaltsas G, Koch C, Kopp P, Korbonits M, Kovacs CS, Kuohung W, Laferrère B, Levy M, McGee EA, McLachlan R, Morley JE, New M, Purnell J, Sahay R, Singer F, Sperling MA, Stratakis CA, Trence DL, Wilson DP, editors. Endotext [Internet]. South Dartmouth (MA): MDText.com, Inc.; 2000–. PMID: 25905161.
2. Vaidya A, Curhan GC, Paik JM, Wang M, Taylor EN. Body Size and the Risk of Primary Hyperparathyroidism in Women: A Cohort Study. J Bone Miner Res. 2017 Sep;32(9):1900-1906. doi: 10.1002/jbmr.3168.
3. Paik JM, Curhan GC, Taylor EN. Calcium intake and risk of primary hyperparathyroidism in women: prospective cohort study. BMJ. 2012 Oct 17;345:e6390. doi: 10.1136/bmj.e6390.
4. Golden SH, Robinson KA, Saldanha I, Anton B, Ladenson PW. Clinical review: Prevalence and incidence of endocrine and metabolic disorders in the United States: a comprehensive review. J Clin Endocrinol Metab. 2009 Jun;94(6):1853-78. doi: 10.1210/jc.2008-2291.
5. Bilezikian JP, Bandeira L, Khan A, Cusano NE. Hyperparathyroidism. Lancet. 2018 Jan 13;391(10116):168-178. doi: 10.1016/S0140-6736(17)31430-7.
6. Johnson NA, Tublin ME, Ogilvie JB. Parathyroid imaging: technique and role in the preoperative evaluation of primary hyperparathyroidism. AJR Am J Roentgenol. 2007 Jun;188(6):1706-15. doi: 10.2214/AJR.06.0938.
7. Parra Ramírez P, Santiago Hernando A, Barquiel Alcalá B, Martín Rojas-Marcos P, Lisbona Catalán A, Álvarez Escolá C. Potential Utility of Contrast-Enhanced Ultrasound in the Preoperative Evaluation of Primary Hyperparathyroidism. J Ultrasound Med. 2019 Oct;38(10):2565-2571. doi: 10.1002/jum.14949.
8. Uller W, Jung EM, Hornung M, Ross C, Jung W, Schlitt HJ, Stroszczynski C, Agha A. Evaluation of the microvascularization of pathologic parathyroid glands in patients with primary hyperparathyroidism using conventional ultrasound and contrast-enhanced ultrasound. Clin Hemorheol Microcirc. 2011;48(1):95-103. doi: 10.3233/CH-2011-1402.
9. Agha A, Hornung M, Rennert J, Uller W, Lighvani H, Schlitt HJ, Jung EM. Contrast-enhanced ultrasonography for localization of pathologic glands in patients with primary hyperparathyroidism. Surgery. 2012 Apr;151(4):580-6. doi: 10.1016/j.surg.2011.08.010.
10. Agha A, Hornung M, Stroszczynski C, Schlitt HJ, Jung EM. Highly efficient localization of pathological glands in primary hyperparathyroidism using contrast-enhanced ultrasonography (CEUS) in comparison with conventional ultrasonography. J Clin Endocrinol Metab. 2013 May;98(5):2019-25. doi: 10.1210/jc.2013-1007.
11. Navarro SM, Malhi H, Deurdulian C, Grant E. Localization of Parathyroid Adenoma Using Contrast-Enhanced Sonography. J Ultrasound Med. 2019 Jan;38(1):259-260. doi: 10.1002/jum.14672.
12. Hornung M, Jung EM, Stroszczynski C, Schlitt HJ, Agha A. Contrast-enhanced ultrasonography (CEUS) using early dynamic in microcirculation for localization of pathological parathyroid glands: first-line or complimentary diagnostic modality? Clin Hemorheol Microcirc. 2011;49(1-4):83-90. doi: 10.3233/CH-2011-1459.
13. Platz Batista da Silva N, Jung EM, Jung F, Schlitt HJ, Hornung M. VueBox® perfusion analysis of contrast-enhanced ultrasound (CEUS) examinations in patients with primary hyperparathyroidism for preoperative detection of parathyroid gland adenoma. Clin Hemorheol Microcirc. 2018;70(4):423-431. doi: 10.3233/CH-189307.
14. Piccin O, D'Alessio P, Cioccoloni E, Burgio L, Poggi C, Altieri P, Vicennati V, Repaci A, Pagotto U, Cavicchi O. Pre-operative imaging workup for surgical intervention in primary hyperparathyroidism: A tertiary referral center experience. Am J Otolaryngol. 2021 Jan-Feb;42(1):102819. doi: 10.1016/j.amjoto.2020.102819.
15. Karakas E, Kann S, Höffken H, Bartsch DK, Celik I, Görg C, Pfestroff A. Does contrast-enhanced cervical ultrasonography improve preoperative localization results in patients with sporadic primary hyperparathyroidism? J Clin Imaging Sci. 2012;2:64. doi: 10.4103/2156-7514.103054.
16. Ruda JM, Hollenbeak CS, Stack BC Jr. A systematic review of the diagnosis and treatment of primary hyperparathyroidism from 1995 to 2003. Otolaryngol Head Neck Surg. 2005 Mar;132(3):359-72. doi: 10.1016/j.otohns.2004.10.005.

***Corresponding author**: Dr. Rana A. Eisa. Health Sciences Department, Colleges of Applied Studies and Community Services, King Saud University Riyadh, Saudi Arabia. E-mail: rana.eisa@gmail.com*

17. Abd Elhameed Elsayed W, Ali RA. Efficacy of Scintigraphy, Ultrasound and Both Scintigraphy and Ultrasonography in Preoperative Detection and Localization of Primary Hyperparathyroidism. Cureus. 2019 Jun 20;11(6):e4960. doi: 10.7759/cureus.4960.
18. Argirò R, Diacinti D, Sacconi B, Iannarelli A, Diacinti D, Cipriani C, Pisani D, Romagnoli E, Biffoni M, Di Gioia C, Pepe J, Bezzi M, Letizia C, Minisola S, Catalano C. Diagnostic accuracy of 3T magnetic resonance imaging in the preoperative localisation of parathyroid adenomas: comparison with ultrasound and 99mTc-sestamibi scans. Eur Radiol. 2018 Nov;28(11):4900-4908. doi: 10.1007/s00330-018-5437-8.
19. Scattergood S, Marsden M, Kyrimi E, Ishii H, Doddi S, Sinha P. Combined ultrasound and Sestamibi scintigraphy provides accurate preoperative localisation for patients with primary hyperparathyroidism. Ann R Coll Surg Engl. 2019 Feb;101(2):97-102. doi: 10.1308/rcsann.2018.0158.
20. Vitetta GM, Neri P, Chiecchio A, Carriero A, Cirillo S, Mussetto AB, Codegone A. Role of ultrasonography in the management of patients with primary hyperparathyroidism: retrospective comparison with technetium-99m sestamibi scintigraphy. J Ultrasound. 2014 Jan 31;17(1):1-12. doi: 10.1007/s40477-014-0067-8.
21. Ibrahim EAG, Elsadawy ME. Combined Tc-99m sesta MIBI scintigraphy and ultrasonography in preoperative detection and localization of parathyroid adenoma. Egypt J Radiol Nucl Med. 2015;46:937-941. 10.1016/j.ejrnm.2015.07.006
22. Akbaba G, Berker D, Isik S, Aydin Y, Ciliz D, Peksoy I, Ozuguz U, Tutuncu YA, Guler S. A comparative study of pre-operative imaging methods in patients with primary hyperparathyroidism: ultrasonography, 99mTc sestamibi, single photon emission computed tomography, and magnetic resonance imaging. J Endocrinol Invest. 2012 Apr;35(4):359-64. doi: 10.3275/7764.
23. Wilhelm SM, Wang TS, Ruan DT, Lee JA, Asa SL, Duh QY, Doherty GM, Herrera MF, Pasieka JL, Perrier ND, Silverberg SJ, Solórzano CC, Sturgeon C, Tublin ME, Udelsman R, Carty SE. The American Association of Endocrine Surgeons Guidelines for Definitive Management of Primary Hyperparathyroidism. JAMA Surg. 2016 Oct 1;151(10):959-968. doi: 10.1001/jamasurg.2016.2310.
24. Agha A, Hornung M, Schlitt HJ, Stroszczynski C, Jung EM. The role of contrast-enhancend ultrasonography (CEUS) in comparison with 99mTechnetium-sestamibi scintigraphy for localization diagnostic of primary hyperparathyroidism. Clin Hemorheol Microcirc. 2014;58(4):515-20. doi: 10.3233/CH-131800.

International Journal of Biomedicine 12(1) (2022) 89-94
http://dx.doi.org/10.21103/Article12(1)_RA4

REVIEW ARTICLE

INTERNATIONAL JOURNAL OF BIOMEDICINE

Magnetic Resonance Imaging in Breast Cancer Screening and Diagnosis

Batil Alonazi, PhD

Department of Radiology and Medical Imaging, College of Applied Medical Sciences, Prince Sattam Bin Abdulaziz University, AlKharj, Saudi Arabia

Abstract

The purpose of this article was to evaluate the diagnostic and screening effectiveness of breast MRI (BMRI) protocols for detecting breast cancer. The current review was based on prior research published in English databases such as PubMed and ScienceDirect in scientific articles published between 2010 and 2020 with the keywords "breast cancer MRI," "diagnostic," "dense breast," "risk factors," and "imaging." BMRI is the most sensitive imaging modality for detecting breast cancer. Annual BMRI is recommended for screening women who are at high risk for breast cancer in addition to mammography. Abbreviated MRI, with shorter image acquisition and interpretation times, increases the availability of breast MRI and reduces the costs. Unenhanced MRI parameters such as DWI are under investigation to be added to abbreviated MRI protocols. It seems feasible to offer a cost-effective screening breast DCE-MRI to a broader population.(**International Journal of Biomedicine. 2022;12(1):89-94.**)

Key Words: breast cancer • MRI • imaging protocol

For citation: Alonazi B. Magnetic Resonance Imaging in Breast Cancer Screening and Diagnosis. International Journal of Biomedicine. 2022;12(1):89-94. doi:10.21103/Article12(1)_RA4

Abbreviations

BMRI, breast MRI; **CESM**, contrast-enhanced spectral mammography; **DCE-MRI**, dynamic contrast-enhanced MRI; **DWI**, diffusion-weighted imaging; **MRI**, magnetic resonance imaging; **PEM**, positron emission mammography: **SPECT**, single-photon emission computerized tomography.

Breast cancer is the most commonly diagnosed cancer among women and the second most prevalent of all malignancies, accounting for 12% of all cancer-related deaths. In a lifetime, a woman also has a 13% chance of acquiring breast cancer.[1-4] In 2021, an estimated 2.3 million women were diagnosed with breast cancer worldwide, with 30.4% of those dying from the disease.[1,5] Breast cancer is caused by a variety of factors, including modern lifestyle (breastfeeding and age at first birth, smoking, and alcohol consumption), hormonal, breast cancer family history, obesity or overweight, null parity or late pregnancy, menstrual history, aging, previous benign breast tumor, and exposure to carcinogenic agents (radiation or chemicals). A hereditary genetic mutation is thought to be responsible for 5% to 10% of breast cancers.[6,7] Breast cancer type 1 (*BRCA1*) and breast cancer type 2 (*BRCA2*) genes are tumor suppressor genes discovered in the 1990s. These genes play an important role in DNA repair, cell cycle control, and overall genomic stability.[8] It was reported that *BRCA1* and *BRCA2* mutation carriers are responsible for 1 in 400 and 1 in 800 women breast cancer in the United States, in that order.[8] Recent estimates suggest that 55 to 65% of *BRCA1* mutation carriers and approximately 45% of *BRCA2* mutation carriers will develop breast cancer by age 70. [9-11]

Breast cancer incidence rates varied widely depending on economic situations and lifestyle. For example, in affluent countries, the incidence is 89.7 cancer cases per 100,000 women in EU countries, whereas, in developing countries, such as Africa, the incidence is 19.3 cancer cases per 100,000 women.[1,12] Dietary impacts along with reproductive factors (first childbirth, lower parity, and shorter nursing) can partly explain the difference in breast cancer incidence between

***Corresponding author**: Batil Alonazi, PhD. Department of Radiology and Medical Imaging, College of Applied Medical Sciences, Prince Sattam Bin Abdulaziz University, AlKharj, Saudi Arabia. E-mail: abdelmoneim_a@yahoo.com*

developing and developed countries.[13] It is worth noting that the incidence is also rising in emerging countries. One of the most likely reasons for the rise in cancer incidence in emerging countries is that all countries now have superior diagnostic imaging technology, which means that more cancer cases are recognized and diagnosed appropriately. Furthermore, today's culture is well informed about the early identification of breast cancer by self-examination and consultation with a qualified physician for additional investigations. Furthermore, from the 1940s through the 1980s, the average life duration of the global population increased.

The purpose of this article was to evaluate the diagnostic and screening effectiveness of breast MRI protocols for detecting breast cancer.

The current review was based on prior research published in English databases such as PubMed and ScienceDirect in scientific articles published between 2010 and 2020 with the keywords "breast cancer MRI," "diagnostic," "dense breast," "risk factors," and "imaging."

Imaging Modalities for Breast Cancer Screening

All health care providers worldwide endorse breast cancer control which involves prevention, early diagnosis, effective treatment with minimal side effects, and palliative health care and rehabilitation.[13] Early detection of breast cancer plays an important role in the treatment and control of the disease.[14]

Currently, there are 3 imaging modalities for breast cancer screening: mammography, MRI, and ultrasound.

Since the introduction of mammography about 30 years ago, breast imaging with this method has improved significantly. The sensitivity of screening mammography varied considerably across BI-RADS density codes, from 78% in women with code 1 to 47% in women with code 4.[15] The average specificity of digital screening mammography in the U.S. is 88.9%.[16] Currently, mammography is recommended for breast cancer screening for 50.0 to 74.0 years old females.[17] Previous studies showed that screening decreased mortality up to 30% compared with control patients.[13,17] Breast cancer screening with mammograms was started in Saudi Arabia in 2007 using mammography as the only screening tool.[18] However, despite recent developments in mammographic equipment and techniques, mammography as a diagnostic and screening modality has many limitations.[19] These include the reduced sensitivity in detection lesions in the radiographic dense breast due to tissue overlap and the similarity in the radiographic appearance of cancer lesions and glandular dense tissue.[20]

The sensitivity of breast magnetic resonance imaging (BMRI) in detecting breast cancer is higher than mammography and ultrasonography.[21-23] BMRI includes numerous post-contrast sequences acquired at different time points after the injection of MR contrast. The MRI cost is deemed high, and each MRI scan takes at least 20-25 minutes.[24] At the same time, BMRI has been shown to detect breast cancer at an earlier stage than mammography in high-risk patients.[25] Most studies have found that the sensitivity of MRI ranged from 71%-100% versus 16%-40% in mammography in high-risk populations.[26] Thus, BMRI is now identified as a valuable modality in diagnosing breast cancer.[27] MRI is a very sensitive method to cancer detection, but its specificity (true negative) is low. Dynamic contrast-enhanced MRI (DCE-MRI), which uses injectable gadolinium, has been recognized as the most powerful method for detecting breast cancer. The disadvantages of using MRI are its high cost and scan time. However, in high-risk patients, this method is recommended in addition to mammography.

The diagnostic power of ultrasound imaging is highly dependent on operator proficiency and the correct selection of ultrasound parameters.

Brest MRI

BMRI is an extremely useful tool for identifying and classifying breast lesions, determining the amount of localized illness, assessing response to therapy, and guiding fine-needle aspiration (FNA) biopsy.[28]

The results of mammography and any other past breast imaging should be compared to the MRI findings, as well as the clinical history, physical examination findings, and the results of mammography and any other prior breast imaging.[28] BMRI currently has specific indications, including evaluation of response to treatment, screening in high-risk patients, the study of occult breast cancer, the study of tumor recurrence, and the assessment of breast prostheses. BMRI can also be recommended for the staging of breast cancer, the study of microcalcifications, breast discharge, premalignant lesions, residual tumor in operated patients, or in cases of inconclusive findings by mammography and ultrasound.[29] BMRI was introduced as a potential diagnostic tool for patients with breast cancer as a result of these qualities.[16]

The MRI with contrast agents enhances the sensibility of images in the region of interest. Contrast agents allow improvement to the quality and the follow-up of molecular processes at the cellular and molecular levels of the region under study. For MRI, the more common contrast agents used are gadolinium-based structures.[30]

Other imaging modalities that could be utilized to diagnose breast cancer patients include positron emission mammography (PEM) and single-photon emission computerized tomography (SPECT). PET imaging uses radioactive isotopes that emit positrons (^{18}F, ^{15}O, ^{13}N, or ^{11}C); whereas SPECT imaging uses isotopes that emit gamma photons (^{99m}Tc, ^{123}I, or ^{125}I).

Both PET and SPECT provide information about the physiological activity, such as glucose metabolism, blood flow and perfusion, and oxygen utilization.[31] In recent years, a hybrid imaging modality has come into existence in the form of combined PET and MRI (PET/MRI). PET/MRI combines the unique tissue characterization of MRI with the quantifiable functional and molecular information provided by PET, thereby providing distinct potential clinical advantages over other imaging modalities.[32]

Breast MRI screening

According to the American College of Radiology (ACR),[28] current indications for breast MRI screening include:

(a) high-risk patients- women with greater than or equal to 20% lifetime risk of breast cancer (for example, individuals with genetic predisposition to breast cancer as determined by either gene testing or family pedigree, or individuals with a history of mantle radiation for Hodgkin lymphoma).[33] For high-risk patients, annual screening MRI is recommended in addition to mammography, preferably after risk assessment.

(b) Intermediate-risk patients – women with a moderately elevated risk of breast cancer (15%-20%). Breast MRI may be considered as a supplement to mammography. Annual screening MRI is recommended for women with a personal history of breast cancer and dense tissue or for those diagnosed with breast cancer under the age of 50.[34] A systematic review found that, among women with dense breasts, MRI has a sensitivity of 75–100%, specificity of 78–94%, and a p*ositive predictive value* of 3–33%.[35]

(c) Patients with a newly diagnosed breast malignancy. Bilateral breast MRI for these patients can detect occult malignancy in the contralateral breast in at least 3% to 5% of patients.[36-38]

(d) Patients with breast augmentation. The integrity of silicone implants can be determined by non-contrast breast MRI. Patients having silicone or saline implants and/or free injections with silicone, paraffin, or polyacrylamide gel in whom mammography is difficult may require contrast BMRI. Contrast-enhanced breast MRI screening may be required for patients who have undergone implant reconstruction following lumpectomy or mastectomy for breast cancer.

The BRMI can also be used to assess the extent of disease**:**[28] invasive carcinoma and ductal carcinoma in situ (DCIS), invasion deep to fascia, postlumpectomy with positive margins, neoadjuvant chemotherapy

MRI in the additional evaluation of clinical or imaging findings is beneficial for breast cancer recurrence, metastatic cancer, lesion characterization, Postoperative tissue reconstruction, MRI-guided biopsy

Screening of the general population, assessment of false-positive cases, treatment planning, inappropriate uses of breast MRI, and abbreviated (fast) MRI protocols are all examples of other considerations for MRI.

BMRI protocol

T1-weighted imaging

A dynamic T1-weighted contrast-enhanced sequence is the basis for any MRI protocol. A 3D-spoiled gradient echo sequence with a short repetition time, short echo time, and shallow flip angle is used for contrast-enhanced T1-weighted imaging.[28, 39] 3D sequences, with their intrinsically higher SNR and small, nearly isotropic voxel dimensions, have several intrinsic advantages for post-processing purposes over 2D sequences, allowing for a more precise determination of spatiotemporal disease activity. 3D images at 3T may be more robust to B1 variations,[40] and, consequently, allow for improved contrast-enhanced images.

After contrast material administration, the T1-weighted acquisition is repeated to depict enhancing abnormalities.[41] The temporal resolution required for breast MRI is determined by the time course of contrast agent uptake.[42] Peak contrast enhancement in malignant lesions typically occurs between 60 and 120 seconds after injection.[43] It is important to correctly capture the morphology and time-enhancement pattern of enhancing breast lesions.[42] Good fat suppression in both precontrast and postcontrast images minimizes the structured noise of misregistration artifacts in subtracted images, allowing detection of smaller enhancing lesions or nonmasslike lesions with greater reliability.[42]

For images obtained without fat suppression, creating subtraction images from the pre- and postcontrast acquisitions is required.[39] Subtraction images are helpful for acquisitions with fat suppression because they help differentiate truly enhancing structures from lesions with native high signal intensity at T1.[44] Generating maximum intensity projections from these subtracted images aids in rapid lesion detection.[45,46]

According to standard practice, BMRI should depict all enhancing cancers 5 mm or larger in size. Therefore, T1-weighted acquisitions should have a section thickness of no more than 2.5 mm. Much higher resolutions (1 mm isotropic and lower) can be achieved with modern MRI equipment and breast coils without lengthening the acquisition time per volume beyond 90 seconds. This enables for reconstruction in any plane, facilitating the evaluation of lesions, especially the distribution of non-mass lesions.[41] As shown by the success of abbreviated protocols for breast MRI, the acquisition of two T1-weighted acquisitions at the indicated time points (one before and one approximately 90 seconds after contrast material administration) is usually sufficient for lesion detection.[47] All other sequences aim to improve breast lesion distinction and avoid false-positive and false-negative classification.[45]

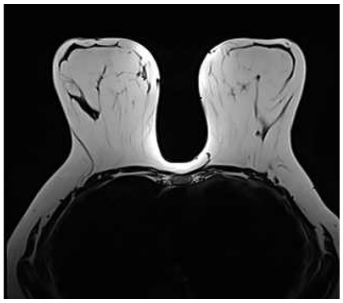

Fig. 1. *BMRI (Dixon protocol) Uuniform fat suppression based on chemical shift .*

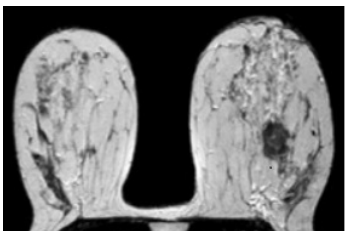

Fig. 2. *T2-weighted BMRI*

Dynamic Evaluation with Time–Signal Intensity Curves

In the previous studies, dynamic analysis has been used to evaluate the permeability of the vessels that supply a lesion.

[48] This approach is carried out by obtaining a series of T1-weighted acquisitions between 5.0 and 7.0 min after gadolinium administration.[49,50] The peak contrast material accumulation will have passed in the case of leaky vessels, and contrast material is being removed from the lesion. The contrast gradient over the vessel wall will still be positive in lesions with less-permeable vessels, and so the lesion will be enhanced. This is reflected in the shape of the time–signal intensity curves; a persistent increase is most commonly seen in benign lesions, whereas a decrease in the late phase is common in malignant lesions.[41,51] Currently, software programs generate color map overlays of the enhancement curve distribution within a lesion, making it easier to extract diagnostic data. [41]

Abbreviated breast MRI

The abbreviated MRI is a shortened version of the standard MRI, consisting of a single early phase DCE series.[52] Abbreviated MRI, with shorter image acquisition and interpretation times, may increase the availability of breast MRI and reduce the costs. Kuhl et al. and Sheth et al.[34,52] introduced the concept of an abbreviated protocol that consisted of one pre- and one postcontrast T1-weighted acquisition and found equivalent diagnostic accuracy for the abbreviated and full protocols. Abbreviated protocols consisting, for instance, of a pre-contrast and an early post-contrast T1-weighted sequence,[34,45,53-56] or, alternatively, a high-resolution ultrafast dynamic imaging protocol, [56] were found suitable to diagnose breast cancer with high accuracy. However, kinetic assessment cannot be performed with the abbreviated protocol, because multiple sets of post-contrast images are necessary for the generation of kinetic curves. [52] Among women with dense breasts undergoing screening, abbreviated breast MRI, compared with digital breast tomosynthesis, was associated with a significantly higher rate of invasive breast cancer detection.[57] Nevertheless, prospective trials with larger patient numbers are warranted to evaluate the true value of abbreviated MRI for breast cancer screening.[58]

Conclusion

Breast MRI is a useful imaging technique for detecting and evaluating breast cancer. It can be used for cancer screening, staging, and evaluating the response to neoadjuvant treatment. The use of BMRI in the evaluation of breast lesions has been researched in the literature, with various publications demonstrating the importance of the topic. BMRI is recognized as the most precise imaging modality in diagnosing malignancy. because of its high sensitivity to soft tissues and ability to provide more comprehensive diagnostic information to identify benign and malignant breast lesions that are not diagnosed by other imaging modalities such as mammography and ultrasound. The current studies have confirmed that the sensitivity of MRI is up to 80%-97.8%, but the specificity is only 46% to 93.3% in diagnosing breast cancer, leading to high rates of misdiagnosis.[59,50] Imaging with DCE-MRI, a technique that samples the influx of contrast agent in the plaque over time using fast T1-weighted (T1w) imaging sequences, has enabled the quantification of several pharmacokinetic parameters, including endothelial permeability and microvascular volume.[61,62] DCE-MRI provides mainly morphological, and, to some extent, functional information about tumor perfusion and vascularity.[63]

A review article by Xiang et al.[64] identified the performance of CESM and MRI for breast cancer diagnosis. The combined data indicating the pooled sensitivity and specificity of CESM and MRI were 0.97 (95% CI: 0.95–0.98), 0.66 (95% CI: 0.59–0.71), 0.97 (95% CI: 0.95–0.98), and 0.52 (95% CI: 0.46–0.58), respectively. The authors concluded that both CESM and MRI are effective methods for the detection of breast cancer with high diagnostic sensitivity.

Xing et al.[60] showed better accuracy, specificity, and false-positive rate of CESM in breast cancer detection than MRI. Contrast-enhanced spectral mammography displayed a good correlation with histopathology in assessing the lesion size of breast cancer, which is consistent with MRI.

In a study by Luczynska et al.,[65] the main goal of this study was to compare CESM and breast magnetic resonance imaging (MRI) with histopathological results and to compare the sensitivity, accuracy, and positive and negative predictive values for both imaging modalities. The results obtained showed that sensitivity was 100% with CESM and 93% with BMRI. Accuracy was 79% with CESM and 73% with BMRI. Contrast-enhanced MRI has been shown to have a very high sensitivity for detecting breast cancer, although reports for specificity have been more variable.

BMRI is critical for the diagnosis of a variety of breast disorders, and it is the most sensitive medical imaging examination for breast cancer detection and diagnosis when compared to mammography, tomosynthesis, and ultrasound imaging. Annual BMRI is recommended for screening women who are at high risk for breast cancer in addition to mammography. Abbreviated MRI, with shorter image acquisition and interpretation times, increases the availability of breast MRI and reduces the costs. Unenhanced MRI parameters such as DWI are under investigation to be added to abbreviated MRI protocols. It seems feasible to offer a cost-effective screening breast DCE-MRI to a broader population.

References

1. Sung H, Ferlay J, Siegel RL, Laversanne M, Soerjomataram I, Jemal A, Bray F. Global Cancer Statistics 2020: GLOBOCAN Estimates of Incidence and Mortality Worldwide for 36 Cancers in 185 Countries. CA Cancer J Clin. 2021 May;71(3):209-249. doi: 10.3322/caac.21660.
2. Tamam N, Al-Mugren KS, Alrebdi HI, Sulieman A, Abdelbasset WK. Evaluating the Quality of Life and Sleep Quality in Saudi Women with Breast Cancer-Related Lymphedema: A Cross-Sectional Correlational Study. Integr Cancer Ther. 2021 Jan-Dec;20:15347354211046192.
3. Tamam N, Salah H, Rabbaa M, Abuljoud M, Sulieman A, Alkhorayef M, Bradley D.Evaluation of patients radiation dose during mammography imaging procedure. Radiation Physics and Chemistry.2021;188,1-7.
4. Sulieman A, Serhan O, Al-Mohammed HI, Mahmoud MZ, Alkhorayef M, Alonazi B, et al. Estimation of cancer risks during mammography procedure in Saudi Arabia. Saudi J Biol Sci. 2019 Sep;26(6):1107-1111. doi: 10.1016/j.sjbs.2018.10.005.
5. Ghoncheh M, Pournamdar Z, Salehiniya H. Incidence and Mortality and Epidemiology of Breast Cancer in the World.

Asian Pac J Cancer Prev. 2016;17(S3):43-6. doi: 10.7314/apjcp.2016.17.s3.43.
6. Apostolou P, Fostira F. Hereditary breast cancer: the era of new susceptibility genes. Biomed Res Int. 2013;2013:747318. doi: 10.1155/2013/747318.
7. Miki Y, Swensen J, Shattuck-Eidens D, Futreal PA, Harshman K, Tavtigian S, et al. A strong candidate for the breast and ovarian cancer susceptibility gene BRCA1. Science. 1994 Oct 7;266(5182):66-71. doi: 10.1126/science.7545954.
8. Gorodetska I, Kozeretska I, Dubrovska A. *BRCA* Genes: The Role in Genome Stability, Cancer Stemness and Therapy Resistance. J Cancer. 2019 May 14;10(9):2109-2127. doi: 10.7150/jca.30410.
9. Godet I, Gilkes DM. BRCA1 and BRCA2 mutations and treatment strategies for breast cancer. Integr Cancer Sci Ther. 2017 Feb;4(1):10.15761/ICST.1000228. doi: 10.15761/ICST.1000228.
10. Antoniou A, Pharoah PD, Narod S, Risch HA, Eyfjord JE, Hopper JL, et al. Average risks of breast and ovarian cancer associated with BRCA1 or BRCA2 mutations detected in case Series unselected for family history: a combined analysis of 22 studies. Am J Hum Genet. 2003 May;72(5):1117-30. doi: 10.1086/375033.
11. Chen S, Parmigiani G. Meta-analysis of BRCA1 and BRCA2 penetrance. J Clin Oncol. 2007 Apr 10;25(11):1329-33. doi: 10.1200/JCO.2006.09.1066.
12. Fahad Ullah M. Breast Cancer: Current Perspectives on the Disease Status. Adv Exp Med Biol. 2019;1152:51-64. doi: 10.1007/978-3-030-20301-6_4.
13. Henson LA, Maddocks M, Evans C, Davidson M, Hicks S, Higginson IJ. Palliative Care and the Management of Common Distressing Symptoms in Advanced Cancer: Pain, Breathlessness, Nausea and Vomiting, and Fatigue. J Clin Oncol. 2020 Mar 20;38(9):905-914. doi: 10.1200/JCO.19.00470.
14. Ferlay J, Ervik M, Lam F, Colombet M, Mery L, Piñeros M, et al. Global Cancer Observatory: Cancer Today. Lyon: International Agency for Research on Cancer; 2020. Available from: https://gco.iarc.fr/today
15. Lynge E, Vejborg I, Andersen Z, von Euler-Chelpin M, Napolitano G. Mammographic Density and Screening Sensitivity, Breast Cancer Incidence and Associated Risk Factors in Danish Breast Cancer Screening. J Clin Med. 2019 Nov 19;8(11):2021. doi: 10.3390/jcm8112021.
16. Lehman CD, Arao RF, Sprague BL, Lee JM, Buist DS, Kerlikowske K, et al. National Performance Benchmarks for Modern Screening Digital Mammography: Update from the Breast Cancer Surveillance Consortium. Radiology. 2017 Apr;283(1):49-58. doi: 10.1148/radiol.2016161174.
17. Sree SV, Ng EY, Acharya RU, Faust O. Breast imaging: A survey. World J Clin Oncol. 2011 Apr 10;2(4):171-8. doi: 10.5306/wjco.v2.i4.171.
18. Abulkhair OA, Al Tahan FM, Young SE, Musaad SM, Jazieh AR. The first national public breast cancer screening program in Saudi Arabia. Ann Saudi Med. 2010 Sep-Oct;30(5):350-7. doi: 10.4103/0256-4947.67078.
19. Coop P, Clawson C. Tomosynthesis as a screening tool for breast cancer: A systematic review. Radiography. 2016, e190-e195.
20. Drukteinis JS, Mooney BP, Flowers CI, Gatenby RA. Beyond mammography: new frontiers in breast cancer screening. Am J Med. 2013 Jun;126(6):472-9. doi: 10.1016/j.amjmed.2012.11.025.
21. Anstey EH, Shoemaker ML, Barrera CM, O'Neil ME, Verma AB, Holman DM. Breastfeeding and Breast Cancer Risk Reduction: Implications for Black Mothers. Am J Prev Med. 2017 Sep;53(3S1):S40-S46. doi: 10.1016/j.amepre.2017.04.024.
22. Oldrini G, Fedida B, Poujol J, Felblinger J, Trop I, Henrot P, Darai E, Thomassin-Naggara I. Abbreviated breast magnetic resonance protocol: Value of high-resolution temporal dynamic sequence to improve lesion characterization. Eur J Radiol. 2017 Oct;95:177-185. doi: 10.1016/j.ejrad.2017.07.025.
23. Ahmed A, Baldo A, Sulieman A, Mirghani H, Abolaban FA, Suliman II, Salih I. Optimisation of T2 and T2* sequences in MRI for better quantification of iron on transfused dependent sickle cell patients. Sci Rep. 2021 Apr 19;11(1):8513. doi: 10.1038/s41598-021-88116-8.
24. Sardanelli F, Boetes C, Borisch B, Decker T, Federico M, Gilbert FJ, et al. Magnetic resonance imaging of the breast: recommendations from the EUSOMA working group. Eur J Cancer. 2010 May;46(8):1296-316. doi: 10.1016/j.ejca.2010.02.015.
25. Kriege M, Brekelmans CT, Boetes C, Besnard PE, Zonderland HM, Obdeijn IM, et al.; Magnetic Resonance Imaging Screening Study Group. Efficacy of MRI and mammography for breast-cancer screening in women with a familial or genetic predisposition. N Engl J Med. 2004 Jul 29;351(5):427-37. doi: 10.1056/NEJMoa031759.
26. Hollingsworth AB. Redefining the sensitivity of screening mammography: A review. Am J Surg. 2019 Aug;218(2):411-418. doi: 10.1016/j.amjsurg.2019.01.039.
27. Salem DS, Kamal RM, Mansour SM, Salah LA, Wessam R. Breast imaging in the young: the role of magnetic resonance imaging in breast cancer screening, diagnosis and follow-up. J Thorac Dis. 2013 Jun;5 Suppl 1(Suppl 1):S9-S18. doi: 10.3978/j.issn.2072-1439.2013.05.02.
28. ACR Ppractice parameter for the performance of contrast enhanced magnetic resonance imaging (MRI) of the breast (2018). Available from: https://www.acr.org/-/media/ACR/Files/Practice-Parameters/mr-contrast-breast.pdf.
29. Alcantara D, Leal MP, García-Bocanegra I, García-Martín ML. Molecular imaging of breast cancer: present and future directions. Front Chem. 2014 Dec 18;2:112. doi: 10.3389/fchem.2014.00112.
30. Ibrahim MA, Hazhirkarzar B, Dublin AB. Gadolinium Magnetic Resonance Imaging. 2021 Jul 9. In: StatPearls [Internet]. Treasure Island (FL): StatPearls Publishing; 2022 Jan–. PMID: 29494094.
31. Kjaer A. Molecular imaging of cancer using PET and SPECT. Adv Exp Med Biol. 2006;587:277-84. PMID: 17163171.
32. Rosenkrantz AB, Friedman K, Chandarana H, Melsaether A, Moy L, Ding YS, et al. Current Status of Hybrid PET/MRI in Oncologic Imaging. AJR Am J Roentgenol. 2016 Jan;206(1):162-72. doi: 10.2214/AJR.15.14968.
33. Saslow D, Boetes C, Burke W, Harms S, Leach MO, Lehman CD, et al.; American Cancer Society Breast Cancer Advisory Group. American Cancer Society guidelines for breast screening with MRI as an adjunct to mammography. CA Cancer J Clin. 2007 Mar-Apr;57(2):75-89. doi: 10.3322/canjclin.57.2.75.
34. Monticciolo DL, Newell MS, Moy L, Niell B, Monsees B, Sickles EA. Breast Cancer Screening in Women at Higher-Than-Average Risk: Recommendations From the ACR. J Am Coll Radiol. 2018 Mar;15(3 Pt A):408-414. doi: 10.1016/j.jacr.2017.11.034.
35. Melnikow J, Fenton JJ, Whitlock EP, Miglioretti DL, Weyrich MS, Thompson JH, Shah K. Supplemental Screening for Breast Cancer in Women With Dense Breasts: A Systematic

Review for the U.S. Preventive Services Task Force. Ann Intern Med. 2016 Feb 16;164(4):268-78. doi: 10.7326/M15-1789. Epub 2016 Jan 12.
36. Lehman CD, Gatsonis C, Kuhl CK, Hendrick RE, Pisano ED, Hanna L, et al.; ACRIN Trial 6667 Investigators Group. MRI evaluation of the contralateral breast in women with recently diagnosed breast cancer. N Engl J Med. 2007 Mar 29;356(13):1295-303. doi: 10.1056/NEJMoa065447.
37. Lehman CD, Blume JD, Thickman D, Bluemke DA, Pisano E, Kuhl C, et al. Added cancer yield of MRI in screening the contralateral breast of women recently diagnosed with breast cancer: results from the International Breast Magnetic Resonance Consortium (IBMC) trial. J Surg Oncol. 2005 Oct 1;92(1):9-15; discussion 15-6. doi: 10.1002/jso.20350.
38. Kim JY, Cho N, Koo HR, Yi A, Kim WH, Lee SH, et al. Unilateral breast cancer: screening of contralateral breast by using preoperative MR imaging reduces incidence of metachronous cancer. Radiology. 2013 Apr;267(1):57-66. doi: 10.1148/radiol.12120629.
39. Flanagan FL, Murray JG, Gilligan P, Stack JP, Ennis JT. Digital subtraction in Gd-DTPA enhanced imaging of the breast. Clin Radiol. 1995 Dec;50(12):848-54. doi: 10.1016/s0009-9260(05)83106-x.
40. Mountford CE, Stanwell P, Ramadan S. Breast MR imaging at 3.0 T. Radiology. 2008 Jul;248(1):319-20; author reply 320. doi: 10.1148/radiol.2481072049. P
41. Mann RM, Cho N, Moy L. Breast MRI: State of the Art. Radiology. 2019 Sep;292(3):520-536. doi: 10.1148/radiol.2019182947.
42. Hendrick RE. High-quality breast MRI. Radiol Clin North Am. 2014 May;52(3):547-62. doi: 10.1016/j.rcl.2013.12.002.
43. Kuhl C. The current status of breast MR imaging. Part I. Choice of technique, image interpretation, diagnostic accuracy, and transfer to clinical practice. Radiology. 2007 Aug;244(2):356-78. doi: 10.1148/radiol.2442051620.
44. Cheung HS, Tse GM, Lai SY, Yeung DK. Relationship between lesion size and signal enhancement on subtraction fat-suppressed MR imaging of the breast. Magn Reson Imaging. 2004 Nov;22(9):1259-64. doi: 10.1016/j.mri.2004.09.001.
45. Mango VL, Morris EA, David Dershaw D, Abramson A, Fry C, Moskowitz CS, et al. Abbreviated protocol for breast MRI: are multiple sequences needed for cancer detection? Eur J Radiol. 2015 Jan;84(1):65-70. doi: 10.1016/j.ejrad.2014.10.004.
46. Kuhl CK, Schrading S, Strobel K, Schild HH, Hilgers RD, Bieling HB. Abbreviated breast magnetic resonance imaging (MRI): first postcontrast subtracted images and maximum-intensity projection-a novel approach to breast cancer screening with MRI. J Clin Oncol. 2014 Aug 1;32(22):2304-10. doi: 10.1200/JCO.2013.52.5386.
47. Leithner D, Moy L, Morris EA, Marino MA, Helbich TH, Pinker K. Abbreviated MRI of the Breast: Does It Provide Value? J Magn Reson Imaging. 2019 Jun;49(7):e85-e100. doi: 10.1002/jmri.26291.
48. Kaiser WA, Zeitler E. MR imaging of the breast: fast imaging sequences with and without Gd-DTPA. Preliminary observations. Radiology. 1989 Mar;170(3 Pt 1):681-6. doi: 10.1148/radiology.170.3.2916021.
49. Kuhl CK, Mielcareck P, Klaschik S, Leutner C, Wardelmann E, Gieseke J, Schild HH. Dynamic breast MR imaging: are signal intensity time course data useful for differential diagnosis of enhancing lesions? Radiology. 1999 Apr;211(1):101-10. doi: 10.1148/radiology.211.1.r99ap38101.
50. Daniel BL, Yen YF, Glover GH, Ikeda DM, Birdwell RL, Sawyer-Glover AM, et al. Breast disease: dynamic spiral MR imaging. Radiology. 1998 Nov;209(2):499-509. doi: 10.1148/radiology.209.2.9807580.
51. Partridge SC, Stone KM, Strigel RM, DeMartini WB, Peacock S, Lehman CD. Breast DCE-MRI: influence of postcontrast timing on automated lesion kinetics assessments and discrimination of benign and malignant lesions. Acad Radiol. 2014 Sep;21(9):1195-203. doi: 10.1016/j.acra.2014.04.013.
52. Sheth D, Abe H. Abbreviated MRI and Accelerated MRI for Screening and Diagnosis of Breast Cancer. Top Magn Reson Imaging. 2017 Oct;26(5):183-189. doi: 10.1097/RMR.0000000000000140.
53. Grimm LJ, Soo MS, Yoon S, Kim C, Ghate SV, Johnson KS. Abbreviated screening protocol for breast MRI: a feasibility study. Acad Radiol. 2015 Sep;22(9):1157-62. doi: 10.1016/j.acra.2015.06.004.
54. Moschetta M, Telegrafo M, Rella L, Stabile Ianora AA, Angelelli G. Abbreviated Combined MR Protocol: A New Faster Strategy for Characterizing Breast Lesions. Clin Breast Cancer. 2016 Jun;16(3):207-11. doi: 10.1016/j.clbc.2016.02.008.
55. Harvey SC, Di Carlo PA, Lee B, Obadina E, Sippo D, Mullen L. An Abbreviated Protocol for High-Risk Screening Breast MRI Saves Time and Resources. J Am Coll Radiol. 2016 Apr;13(4):374-80. doi: 10.1016/j.jacr.2015.08.015.
56. Mann RM, Mus RD, van Zelst J, Geppert C, Karssemeijer N, Platel B. A novel approach to contrast-enhanced breast magnetic resonance imaging for screening: high-resolution ultrafast dynamic imaging. Invest Radiol. 2014 Sep;49(9):579-85.
57. Comstock CE, Gatsonis C, Newstead GM, Snyder BS, Gareen IF, Bergin JT, et al. Comparison of Abbreviated Breast MRI vs Digital Breast Tomosynthesis for Breast Cancer Detection Among Women With Dense Breasts Undergoing Screening. JAMA. 2020 Feb 25;323(8):746-756. doi: 10.1001/jama.2020.0572. Erratum in: JAMA. 2020 Mar 24;323(12):1194.
58. Leithner D, Wengert GJ, Helbich TH, Thakur S, Ochoa-Albiztegui RE, Morris EA, Pinker K. Clinical role of breast MRI now and going forward. Clin Radiol. 2018 Aug;73(8):700-714. doi: 10.1016/j.crad.2017.10.021.
59. Evans DG, Maxwell AJ. MRI Screening in Women With a Personal History of Breast cancer. J Natl Cancer Inst. 2015 Nov 30;108(3):djv373. doi: 10.1093/jnci/djv373.
60. Xing D, Lv Y, Sun B, Xie H, Dong J, Hao C, Chen Q, Chi X. Diagnostic Value of Contrast-Enhanced Spectral Mammography in Comparison to Magnetic Resonance Imaging in Breast Lesions. J Comput Assist Tomogr. 2019 Mar/Apr;43(2):245-251. doi: 10.1097/RCT.0000000000000832.
61. Coolen BF, Calcagno C, van Ooij P, Fayad ZA, Strijkers GJ, Nederveen AJ. Vessel wall characterization using quantitative MRI: what's in a number? MAGMA. 2018 Feb;31(1):201-222. doi: 10.1007/s10334-017-0644-x.
62. Xiao YD, Paudel R, Liu J, Ma C, Zhang ZS, Zhou SK. MRI contrast agents: Classification and application (Review). Int J Mol Med. 2016 Nov;38(5):1319-1326.
63. Marino MA, Helbich T, Baltzer P, Pinker-Domenig K. Multiparametric MRI of the breast: A review. J Magn Reson Imaging. 2018 Feb;47(2):301-315. doi: 10.1002/jmri.25790.
64. Xiang W, Rao H, Zhou L. A meta-analysis of contrast-enhanced spectral mammography versus MRI in the diagnosis of breast cancer. Thorac Cancer. 2020 Jun;11(6):1423-1432. doi: 10.1111/1759-7714.13400.
65. Łuczyńska E, Heinze-Paluchowska S, Hendrick E, Dyczek S, Ryś J, Herman K, Blecharz P, Jakubowicz J. Comparison between breast MRI and contrast-enhanced spectral mammography. Med Sci Monit. 2015 May 12;21:1358-67.

International Journal of Biomedicine 12(1) (2022) 95-99
http://dx.doi.org/10.21103/Article12(1)_RA5

REVIEW ARTICLE

INTERNATIONAL JOURNAL OF BIOMEDICINE

Prevalence of Metabolic Syndrome in PCOS Patients

Ilia A. Igumnov*; Nadezhda A. Kurashova, PhD, ScD; Liliya V. Belenkaya, PhD; Natalia I. Vilson; Larisa V. Suturina, PhD, ScD

Scientific Centre for Family Health and Human Reproduction Problems
Irkutsk, the Russian Federation

Abstract

The purpose of the review was to systematize the available data on the epidemiology and diagnosis of the metabolic syndrome (MetS) in polycystic ovary syndrome (PCOS). The information search was conducted using Internet resources (PubMed, EMBASE, Google Scholar, E-Library) and literature sources for the years 2000-2020. **T**he modern **s**tudies indicate that the prevalence of metabolic disorders varies in groups of women with different PCOS phenotypes. Numerous risk factors in PCOS lead to a significant increase in risk for cardiovascular diseases. Patients with PCOS diagnosed according to AE-PCOS Society criteria have the most severe metabolic features and risk of cardiovascular disease. Hyperandrogenism in PCOS is closely related to the aggravation of abdominal obesity, and together with insulin resistance forms the metabolic core for the development of cardiovascular diseases.(**International Journal of Biomedicine. 2022;12(1):95-99.**)

Key Words: metabolic syndrome • obesity • insulin resistance • hyperandrogenism • polycystic ovary syndrome

For citation: Igumnov IA, Kurashova NA, Belenkaya LV, Vilson NI, Suturina LV. Prevalence of Metabolic Syndrome in PCOS Patients. International Journal of Biomedicine. 2022;12(1):95-99. doi:10.21103/Article12(1)_RA5

Abbreviations

BMI, body mass index; **CVD**, cardiovascular diseases; **DM**, diabetes mellitus; **HDL-C**, high-density lipoprotein cholesterol; **HA**, hyperandrogenism; **IR**, insulin resistance; **IGT**, impaired glucose tolerance; **LDL-C**, low-density lipoprotein cholesterol; **MetS**, metabolic syndrome; **PCOS**, polycystic ovary syndrome; **PCOM**, polycystic ovarian morphology; **T2D**, type 2 diabetes; **WC**, waist circumference.

Metabolic syndrome (MetS) is one of the most important health problems in different countries. Experts of the World Health Organization (WHO) have described MetS as a pandemic of the twenty-first century.[1-5] MetS (also known as syndrome X, Reaven syndrome, insulin resistance syndrome) is a combination of hormonal and metabolic disorders that significantly accelerate the development of CVD. The high variability in the prevalence of MetS, according to various studies, is primarily associated with an insufficiently clear, consistent definition of diagnostic criteria. The main sources of information are epidemiological data and prognostic studies conducted in the *United States* and countries of Western Europe, and single epidemiological studies on the prevalence of MetS in Russia.

Several clinical definitions of MS have been proposed and widely used over the past decade, including those by the World Health Organisation (WHO),[6] National Cholesterol Education Programme Adult Treatment Panel III (NCEP-ATPIII),[7] International Diabetes Federation (IDF),[8] American Heart Association/National Heart, Lung, and Blood Institute(AHA/NHLBI),[1] and The European Group for Study of Insulin Resistance (EGIR).[9]

The 2009 harmonized definition of MetS requires the presence of any 3 of the following: increased WC (men: ≥94 cm, women: ≥80 cm), low HDL-C (men: <40 mg/dL (1 mmol/L), women: <50 mg/dL (1.3 mmol/L)), hypertriglyceredimia ≥150 mg/dL (1.7 mmol/L), elevated BP (systolic BP ≥130 mmHg

***Corresponding author:** Ilia A. Igumnov. Scientific Centre for Family Health and Human Reproduction Problems, Irkutsk, the Russian Federation. E-mail: iigumnov7@gmail.com*

and/or diastolic ≥85 mmHg or drug treatment for hypertension) and elevated blood sugar (FPG ≥100 mg/dL (5.6 mmol/L) or diabetes mellitus.[10]

The prevalence of MetS varies within 20%-40%, averaging 26% among the adult population of the planet, according to an INTERHEART study.[11] In Russia, according to research results, 40% of the population has 2 components of MS, 11% – 3 or more of its components. It is more common in middle-aged and older people.[12] MetS prevalence is high among obese patients; among people with IGT, the frequency of MetS is 50%, and in DM - 80%. In addition, there is a steady trend of increasing prevalence of MetS. Currently, the number of patients with MetS is 2 times higher than the number of patients with T2D; in the next 20 years, an increase of 50% in the frequency of MetS is expected. The majority of patients with MetS are the working-age population, but over the past 2 decades, the MetS frequency has shown a steady increase among young people.[13]

The prevalence of MetS in PCOS

MetS is also associated with ovulation, conception, and pregnancy complications: increase of pregnancy losses and decrease of the number of live-born children. There is evidence of an increased prevalence of MetS among overweight or obese women with PCOS (OR=1.88; 95% CI: 1.16-3.04), but not among women with a normal BMI, even in the presence of PCOS(OR=1.45; 95% CI:0.35-6.12).[14] In addition, it is known that the presence of MetS in patients with PCOS reduces the chances of pregnancy and negatively affects the results of in vitro fertilization in infertile women with PCOS. MetS in patients with PCOS can reduce the antioxidant activity of the body and lead to the development of oxidative stress. A decrease in antioxidant activity in PCOS with MetS is associated with an increased level of triglycerides and LDL-C, which can worsen the course of these diseases.[14,15]

The main mechanisms of the pathogenesis of PCOS include disorders of the steroid-producing function of the ovaries[16] with an increase in the production of androgens and a violation of their conversion to estrogens, as well as an increase in the level of free testosterone against the background of low content of sex hormone-binding globulin.[17] In turn, hyperandrogenism (HA) is associated with an abdominal type of obesity and changes in the lipid profile.[18] In addition, PCOS is characterized by the presence of gonadotropic dysfunction, which naturally leads to anovulation or at least to progesterone deficiency. Along with this, anovulation and small-cystic ovarian transformation are the results of the so-called follicular arrest associated with excessive secretion of anti-müllerian hormone.

The prevalence of PCOS is usually influenced by the characteristics of the population sample. Thus, in a non-selective sample of women of reproductive age, the PCOS prevalence ranges from 6% to 19.9%, in menstrual disorders - from 17.4% to 46.4%, in women with clinical manifestations of HA -72.1%-82%, and in anovulatory infertility - in 55-91% of cases.[19,20] Chronic anovulation in women with PCOS is a risk factor for endometrial hyperplasia and cancer, which is largely facilitated by the presence of overweight or obesity in 40%-85% of women with PCOS. Along with reproductive disorders, PCOS, especially its classical phenotype, is associated with IR, IGT, DM, CVD, all of which determine the long-term consequences of this disease.[21]

PCOS is the most common cause of HA, a common endocrine disorder, the main clinical markers of which are skin problems and menstrual cycle disorders such as hypomenstrual syndrome.[22] The diagnosis of PCOS is based on the criteria presented and approved in various consensuses. The NIH criteria (1990) established the presence of oligo-/anovulation and HA as a necessary condition for the diagnosis of PCOS (after excluding conditions with similar symptoms).[23] At the same time, the appearance of a polycystic ovarian structure by ultrasound is not considered a mandatory sign of PCOS.

Possible combinations of components of the Rotterdam criteria have allowed identifying 4 PCOS phenotypes:[24-27] phenotype A (oligo-/anovulation (OA), clinical and/or biochemical HA, and PCOM), phenotype B (HA+OA), phenotype C (HA+PCOM), and phenotype D (OA+PCOM). The more severe PCOS phenotypes are associated with a greater magnitude of CVD risk and this has been found in obese and non-obese women.[28]

The Harmonized Criteria of the European Society for Human Reproduction and Embryology and the American Society for Reproductive Medicine (ASRM/ESHRE), adopted in Rotterdam,[24] are currently used to diagnose PCOS. According to this consensus, the diagnosis of PCOS can be confirmed by the presence of at least two of the following three criteria: oligo- or anovulation, clinical or biochemical signs of HA, polycystic ovarian morphology on ultrasound.

Based on the available data, in 2006, the Androgen Excess and PCOS Society (AE-PCOS) experts proposed their version of the PCOS diagnostic criteria. According to the AE-PCOS consensus, PCOS should have been diagnosed with the obligatory presence of HA(clinical and/or biochemical) in combination with ovarian dysfunction (oligo-anovulation and/or polycystic ovaries), and the exclusion of related disorders.[25,29]

The prevalence of MetS among 248 women with different PCOS phenotypes was analyzed in a study by Bahadur et al.[4] The prevalence of phenotypes A, B, C, and D were 36.7%, 10.1%, 4.4%, and 48.8%, respectively. Phenotype D had the highest prevalence of MetS. Phenotype A was at higher risk of adverse MetS risk profile.

A study performed by Karee et al.[30] included 382 Indian women with PCOS. MetS was present in 147(38.5%) PCOS women. The most frequently observed individual components of MetS were increased WC and decreased HDL-C.

A retrospective cohort study conducted in Germany found that the prevalence of underweight in patients with PCOS is very low. Underweight in PCOS was associated with higher postprandial insulin levels.[31]

A study conducted by Kim et al.[32] investigated the various HOMA-IR cutoff values in a population of healthy controls (n=579) and evaluated the prevalence of IR in women with PCOS(n=699). Overweight/obese PCOS patients were the most high-risk group, but lean patients also showed an elevated prevalence of IR similar to that of overweight/obese controls. The authors concluded that although IR is common

in women with PCOS, it does not seem to be universal, and patients without IR had reassuring metabolic features**.**

A study performed by Carmina et al.[33] investigated the prevalence of MetS according to ATP-III and WHO criteria in 282 women with PCOS, aged 18-40 years, living in western Sicily. Patients were divided into 2 groups: Group 1 included 225 patients with chronic anovulation and hyperandrogenism (classic PCOS); Group 2 included 57 patients with hyperandrogenism and polycystic ovaries who were ovulatory (ovulatory PCOS). In classic PCOS patients, MetS was higher (8.9% by ATP-III, 17.3% by WHO) than in ovulatory PCOS (5% and 10.6%, respectively).

In a study performed by Dargham et al.,[34] the prevalence and metabolic features of PCOS among 750 Qatari women aged between 18-40 years were estimated. By NIH guidelines, the prevalence of PCOS in this Qatari cohort was 12.1%, which would likely reflect 20% by Rotterdam criteria. Over 61% of investigated women identified were either overweight (BMI 26–29.9; 31.4%) or obese (BMI greater than 30; 29.7%). Clinical HA defined by the Ferriman and Gallwey score was not validated in that ethnic population.

The systematic review and meta-analysis conducted by Behboudi-Gandevani et al.[35] showed that in PCOS patients, regardless of age, BMI and recruitment sources of samples had higher odds of MetS than healthy controls (OR=2.5, 95% CI: 2.0-3.2). Adolescents with PCOS had an increased OR of MetS compared to healthy adolescents in population- and nonpopulation-based studies (OR=4.7, 95% CI: 1.8-11.9; OR=6.1, 95% CI: 6.0-6.1, respectively). Subgroup analysis based on PCOS diagnostic criteria showed that HA is an important component of this disorder.

The prevalence of MetS in PCOS has been studied in different populations. Reported prevalence is 43% in U.S., 28.4% in Brazil, 24.9% in Hong Kong Chinese women, and only 1.6% in Czech women.[36-39] The prevalence of MetS in PCOS is strongly influenced by the criteria used to diagnose MetS as well as the criteria used to diagnose PCOS. The prevalence of MetS (the ATP-III criteria) among women from southern Italy was only 8.2% in comparison with a prevalence of 43%–46% reported in the USA.[40,41]

A prospective cross-sectional study performed by Mandrelle et al.[42] in infertile Indian women with PCOS, according to Rotterdam criteria (2003), showed that the overall prevalence of MetS, according to the modified AHA/NHLBI ATP III (2005) criteria, was 37.5%. A total of 5.8 % cases were found to have DM, 8.3% had impaired fasting glucose, and 11.7 % had an IGT.

A case-control, cross-sectional, observational study of consecutive women with anovular PCOS (47 South Asians, 40 Caucasians) and their age-matched controls (11 South Asians and 22 Caucasians) [43] showed that South Asians with anovular PCOS seek treatment at a younger age and have more serious symptoms, higher fasting insulin concentrations and lower insulin sensitivity than Caucasians.

In 2019, a retrospective study of 1,215 Mediterranean women from Sicily was conducted to better characterize the metabolic alterations in various phenotypes of PCOS. [44] Among 1,215 women with PCOS, phenotype A was diagnosed in 701(57.7%), phenotype B - in 112(9.2%), phenotype C - in 364(30%), and phenotype D - in 38(3.1%). According to the results of the study, the prevalence of obesity was 31%, MetS - 6.6%, DM - 2.1%, altered glucose metabolism - 13.1%, and abnormal lipid profile - 60%. Phenotype B was characterized by the highest prevalence of obesity, MetS, IGT, and lipid abnormalities, compared to other PCOS phenotypes and controls. Women with phenotype A were more obese and more women had MS, than women with phenotypes C and D; however, women with phenotype C had a prevalence of altered glucose metabolism and lipid abnormalities similar to phenotype A. These metabolic abnormalities in phenotypes A and C were higher than in phenotype D and controls. Multivariate analysis showed that BMI allows predicting only deviations in fasting glucose and triglycerides, regardless of the level of androgens. Only women with norm-androgenic phenotype D had no metabolic abnormalities. Thus, the risk of MetS and CVD may vary depending on the PCOS phenotype, based on the Rotterdam criteria.

To compare the prevalence of various metabolic and cardiovascular risk factors and IR between PCOS patients with or without HA, a retrospective cross-sectional study involving women with PCOS, as diagnosed according to AE-PCOS Society criteria (n=504), and women with normoandrogenemic PCOS (n=183) was performed.[45] Women with PCOS diagnosed according to the AE-PCOS Society criteria had a significantly higher prevalence of MetS than in the normoandrogenemic PCOS phenotype (25.4% vs. 10.3%; P=0.01). There was no significant difference in the prevalence of the IGT test between the groups. The prevalence of HDL-C<50 mg/dL in the group under the AE-PCOS criteria was higher than in the normoandrogenemic PCOS group (59.4 vs 41.2%, respectively; P=0.002).

The evidence currently suggests that patients with PCOS diagnosed according to AE-PCOS Society criteria have the most severe metabolic features.[29,46] Rizzo et al.[47] found that women with hyperanderogenemic PCOS showed the most atherogenic lipid profiles, with higher apolipoprotein B than the other PCOS phenotypes.

Conclusion

The modern **s**tudies indicate that the prevalence of metabolic disorders varies in groups of women with different PCOS phenotypes. Numerous risk factors in PCOS lead to a significant increase in risk for cardiovascular diseases. Patients with PCOS diagnosed according to AE-PCOS Society criteria have the most severe metabolic features and risk of cardiovascular disease. HA in PCOS is closely related to the aggravation of abdominal obesity, and together with insulin resistance forms the metabolic core for the development of cardiovascular diseases.

Competing Interests

The authors declare that they have no competing interests.

References

1. Grundy SM, Cleeman JI, Daniels SR, Donato KA, Eckel RH, Franklin BA, et al.; American Heart Association; National Heart, Lung, and Blood Institute. Diagnosis and management of the metabolic syndrome: an American Heart Association/ National Heart, Lung, and Blood Institute Scientific Statement. Circulation. 2005 Oct 25;112(17):2735-52. doi: 10.1161/ CIRCULATIONAHA.105.169404.
2. Ford ES, Giles WH. A comparison of the prevalence of the metabolic syndrome using two proposed definitions. Diabetes Care. 2003 Mar;26(3):575-81. doi: 10.2337/diacare.26.3.575.
3. Panov AV, Dikalov SI, Darenskaya MA, Rychkova LV, Kolesnikova LI, Kolesnikov SI. [Mitochondria: Aging, Metabolic Syndrome, and Cardiovascular Pathology. Formation of a new paradigm]. Acta Biomedica Scientifica. 2020;5(4):33-44. doi: 10.29413/ABS.2020-5.4.5. [Article in Russian].
4. Bahadur A, Mundhra R, Kashibhatla J, Rajput R, Verma N, Kumawat M. Prevalence of metabolic syndrome among women with different PCOS phenotypes - a prospective study. Gynecol Endocrinol. 2021 Jan;37(1):21-25. doi: 10.1080/09513590.2020.1775193.
5. The Recommendations of the Experts of the All-Russia Scientific Society of Cardiologists for the Diagnosis and Treatment of Metabolic Syndrome. The 2-nd review. Moscow; 2009. [In Russian].
6. Alberti KG, Zimmet PZ. Definition, diagnosis and classification of diabetes mellitus and its complications. Part 1: diagnosis and classification of diabetes mellitus provisional report of a WHO consultation. Diabet Med. 1998 Jul;15(7):539-53. doi: 10.1002/(SICI)1096-9136(199807)15:7<539::AID-DIA668>3.0.CO;2-S.
7. National Cholesterol Education Program (NCEP) Expert Panel on Detection, Evaluation, and Treatment of High Blood Cholesterol in Adults (Adult Treatment Panel III). Third Report of the National Cholesterol Education Program (NCEP) Expert Panel on Detection, Evaluation, and Treatment of High Blood Cholesterol in Adults (Adult Treatment Panel III) final report. Circulation. 2002 Dec 17;106(25):3143-421.
8. Alberti KG, Zimmet P, Shaw J; IDF Epidemiology Task Force Consensus Group. The metabolic syndrome--a new worldwide definition. Lancet. 2005 Sep 24-30;366(9491):1059-62. doi: 10.1016/S0140-6736(05)67402-8.
9. Balkau B, Charles MA. Comment on the provisional report from the WHO consultation. European Group for the Study of Insulin Resistance (EGIR). Diabet Med. 1999 May;16(5):442-3. doi: 10.1046/j.1464-5491.1999.00059.x.
10. Alberti KG, Eckel RH, Grundy SM, Zimmet PZ, Cleeman JI, Donato KA, Fruchart JC, James WP, Loria CM, Smith SC Jr; International Diabetes Federation Task Force on Epidemiology and Prevention; National Heart, Lung, and Blood Institute; American Heart Association; World Heart Federation; International Atherosclerosis Society; International Association for the Study of Obesity. Harmonizing the metabolic syndrome: a joint interim statement of the International Diabetes Federation Task Force on Epidemiology and Prevention; National Heart, Lung, and Blood Institute; American Heart Association; World Heart Federation; International Atherosclerosis Society; and International Association for the Study of Obesity. Circulation. 2009 Oct 20;120(16):1640-5. doi: 10.1161/ CIRCULATIONAHA.109.192644.
11. Thomas GN, Ho SY, Janus ED, Lam KS, Hedley AJ, Lam TH; Hong Kong Cardiovascular Risk Factor Prevalence Study Steering Committee. The US National Cholesterol Education Programme Adult Treatment Panel III (NCEP ATP III) prevalence of the metabolic syndrome in a Chinese population. Diabetes Res Clin Pract. 2005 Mar;67(3):251-7. doi: 10.1016/j.diabres.2004.07.022.
12. Rotar OP, Libis RA, Isaeva EN et al. Metabolic syndrome prevalence in Russian cities. Russian Journal of Cardiology. 2012;17(2):55-62.
13. Alberti KG, Zimmet P, Shaw J. Metabolic syndrome--a new world-wide definition. A Consensus Statement from the International Diabetes Federation. Diabet Med. 2006 May;23(5):469-80. doi: 10.1111/j.1464-5491.2006.01858.x.
14. Kolesnikova LI, Kolesnikov SI, Darenskaya MA, Grebenkina LA, Nikitina OA, Lazareva LM, Suturina LV, Danusevich IN, Druzhinina EB, Semendyaev AA. Activity of LPO Processes in Women with Polycystic Ovarian Syndrome and Infertility. Bull Exp Biol Med. 2017 Jan;162(3):320-322. doi: 10.1007/s10517-017-3605-5.
15. Suturina LV, Atalyan AV, Darzhaev ZY, et al. Overweight and obesity prevalence in referral population of infertile women with polycystic ovary syndrome. Adv Obes Weight Manag Control. 2017;7(1):237-240. doi: 10.15406/ aowmc.2017.07.00188.
16. Rosenfield RL, Ehrmann DA. The Pathogenesis of Polycystic Ovary Syndrome (PCOS): The Hypothesis of PCOS as Functional Ovarian Hyperandrogenism Revisited. Endocr Rev. 2016 Oct;37(5):467-520. doi: 10.1210/er.2015-1104.
17. Lizneva D, Kirubakaran R, Mykhalchenko K, Suturina L, Chernukha G, Diamond MP, Azziz R. Phenotypes and body mass in women with polycystic ovary syndrome identified in referral versus unselected populations: systematic review and meta-analysis. Fertil Steril. 2016 Nov;106(6):1510-1520.e2. doi: 10.1016/j.fertnstert.2016.07.1121.
18. Wijeyaratne CN, Balen AH, Barth JH, Belchetz PE. Clinical manifestations and insulin resistance (IR) in polycystic ovary syndrome (PCOS) among South Asians and Caucasians: is there a difference? Clin Endocrinol (Oxf). 2002 Sep;57(3):343-50. doi: 10.1046/j.1365-2265.2002.01603.x.
19. Lizneva D, Suturina L, Walker W, Brakta S, Gavrilova-Jordan L, Azziz R. Criteria, prevalence, and phenotypes of polycystic ovary syndrome. Fertil Steril. 2016 Jul;106(1):6-15. doi: 10.1016/j.fertnstert.2016.05.003.
20. Li R, Zhang Q, Yang D, Li S, Lu S, Wu X, Wei Z, Song X, Wang X, Fu S, Lin J, Zhu Y, Jiang Y, Feng HL, Qiao J. Prevalence of polycystic ovary syndrome in women in China: a large community-based study. Hum Reprod. 2013 Sep;28(9):2562-9. doi: 10.1093/humrep/det262.
21. Belenkaia LV, Lazareva LM, Walker W, Lizneva DV, Suturina LV. Criteria, phenotypes and prevalence of polycystic ovary syndrome. Minerva Ginecol. 2019 Jun;71(3):211-223. doi: 10.23736/S0026-4784.19.04404-6.
22. Zore T, Joshi NV, Lizneva D, Azziz R. Polycystic Ovarian Syndrome: Long-Term Health Consequences. Semin Reprod Med. 2017 May;35(3):271-281. doi: 10.1055/s-0037-1603096.
23. March WA, Moore VM, Willson KJ, Phillips DI, Norman RJ, Davies MJ. The prevalence of polycystic ovary syndrome in a community sample assessed under contrasting diagnostic criteria. Hum Reprod. 2010 Feb;25(2):544-51. doi: 10.1093/ humrep/dep399.

24. Rotterdam ESHRE/ASRM-Sponsored PCOS consensus workshop group. Revised 2003 consensus on diagnostic criteria and long-term health risks related to polycystic ovary syndrome (PCOS). Hum Reprod. 2004 Jan;19(1):41-7. doi: 10.1093/humrep/deh098.
25. Azziz R, Carmina E, Dewailly D, Diamanti-Kandarakis E, Escobar-Morreale HF, Futterweit W, Janssen OE, Legro RS, Norman RJ, Taylor AE, Witchel SF; Androgen Excess Society. Positions statement: criteria for defining polycystic ovary syndrome as a predominantly hyperandrogenic syndrome: an Androgen Excess Society guideline. J Clin Endocrinol Metab. 2006 Nov;91(11):4237-45. doi: 10.1210/jc.2006-0178.
26. Carmina E, Azziz R. Diagnosis, phenotype, and prevalence of polycystic ovary syndrome. Fertil Steril. 2006 Jul;86 Suppl 1:S7-8. doi: 10.1016/j.fertnstert.2006.03.012.
27. Azziz R. Polycystic Ovary Syndrome. Obstet Gynecol. 2018 Aug;132(2):321-336. doi: 10.1097/AOG.0000000000002698.
28. Amsterdam ESHRE/ASRM-Sponsored 3rd PCOS Consensus Workshop Group. Consensus on women's health aspects of polycystic ovary syndrome (PCOS). Hum Reprod. 2012 Jan;27(1):14-24. doi: 10.1093/humrep/der396.
29. Azziz R, Carmina E, Dewailly D, Diamanti-Kandarakis E, Escobar-Morreale HF, Futterweit W, Janssen OE, Legro RS, Norman RJ, Taylor AE, Witchel SF; Task Force on the Phenotype of the Polycystic Ovary Syndrome of The Androgen Excess and PCOS Society. The Androgen Excess and PCOS Society criteria for the polycystic ovary syndrome: the complete task force report. Fertil Steril. 2009 Feb;91(2):456-88. doi: 10.1016/j.fertnstert.2008.06.035.
30. Karee M, Gundabattula SR, Sashi L, Boorugu H, Chowdhury A. Prevalence of metabolic syndrome in women with polycystic ovary syndrome and the factors associated: A cross sectional study at a tertiary care center in Hyderabad, south-eastern India. Diabetes Metab Syndr. 2020 Jul-Aug;14(4):583-587. doi: 10.1016/j.dsx.2020.05.006.
31. Anastasiou OE, Canbay A, Fuhrer D, Reger-Tan S. Metabolic and androgen profile in underweight women with polycystic ovary syndrome. Arch Gynecol Obstet. 2017 Aug;296(2):363-371. doi: 10.1007/s00404-017-4422-9.
32. Kim JJ, Hwang KR, Oh SH, Chae SJ, Yoon SH, Choi YM. Prevalence of insulin resistance in Korean women with polycystic ovary syndrome according to various homeostasis model assessment for insulin resistance cutoff values. Fertil Steril. 2019 Nov;112(5):959-966.e1. doi: 10.1016/j.fertnstert.2019.06.035.
33. Carmina E, Napoli N, Longo RA, Rini GB, Lobo RA. Metabolic syndrome in polycystic ovary syndrome (PCOS): lower prevalence in southern Italy than in the USA and the influence of criteria for the diagnosis of PCOS. Eur J Endocrinol. 2006 Jan;154(1):141-5. doi: 10.1530/eje.1.02058.
34. Dargham SR, Ahmed L, Kilpatrick ES, Atkin SL. The prevalence and metabolic characteristics of polycystic ovary syndrome in the Qatari population. PLoS One. 2017 Jul 19;12(7):e0181467. doi: 10.1371/journal.pone.0181467.
35. Behboudi-Gandevani S, Amiri M, Bidhendi Yarandi R, Noroozzadeh M, Farahmand M, Rostami Dovom M, Ramezani Tehrani F. The risk of metabolic syndrome in polycystic ovary syndrome: A systematic review and meta-analysis. Clin Endocrinol (Oxf). 2018 Feb;88(2):169-184. doi: 10.1111/cen.13477.
36. Essah PA, Nestler JE. Metabolic syndrome in women with polycystic ovary syndrome. Fertil Steril. 2006 Jul;86 Suppl 1:S18-9. doi: 10.1016/j.fertnstert.2006.04.013.
37. Soares EM, Azevedo GD, Gadelha RG, Lemos TM, Maranhão TM. Prevalence of the metabolic syndrome and its components in Brazilian women with polycystic ovary syndrome. Fertil Steril. 2008 Mar;89(3):649-55. doi: 10.1016/j.fertnstert.2007.03.081.
38. Cheung LP, Ma RC, Lam PM, Lok IH, Haines CJ, So WY, Tong PC, Cockram CS, Chow CC, Goggins WB. Cardiovascular risks and metabolic syndrome in Hong Kong Chinese women with polycystic ovary syndrome. Hum Reprod. 2008 Jun;23(6):1431-8. doi: 10.1093/humrep/den090.
39. Vrbíková J, Vondra K, Cibula D, Dvoráková K, Stanická S, Srámková D, Sindelka G, Hill M, Bendlová B, Skrha J. Metabolic syndrome in young Czech women with polycystic ovary syndrome. Hum Reprod. 2005 Dec;20(12):3328-32. doi: 10.1093/humrep/dei221.
40. Glueck CJ, Papanna R, Wang P, Goldenberg N, Sieve-Smith L. Incidence and treatment of metabolic syndrome in newly referred women with confirmed polycystic ovarian syndrome. Metabolism. 2003 Jul;52(7):908-15. doi: 10.1016/s0026-0495(03)00104-5.
41. Apridonidze T, Essah PA, Iuorno MJ, Nestler JE. Prevalence and characteristics of the metabolic syndrome in women with polycystic ovary syndrome. J Clin Endocrinol Metab. 2005 Apr;90(4):1929-35. doi: 10.1210/jc.2004-1045.
42. Mandrelle K, Kamath MS, Bondu DJ, Chandy A, Aleyamma T, George K. Prevalence of metabolic syndrome in women with polycystic ovary syndrome attending an infertility clinic in a tertiary care hospital in south India. J Hum Reprod Sci. 2012 Jan;5(1):26-31. doi: 10.4103/0974-1208.97791.
43. Wijeyaratne CN, Balen AH, Barth JH, Belchetz PE. Clinical manifestations and insulin resistance (IR) in polycystic ovary syndrome (PCOS) among South Asians and Caucasians: is there a difference? Clin Endocrinol (Oxf). 2002 Sep;57(3):343-50. doi: 10.1046/j.1365-2265.2002.01603.x.
44. Carmina E, Nasrallah MP, Guastella E, Lobo RA. Characterization of metabolic changes in the phenotypes of women with polycystic ovary syndrome in a large Mediterranean population from Sicily. Clin Endocrinol (Oxf). 2019 Oct;91(4):553-560. doi: 10.1111/cen.14063.
45. Çelik E, Türkçüoğlu I, Ata B, Karaer A, Kırıcı P, Eraslan S, Taşkapan Ç, Berker B. Metabolic and carbohydrate characteristics of different phenotypes of polycystic ovary syndrome. J Turk Ger Gynecol Assoc. 2016 Dec 1;17(4):201-208. doi: 10.5152/jtgga.2016.16133.
46. Moran L, Teede H. Metabolic features of the reproductive phenotypes of polycystic ovary syndrome. Hum Reprod Update. 2009 Jul-Aug;15(4):477-88. doi: 10.1093/humupd/dmp008.
47. Rizzo M, Berneis K, Hersberger M, Pepe I, Di Fede G, Rini GB, Spinas GA, Carmina E. Milder forms of atherogenic dyslipidemia in ovulatory versus anovulatory polycystic ovary syndrome phenotype. Hum Reprod. 2009 Sep;24(9):2286-92. doi: 10.1093/humrep/dep121.

International Journal of Biomedicine 12(1) (2022) 100-103
http://dx.doi.org/10.21103/Article12(1)_RA6

BRIEF REVIEW

INTERNATIONAL JOURNAL OF BIOMEDICINE

Polycystic Ovarian Morphology: Diagnostic Criteria and Prevalence

Lyudmila M. Lazareva*, PhD; Larisa V. Suturina, PhD, ScD

Scientific Centre for Family Health and Human Reproduction Problems
Irkutsk, the Russian Federation

Abstract

The purpose of this brief review was to systematize the current information on the diagnosis, prevalence, and ethnic aspects of polycystic ovarian morphology (PCOM). The information search was conducted using Internet resources (Medline, Pubmed, Cochrane Library, and Google Scholar) and literature sources for the period from January 1999 to August 2021. The review includes only full-text articles. Based on the analysis of the literature, we demonstrated that the diagnostic value of PCOM has changed since the moment of the first description of polycystic ovarian syndrome (PCOS). Currently, ovarian size, ovarian volume and antral follicle count are key criteria for most PCOS phenotypes and complications. The diagnostic value of PCOM depends on age and racial characteristics, which requires large-scale epidemiological studies to determine PCOM characteristics in different populations. Standardizing PCOM diagnostic criteria is the key to PCOS effective diagnosis and, consequently, to preventing complications and comorbidities associated with PCOS.(**International Journal of Biomedicine. 2021;11(4):100-103.**)

Key Words: PCOM • PCOS • insulin resistance • hyperandrogenism • ultrasound criteria

For citation: Lazareva LM, Suturina LV. Polycystic Ovarian Morphology: Diagnostic Criteria and Prevalence. International Journal of Biomedicine. 2022;12(1):100-103. doi:10.21103/Article12(1)_RA6

Abbreviations

AMH, anti-müllerian hormone; **FNPO**, follicle number per ovary; **FSH**, follicle-stimulating hormone; **IR**, insulin resistance; **OV**, ovarian volume; **PCOM**, polycystic ovarian morphology; **PCOS**, polycystic ovarian syndrome; **SHBG**, sex hormone binding globulin.

Introduction

Polycystic ovarian syndrome (PCOS) takes a leading position among endocrine diseases and is associated with a wide range of reproductive[1-4] and metabolic disorders.[4-7] Currently, polycystic ovarian morphology (PCOM) is a key criterion for PCOS in most cases. The definition of PCOS symptoms has significantly changed since the first description [8] of this syndrome in 1935 and remains a subject of debate among clinicians and scientits around the world. In 1990, a panel of experts from the National Institutes of Health (NIH) defined this condition as a combination of hyperandrogenism and chronic anovulation after excluding other causes of anovulation.[8] Subsequently, the NIH criteria were criticized because they did not include ultrasound (US) signs of PCOM, which was considered to be a significant marker of PCOS by many scientists.

In 2003, ESHRE/ASRM experts in Rotterdam adopted updated criteria for PCOS,[9] which represented an extended version of the 1990 NIH consensus and included polycystic ovarian changes as one of the criteria for diagnosing PCOS.[8,9] Parameters providing sufficient sensitivity and specificity of PCOM were approved. They included the presence in at least one ovary with follicle number per ovary (FNPO) of ≥12 with a diameter of 2–9mm and/or ovarian volume (OV) of ≥10 cm^3. It was noted that the number of follicles should be assessed both in longitudinal and anteroposterior sections of the ovaries, and follicles with a size of 10mm should denominate the average value of the diameters measured in two sections. To calculate the volume of the ovary, a formula was proposed for an elongated ellipsoid (0.523×length×width×thickness). For sexually active women, transvaginal access was recognized as a priority, especially in obese patients. Women with regular menstruation were advised to undergo a pelvic ultrasound

***Corresponding author:** *Lyudmila M. Lazareva, PhD. Scientific Centre for Family Health and Human Reproduction Problems, Irkutsk, the Russian Federation. E-mail: lirken_@mail.ru*

on the early follicular phase of the natural cycle, or, if oligo-amenorrhea occurs, regardless of the day of the cycle or after withdrawal bleeding caused by pharmaceuticals. In case of the follicle/cyst diameter more than 10mm or corpus luteum presence, a repeat US was recommended.

The unacceptability of the criteria for the diagnosis of PCOM in women taking oral contraceptives (both healthy and with a diagnosis of PCOS) was noted due to changes in the structure of the ovary during intake of these medicines. It was recommended not to overestimate the distribution of follicles in the ovary, the increase in echogenicity, and the stroma volume as the parameters of polycystic morphology, due to the presence of a more sensitive marker - OV. The role of pelvic ultrasound estimates in the prognosis of hyperstimulation and in response to ovarian stimulation and the outcomes of in vitro oocyte maturation was demonstrated as significant, as was the use of modern equipment. In addition, the importance of appropriate training of specialists and the inadmissibility of replacing measurements according to the protocol with a subjective assessment was emphasized.[9]

The introduction of these criteria naturally led to an increase in the frequency of PCOS detection due to the so-called "non-androgenic" and "ovulatory" phenotypes. Possible combinations of components of the Rotterdam criteria have allowed identifying four PCOS phenotypes:[6,10] phenotype A (oligo-/anovulation (OA), clinical and/or biochemical hyperandrogenism (HA), and PCOM), phenotype B (HA+OA), phenotype C (HA+PCOM), and phenotype D (OA+PCOM).[9-12]

In 2006, the AE-PCOS experts proposed their version of the PCOS diagnostic criteria. These criteria focused on the manifestations of hyperandrogenism, which was recognized as a necessary symptom of PCOS. According to the AE-PCOS consensus, PCOS should have been diagnosed with the obligatory presence of hyperandrogenism in combination with menstrual dysfunction and/or a polycystic ovarian structure, according to ultrasound data.[10,13] The Rotterdam 2003 PCOM ultrasound diagnostic criteria (presence of at least one ovary with 12 follicles of 2–9 mm in size or OV>10 mL, in the absence of a dominant follicle >0 mm) were supported in this document as well. However, the working group noted the likelihood of a high incidence of false-positive PCOM results and suggested that hyperandrogenism and oligo/anovulation should be considered priority criteria for PCOS.

In 2013, the experts from the Endocrine Society Working Group [14] published a document in which they recommended the criteria proposed in Rotterdam in 2003 for the diagnosis of PCOM (the presence of at least one ovary with 12 follicles 2-9 mm in size or >10mL, in the absence of a dominant follicle of >10 mm), the preference for the transvaginal approach to imaging was also supported. At the same time, the need to standardize the ultrasound characteristics of PCOS was pronounced, considering the age and possible limitations of the method associated with the technical characteristics of the equipment and ethical aspects.[14]

The improvement in the technical capabilities of ultrasound diagnostic devices has led to a clearer visualization of the ovarian structure and requests for a revision of the ultrasound criteria for PCOS. In this regard, it was proposed to increase the threshold value of the number of follicles or ovarian volume.[4,14]

The latest guideline on the diagnosis and management of PCOS, published in 2018,[4] proposes to consider the provisions adopted in Rotterdam as the basis for the diagnosis of PCOS.[4] However, the need to take into account racial and age characteristics was noted. This document establishes the standard protocol for clinical assessment of polycystic ovarian structure for sexually active women, including a transvaginal ultrasound examination in the early follicular phase of the natural cycle or after withdrawal of bleeding caused by pharmaceutical drugs. The 2018 ESHRE PCOS guideline group suggested a threshold of >20 FNPO with or without an OV ≥10 mL, without any dominant follicles, cysts, or corpus luteum in either ovary using transvaginal ultrasound transducers with a frequency bandwidth of 8MHz to diagnose PCOM in women aged 18-35.[4,15] It has been emphasized that a cut-off OV value of ≥10 mL is much more reliable than the number of follicles for the diagnosis of PCOM.[4,15] This parameter is especially useful when utilizing outdated ultrasound equipment or transabdominal imaging[15] in sexually inactive women.[4] The above-mentioned approach to determining PCOM is also used in the Russian national clinical guidelines for the management of women with PCOS.

It should be noted that in patients with hyperandrogenism and irregular menstrual cycles, ultrasound examination of the pelvic organs is not necessary for the diagnosis of PCOS; however, it is important to clarify the clinical phenotype.[4] Also, the latest international guidelines do not recommend using PCOM as a diagnostic criterion for PCOS within 8 years after menarche.[4]

The ovarian stroma was considered by researchers as a tool to improve the quality of PCOM diagnostics.[16] However, due to the technical features of the implementation and the high correlation between stromal volume and the size of the ovaries, this approach is not used in clinical practice.[4,15] There is also no reliable data on the diagnostic value of measuring blood flow in the ovaries to detect PCOM, nor are there threshold values for differentiating the blood flow of polycystic and normal ovaries.[4,15]

Ethnic differences in the number of follicles and/or volume of the ovaries are being actively studied. For example, in Chinese women, the lower OV and FNPO, compared to women in the European population (≥6.3 cm^3 and ≥10), are considered as sufficient criteria for determining PCOM.[17] Turkish women also showed lower values than the Western population. The threshold PCOM criteria for them are OV of 6.43 cm^3 and FNPO of >8.[18] In the population of Korean patients, FNPO is considered to be a more significant criterion for polycystic disease than the OV, due to the smaller volume of ovaries specific for the Asian race.

The OV and FNPO change during the woman's reproductive period, reaching a maximum in adolescence with a gradual decrease in adulthood and a fast decrease in the age of menopause. For example, in women over age 35, the prevalence of PCOM is 7.8%, compared with 21% in younger women.[19] Moreover, a decrease in FNPO happens faster than

in OV.[20] Age-related processes in women suggest a reduction in the number of growing antral follicles.[20] A progressive decrease in the number of antral follicles leads to significant changes in typical ultrasound signs of PCOS, associated with a decrease in inhibin B and AMH levels,[20,21] and an increase in FSH levels.[20] FSH contributes a temporary more complete maturation of follicles with a reduction in the duration of the menstrual cycle,[20,21] and a decrease in the level of androgens in the blood serum. In this regard, aging in women with PCOS is associated with an improvement in the main characteristics of PCOS: a decrease in the prevalence of PCOM and a rise in the proportion of women with regular menstrual cycles.[20]

The use of various criteria for polycystic ovarian transformation also determines the inconsistency of information about the prevalence of PCOM. In general, the prevalence of polycystic morphology in a non-selective population, according to several authors, ranges from 33% to 22%.[22] At the same time, PCOM, according to the results of the ultrasound examination, is a common condition that can occur in 16%-25% of healthy women with regular menstrual cycles.[19] According to a few studies, the polycystic ovarian structure was detected in 92% of women with hirsutism with regular menstrual cycles, in 87% of women with oligomenorrhea, in 57% of women with anovulation, and in 26% of women with amenorrhea.[19,23] Interestingly, 25% of women with signs of PCOM had no other PCOS symptoms. Of women with anovulation and regular menstruation, 91% showed polycystic ovarian changes.[19]

The incidence of polycystic ovaries in Japanese women was comparable to that in women from the United States and Italy and was detected in 68%-80% of patients diagnosed with PCOS.[23] The prevalence of polycystic morphology in English women aged 20-25 years is 22%-33%, in Finnish women <36 years –21.6%, in New Zealand – 21%, and in Australia – 23%.[19] The prevalence of polycystic ovaries may be less if the study had been conducted using a transabdominal approach.[4]

Insulin resistance (IR) and hyperandrogenism are closely interrelated, exacerbating the pathogenesis of PCOS. Hyperandrogenemia favors the development of IR by directly altering the action of insulin in skeletal muscle and adipocytes and decreasing the secretion of adiponectin. IR also enhances hyperandrogenemia due to the induction of steroidogenesis in the ovaries and adrenal glands and a decrease in the synthesis of SHBG. In addition, hyperandrogenism correlates with follicular excess in PCOS.[4,24] According to a cross-sectional study, PCOS patients with IR and hyperinsulinemia had a larger OV than patients without abnormal biochemical markers.[4,25,26] However, there was no correlation between laboratory parameters of IR and FNPO.[25] Therefore, the authors consider OV as an important risk factor for metabolic disorders in patients with PCOS.[4,25] Even in women with normal menstrual function and without clinical signs of hyperandrogenism, PCOM is associated with higher androgen and insulin levels and lower SHBG levels.[27] On the other hand, hirsutism, oligomenorrhea, and irregular cycles were equally present in patients with normal OV and enlarged ovaries.[4]

There is a positive correlation between the FNPO and AMH levels. Some authors have proposed the use of AMH as an alternative marker of ovarian dysfunction and PCOM, especially in cases with an ambiguous assessment of PCOM, as well as when it is impossible to use a transvaginal approach (for example, in virgins, in the absence of equipment of a certain class, and in obese patients). However, a single threshold for AMH as a diagnostic criterion has not been determined yet.[4,28]

Conclusion

Thus, the results of the conducted literature review emphasize the importance of assessing PCOM, which is an independent criterion for diagnosing PCOS and determining its clinical phenotype. The review illustrates the role of PCOM, not only as an indicator of ovarian dysfunction but also as a marker of disease severity and a factor in assessing metabolic risks. The diagnostic significance of PCOM varies with age and race, requiring large-scale epidemiological studies to determine the PCOM characteristics for different populations. Standardization of PCOM diagnostic criteria is the key to the effective diagnosis of PCOS and, accordingly, to the prevention of complications and comorbidities associated with PCOS.

Competing Interests

The authors declare that they have no competing interests.

Acknowledgments

This article contains material that has been discussed at the VIII International Research and Practical Conference «FUNDAMENTAL AND APPLIED ASPECTS OF REPRODUCTION» (December 2021, Irkutsk, Russia). The author thanks all researchers who participated in the oral discussion.

References

1. Kolesnikova LI, Kolesnikov SI, Darenskaya MA, Grebenkina LA, Nikitina OA, Lazareva LM, Suturina LV, Danusevich IN, Druzhinina EB, Semendyaev AA. Activity of LPO Processes in Women with Polycystic Ovarian Syndrome and Infertility. Bull Exp Biol Med. 2017 Jan;162(3):320-322. doi: 10.1007/s10517-017-3605-5.
2. Darenskaya MA, Kolesnikov SI, Grebenkina LA, Danusevich IN, Lazareva LM, Nadelyaeva YaG, et al. [Analysis of pro-and antioxidant activity in the blood of women with different phenotypes of polycystic ovary syndrome and infertility]. Akusherstvo i Ginekologiya. 2017; (8):86–91. doi: 10.18565/aig.2017.8.86-91. [Article in Russian].
3. Atalyan AV, Kolesnikova LI, Kolesnikov SI, Grzhibovskiy AM, Suturina LV. Research electronic data capture (REDCap) for building and managing databases for population-based biomedical studies. Ekologiya Cheloveka. 2019; (2):52-59. doi: 10.1016/10.33396/1728-0869-2019-2-52-59. [Article in Russian].
4. Teede HJ, Misso ML, Costello MF, Dokras A, Laven

J, Moran L, Piltonen T, Norman RJ; International PCOS Network. Recommendations from the international evidence-based guideline for the assessment and management of polycystic ovary syndrome. Clin Endocrinol (Oxf). 2018 Sep;89(3):251-268. doi: 10.1111/cen.13795.
5. Belenkaia LV, Lazareva LM, Walker W, Lizneva DV, Suturina LV. Criteria, phenotypes and prevalence of polycystic ovary syndrome. Minerva Ginecol. 2019 Jun;71(3):211-223. doi: 10.23736/S0026-4784.19.04404-6.
6. Lizneva D, Kirubakaran R, Mykhalchenko K, Suturina L, Chernukha G, Diamond MP, Azziz R. Phenotypes and body mass in women with polycystic ovary syndrome identified in referral versus unselected populations: systematic review and meta-analysis. Fertil Steril. 2016 Nov;106(6):1510-1520.e2. doi: 10.1016/j.fertnstert.2016.07.1121.
7. Igumnov IA, Sharifulin EM, Belenkaia LV, Lazareva LM, Atalyan AV, Vilson NI, Suturina LV. [Chronic systemic inflammation in pathways of metabolic syndrome associated with hyperandrogenism (review)]. Pathogenesis. 2020; 18(3):12-18. doi: 10.25557/2310-0435.2020.03.12-18. [Article in Russian].
8. Lesnoy SK. [Partial resection of the ovaries with oligomenorrhea and amenorrhea]. Gynecol Obstetrics. 1928:2:184-191. [Article in Russian].
9. Rotterdam ESHRE/ASRM-Sponsored PCOS consensus workshop group. Revised 2003 consensus on diagnostic criteria and long-term health risks related to polycystic ovary syndrome (PCOS). Hum Reprod. 2004 Jan;19(1):41-7. doi: 10.1093/humrep/deh098.
10. Carmina E, Azziz R. Diagnosis, phenotype, and prevalence of polycystic ovary syndrome. Fertil Steril. 2006 Jul;86 Suppl 1:S7-8. doi: 10.1016/j.fertnstert.2006.03.012.
11. Azziz R. Polycystic Ovary Syndrome. Obstet Gynecol. 2018 Aug;132(2):321-336. doi: 10.1097/AOG.0000000000002698.
12. Azziz R, Carmina E, Dewailly D, Diamanti-Kandarakis E, Escobar-Morreale HF, Futterweit W, et al.; Androgen Excess Society. Positions statement: criteria for defining polycystic ovary syndrome as a predominantly hyperandrogenic syndrome: an Androgen Excess Society guideline. J Clin Endocrinol Metab. 2006 Nov;91(11):4237-45. doi: 10.1210/jc.2006-0178.
13. DeUgarte CM, Woods KS, Bartolucci AA, Azziz R. Degree of facial and body terminal hair growth in unselected black and white women: toward a populational definition of hirsutism. J Clin Endocrinol Metab. 2006 Apr;91(4):1345-50. doi: 10.1210/jc.2004-2301.
14. Legro RS, Arslanian SA, Ehrmann DA, Hoeger KM, Murad MH, Pasquali R, Welt CK; Endocrine Society. Diagnosis and treatment of polycystic ovary syndrome: an Endocrine Society clinical practice guideline. J Clin Endocrinol Metab. 2013 Dec;98(12):4565-92. doi: 10.1210/jc.2013-2350. Epub 2013 Oct 22. Erratum in: J Clin Endocrinol Metab. 2021 May 13;106(6):e2462.
15. Rao P, Bhide P. Controversies in the diagnosis of polycystic ovary syndrome. Ther Adv Reprod Health. 2020 Jun 29;14:2633494120913032. doi: 10.1177/2633494120913032.
16. Fulghesu AM, Angioni S, Frau E, Belosi C, Apa R, Mioni R, et al. Ultrasound in polycystic ovary syndrome--the measuring of ovarian stroma and relationship with circulating androgens: results of a multicentric study. Hum Reprod. 2007 Sep;22(9):2501-8. doi: 10.1093/humrep/dem202.
17. Chen X, Yang D, Mo Y, Li L, Chen Y, Huang Y. Prevalence of polycystic ovary syndrome in unselected women from southern China. Eur J Obstet Gynecol Reprod Biol. 2008 Jul;139(1):59-64. doi: 10.1016/j.ejogrb.2007.12.018.
18. Köşüş N, Köşüş A, Turhan NÖ, Kamalak Z. Do threshold values of ovarian volume and follicle number for diagnosing polycystic ovarian syndrome in Turkish women differ from western countries? Eur J Obstet Gynecol Reprod Biol. 2011 Feb;154(2):177-81. doi: 10.1016/j.ejogrb.2010.10.007.
19. Azziz R, Carmina E, Dewailly D, Diamanti-Kandarakis E, Escobar-Morreale HF, Futterweit W, Janssen OE, Legro RS, Norman RJ, Taylor AE, Witchel SF; Task Force on the Phenotype of the Polycystic Ovary Syndrome of The Androgen Excess and PCOS Society. The Androgen Excess and PCOS Society criteria for the polycystic ovary syndrome: the complete task force report. Fertil Steril. 2009 Feb;91(2):456-88. doi: 10.1016/j.fertnstert.2008.06.035.
20. Hsu MI. Changes in the PCOS phenotype with age. Steroids. 2013 Aug;78(8):761-6. doi: 10.1016/j.steroids.2013.04.005.
21. Quinn MM, Kao CN, Ahmad AK, Haisenleder DJ, Santoro N, Eisenberg E, Legro RS, Cedars MI, Huddleston HG; NIH/NICHD Reproductive Medicine Network. Age-stratified thresholds of anti-Müllerian hormone improve prediction of polycystic ovary syndrome over a population-based threshold. Clin Endocrinol (Oxf). 2017 Dec;87(6):733-740. doi: 10.1111/cen.13415.
22. Hart R, Doherty DA. The potential implications of a PCOS diagnosis on a woman's long-term health using data linkage. J Clin Endocrinol Metab. 2015 Mar;100(3):911-9. doi: 10.1210/jc.2014-3886. Epub 2014 Dec 22. Erratum in: J Clin Endocrinol Metab. 2015 Jun;100(6):2502.
23. Han YS, Lee AR, Song HK, Choi JI, Kim JH, Kim MR, Kim MJ. Ovarian Volume in Korean Women with Polycystic Ovary Syndrome and Its Related Factors. J Menopausal Med. 2017 Apr;23(1):25-31. doi: 10.6118/jmm.2017.23.1.25.
24. Homburg R. Androgen circle of polycystic ovary syndrome. Hum Reprod. 2009 Jul;24(7):1548-55. doi: 10.1093/humrep/dep049.
25. Reid SP, Kao CN, Pasch L, Shinkai K, Cedars MI, Huddleston HG. Ovarian morphology is associated with insulin resistance in women with polycystic ovary syndrome: a cross sectional study. Fertil Res Pract. 2017 May 30;3:8. doi: 10.1186/s40738-017-0035-z.
26. Hong SH, Sung YA, Hong YS, Jeong K, Chung H, Lee H. Polycystic ovary morphology is associated with insulin resistance in women with polycystic ovary syndrome. Clin Endocrinol (Oxf). 2017 Oct;87(4):375-380. doi: 10.1111/cen.13380.
27. Adams JM, Taylor AE, Crowley WF Jr, Hall JE. Polycystic ovarian morphology with regular ovulatory cycles: insights into the pathophysiology of polycystic ovarian syndrome. J Clin Endocrinol Metab. 2004 Sep;89(9):4343-50. doi: 10.1210/jc.2003-031600.
28. Ahmed AA, Moselhy SS, Kumosani TA, Huwait EA, Al-Ghamdi MA, Al-Madani KA, AlToukhi MH, Kumosani AT. Ultrasonographic and biochemical assessments as early prediction of polycystic ovarian syndrome in obese women. Afr Health Sci. 2020 Jun;20(2):676-681. doi: 10.4314/ahs.v20i2.18.

International Journal of Biomedicine 12(1) (2022) 104-108
http://dx.doi.org/10.21103/Article12(1)_OA9

ORIGINAL ARTICLE

Cardiology

INTERNATIONAL JOURNAL OF BIOMEDICINE

Comparison of the Impacts of Insulin and Oral Treatment, with or without Dietary Control and Physical Activity Management, on the Carotid Intima-Media Thickness of Patients with Type 2 Diabetes

Hassan A. Hamad[1]; Moawia Gameraddin[2*]; Sultan Alshoabi[2]; Mohamed Adam[3]; Salah Aloub[1]; Bushra A. Abdelmalik[4]

[1]*Diagnostic Radiologic Department, Alghad International Colleges, Almadinah, Saudi Arabia*
[2]*Department of Diagnostic Radiologic Technology, Faculty of Applied Medical Sciences, Taibah University, Almadinah, Saudi Arabia*
[3]*College of Applied Medical Science, Radiology Department, King Khalid University, Abha, Saudi Arabia*
[4]*Department of Diagnostic Radiology Sciences, College of Medical Applied Sciences, Hail University, Hail, Saudi Arabia*

Abstract

The aim of this study was to assess carotid intima-media thickness (CIMT) changes in relation to the treatment options of type 2 diabetes (T2D).

***Methods and Results*:** This cross-sectional descriptive study included 92 adults (57.61% female and 42.39% male) diagnosed with T2D with the mean age of 48.59±8.24 years and mean disease duration of 6.0±3.03 years. All patients were categorized into three groups according to the treatment types: Croup A included patients (n=21) treated with insulin injections; Group B included patients (n=33) treated with pills; and Group C included patients (n=38) treated with pills, dietary control, and regular exercise. The control group included 83 healthy people. High-resolution B-mode sonographic evaluations of common carotid arteries (CCAs) were performed. CIMT was measured at a point 1cm distal from the bulb of the carotid artery. The random blood glucose (RBG) test was performed at the time of the sonographic investigation.

In T2D patients, the CIMT was significantly higher than in the healthy participants (P<0.001).The CIMT of the left CCA in Group C was significantly lower than in Groups A and B (P=0.033). The age of participants and the duration of T2D were significantly associated with increased CIMT (P=0.021 and P=0.015, respectively).

Conclusion: Dietary control and physical activity should be considered significant factors in controlling CIMT in T2D. (**International Journal of Biomedicine. 2022;12(1):104-108.**)

Key Words: carotid intima-media thickness • type 2 diabetes • dietary control • physical activity • insulin injection

For citation: Hamad HA, Gameraddin M, Alshoabi S, Adam M, Aloub S, Abdelmalik BA. Comparison of the Impacts of Insulin and Oral Treatment, with or without Dietary Control and Physical Activity Management, on the Carotid Intima-Media Thickness of Patients with Type 2 Diabetes International Journal of Biomedicine. 2022;12(1):104-108. doi:10.21103/Article12(1)_OA9

Abbreviations

CCAs, common carotid arteries; **CVD**; cardiovascular disease; **CIMT,** carotid intima-media thickness; **DM,** diabetes mellitus; **RBG**, random blood glucose; **T2D**, type 2 diabetes.

Introduction

Diabetes mellitus (DM) is a significant health problem and a key risk factor for atherosclerosis and several cardiovascular issues, such as myocardial infarction, stroke, and vascular death. Compared to people without DM, those with diabetes have a higher risk of CVD events and cardiovascular death.[1,2]

Carotid intima-media thickness (CIMT) is an important ultrasound biomarker for the evaluation of atherosclerosis and is considered a predictor of organ damage. People with DM exhibit a higher CIMT than those without DM.[3-5]

The control of DM has a significant role in the prevention of CVDs. Uncontrolled DM can damage various organs, such as the eyes, nerves, kidneys, and cardiovascular system.[6] A large number of prospective and retrospective studies have reported significant associations between control of T2D and reduction of the progressive effect of CIMT.[7] For T2D, a diet rich in fiber has been found to have a beneficial effect on cardiovascular risk factors.[8] Regular physical activity has also been shown to reduce CIMT.[9]

The aim of this study was to assess CIMT changes in relation to the treatment options of T2D.

Materials and Methods

This cross-sectional descriptive study was conducted at Ribat University Hospital and Military Hospital in Khartoum State from January 2015 to November 2017. A total of 92 adults (57.61% female and 42.39% male) diagnosed with T2D with the mean age of 48.59±8.24 years and mean disease duration of 6.0±3.03 years were categorized into three groups according to the treatment types (Table 1): Croup A included patients (n=21) treated with insulin injections; Group B included patients (n=33) treated with pills; and Group C included patients (n=38) treated with pills, dietary control, and regular exercise. The participants were asked for regular exercise and dietary control using a designed data collection sheet.

Table 1.
Demographic characteristics of patients with T2D

Variable	Mean ± SD
CIMT (Male; n=53)	1.675±0.088 mm
CIMT (Female; n =39)	1.907±0.168 mm
Age	48.59±8.25 years
Duration of the disease	6±3.03 years
RBG Group C Group A Group B	 125±8 mg/dL 150±11 mg/dL 170±9 mg/dL

The dietary control was implemented through medical nutrition therapy utilized for improving diabetes management. RBG was taken at the time of the sonographic investigation.

Patients were excluded from the study if they had any history of previous ischemic stroke, hypertension, familial hyperlipidemia, CVDs, carotid or peripheral vascular surgery, or renal insufficiency. The control group included 83 healthy participants.

Sonographic examination

The patients were investigated using an ultrasound machine (Sonoline G 60S) equipped with a linear probe with a frequency of 7–10MHz. High-resolution B-mode sonographic evaluations were performed. Patients were examined in a supine position with the sonographer seated beside the patient's head. The sonographic scanning of the neck was obtained by tilting and rotating the head away from the side being investigated. The CCAs were scanned in several transducer positions, such as long-axis (longitudinal) and short-axis (transverse) planes. The views of the CCAs were obtained from the anterior, lateral, and posterior-lateral approaches. CIMT was measured at a point 1cm distal from the bulb of the carotid artery.

Statistical analysis was performed using the standard Statistical Package for the Social Sciences (IBM SPSS Statistics for Windows, Version 23.0. Armonk, NY: IBM Corp). Continuous variables were presented as mean±standard deviation (SD). For data with normal distribution, inter-group comparisons were performed using Student's t-test. Multiple comparisons were performed with one-way ANOVA. The linear regression test was applied. A probability value of $P<0.05$ was considered statistically significant.

The study was approved by the ethical committee of the College of Medical Radiologic Science at the Sudan University for Science and Technology (SUST). Written informed consent was obtained from all participants.

Results

The results of biochemical analysis were not significantly different between the groups; the range of the RBG was 125–170 mg/dl for the three groups (Table 1). In T2D patients, the CIMT was significantly higher than in the healthy participants ($P<0.001$) (Table 2).

Table 2.
CIMT in patients with T2D and Control group

Variables	Participants	n	Mean±SD	P-value	95% CI
Right CCA CIMT, mm	T2D	92	1.47±.268	< 0.001	.745─.86
	Control group	83	0.66±0.079		
Left CCA CIMT, mm	T2D	92	1.52±0.220	< 0.001	.869─.97
	Control group	83	0.59±0.098		

The CIMT of the left and right CCAs was not significantly different between Group A and Group B. In contrast, the CIMT of the left CCA in Group C was significantly lower than in Groups A and B ($P=0.033$) (Table 3).

The right CIMT was also lower in Group C than in Group A, but differences were not statistically significant (Table 4). Figure 1 summarizes the changes in the mean CIMT in the study groups.

We applied a linear regression test to determine the risk factors and predictors that may affect the carotid IMT. We found that the age of participants and the duration of T2D are significantly associated with increased CIMT ($P=0.021$ and $P=0.015$, respectively). Importantly, the treatment of T2D with dietary control and exercise has a significant association

with CIMT (*P*=0.022). After adjusting for age, duration of T2D, and gender, the mean CIMT maintained a significant difference depending on the type of treatment (Table 5).

Table 3.

CIMT in patients according to the type of treatment

Group	n	Right CCA CIMT, mm	Left CCA CIMT, mm	Duration of T2D, years
Group C	38	1.44±.27	1.46±.19	4.79±2.24
Group A	21	1.48±.31	1.61±.18	8.19±3.23
Group B	33	1.48±.23	1.52±.25	6.00±2.98
P-value (ANOVA test)		0.836	0.033	< 0.001

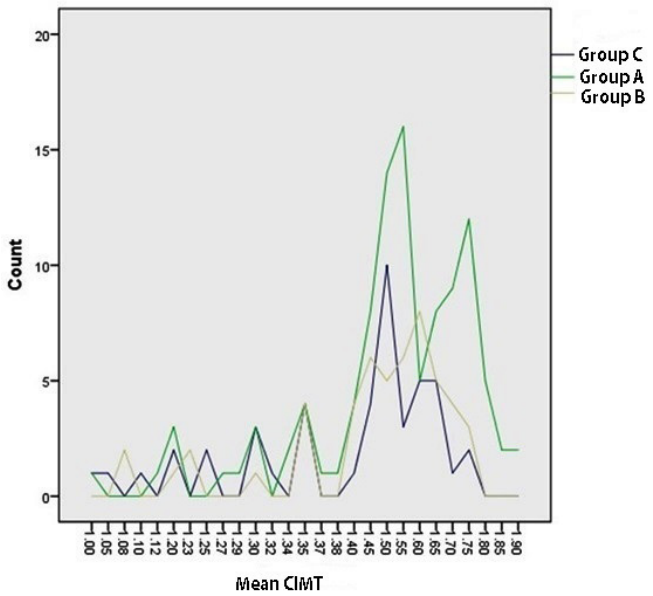

Fig.1. *CIMT in patients according to the type of treatment*

Table 4.

CIMT of the left and right CCAs in groups of patients according to the type of treatment

CIMT	Group	Mean ± SD, mm	*P*-value	95% CI
Left CCA CIMT, mm	Group C	1.46±0.19	.005	-.25957 — -.04896
	Group A	1.61 ±0.18		
Right CCA CIMT, mm	Group C	1.44±0.28	.66	-.19145 — .12333
	Group A	1.48±0.31		
LT CCA CIMT, mm	Group A	1.61±0.18	.183	-.04122— -.03344
	Group B	1.52±.25		
RT CCA CIMT, mm	Group A	1.48±.31	.996	-.14934 — .14856
	Group B	1.48±.23		

Table 5.

CIMT in the linear regression test

Model	Unstandardized coefficient		Standardized coefficient	t	*P*	95.0% CI for B
	B	Std. Error	Beta			
Age	.035	.015	.275	2.357	.021	.005–.064
Gender	.492	.209	.233	2.356	.021	.077–.908
Dietary and exercise control	.523	.224	.247	2.335	.022	.078–.968
Duration of T2D	-.101-	.041	-.293-	-2.480-	.015	-.183–-.020
(Constant)	-.734-	.759	--	-.968-	.336	-2.242–.774

Discussion

Atherosclerosis is a major cause of death and disability in patients with T2D.[10] The CIMT is a risk marker for CVD.[11-13] The present study explored the expected change in the CIMT of T2D patients undergoing three types of treatment.

We found that the CIMT was significantly higher in the T2D group than in the control group. A previous study also reported that the average common CIMT was 0.13mm greater in patients with DM,[14] and several other studies have found a significant relationship between CIMT and DM.[15,16]

The present study revealed that age and duration of DM were significantly associated with increased CIMT. This finding consistently agreed with previous studies, which reported a significant impact of age and DM duration on CIMT.[17,18] Despite the significant relationship between gender and CIMT, as reported in previous studies,[19,20] the current study found an insignificant correlation.

In our study, oral treatment with dietary control and exercise had a more significant impact on reducing the CIMT than oral treatment without exercise and dietary control. A previous study reported the beneficial effect of dietary control on T2D and glucose metabolism in general, reducing the risk of microvascular complications.[21] Epidemiological data have shown that a higher intake of some foods, such as whole grains, fruit, and soluble fibers, and lower consumption of saturated fat are associated with a decrease in CIMT. Lower CIMT has been reported with consumption of more than 0.79 servings/day of whole grains and more than 25g/day of fiber, predominately in a soluble form, and dietary control has thus been correlated with a significant decrease in CIMT.[22]

In the current study, the pills, diet, and exercise group had significantly lower CIMT. In the literature, it has been reported that regular exercise has a beneficial effect in reducing CIMT, which in turn helps to prevent carotid plaques. Byrkjeland et al.[23] reported that there was a significant effect of exercise on the presence of carotid plaques (*P*=0.013), with significantly lower CIMT in their exercise group than in the control group in patients without identified carotid plaques. Long-term physical activity may also have a positive effect

against atherosclerosis in healthy asymptomatic individuals.[24,25] These studies support our finding that dietary control and physical activity are related to significantly lower CIMT than insulin injections alone for T2D.

The current recommendations for the treatment of patients with T2D highlight the importance of diet and exercise.[26-30] Dietary knowledge and exercise for the treatment of T2D lead to better control of the disease and prevent carotid atherosclerosis, which is a key factor in cardiovascular events.

Limitations

The findings of this study should be interpreted in the context of some specific limitations. The diabetic treatments may not have been controlled perfectly in accordance with clinician instructions, and some patients may not have optimally implemented physical activity and dietary control. Secondly, the sample size is not large enough, and this may influence the statistical or clinical conclusion. These situations may affect the current results.

In conclusion, both insulin and oral treatment without other forms of management had no significant impact on reducing the progressive effect of CIMT. In contrast, oral treatment with dietary control and exercise saw significant differences. Therefore, dietary control and physical activity should be considered significant factors in controlling CIMT in T2D. Further studies are required to understand the correlation between diet, physical activity, and changes in CIMT.

Competing Interests

The authors declare that they have no competing interests.

References

1. Emerging Risk Factors Collaboration, Sarwar N, Gao P, Seshasai SR, Gobin R, Kaptoge S, Di Angelantonio E, Ingelsson E, Lawlor DA, et al. Diabetes mellitus, fasting blood glucose concentration, and risk of vascular disease: a collaborative meta-analysis of 102 prospective studies. Lancet. 2010 Jun 26;375(9733):2215-22. doi: 10.1016/S0140-6736(10)60484-9. Erratum in: Lancet. 2010 Sep 18;376(9745):958. Hillage, H L [corrected to Hillege, H L].
2. Woodward M, Zhang X, Barzi F, Pan W, Ueshima H, Rodgers A, MacMahon S; Asia Pacific Cohort Studies Collaboration. The effects of diabetes on the risks of major cardiovascular diseases and death in the Asia-Pacific region. Diabetes Care. 2003 Feb;26(2):360-6. doi: 10.2337/diacare.26.2.360.
3. Lorenz MW, Price JF, Robertson C, Bots ML, Polak JF, Poppert H, et al. Carotid intima-media thickness progression and risk of vascular events in people with diabetes: results from the PROG-IMT collaboration. Diabetes Care. 2015 Oct;38(10):1921-9. doi: 10.2337/dc14-2732.
4. Qu B, Qu T. Causes of changes in carotid intima-media thickness: a literature review. Cardiovasc Ultrasound. 2015 Dec 15;13:46. doi: 10.1186/s12947-015-0041-4.
5. Roumeliotis A, Roumeliotis S, Panagoutsos S, Theodoridis M, Argyriou C, Tavridou A, Georgiadis GS. Carotid intima-media thickness is an independent predictor of all-cause mortality and cardiovascular morbidity in patients with diabetes mellitus type 2 and chronic kidney disease. Ren Fail. 2019 Nov;41(1):131-138. doi: 10.1080/0886022X.2019.1585372.
6. Sami W, Ansari T, Butt NS, Hamid MRA. Effect of diet on type 2 diabetes mellitus: A review. Int J Health Sci (Qassim). 2017 Apr-Jun;11(2):65-71.
7. Forouhi NG, Misra A, Mohan V, Taylor R, Yancy W. Dietary and nutritional approaches for prevention and management of type 2 diabetes. BMJ. 2018 Jun 13;361:k2234. doi: 10.1136/bmj.k2234.
8. lurink IA, Soedamah-Muthu SS. Dietary Fibre and Cardiovascular Risk in Diabetes Mellitus. J Clin Nutr Diet. 2016; 2:3. doi: 10.4172/2472-1921.100021.
9. Kadoglou NP, Iliadis F, Liapis CD. Exercise and carotid atherosclerosis. Eur J Vasc Endovasc Surg. 2008 Mar;35(3):264-72. doi: 10.1016/j.ejvs.2007.08.022.
10. Low Wang CC, Hess CN, Hiatt WR, Goldfine AB. Clinical Update: Cardiovascular Disease in Diabetes Mellitus: Atherosclerotic Cardiovascular Disease and Heart Failure in Type 2 Diabetes Mellitus - Mechanisms, Management, and Clinical Considerations. Circulation. 2016 Jun 14;133(24):2459-502. doi: 10.1161/CIRCULATIONAHA.116.022194.
11. Lorenz MW, Markus HS, Bots ML, Rosvall M, Sitzer M. Prediction of clinical cardiovascular events with carotid intima-media thickness: a systematic review and meta-analysis. Circulation. 2007 Jan 30;115(4):459-67. doi: 10.1161/CIRCULATIONAHA.106.628875.
12. Sibal L, Agarwal SC, Home PD. Carotid intima-media thickness as a surrogate marker of cardiovascular disease in diabetes. Diabetes Metab Syndr Obes. 2011 Jan 19;4:23-34. doi: 10.2147/DMSO.S8540.
13. Lorenz MW, Polak JF, Kavousi M, Mathiesen EB, Völzke H, Tuomainen TP, et al.; PROG-IMT Study Group. Carotid intima-media thickness progression to predict cardiovascular events in the general population (the PROG-IMT collaborative project): a meta-analysis of individual participant data. Lancet. 2012 Jun 2;379(9831):2053-62. doi: 10.1016/S0140-6736(12)60441-3.
14. Kasliwal RR, Bansal M, Desai N, Kotak B, Raza A, Vasnawala H, Kumar A; SCORE-India collaborators. A Study to derive distribution of carotid intima media thickness and to determine its COrrelation with cardiovascular Risk factors in asymptomatic nationwidE Indian population (SCORE-India). Indian Heart J. 2016 Nov-Dec;68(6):821-827. doi: 10.1016/j.ihj.2016.04.009.
15. Zhang F, Feng L, Chen Y, Geng Z, Xu X. Relationship between carotid artery intima-media thickness and cardiovascular risk factors in Chinese Uygur population. Int J Clin Exp Med. 2014 Dec 15;7(12):5412-20.
16. Fusaro MF, Zanini JL, Silva IN. Increased carotid intima-media thickness in Brazilian adolescents with type 1 diabetes mellitus. Diabetol Metab Syndr. 2016 Nov 11;8:74. doi: 10.1186/s13098-016-0190-0.
17. Bashir F, Nageen A, Kidwai SS, Ara J. Carotid intima-media thickness and cardiometabolic risk factors in Pakistani type 2 diabetics. Saudi J Health Sci 2017;6:145-50. doi: 10.4103/sjhs.sjhs_66_17

***Corresponding author:** Dr. Moawia Gameraddin, Department of Diagnostic Radiologic Technology, Faculty of Applied Medical Sciences, Taibah University, Almadinah, Saudi Arabia. E-mail: gameradinm@gmail.com*

18. Jin Y, Kim D, Cho J, Lee I, Choi K, Kang H. Association between Obesity and Carotid Intima-Media Thickness in Korean Office Workers: The Mediating Effect of Physical Activity. Biomed Res Int. 2018 Aug 1;2018:4285038. doi: 10.1155/2018/4285038.
19. Momeni A, Taheri A, Mansuri M, Bazdar A, Sedehi M, Amiri M. Association of carotid intima-media thickness with exercise tolerance test in type 2 diabetic patients. Int J Cardiol Heart Vasc. 2018 Oct 17;21:74-77. doi: 10.1016/j.ijcha.2018.10.002.
20. Zanini JLSS, Rodrigues TMB, Barra CB, Filgueiras MFTF, Silva IN. INTIMA-MEDIA THICKNESS OF THE CAROTID ARTERIES IS AFFECTED BY PUBERTAL MATURATION IN HEALTHY ADOLESCENTS. Rev Paul Pediatr. 2019 Jul 4;37(4):428-434. doi: 10.1590/1984-0462/;2019;37;4;00010.
21. Fox CS, Golden SH, Anderson C, Bray GA, Burke LE, de Boer IH, et al.; American Heart Association Diabetes Committee of the Council on Lifestyle and Cardiometabolic Health; Council on Clinical Cardiology, Council on Cardiovascular and Stroke Nursing, Council on Cardiovascular Surgery and Anesthesia, Council on Quality of Care and Outcomes Research; American Diabetes Association. Update on Prevention of Cardiovascular Disease in Adults With Type 2 Diabetes Mellitus in Light of Recent Evidence: A Scientific Statement From the American Heart Association and the American Diabetes Association. Diabetes Care. 2015 Sep;38(9):1777-803. doi: 10.2337/dci15-0012. Epub 2015 Aug 5.
22. Petersen KS, Clifton PM, Keogh JB. The association between carotid intima media thickness and individual dietary components and patterns. Nutr Metab Cardiovasc Dis. 2014 May;24(5):495-502. doi: 10.1016/j.numecd.2013.10.024.
23. Byrkjeland R, Stensæth KH, Anderssen S, Njerve IU, Arnesen H, Seljeflot I, Solheim S. Effects of exercise training on carotid intima-media thickness in patients with type 2 diabetes and coronary artery disease. Influence of carotid plaques. Cardiovasc Diabetol. 2016 Jan 22;15:13. doi: 10.1186/s12933-016-0336-2.
24. Kwaśniewska M, Jegier A, Kostka T, Dziankowska-Zaborszczyk E, Rębowska E, Kozińska J, Drygas W. Long-term effect of different physical activity levels on subclinical atherosclerosis in middle-aged men: a 25-year prospective study. PLoS One. 2014 Jan 20;9(1):e85209. doi: 10.1371/journal.pone.0085209.
25. Ried-Larsen M, Grøntved A, Kristensen PL, Froberg K, Andersen LB. Moderate-and-vigorous physical activity from adolescence to adulthood and subclinical atherosclerosis in adulthood: prospective observations from the European Youth Heart Study. Br J Sports Med. 2015 Jan;49(2):107-12. doi: 10.1136/bjsports-2013-092409.
26. American Diabetes Association Standards of medical care in diabetes—2015. Diabetes Care 2015;38(Suppl. 1): S1–S89. https://doi.org/10.2337/dc15-S001. Available from: https://www.sahta.com/docs/standardsDiabetes.pdf
27. Expert Panel on Detection, Evaluation, and Treatment of High Blood Cholesterol in Adults. Executive Summary of The Third Report of The National Cholesterol Education Program (NCEP) Expert Panel on Detection, Evaluation, And Treatment of High Blood Cholesterol In Adults (Adult Treatment Panel III). JAMA. 2001 May 16;285(19):2486-97. doi: 10.1001/jama.285.19.2486.
28. American Heart Association Nutrition Committee, Lichtenstein AH, Appel LJ, Brands M, Carnethon M, Daniels S, Franch HA, Franklin B, Kris-Etherton P, Harris WS, Howard B, Karanja N, Lefevre M, Rudel L, Sacks F, Van Horn L, Winston M, Wylie-Rosett J. Diet and lifestyle recommendations revision 2006: a scientific statement from the American Heart Association Nutrition Committee. Circulation. 2006 Jul 4;114(1):82-96. doi: 10.1161/CIRCULATIONAHA.106.176158.
29. Handelsman Y, Bloomgarden ZT, Grunberger G, Umpierrez G, Zimmerman RS, Bailey TS, et al. American association of clinical endocrinologists and american college of endocrinology - clinical practice guidelines for developing a diabetes mellitus comprehensive care plan - 2015. Endocr Pract. 2015 Apr;21 Suppl 1(Suppl 1):1-87. doi: 10.4158/EP15672.GL.
30. Evert AB, Boucher JL, Cypress M, Dunbar SA, Franz MJ, Mayer-Davis EJ, Neumiller JJ, Nwankwo R, Verdi CL, Urbanski P, Yancy WS Jr. Nutrition therapy recommendations for the management of adults with diabetes. Diabetes Care. 2014 Jan;37 Suppl 1:S120-43. doi: 10.2337/dc14-S120.

International Journal of Biomedicine 12(1) (2022) 109-114
http://dx.doi.org/10.21103/Article12(1)_OA10

ORIGINAL ARTICLE

Oncology

INTERNATIONAL JOURNAL OF BIOMEDICINE

Simultaneous Detection of the HPV L1 Gene and the Human β-Globin Gene in the Blood Components of Cervical Cancer Patients Living in Yakutia

Irina V. Kononova[1*], PhD; Sargylana N. Mamaeva[2], PhD; V. A. Alekseev[1]; Nadezhda A. Nikolaeva[2]; L. N. Afanasyeva[2], PhD; Petr V. Nikiforov[2,3]; N. A. Vasilyeva[2]; I. V. Vasiliev[3]; Georgy V. Maximov[4,5], PhD, ScD

[1]*Yakut Scientific Center of Complex Medical Problems, Yakutsk, Sakha (Yakutia) Republic, Russia*
[2]*M.K. Ammosov North-Eastern Federal University, Yakutsk, Sakha (Yakutia) Republic, Russia*
[3]*Yakut Republican Oncology Center, Yakutsk, Sakha (Yakutia) Republic, Russia*
[4]*Lomonosov Moscow State University, Moscow, Russia*
[5]*National University of Science and Technology "MISiS," Moscow, Russia*

Abstract

Background: To create a test for the early detection of cervical cancer (CC), we conducted exploratory studies on detecting HPV genes and genes of the human β-globin locus in plasma (Pl) and red blood cell (RBC) suspension (RBCsus) samples from patients with newly detected CC (NDCC).

Methods and Results: Smears of venous blood containing K3-EDTA from five anonymous patients aged from 45 to 55 years (residents of Yakutia), with NDCC were obtained. Three types of blood component samples were prepared – Pl, RBCsus, and the erythrocyte fraction treated with trypsin (RBCsus-Try). To detect circulating cell-free DNA (cfDNA) in NDCC patients, we studied the presence of genes corresponding to the HPV L1 protein region and genes of the human β-globin locus by real-time PCR (qPCR) using appropriate primers.

The genes of β-globin locus and HPV L1 were detected in Pl of NDCC patients in 20% of cases, and in RBCsus in 60% of cases. The amplified gene products using primers were present in RBCsus-Try in only one patient (20% of cases).In patients with uncertain amplification, electrophoresis showed the absence of amplified products in Pl and their presence in RBCsus.

Conclusion: In NDCC patients, HPV L1 and β-globin genes can be detected in both Pl and RBCsus. In addition, in RBC samples, these genes were detected more often than in plasma samples, and no absolute absence of amplification products was observed in RBC samples. The research needs to be continued.(**International Journal of Biomedicine. 2022;12(1):109-114.**)

Key Words: cervical cancer • human papillomavirus • circulating cell-free DNA • quantitative PCR

For citation: Kononova IV, Mamaeva SN, Alekseev VA, Nikolaeva NA, Afanasyeva LN, Nikiforov PV, Vasilyeva NA, Vasiliev IV, Maximov GV. Simultaneous Detection of the HPV L1 Gene and the Human β-Globin Gene in the Blood Components of Cervical Cancer Patients Living in Yakutia. International Journal of Biomedicine. 2022;12(1):109-114. doi:10.21103/Article12(1)_OA10

Abbreviations

CC, cervical cancer; **Pl**, plasma; **RBC**, red blood cells; **NDCC**, newly detected CC; **HPV**, human papillomavirus; **ctDNA**, circulating tumor DNA; **cfDNA**, circulating cell-free DNA; **qPCR**, quantitative PCR; **csbDNA**, cell-surface-bound extracellular DNA.

Introduction

Cervical cancer (CC) is common cancer among women around the world. The high burden of CC is among people living in low- and middle-income countries where access to public health services is limited.(1) In Russia, a middle-income country,(2) cytological screening is primarily used for CC early detection. Cytological screening is carried out

free of charge for Russian citizens once every 3 years. At the same time, in Russia, the CC incidence and mortality have not been decreasing and significantly exceed the target level established by the WHO.[3] Therefore, research on creating new tests for CC early detection is highly relevant. For such tests, the researchers suggest, among others, the detection of ctDNA isolated from human bodily fluids since in CC patients, ctDNA has a high genetic similarity to the tumor cell DNA.[4,5] ctDNA can be detected before treatment in patients with early-stage primary cancer; however, ctDNA is generally detected at a lower rate than in advanced cancer.[6-8]

For CC detection, researchers often detect circulating cell-free HPV DNA, which can be considered as CC-ctDNA, since it is believed that cfDNA containing one or more copies of the HPV genome originates from transformed cells.[5,9]

The aim of our study was to create an affordable and easily reproducible method for the early detection of CC using cfDNA as a CC biomarker.

To detect cfDNA in NDCC patients, we studied the presence of genes corresponding to the HPV L1 protein region and genes of the human β-globin locus by real-time PCR (qPCR) using appropriate primers. It is known that CC-ctDNA contains human genes and HPV genes.[5] We detected cfDNA, which can be a CC biomarker in NDCC patients, in samples of plasma (Pl) and red blood cell (RBC) suspension (RBCsus) since these blood fractions do not contain human cell nuclei.

A meta-analysis conducted by Y. Gu et al.[9] showed that detection of HPV cDNA in patients with CC could be used as a noninvasive early dynamic biomarker of tumors, with high specificity and moderate sensitivity.

Human β-globin is expressed by cervical carcinoma cells and plays a cytoprotective role against oxidative damage.[10] In cancer patients, cfDNA carries tumor-related genetic alteration of transformed cells.[11] Therefore, we expected that in CC patients, genes of the human β-globin locus should be detected in blood fractions that do not contain human cell nuclei in significant quantities. In ovarian cancer, for example, genes of the human β-globin locus are detected in plasma in significantly greater numbers than in healthy patients.[12]

Genes corresponding to the HPV L1 protein region and genes of the human β-globin locus are often detected in scientific research and in clinical practice; their primers are available on the market and have an optimal value. In addition, we decided to find out whether the cfDNA detected from RBCsus is the RBC-bound cfDNA. Therefore, we determined the presence of cfDNA in the erythrocyte fraction treated with trypsin (RBCsus-Try).

Materials and Methods

Smears of venous blood containing K3-EDTA from five anonymous patients aged from 45 to 55 years (residents of Yakutia), with NDCC were obtained. The blood was collected in 2018-2019 and in the same years, it was investigated. At the time of blood sampling, the patients were not given any type of cervical cancer treatment.

Three types of blood component samples were prepared – Pl, RBCsus and RBCsus-Try. To obtain blood fractionation, blood samples were centrifuged at 1600 g for 10 minutes. After fractionation, PI samples were obtained.

RBC samples were obtained from 1ml of the erythrocyte fraction then washed three times in a phosphate buffer. RBCsus-Try samples were obtained as follows: The RBC samples described above were split in half; a solution of 0.25% trypsin was added to one half in a ratio of 1:1 and incubated at 37°C for 10 minutes. After incubation, it was centrifuged to obtain sediment. Then the lower part of the sediment was washed three times in a phosphate buffer, and these samples were included in this study as RBCsus-Try.

All samples were stored at a temperature of –20°C before DNA isolation and qPCR. For DNA extraction, 200 µl of previously prepared samples with markings Pl, RBCsus, RBCsus-Try were used. TRIzol™ and chloroform were added to each sample in an amount of 1000 µl and 200 µl, respectively. The concentration of the isolated DNA was determined on a spectrophotometer, following the manufacturer's instructions.[13]

To detect cfDNA, the CFX96 Touch Real-Time PCR Detection System was used. qPCR was performed using the 5x qPCRmix-HS SYBR+LowROX, designed for setting up PCR with SYBR Green I in the presence of a reference dye ROX, according to the manufacturer's amplification protocol.[14]

Genes of the human β-globin locus were detected using PC03/04 primers (5'-ACACAACTGTGTTCACTAGC-3'/5'-CAACTTCATCCACGTTCACC-3').

Primers MY09/11 (5'-CGTCCMARRGGAWACTGATC-3'/5'-GCMCAGGGWCATAAYAATGG-3') were used to detect genes corresponding to the HPV L1 protein DNA region. The length of the amplicons was determined by DNA electrophoresis in 2% agarose gel.

Given the small number of patients and the exploratory nature of the study, the results are presented as a percentage.

The study was conducted in accordance with ethical principles of the WMA Declaration of Helsinki (1964, ed. 2013) and approved by the Ethics Committee of the M.K. Ammosov North-Eastern Federal University (protocol No. 13 of April 4, 2018, decision No. 2). Written informed consent was obtained from each patient.

Results

In all 15 samples (3 samples [Pl, RBCsus, and RBCsus-Try] from each of the five CC patients), DNA was detected and isolated in sufficient amounts (Table 1).

The results of qPCR using primers PC03/04 and MY09/11 (Table 2) showed the joint presence of genes corresponding to the human β-globin region and HPV L1 protein DNA region in Pl from Patient #5 (20% of cases), in RBCsys from Patients #3-5 (60% of cases) and in RBCsus-Try from Patient #5 (20% of cases).

Uncertain amplification results using both primers were detected for DNA isolated from Pl of Patients #1 and #4 (40% of cases), for DNA isolated from RBCsus of Patients

Table 1.

DNA concentration (ng/ml)

	Pl	RBCsus	RBCsus -Try
Patient 1	High	High	High
Patient 2	High	High	High
Patient 3	High	3773	High
Patient 4	High	High	High
Patient 5	3390	2808	2753

"High" means that the concentration of the isolated DNA is higher than the linear range of the spectrophotometer.

#1 and #2 (40% of cases), and for DNA isolated from the RBCsus-Try of Patients #1, #3 and #4 (60% of cases). No amplification results using both primers were detected for DNA in Pl from Patients #2 and #3 (40% of cases) and in RBCsus-Try from Patient #2 (20% of cases).

The results of qPCR products were validated based on the DNA gel electrophoresis. The agarose gel electrophoresis confirmed the qPCR amplification and no amplification. Regarding CC patients with uncertain amplification for DNA isolated from Pl (Patients #1 and #4), in Patient #1, electrophoresis showed the presence of amplified products using PC03/04 primers, but electrophoresis to confirm amplification using MY09/11 primer products could not be performed because we ran out of biomaterial; in Patient #4, electrophoresis showed the absence of amplified products using both primers.

Patients #1 and #2 with uncertain amplification for DNA isolated from RBCsus, electrophoresis showed the presence of amplified products using both primers. In Patients #1, #3, and #4 with uncertain amplification results for DNA isolated from RBCsus-Try, electrophoresis did not confirm the presence of amplified products using both primers.

Electrophoresis revealed that the size of qPCR products ranges from 50 bp to 200 bp. This size corresponds to the recommended amplicon sizes for obtaining consistent and reliable results by the real-time PCR method.[15]

Thus, in NDCC patients, genes corresponding to the HPV L1 protein DNA region and the human β-globin region were detected in RBCsus more often than in Pl. Also, in RBCsus, there was no undoubted absence of amplified products using primers for these gene products. Considering that the amplified gene products using primers were present in RBCsus-Try in only one patient, we can say that the cfDNA that can be a CC biomarker might be an RBC-bound cfDNA.

Discussion

HPV cDNA has become a major focus, providing a strong basis for early diagnosis and prognosis in cervical cancer.[5,16,17] The E7 proteins encoded by the high-risk type HPVs, such as HPV 16 and HPV 18, bind Rb with a much higher affinity compared to those encoded by the low-risk type HPVs, such as HPV 6 and HPV 11.[18] The ability to target the retinoblastoma (Rb) family of proteins and p53 and to induce telomerase are some of the critical events that contribute to the development of malignancy.[19]

HPV DNA for CC detection is isolated by researchers mainly from plasma and serum samples(6) using primers for HPV16/18 E7.[20-22] It is believed that the DNA fragment corresponding to the HPV16/18 E7 protein region is the optimal candidate for a CC biomarker.[22,23]

The papillomavirus major capsid protein, L1, encoded by late gene 1, can spontaneously self-assemble into a highly immunogenic structure,virus-like particles, that closely mimic the natural surface of native papillomavirus virions. The late phase of the viral life cycle, during which new virions are assembled, occurs only in keratinocytes, which form the outer layer of the skin (epidermis), as well as the surface of other stratified squamous epithelia, including the genitals.[24]

Table 2.

The results of qPCR using primers PC03/04 and MY09/11

	Pl		RBCsus		RBCsus -Try	
	PC03/04	MY09/11	PC03/04	MY09/11	PC03/04	MY09/11
Patient #1	-+ (+)	-+(N/A)	-+ (+)	-+ (+)	-+ (-)	-+ (-)
Patient #2	- (-)	- (-)	-+\+	-+ (+)	- (-)	- (-)
Patient #3	- (-)	- (-)	+ (+)	+ (+)	-+ (-)	-+ (-)
Patient #4	-+ (-)	-+ (-)	+ (+)	+ (+)	-+ (-)	-+ (-)
Patient #5	+ (+)	+ (+)	+ (+)	+ (+)	+ (+)	+ (+)

The "+" indicates the amplification; the "-"indicates no amplification; the "-+" indicates an uncertain amplification. In parentheses - the results of electrophoresis with the RT-PCR products.

We have not found any published studies on CC detection based on the presence of circulating HPV DNA using primers for HPV L1 DNA. Also, we have not found published studies on the detection of HPV DNA and ctDNA in the erythrocyte fraction of CC patients. There is a study that shows that in healthy male blood donors, HPV DNA is found among leukocytes, but not in the erythrocyte fraction.[25]

Protein L1 alone forms the surface of the HPV virion and provides the initial interaction of the HPV capsid with the host cells.[24] In a study by Cao et al.,[26] circulating HPV DNA (in the plasma) was detected by conventional PCR using the L1 G5+/6+ primer (L1 primer) in most patients with HPV(+) oropharyngeal carcinoma. In a study by Cocuzza et al.,[27] HPV DNA detection was carried out in both plasma and cervical samples using type-specific real-time quantitative PCR assays identifying oncogenic HPV 16, 18, 31, 33, 45, 51, and 52. Overall, 34.2% (41/120) of plasma samples were shown to be positive for HPV DNA detection; HPV 45(46.3%), HPV-51(29.6%), and HPV 16(18.5%) were the most frequently identified genotypes. HPV 16 was the most common genotype identified in women found to be HPV DNA positive in both cervical and plasma samples.

We chose primers for HPV L1 and the human β-globin region for early detection of CC, not only in Pl, but also in RBC suspensions because we speculated on the following:

(i) It is known that with the CC progression, changes in an infected cell interrupt the HPV replicative life cycle; therefore, progeny virions cannot be obtained,[28] and L1expression is only poorly supported,[29] but not all infected cells in CC patients undergo cancer transformation, and that means HPV replication may still be present;

(ii) there is a possibility that HPV can bind to the erythrocyte surface; it is known that virus-like particles having the L1 protein derived from bovine papillomavirus type 1 (BPV-1) can bind to surface receptors of erythrocytes;[30] in addition, heparan sulfate, the HPV receptor,[25] has been identified on human erythrocytes.[31]

(iii) With the probable fulfillment of the events described in (i) and (ii), the biomarker of malignancy can be the simultaneous presence of genes corresponding to the HPV L1 protein DNA region, as well as genes of the human β-globin locus, since the human β-globin gene cluster is expressed by cervical carcinoma cells;[10]

(iv) erythrocytes carry extracellular vesicles on their surface,[32] some of which are represented by exosomes[33] including, in our opinion, tumor exosomes, and it is possible that DNA of tumor exosomes contains genes corresponding to the HPV L1 protein DNA region and genes of the human β-globin locus;

(v) erythrocytes are capable of carrying csbDNA[34] and, in our opinion, it is possible that erythrocytes are also capable of carrying csbDNA—RBC-bound ctDNA.

Our study has certain limitations. We do not exclude technical errors, so the study should be repeated. In future research, we should include in the study a larger number of patients, both with CC and cervical neoplasia, as well as healthy patients. We should also get, if possible, consent from patients for more of their medical information.

A review by ASCO and the College of American Pathologists analyzed information on clinical ctDNA assays and found no evidence for clinical utility and little evidence for clinical validity of ctDNA assays in cancer early detection, treatment monitoring, and detection of residual disease. There is also a lack of evidence for the clinical validity and clinical usefulness of ctDNA assays for cancer screening outside of clinical trials.[35] The authors emphasize that "Given the rapid pace of research, re-evaluation of the literature will shortly be required, along with the development of tools and guidance for clinical practice."[35]

We want to emphasize that this study was performed for the detection of CC at any stage. Our study and similar studies by other researchers are relevant, for example, for patients for whom it is important that the procedure for taking their samples for testing is psychologically comfortable.

For example, CC screening tends to induce psychological discomfort, since all patients experience anxiety before a gynecological examination,[36] while the level of anxiety during venipuncture is very low.[37] Patients can be expected to shy away somewhat less from tests that detect CC markers in the blood than from screening for CC.

We hope that the continuation of the study will allow us to create an affordable and easily reproducible method for detecting cfDNA, which can be a CC biomarker.

Acknowledgments

This study was supported by “The Fund of target capital management North-Eastern Federal University named after M. K. Ammosov.”

Competing Interests

The authors declare that they have no competing interests.

References

1. World Health Organization. 73rd World Health Assembly Decisions. Available from: https://www.who.int/news-room/feature-stories/detail/73rd-world-health-assembly-decisions
2. The World Bank. Available from: https://datahelpdesk.worldbank.org/knowledgebase/articles/906519
3. Kononova IV, Kirillina MP, Sofronova SI, Illarionova NA, Mamaeva SN, Arzhakova LI, et al. [Disparities of cervical cancer incidence and mortality in the republics located in Siberia and all over Russia in the period from 2007 to 2019]. Yakut Medical Journal. 2021;73(1):50-53. doi: 10.25789/YMJ.2021.73.14 [Article in Russian].
4. Liu K, Tong H, Li T, Chen Y, Mao X. Potential value of circulating tumor DNA in gynecological tumors. Am J Transl Res. 2020 Jul 15;12(7):3225-3233.
5. Pornthanakasem W, Shotelersuk K, Termrungruanglert W, Voravud N, Niruthisard S, Mutirangura A. Human

***Corresponding author:** Irina V. Kononova, PhD. Yakut Scientific Center of Complex Medical Problems, Yakutsk, Russia. E-mail: irinakon.07@mail.ru*

papillomavirus DNA in plasma of patients with cervical cancer. BMC Cancer. 2001;1:2. doi: 10.1186/1471-2407-1-2.
6. Oshiro C, Kagara N, Naoi Y, Shimoda M, Shimomura A, Maruyama N, Shimazu K, Kim SJ, Noguchi S. PIK3CA mutations in serum DNA are predictive of recurrence in primary breast cancer patients. Breast Cancer Res Treat. 2015 Apr;150(2):299-307. doi: 10.1007/s10549-015-3322-6.
7. Newman AM, Bratman SV, To J, Wynne JF, Eclov NC, Modlin LA, Liu CL, Neal JW, Wakelee HA, Merritt RE, Shrager JB, Loo BW Jr, Alizadeh AA, Diehn M. An ultrasensitive method for quantitating circulating tumor DNA with broad patient coverage. Nat Med. 2014 May;20(5):548-54. doi: 10.1038/nm.3519.
8. Bettegowda C, Sausen M, Leary RJ, Kinde I, Wang Y, Agrawal N, Bartlett BR, Wang H, Luber B, Alani RM, Antonarakis ES, Azad NS, Bardelli A, Brem H, Cameron JL, Lee CC, Fecher LA, Gallia GL, Gibbs P, Le D, Giuntoli RL, Goggins M, Hogarty MD, Holdhoff M, Hong SM, Jiao Y, Juhl HH, Kim JJ, Siravegna G, Laheru DA, Lauricella C, Lim M, Lipson EJ, Marie SK, Netto GJ, Oliner KS, Olivi A, Olsson L, Riggins GJ, Sartore-Bianchi A, Schmidt K, Shih lM, Oba-Shinjo SM, Siena S, Theodorescu D, Tie J, Harkins TT, Veronese S, Wang TL, Weingart JD, Wolfgang CL, Wood LD, Xing D, Hruban RH, Wu J, Allen PJ, Schmidt CM, Choti MA, Velculescu VE, Kinzler KW, Vogelstein B, Papadopoulos N, Diaz LA Jr. Detection of circulating tumor DNA in early- and late-stage human malignancies. Sci Transl Med. 2014 Feb 19;6(224):224ra24. doi: 10.1126/scitranslmed.3007094.
9. Gu Y, Wan C, Qiu J, Cui Y, Jiang T, Zhuang Z. Circulating HPV cDNA in the blood as a reliable biomarker for cervical cancer: A meta-analysis. PLoS One. 2020 Feb 6;15(2):e0224001. doi: 10.1371/journal.pone.0224001.
10. Li X, Wu Z, Wang Y, Mei Q, Fu X, Han W. Characterization of adult α- and β-globin elevated by hydrogen peroxide in cervical cancer cells that play a cytoprotective role against oxidative insults. PLoS One. 2013;8(1):e54342. doi: 10.1371/journal.pone.0054342.
11. Schwarzenbach H, Hoon DS, Pantel K. Cell-free nucleic acids as biomarkers in cancer patients. Nat Rev Cancer. 2011 Jun;11(6):426-37. doi: 10.1038/nrc3066.
12. Kamat AA, Sood AK, Dang D, Gershenson DM, Simpson JL, Bischoff FZ. Quantification of total plasma cell-free DNA in ovarian cancer using real-time PCR. Ann N Y Acad Sci. 2006 Sep;1075:230-4. doi: 10.1196/annals.1368.031.
13. NanoPhotometer® P-Class User Manual P 300 / P 330 / P 360. Available from: https://www.implen.de/wp-content/uploads/2015/04/NanoPhotometer-P-Class-User-Manual-2.1.pdf
14. Evrogen. Available from: https://evrogen.ru/kit-user-manuals/qPCRmix-HS-SYBR-LowROX_PK156.pdf [in Russian]
15. Quellhorst G, Rulli S. A systematic guideline for developing the best real-time PCR primers. Lessons learned from designing assays for more than 14,000 genes. Qiagen. 2012;1–9. Available from: file:///C:/Users/Admin/Downloads/1073958_A_systematic_guideline_for_developing_the_best_real-time_PCR_primers.pdf
16. Mazurek AM, Fiszer-Kierzkowska A, Rutkowski T, Składowski K, Pierzyna M, Sciegliński D, Woźniak G, Głowacki G, Kawczyński R, Małusecka E. Optimization of circulating cell-free DNA recovery for KRAS mutation and HPV detection in plasma. Cancer Biomark. 2013;13(5):385-94. doi: 10.3233/CBM-130371.
17. Takakura M, Matsumoto T, Nakamura M, Mizumoto Y, Myojyo S, Yamazaki R, Iwadare J, Bono Y, Orisaka S, Obata T, Iizuka T, Kagami K, Nakayama K, Hayakawa H, Sakurai F, Mizuguchi H, Urata Y, Fujiwara T, Kyo S, Sasagawa T, Fujiwara H. Detection of circulating tumor cells in cervical cancer using a conditionally replicative adenovirus targeting telomerase-positive cells. Cancer Sci. 2018 Jan;109(1):231-240. doi: 10.1111/cas.13449.
18. Yim EK, Park JS. The role of HPV E6 and E7 oncoproteins in HPV-associated cervical carcinogenesis. Cancer Res Treat. 2005 Dec;37(6):319-24. doi: 10.4143/crt.2005.37.6.319.
19. IARC Working Group on the Evaluation of Carcinogenic Risks to Humans. Human papillomaviruses. IARC Monogr Eval Carcinog Risks Hum. 2007;90:1-636.
20. Rungkamoltip P, Temisak S, Piboonprai K, Japrung D, Thangsunan P, Chanpanitkitchot S, Chaowawanit W, Chandeying N, Tangjitgamol S, Iempridee T. Rapid and ultrasensitive detection of circulating human papillomavirus E7 cell-free DNA as a cervical cancer biomarker. Exp Biol Med (Maywood). 2021 Mar;246(6):654-666. doi: 10.1177/1535370220978899.
21. Jeannot E, Becette V, Campitelli M, Calméjane MA, Lappartient E, Ruff E, Saada S, Holmes A, Bellet D, Sastre-Garau X. Circulating human papillomavirus DNA detected using droplet digital PCR in the serum of patients diagnosed with early stage human papillomavirus-associated invasive carcinoma. J Pathol Clin Res. 2016 Jun 28;2(4):201-209. doi: 10.1002/cjp2.47.
22. Campitelli M, Jeannot E, Peter M, Lappartient E, Saada S, de la Rochefordière A, Fourchotte V, Alran S, Petrow P, Cottu P, Pierga JY, Lantz O, Couturier J, Sastre-Garau X. Human papillomavirus mutational insertion: specific marker of circulating tumor DNA in cervical cancer patients. PLoS One. 2012;7(8):e43393. doi: 10.1371/journal.pone.0043393.
23. Jeannot E, Latouche A, Bonneau C, Calméjane MA, Beaufort C, Ruigrok-Ritstier K, Bataillon G, Larbi Chérif L, Dupain C, Lecerf C, Popovic M, de la Rochefordière A, Lecuru F, Fourchotte V, Jordanova ES, von der Leyen H, Tran-Perennou C, Legrier ME, Dureau S, Raizonville L, Bello Roufai D, Le Tourneau C, Bièche I, Rouzier R, Berns EMJJ, Kamal M, Scholl S. Circulating HPV DNA as a Marker for Early Detection of Relapse in Patients with Cervical Cancer. Clin Cancer Res. 2021 Nov 1;27(21):5869-5877. doi: 10.1158/1078-0432.CCR-21-0625.
24. Buck CB, Day PM, Trus BL. The papillomavirus major capsid protein L1. Virology. 2013 Oct;445(1-2):169-74. doi: 10.1016/j.virol.2013.05.038.
25. Chen AC, Keleher A, Kedda MA, Spurdle AB, McMillan NA, Antonsson A. Human papillomavirus DNA detected in peripheral blood samples from healthy Australian male blood donors. J Med Virol. 2009 Oct;81(10):1792-6. doi: 10.1002/jmv.21592.
26. Cao H, Banh A, Kwok S, Shi X, Wu S, Krakow T, Khong B, Bavan B, Bala R, Pinsky BA, Colevas D, Pourmand N, Koong AC, Kong CS, Le QT. Quantitation of human papillomavirus DNA in plasma of oropharyngeal carcinoma patients. Int J Radiat Oncol Biol Phys. 2012 Mar 1;82(3):e351-8. doi: 10.1016/j.ijrobp.2011.05.061.
27. Cocuzza CE, Martinelli M, Sina F, Piana A, Sotgiu G, Dell'Anna T, Musumeci R. Human papillomavirus DNA detection in plasma and cervical samples of women with a recent history of low grade or precancerous cervical dysplasia. PLoS One. 2017 Nov 28;12(11):e0188592.

28. Graham SV. The human papillomavirus replication cycle, and its links to cancer progression: a comprehensive review. Clin Sci (Lond). 2017 Aug 10;131(17):2201-2221. doi: 10.1042/CS20160786.
29. Middleton K, Peh W, Southern S, Griffin H, Sotlar K, Nakahara T, El-Sherif A, Morris L, Seth R, Hibma M, Jenkins D, Lambert P, Coleman N, Doorbar J. Organization of human papillomavirus productive cycle during neoplastic progression provides a basis for selection of diagnostic markers. J Virol. 2003 Oct;77(19):10186-201. doi: 10.1128/jvi.77.19.10186-10201.2003.
30. Roden RB, Hubbert NL, Kirnbauer R, Breitburd F, Lowy DR, Schiller JT. Papillomavirus L1 capsids agglutinate mouse erythrocytes through a proteinaceous receptor. J Virol. 1995 Aug;69(8):5147-51. doi: 10.1128/JVI.69.8.5147-5151.1995.
31. Vogt AM, Winter G, Wahlgren M, Spillmann D. Heparan sulphate identified on human erythrocytes: a Plasmodium falciparum receptor. Biochem J. 2004 Aug 1;381(Pt 3):593-7. doi: 10.1042/BJ20040762.
32. Mamaeva SN, Kononova IV, Alekseev VA, Nikolaeva NA, Pavlov AN, Semenova MN, et al. Determination of Blood Parameters using Scanning Electron Microscopy as a Prototype Model for Evaluating the Effectiveness of Radiation Therapy for Cervical Cancer. International Journal of Biomedicine. 2021;11(1):32-38. doi:10.21103/Article11(1)_OA6
33. Doyle LM, Wang MZ. Overview of Extracellular Vesicles, Their Origin, Composition, Purpose, and Methods for Exosome Isolation and Analysis. Cells. 2019 Jul 15;8(7):727. doi: 10.3390/cells8070727.
34. Tamkovich S, Laktionov P. Cell-surface-bound circulating DNA in the blood: Biology and clinical application. IUBMB Life. 2019 Sep;71(9):1201-1210. doi: 10.1002/iub.2070.
35. Merker JD, Oxnard GR, Compton C, Diehn M, Hurley P, Lazar AJ, Lindeman N, Lockwood CM, Rai AJ, Schilsky RL, Tsimberidou AM, Vasalos P, Billman BL, Oliver TK, Bruinooge SS, Hayes DF, Turner NC. Circulating Tumor DNA Analysis in Patients With Cancer: American Society of Clinical Oncology and College of American Pathologists Joint Review. J Clin Oncol. 2018 Jun 1;36(16):1631-1641. doi: 10.1200/JCO.2017.76.8671.
36. Yilmaz FT, Demirel G. The relationship between body privacy and anxiety in women having gynecological examination. J Obstet Gynaecol. 2021 Oct;41(7):1112-1115. doi: 10.1080/01443615.2020.1835845.
37. Deacon B, Abramowitz J. Fear of needles and vasovagal reactions among phlebotomy patients. J Anxiety Disord. 2006;20(7):946-60. doi: 10.1016/j.janxdis.2006.01.004.

International Journal of Biomedicine 12(1) (2022) 115-119
http://dx.doi.org/10.21103/Article12(1)_OA11

ORIGINAL ARTICLE

Radiology

INTERNATIONAL JOURNAL OF BIOMEDICINE

Assessment of Radiation Exposure and Attributed Risk During Chest, Abdominal and Pelvic Computed Tomography Procedures

Essam H. Mattar

Department of Radiological Sciences, College of Applied Medical Sciences, King Saud University Riyadh, Saudi Arabia

Abstract

Adult patients' exposure and ascribed cancer risk were calculated using CT-Expo dosimetry software. A total of eight CT scanners and 395 examination patients were used in the study. The predicted effective dose values for chest CT, abdominal CT, and pelvic CT were 8.0 mSv, 10.9 mSv, and 5.6 mSv, respectively. The estimated dose–length product to effective dose (ICRP 103) conversion coefficients for chest CT, abdominal CT, and pelvic CT were 0.020 $mSv \cdot mGy^{-1}$, 0.016 $mSv \cdot mGy^{-1}$, and 0.013 $mSv \cdot mGy^{-1}$, respectively. In chest CT, organ doses were 16.6 mSv (lung), 14.9 mSv (esophagus), and 10.8 mSv (breast); in abdominal CT: 15.5 mSv (stomach) and 13.7 mSv (liver); and in pelvic CT: 17.9 mSv (bladder) and 11.3 mSv (colon). The estimated cancer incident cases per million were 168 for lung cancer (chest CT) and 103 for stomach cancer (abdominal CT). The study allows comparing the risk of CT examinations to those of other radiological procedures.(**International Journal of Biomedicine. 2022;12(1):115-119.**)

Key Words: computed tomography • organ-equivalent doses • effective doses • cancer risk • radiation protection

For citation: Mattar EH. Assessment of Radiation Exposure and Attributed Risk During Chest, Abdominal and Pelvic Computed Tomography Procedures.. International Journal of Biomedicine. 2022;12(1):115-119. doi:10.21103/Article12(1)_OA11

Introduction

Because computed tomography (CT) is the major contribution to patient radiation exposure in diagnostic radiology, it merits special consideration. The frequency of CT examinations is expanding worldwide, owing to technical developments that have contributed to the clear benefit supplied to the tested persons. The number of different types of CT tests is likewise growing. Increasing concerns regarding the growing population's exposure to radiation are correlated to its increasing use.[1-3] The amount of radiation used in CT scans is a significant source of worry for the medical imaging community. As a result, physicians must have realistic instruments to allow for the console-displayed dose (i.e., dose length product $P_{KL,CT}$), which can be converted into a radiation protection, risk-related dose quantity that is understandable to the medical imaging community. Practitioners who are aware of radiation dangers are more likely to take the necessary precautions to keep all patient exposures as low as reasonably possible, especially in CT and other high-dose imaging modalities.[4] Radiation risk in CT and other ionizing radiation-based diagnostic methods can be calculated using two radiation protection quantities: organ dose and effective dose. The effective dose accounts for the radiosensitivity of different body organs and tissues, whereas the body organ dose considers the relative biological effectiveness (RBE) of different radiation types.[5] A significant amount of work has been done in CT dosimetry in the last few years.[2,6] To optimize and create national diagnostic reference levels, doses were expressed in terms of the CT air kerma index and the CT dose–length product. Estimates of radiation protection risk-related variables (organ and effective doses) and ascribed cancer risk have recently received attention.[7] The current investigation was undertaken as part of these attempts to quantify organ doses, effective doses, and associated cancer risk following adult CT scans. For the first time, body organ doses are reported, adding to the national databank on radiation exposure. Because effective dose values and radiation risk incidents in CT are assessed using tissue-weighting factors from the International Commission on Radiological Protection (ICRP) Report 103, the findings of this study are critical for updating effective dose values and radiation risk incidents in CT.[2,5]

***Corresponding Author**: Dr. Essam H. Mattar. Department of Radiological Sciences, College of Applied Medical Sciences, King Saud University, Riyadh, Saudi Arabia. E-mail:emattar@ksu.edu.sa*

Materials and Methods

Survey of the ionizing radiation dose

In this investigation, organ and effective doses were computed for 395 patient examinations in eight hospitals using CT-Expo CT dosimetry software version 2.5.[8] To evaluate radiation protection risk-related variables, such as the organ-equivalent dose and effective dose (E), patient doses were calculated using the volume CT air kerma index (C_{vol} (mGy) and CT air kerma length product ($P_{KL,CT}$).[9-11]

CT dose descriptors

For a multislice scanner with N_i and slice thickness T_i, C_K, the CT air kerma index in-phantom for an integration length of 100 mm, $C_{K,PMMA,100}$, is defined as follows: [10,11]

$$C_{k,PMMA,100} = \int_{-50}^{+50} \frac{K_{a,PMMA}(Z)dZ}{N_i T_i}$$

In clinical applications, an ionization chamber (pencil-type) with an active length of 10 cm, placed along the CT machine's axis of rotation, with its center at the center of the scanning plane, can be utilized to generate a reasonable assessment of $C_{K,PMMA,100}$. $C_{K,PMMA,100}$ is derived from the expression:

$$C_{K,PMMA,100} = \frac{DL}{T} \text{ [mGy],}$$

in which D is the radiation dose measured by the ionisation chamber and L is the sensitive length of the chamber (in this case, 100 cm).

The measurement can be performed either free-in-air (Cair) or in the center (C100,c) and periphery (C100,p) of a typical head or body CT dosimetry phantom.[9] The average dose (in the air) can be described by the weighted C:D ratio, assuming that the dose decays exponentially with radial position from the top to the middle of the phantom:

$$C_w = C_{K,PMMA,w} = \frac{1}{3} \cdot C_{K,PMMA,100,c} + \frac{2}{3} \cdot C_{K,PMMA,100,p}$$

Organ and effective doses and risk estimates

In addition to the main CT radiation dose units (C_{vol} and $P_{KL,CT}$), the software is capable of quantifying the organ-equivalent and effective radiation doses (mSv) in accordance with the recent ICRP recommendations. Effective doses were calculated using: (1) tissue-weighting factors given in ICRP-60; and (2) tissue-weighting factors given in ICRP-103. The ratios of the effective doses (E103/E60) and conversion coefficients (E103/$P_{KL,CT}$) are also provided. Detailed descriptions of the dose survey, including presentation of the common patient dose descriptors, are presented in our previous publication.[2] Organ-equivalent doses are used to calculate attributed cancer risk incidence using the cancer incidence risk coefficient given in ICRP-103[5]:

$$Risk\ Index = \sum_T r_T H_T$$

Results

This study contained a total of eight CT machines: two 16-slice CT machines, five dual-slice CT machines, and one single-slice CT machine. The diversity of manufacturers and types, as well as the year of installation and the measured CT air kerma index, are summarized in Table 1. Dose estimates were produced for 395 patients who had a routine chest, abdomen, or pelvic CT scan. Doses were computed using CT-Expo software and patient scan information obtained during a countrywide exposure survey conducted throughout the country.

Table 2 presents the mean scan parameter, CT dose descriptors (C_{vol} and $P_{KL,CT}$). The effective doses for chest, abdomen, and pelvic CT have been determined. The tissue-weighting factor described in ICRP publication 60 (E60) and ICRP publication 103 was used to derive the effective doses shown here (E103). An increase in the breast tissue-weighting factor from 0.05 to 0.12 and a reduction in the gonad tissue-weighting factor from 0.2 to 0.08 are significant modifications from the preceding tissue-weighting factors described in ICRP Guideline 60 (ICRP, 1991). (ICRP, 2007). Changes in risk estimates from E60 to E103 were normalized to E60 to demonstrate changes in risk estimates due to changes in the tissue-weighting factor, which represents the effective dose.

Conversely, the conversion coefficients (E103/$P_{KL,CT}$) were also determined; these were used to convert the values of the console-displayed $P_{KL,CT}$ into a corresponding effective dose.

Table 2 shows that abdominal CT had the highest effective dosage (10.9 mSv), followed by chest CT (8.0 mSv), and pelvic CT (5.7 mSv). CT scans of certain bodily regions have a longer scan length, which allows them to cover the majority of radiosensitive organs. Physicians may ask that chest–abdomen or abdomen–pelvis tests be performed as a single operation, resulting in greater extended scan coverage, high total mAs, and consequently increased radiation dosage to the patient, depending on the physicians' explanations.

Table 3 presents a comparison of the E103/$P_{KL,CT}$(μSv/mGy.cm) coefficients and the E103/E60 ratios obtained in this study with those from the literature. The E103/E60 ratios are below unity for the abdomen (0.85) and pelvis (0.76), but above unity for the chest, which is expected due to the increased tissue weighting of certain organs in ICRP 103.[5]

In Figure 1, the mean organ-equivalent doses are presented in chest, abdominal, and pelvic CT. In chest CT, the lung (16.6 mSv) presented with the highest dose, followed by the esophagus (14.9 mSv) and the breast (10.8 mSv). In abdominal CT, organ-equivalent doses as high as 20.7mSv (urinary bladder) and 15.5 mSv (stomach) are presented. With respect to pelvic CT, the colon (5.6 mSv) presents the highest organ dose, followed by the gonads (7.2 mSv). Radiation doses to the gonads serve as indicators for possible cancer risk in the offspring of exposed individuals.

Table 4 shows the cancer risk estimates for adult patients that were computed using the sex-averaged, organ-specific cancer risk coefficients given in E103. Projected risk incidence rates as high as 168 per million people are presented for lung cancer (chest CT), whereas the incidence rate is as high as 102 per million people among those with stomach cancer (abdominal CT).

Table 1.

Summary of characteristic performance parameters for the CT systems used for dose calculation

Scanner Code	Made	Type	Number of detectors	U_{ref}(kV)	Brain mode		Trunk mode	
					${}_nC_{w,}$ (mGy/mAs)	P_H	${}_nC_{w,}$(mGy/mAs)	P_B
GE I	GE	CT/e	1	120	0.160	0.70	0.072	0.32
GE II		CTe dual	2	120	0.154	0.71	0.154	0.71
GE III		High Speed Nx/i	2	120	0.151	0.63	0.072	0.30
S I	Siemens	Emotion Duo	2	130	0.215	0.71	0.215	0.71
S II		Sensation 16	16	120	0.184	0.76	0.131	0.77
S II		Sensation 16	16	120	0.184	0.76	0.131	0.77
T I	Toshiba	Steion dual	2	120	0.293	0.65	0.149	0.32
T II		Steion TSX	2	120	0.067	0.30	0.135	0.61

P_H: Scanner-specific (C_w/C_{air}) ratio for the head (16 cm) CT dosimetry phantom.

P_B: Scanner-specific (C_w/C_{air}) ratio for the body (32 cm) CT dosimetry phantom.

Table 2.

CT scan parameters, dose indices, and conversion coefficients

Scanner	N	Scan parameters			CT Doses	Effective Dose (mSv)			E103/$P_{KL,CT}$ (mSv/mGy.cm)
		mAs	L (cm)	C_{vol}(mGy)	$P_{KL,CT}$ (mGy.cm)	ICRP 60	ICRP 103	E103/E60	
Chest CT									
GII	5	63	15	2.9	61.2	1.1	1.2	1.08	0.020
GIII	11	131	25	9	237.9	4.3	5.0	1.12	0.021
SI	9	83	46	5.1	94.1	1.7	1.9	1.10	0.020
SII	9	105	40	9	410.2	6.5	8.0	1.23	0.020
SIII	16	41	28	3.1	98.1	1.6	1.9	1.12	0.019
TI	5	210	24	31.7	1123	24.0	22.0	1.17	0.022
TII	18	150	33	18.5	799.7	14.1	16	1.13	0.020
Average	10.4	111.9	30.1	11.3	403.5	7.61	8.00	1.14	0.020
Abdominal CT									
GI	22	102	29	4.9	164.4	2.9	2.4	0.79	0.015
GIII	19	119	20	15.9	286.7	5.3	3.8	0.72	0.013
SI	32	63	36	5.0	195.2	3.3	2.9	0.88	0.015
SII	22	73	43	6.1	270.5	4.9	4.3	0.87	0.016
SIII	21	60	38	9.3	516.7	9.4	8.9	0.94	0.017
TI	10	253	38	51.6	2309	42	36	0.84	0.016
TII	20	150	42	20.1	1012.6	20	18	0.90	0.018
Average	20.9	117.1	35.1	16.1	679.3	12.54	10.90	0.85	0.016
Pelvic CT									
GIII	10	104	12	10.4	229.3	4.0	3.0	0.77	0.013
SI	10	28	22	2.7	72.3	1.2	0.9	0.75	0.012
TII	12	200	24	25.8	902.4	17.2	12.8	0.75	0.014
Average	10.7	110.7	19.3	13.0	401.3	7.47	5.57	0.76	0.013

E103 refers to the effective dose calculated according to the recommendation of the ICRP 103.

E60 refers to the effective dose calculated according to the recommendation of the ICRP 60.

Table 3.

Comparison of E103/E60 (μSv/mGy cm) coefficients and (E103/E60) ratios (mSv/mSv) obtained in this study and the presented data

Study		Chest (32 cm)	Abdomen (32 cm)	Pelvis (32 cm)
This study (2016)	E103/ $P_{KL,CT}$	20.4	16.0	13
	E103/E60	1.14	0.85	0.76
	Scan length (cm)	30.1	35.1	19.3
Deak et al. (2010)	E103/ $P_{KL,CT}$	14.5	15.3	12.9
	E103/E60	1.07	0.99	0.77
	Scan length (cm)	22.6	20.2	21.1
Huda et al. (2011)	E103/ $P_{KL,CT}$	20.4	16.3	14.3
	E103/E60	1.20	1.02	0.75
	Scan length (cm)	35	24	20

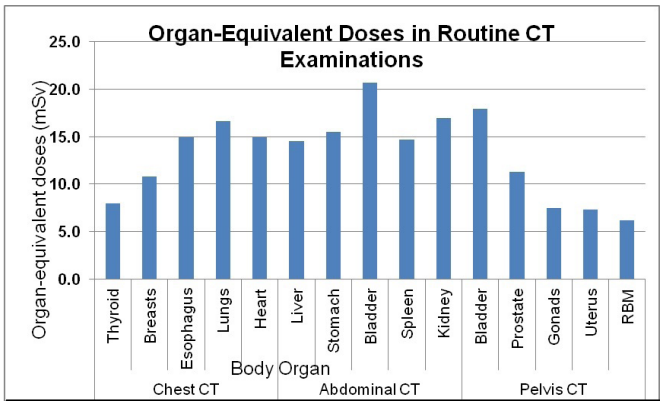

Fig. 1. *Mean organ-equivalent doses in chest, abdominal, and pelvic CT.*

Table 4.

Cancer risk estimates for adult patients during CT exams

Organs	Organ doses (mSv)	Nominal risk coefficients (cases per 10,000 persons per Sv)		Radiation-induced cancerprobability per 10^6	
		Non-Fatal	Fatal	Non-Fatal	Fatal
Esophagus	14.9	14.0	1.1	21	2
Stomach	15.5	65.5	3.5	102	5
Colon	11.3	31.3	34.2	35	39
Liver	13.7	28.9	1.4	40	2
Lung	16.6	101.5	12.6	168	21
Breast	10.8	33.0	79.1	36	85
Ovary	5.7	6.0	4.6	3	3
Bladder	17.9	12	31	21	55
Thyroid	8.0	2.2	30.3	2	24
Bone Marrow	6.2	28.0	13.9	17	9
Gonads (Heritable)	7.5	16	4.0	12	3

Discussion

Doses were determined for patients undergoing CT procedures of the chest, abdomen, and pelvis. Head CT was excluded due to large inaccuracies in determining the organs included in the scan; there was also a great deal of uncertainty when determining organ and effective doses.

Computing the effective dose is of paramount importance, as it provides a common measure by which to compare exposure in different radiological procedures, as well that from natural background radiation.[12] The annual dose limit for occupational exposure, the yearly dose limit for public exposure(1 mSv), and the annual effective dose from natural background radiation (2.4 mSv) can all be compared to the effective dose in body CT exams.[1,5]

The E103/E60 ratios obtained in this study for chest (1.18) and pelvic (0.76) CT are not much different from those reported by Huda and He,(13) who presented with ratios of 1.20 (chest CT) and 0.75 (pelvic CT), and these are very similar to the results reported by Deak et al.[14] Both results showed an E103/E60 ratio below unity for abdominal CT. It is crucial to report that the current results are averaged over eight scanners, as compared to the one scanner that was used in the study by Huda and He,[13] and the two scanners that were employed in the study by Deak et al.[14] The average conversion factor (E103/E60) per CT procedure could be used to attain a reasonable estimation of effective doses from previous studies, which were calculated using ICRP 60. In Tanzania, Ngaile and Msaki [15] found that the mean organ doses for the lens of the eyes (for head), the thyroid (chest CT), breast(chest CT), stomach(abdominal CT), and gonads (for pelvis) were 63.9 mGy, 12.3 mGy, 26.1 mGy, 35.6 mGy, and 24.0 mGy, respectively. When compared to the results of this study, the organ doses reported in Tanzania are much higher. This may be primarily attributed to the old scanner model used in Tanzania. All scanners were single-slice, as compared to the 4- and 16-multislice CT scanner used in this study.

Projected risk incidents as high as 168 per million people are presented for lung cancer during chest CT (Table 3). These values are much higher than the cancer incidence rate previously reported for multiple-radiograph intravenous urography.[7] In a study by Andrade et al.,[16] the effective attributed cancer risk per million during chest CT ranged from 203–330, whereas in abdominal CT, this rate ranged from 113–270 per million. The current values are lower than those previously reported by Andrade et al.[16] Those authors presented the effective average attributed cancer risk in a given bodily region (chest/abdomen), whereas in our study, attributed cancer risks were computed for each body organ of interest. Attributed cancer risk determines which organ-equivalent doses are more appropriate, as their incidence rates depend upon which organ is irradiated; that organ is thus added to the individual's organ sensitivity.[5,17-24]

Variations in organ-equivalent dose indicate that dose reduction can be achieved without jeopardizing the quality of diagnostic information. High doses were mainly due to using the same protocol for all patients regardless of their sizes (Scanner SIII), as well as using inappropriate technique factors, primarily including higher mAs than necessary(TI scanner). Dose optimization using various technique factors involved

decreasing mAs, using tube-current modulation where possible, and limiting scan coverage.[2,17,18,25,26] Shielding radioprotective organs during CT procedures may better mitigate the health consequences of ionizing radiation.

Conclusion

The effective radiation dose is a useful metric for comparing exposure during various radiological treatments, whereas organ doses are better for predicting cancer induction. The input of estimated dosages to the national patient exposure databank is critical. They allow for a comparison of the risks associated with CT scans to those associated with other radiological techniques. The conversion of the dose length product to effective dose conversion coefficients gives radiologists operating without medical physics support with an accessible and user-friendly method for determining CT-effective doses. The most recent ICRP was used to calculate current effective dosage values.

Competing interests

The author declares that there is no conflict of interest.

Acknowledgments

The author extends his appreciation to the College of Applied Medical Sciences Research Centre and Deanship of Scientific Research at King Saud University for funding this project.

References

1. Sources and Effects of Ionizing Radiation. UNSCEAR 2008. Report to the General Assembly with Scientific Annexes. UNITED NATIONS. New York, 2010.
2. Suliman II, Abdalla SE, Ahmed NA, Galal MA, Salih I. Survey of computed tomography technique and radiation dose in Sudanese hospitals. Eur J Radiol. 2011 Dec;80(3):e544-51.
3. Vassileva J, Rehani MM, Applegate K, Ahmed NA, Al-Dhuhli H, Al-Naemi HM, et al. IAEA survey of paediatric computed tomography practice in 40 countries in Asia, Europe, Latin America and Africa: procedures and protocols. Eur Radiol. 2013 Mar;23(3):623-31. doi: 10.1007/s00330-012-2639-3.
4. Oikarinen H, Meriläinen S, Pääkkö E, Karttunen A, Nieminen MT, Tervonen O. Unjustified CT examinations in young patients. Eur Radiol. 2009 May;19(5):1161-5. doi: 10.1007/s00330-008-1256-7.
5. The 2007 Recommendations of the International Commission on Radiological Protection. ICRP publication 103. Ann ICRP. 2007;37(2-4):1-332. doi: 10.1016/j.icrp.2007.10.003.
6. Suliman II, Khamis HM, Ombada TH, Alzimami K, Alkhorayef M, Sulieman A. Radiation exposure during paediatric CT in Sudan: CT dose, organ and effective doses. Radiat Prot Dosimetry. 2015 Dec;167(4):513-8. doi: 10.1093/rpd/ncu321.
7. Suliman II, Al-Jabri AJ, Badawi AA, Halato MA, Alzimami K, Sulieman A. Radiation dose and cancer risk in patients undergoing multiple radiographs in intravenous urography X-ray examinations. Radiat Phys Chem. 2014;104:272-5.
8. Stamm G, Nagel HD. CT-Expo - ein neuartiges Programm zur Dosisevaluierung in der CT [CT-expo--a novel program for dose evaluation in CT]. Rofo. 2002 Dec;174(12):1570-6. doi: 10.1055/s-2002-35937. [Article in German]..
9. CEC (Commission for European Community). European Guidelines on quality criteria for diagnostic radiographic images. EUR 16260 EN. Luxembourg: Office for Official Publication of the European Community, 1996.
10. ICRU – REPORT 74. Patient Dosimetry for X-rays used in Medical Imaging. ICRU, 2006. (Bethesda, MD, USA).
11. IAEA. Dosimetry in Diagnostic Radiology: An International Code of Practice. IAEA TRS. No 457, IAEA, Vienna. 2007.
12. Brenner D, Huda W. Effective dose: a useful concept in diagnostic radiology. Radiat Prot Dosimetry. 2008;128(4):503-8. doi: 10.1093/rpd/ncn056.
13. Huda W, He W. Estimating cancer risks to adults undergoing body CT examinations. Radiat Prot Dosimetry. 2012 Jun;150(2):168-79. doi: 10.1093/rpd/ncr376.
14. Deak PD, Smal Y, Kalender WA. Multisection CT protocols: sex- and age-specific conversion factors used to determine effective dose from dose-length product. Radiology. 2010 Oct;257(1):158-66. doi: 10.1148/radiol.10100047.
15. Ngaile JE, Msaki PK. Estimation of patient organ doses from CT examinations in Tanzania. J Appl Clin Med Phys. 2006 Aug 24;7(3):80-94. doi: 10.1120/jacmp.v7i3.2200.
16. Andrade ME, Borrás C, Khoury HJ, Dias SK, Barros VS. Organ doses and risks of computed tomography examinations in Recife, Brazil. J Radiol Prot. 2012 Sep;32(3):251-60. doi: 10.1088/0952-4746/32/3/251.
17. Sulieman A, Adam H, Elnour A, Tamam N, Alhaili A, Alkhorayef M, et al. Patient radiation dose reduction using a commercial iterative reconstruction technique package. Radiat Phys Chem. 2021;178:1-7.
18. Saeed MK, Tamam N, Sulieman A. Assessment of dose reduction and influence of gantry rotation time in CT abdomen examination. Int J Radiat Res. 2021;19(1): 223-230.
19. Manssor E, Abuderman A, Osman S, Alenezi SB, Almehemeid S, Babikir E, et al. Radiation doses in chest, abdomen and pelvis CT procedures. Radiat Prot Dosimetry. 2015 Jul;165(1-4):194-8. doi: 10.1093/rpd/ncv107.
20. Alzimami K, Sulieman A, Omer E, Suliman II, Alsafi K. Effective dose estimation during conventional and CT urography. Radiat. Phys Chem. 2014;104:154-157.
21. Sulieman A, Elzaki M, Kappas C, Theodorou K. Radiation dose measurement in gastrointestinal studies. Radiat Prot Dosimetry. 2011 Sep;147(1-2):118-21. doi: 10.1093/rpd/ncr277.
22. Sulieman A, Mahmoud MZ, Serhan O, Alonazi B, Alkhorayef M, Alzimami K, Bradley D. CT examination effective doses in Saudi Arabia. Appl Radiat Isot. 2018 Nov;141:261-265. doi: 10.1016/j.apradiso.2018.07.011.
23. Geso M, Alghamdi SS, Tajaldeen A, Aljondi R, Alghamdi H, Zailae A, et al. Modified Contrast-Detail Phantom for Determination of the CT Scanners Abilities for Low-Contrast Detection. Appl. Sci. 2021;11:6661.
24. Alsufayan M, Sulieman A, Moslem R, Asiri A, Alomary A, Alanazi BM, et al. Assessment of Imaging Protocol and Patients Radiation Exposure in Computed Tomography Colonography. Appl. Sci. 2021;11:4761.
25. Sulieman A, Vlychou M, Tsougos I, Theodorou K. Radiation doses to paediatric patients and comforters undergoing chest X rays. Radiat Prot Dosimetry. 2011 Sep;147(1-2):171-5. doi: 10.1093/rpd/ncr295.
26. Suliman II, Sulieman A, Mattar E. Radiation Protection Evaluations Following the Installations of Two Cardiovascular Digital X-ray Fluoroscopy Systems. Appl. Sci. 2021;11(20):9749. doi: 10.3390/app11209749

International Journal of Biomedicine 12(1) (2022) 120-123
http://dx.doi.org/10.21103/Article12(1)_OA12

ORIGINAL ARTICLE

Obstetrics and Gynecology

INTERNATIONAL JOURNAL OF BIOMEDICINE

Structure of Gynecological Diseases and Comorbidity in Women with HIV Infection and Reproductive Disorders

Olga Leshchenko[1*], PhD, ScD; Margarita Bazyaeva[2]; Elena Genich[1]; Albina Labygina[1], PhD; Leonid Sholokhov[1], PhD, ScD

[1]*Scientific Centre for Family Health and Human Reproduction Problems*
[2]*Irkutsk State Medical University*
Irkutsk, the Russian Federation

Abstract

Background: The increase in the number of HIV-infected women of fertile age, as well as their reproductive plans to have healthy children, was the reason for studying the features of reproductive health disorders and comorbid conditions in women with HIV infection.

Methods and Results: Women meeting the inclusion criteria were divided into two groups: Group 1 included 27 HIV-infected women (average age of 30.8±2.9 years) with reproductive disorders; Group 2 included 23 HIV-infected women (average age of 31.4±7.1 years) without reproductive disorders. In study groups, the main route of HIV transmission was sexual contact. When assigning women to a particular category (fertile or infertile), the WHO classification of fertility was used: fertile, presumably fertile, primarily infertile, secondarily infertile, women with unknown fertility. There was a statistically significant difference in the incidence of medical abortion in Group 1 [14(60.9%)] than in Group 2 [8(29.6%)] (P=0.026). There were no statistically significant differences in the incidence of chronic co-morbidities (ENT disorders, gastritis/duodenitis, pancreatitis, cystitis, viral hepatitis (B, C), papillomavirus infection) in Groups 1 and 2 (P>0.05). The incidence of pelvic inflammatory diseases was 2 times higher in Group 1 than in Group 2. No statistically significant differences in the incidence of uterine myoma, chronic cervicitis, chronic endometritis, vulvovaginal candidiasis,, and cervical dysplasia were found. A significant prevalence of chronic salpingo-oophoritis, secondary dysmenorrhea, secondary amenorrhea, opsomenorrhea, and secondary oligomenorrhea was detected significantly more frequently in Group 1 than in Group 2. The syndrome of hyperprolactinemia was also 2.6 times more frequent in Group 1 than in Group 2. Reproductive disorders in HIV-infected women were associated with a high incidence of STI combinations (trichomoniasis, gonorrhea, syphilis, chlamydia).

Conclusion: Early detection of menstrual dysfunctions, prevention of abortion and sexually transmitted diseases, and timely treatment of infertility, are essential for women living with HIV.(**International Journal of Biomedicine. 2022;12(1):120-123.**)

Key Words: fertility • infertility • HIV infection • comorbidity

For citation: Leshchenko O, Bazyaeva M, Genich E, Labygina A, Sholokhov L. Structure of Gynecological Diseases and Comorbidity in Women with HIV Infection and Reproductive Disorders. International Journal of Biomedicine. 2022;12(1):120-123. doi:10.21103/Article12(1)_OA12

Introduction

In recent years, the proportion of HIV-infected women has been increasing, and the role of sexual transmission is increasing, as well as the active involvement of women of reproductive age in the HIV epidemic.[1,2] HIV infection can reduce the fertility of women at any stage of the disease; menstrual cycle and ovulation disorders, decreased ovarian reserve and oocyte quality have been reported.[3,4] Hormonal disorders are an important link in the pathogenesis of many disorders, including reproductive,[5] and may also contribute to the more rapid development of acquired immunodeficiency syndrome (AIDS), so monitoring of this system provides additional information on opportunities and ways to prevent the progression of HIV infection, and improve the possibility of giving birth to a healthy child.[6,7] The increase in the number of HIV-infected women of fertile age, as well as their reproductive plans to have healthy children, was the reason for studying the features of reproductive health disorders and comorbid conditions in women with HIV infection.

Materials and Methods

We performed a cross-sectional study of 83 women of reproductive age with HIV stage 4B. Inclusion criteria were age 18-45; HIV infection stage 4B, diagnosed on the basis of epidemiological, clinical data and confirmed by detection of specific antibodies by ELISA and immune blotting to HIV type 1 proteins; signature of informed consent; regular sexual activity for a year in the absence of contraception. Exclusion criteria were anything that would place the individual at increased risk or preclude the individual's full compliance with or completion of the study; history of hysterectomy, bilateral oophorectomy; HIV-infected women with unknown fertility.

Women meeting the inclusion criteria were divided into two groups: Group 1 included 27 HIV-infected women (average age of 30.8±2.9 years) with reproductive disorders; Group 2 included 23 HIV-infected women (average age of 31.4±7.1 years) without reproductive disorders. In study groups, the main route of HIV transmission was sexual contact.

When assigning women to a particular category (fertile or infertile), the WHO classification of fertility was used: fertile (women who had a pregnancy during the current year), presumably fertile(women who had a history of pregnancy more than 1 year ago), primarily infertile(women who did not have a history of pregnancy, despite regular sexual contact during the year and provided that no contraceptive methods were used), secondarily infertile(infertile women with a history of pregnancy), women with unknown fertility(women with no history of pregnancy due to the use of contraceptive methods, and/or with irregular sexual contact).

All women answered a questionnaire survey (menarche, parity, live-births, abortions, missed abortions, use of hormonal or other contraceptives, gynecological operations) and underwent general clinical, gynecological, and laboratory-instrumental examination.

Blood samples (5 ml) were collected from the ulnar vein in standard vacuum tubes with EDTA in the morning after night fasting, taking into account the phases of the menstrual cycle or amenorrhea. The levels of prolactin, luteinizing hormone, follicle-stimulating hormone, testosterone, cortisol, 17-OH progesterone, estradiol, thyroid-stimulating hormone, free triiodothyronine, free thyroxine, progesterone, dehydroepiandrosterone sulfate, anti-müllerian hormone were assessed by competitive solid-phase enzyme immunoassay using test system "ALKOR-BIO" on a Cobos ELL immunoassay analyzer (USA).

The percentages and absolute counts of blood lymphocytes (CD3+ and CD4+ cells) were determined by the method of indirect immunofluorescence with monoclonal antibodies using the BD FACSCalibur flow cytometer (USA).

The diagnosis of HIV infection was made on the basis of epidemiological and clinical data and was confirmed by the detection of specific antibodies by ELISA and immune blotting for HIV type 1 protein.

Statistical analysis was performed using the Statistica 8.0 software package (Stat-Soft Inc., USA). The normality of the distribution of continuous variables was tested by a one-sample Kolmogorov-Smirnov test. Continuous variables with normal distribution were presented as the mean and standard error of the mean [SEM]. Means of 2 continuous normally distributed variables were compared by independent samples Student's t-test. Mann-Whitney U test was used to compare means of 2 groups of variables not normally distributed. The frequencies of categorical variables were compared using Pearson's chi-squared test or Fisher's exact test (2-tail), when appropriate. A value of $P<0.05$ was considered significant.

The study was approved by the Ethics Committee of the Scientific Center for Family Health and Human Reproduction Problems. Written informed consent was obtained from each participant.

Results and Discussion

Group 1 consisted of women with primary and secondary infertility. Group 2 consisted of fertile and presumably fertile women. The HIV status of women in both groups did not differ (Table 1).

Table1.

Characteristics of HIV status in women with reproductive disorders

Indicators	Group 1 n=23	Group 2 n=27	*P*-level
Mean duration of HIV infection	10.0±1.5	8.0±2.5	0.496
HAART	8(34.8%)	11(40.7%)	0.666
STI	18(78.3%)	24(88.9%)	0.307
Parenteral route of HIV transmission	5(21.7%)	3(11.1%)	0.444

In Groups 1 and 2, the mean duration of the HIV infection was 10±1.5 years and 8±2.5 years, respectively ($P>0.05$). Highly active antiretroviral therapy (HAART) was received by 35% of women in Group 1 and 40% women in Group 2. The main route of transmission was sexual in the 2 groups.

According to the active detection of infertility in the Irkutsk region, the proportion of infertile women in a healthy population was 19.56±1.1%, primary infertility - 32.5±0.7%, secondary infertility - 67.5±0.7%.[8] Comparing the data obtained in our study, the fertility status of HIV-infected women is characterized by a low level.

In a study by Zaba et al.,[9] fertility of HIV-positive women was lower than that of HIV-negative women in all except the youngest age group. This controversial observation has been attributed to earlier sexual activity in this patient group. Comparison with the general female population showed that fertility in HIV-infected women was 40% lower than in uninfected controls. Decreased fertility rates in HIV-infected women have been described in the United States in more recent studies.[10-12] Kushnir et al.[3] concluded that psychosocial factors, in addition to biological alterations in reproductive physiology, might affect reproductive desires in HIV-infected patients.

In our study, a parity analysis of HIV-infected women in Group 1 revealed the following: anamnesis births in 56% (in women with secondary infertility), pregnancy failure in 17%, medical abortion in 61%, ectopic pregnancy in 8%, complications after medical abortion and delivery in 25%, primary infertility in 43%, secondary infertility in 57%. There was a statistically significant difference in the incidence of medical abortion in Group 1 [14(60.9%)] than in Group 2 [8(29.6%)] (P=0.026).

Comorbid conditions in HIV-infected women are presented in Table 2. There were no statistically significant differences in the incidence of chronic co-morbidities (ENT disorders, gastritis/duodenitis, pancreatitis, cystitis, viral hepatitis (B, C), papillomavirus infection) in Groups 1 and 2 (P>0.05). The incidence of pelvic inflammatory diseases was 2 times higher in Group 1 than in Group 2.

Table 2.

Comorbid conditions n (%) in HIV-infected women

ICD-10 codes	Group 1 n=23	Group 2 n=27	P-level
Chronic diseases of the tonsils - J35.0	10(43.5%)	15(55.6%)	0.394
Chronic gastritis/duodenitis - K 29.5	5(21.7%)	7(25.9%)	0.730
Chronic viral hepatitis B - B18.1 Chronic viral hepatitis C - B18.2	11(47.8%)	12(44.4%)	0.811
Chronic pancreatitis - K86.1	3(13.0%)	4(14.8%)	1
Chronic cystitis - N30.1	2(8.7%)	4(14.8%)	0.674
STI combinations -Chlamydial infection of pelvi-peritoneum and other genitourinary organs - A56.1 -Gonococcal infection of lower genitourinary tract without periurethral or accessory gland abscess - A54 -Latent syphilis, unspecified as early or late - A53 -Urogenital trichomoniasis - A59	15(65.2%)	9(33.3%)	0.024
Papillomavirus - B97.7	10(45%)	12(40%)	0.944

The structure of gynecological diseases is presented in Table 3. No statistically significant differences in the incidence of uterine myoma, chronic cervicitis, chronic endometritis, vulvovaginal candidiasis, and cervical dysplasia were found. A significant prevalence of chronic salpingo-oophoritis, secondary dysmenorrhea, secondary amenorrhea, opsomenorrhea, and secondary oligomenorrhea was detected significantly more frequently in Group 1 than in Group 2. The syndrome of hyperprolactinemia was also 2.6 times more frequent in Group 1 than in Group 2.

Biological changes in reproductive physiology may explain the lack of fertility in HIV-infected women.[4,5] Systemic disease, stress, weight loss, and substance abuse can affect reproductive potential.[13-15] HIV-infected women are more likely to suffer from prolonged anovulation and amenorrhea;[3,4,16] the mechanisms underlying this clinical observation are unknown and debated. However, there are studies that have found no association between HIV infection and amenorrhea after adjusting for age, body mass index, and substance use.[3] The number of ovulatory cycles and frequency of sexual intercourse correlate with the severity of HIV/AIDS clinical status and can obviously affect fertility and may reflect the degree of depletion and immunosuppression.[3,4] A direct link between HIV and gonadal deficiency in men and women has been suggested, but no evidence for this hypothesis is yet available.

Table 3.

Gynecological diseases n (%) in HIV-infected women

ICD -10 codes	Group 1 n=23	Group 2 n=27	P-level
Moderate cervical dysplasia - N87.1	7(30.4%)	4(14.8%)	0.305
Chronic salpingo-oophoritis - N70.1	15(65.2 %)	8(29.6%)	0.012
Secondary amenorrhea - N92.1	5(21.8%)	0	0.016
Opsomenorrhea - N91.3	6(26.1 %)	1(3.7%)	0.039
Secondary oligomenorrhea - N91.4	8(34.8%)	2(7.4 %)	0.030
Cervicitis - N72	12(52.2%)	8(29.6%)	0.105
Chronic vulvovaginitis - N76.1	14(60.9%)	11(40.7 %)	0.156
Chronic inflammatory diseases of the uterus - N71.1	9(39.1%)	3(11.1 %)	0.044
Secondary dysmenorrhea - N94.5	16(69.6%)	10(37.0 %)	0.022
Myoma of the uterus - D25.1	1(4.3%)	2(7.4%)	1
External genital and vaginal candidiasis - B37.3	12(52.2%)	10(37.0 %)	0.283
Hyperprolactinemia - E22.1	13(56.5%)	5(18.5 %)	0.008
Female infertility associated with anovulation - N97.0	7(30.4%)	0	0.002

In our study, reproductive disorders in HIV-infected women are associated with a high incidence of gynecological and endocrine pathology: secondary dysmenorrhea, pelvic inflammatory disease, STI combinations (trichomoniasis, gonorrhea, syphilis, chlamydia), hyperprolactinemia, anovulation, oligomenorrhea, and secondary amenorrhea. As more and more young HIV-infected patients live longer, reproductive problems are becoming more prominent in public health. It can be concluded that fertility treatment is a relevant option for HIV-infected couples. Future treatments should be designed to help minimize the risk of HIV transmission and improve understanding of the impact of HIV and its treatments on fertility and reproductive competence.

Competing Interests

The authors declare that they have no competing interests.

References

1. World Health Organization. Draft global health sector strategy on HIV, 2016–2021. Available from: https://apps.who.int/gb/ebwha/pdf_files/WHA69/A69_31-en.pdf?ua=1.
2. UNAIDS. 2020 Global AIDS Update — Seizing the moment — Tackling entrenched inequalities to end epidemics. Available from: https://www.unaids.org/en/resources/documents/2020/global-aids-report
3. Kushnir VA, Lewis W. Human immunodeficiency virus/acquired immunodeficiency syndrome and infertility: emerging problems in the era of highly active antiretrovirals. Fertil Steril. 2011 Sep;96(3):546-53. doi: 10.1016/j.fertnstert.2011.05.094.
4. Leshchenko OY, Genich EV. [Reproductive disorders and their pathogenetic mechanisms in women with HIV]. HIV Infection and Immunosuppressive Disorders. 2019;11(4):20-29. doi:10.22328/2077-9828-2019-11-4-20-29. [Article in Russian].
5. Leshchenko OY, Genich EV, Darenskaya MA, Kolesnikova LI. [HIV and infertility: neuro-endocrine and metabolic aspects]. HIV Infection and Immunosuppressive Disorders. 2020;12(4):73-80. doi:10.22328/2077-9828-2020-12-4-73-80. [Article in Russian].
6. Kolesnikov SI, Savilov ED, Savchenkov MF, Leshchenko YaA, Malov IV, Anganova EV, et al. [Sanitary-Epidemiological Status of Siberian Population (Medico-Demographic and Epidemiological Characteristics)]. Annals of the Russian Academy of Medical Sciences. 2016;71(6):472-481. doi: 10.15690/vramn640. [Article in Russian].
7. Darenskaya MA., Kolesnikov SI., Grebenkina LA., Timofeeva E, Leshenko OYa., Nikitina O, Kolesnikova LI. The correlation between antioxidant deficiency and reproductive disorders in women with HIV-infection. Free Radical Biology & Medicine. 2017;112(S1):129. DOI: 10.1016/j.freeradbiomed.2017.10.194
8. Leshchenko O.Ya. [Reproductive potential status of women in Irkutsk region]. Acta Biomed. Scientifica. 2011; 3-2: 106-11. [Article in Russian].
9. Zaba B, Gregson S. Measuring the impact of HIV on fertility in Africa. AIDS. 1998;12 Suppl 1:S41-50.
10. Massad LS, Springer G, Jacobson L, Watts H, Anastos K, Korn A, Cejtin H, Stek A, Young M, Schmidt J, Minkoff H. Pregnancy rates and predictors of conception, miscarriage and abortion in US women with HIV. AIDS. 2004 Jan 23;18(2):281-6. doi: 10.1097/00002030-200401230-00018.
11. Ethics Committee of American Society for Reproductive Medicine. Human immunodeficiency virus (HIV) and infertility treatment: a committee opinion. Fertil Steril. 2015 Jul;104(1):e1-8. doi: 10.1016/j.fertnstert.2015.04.004.
12. Brickley DB, Almers L, Kennedy CE, Spaulding AB, Mirjahangir J, Kennedy GE, Packel L, Osborne K, Mbizvo M, Collins L. Sexual and reproductive health services for people living with HIV: a systematic review. AIDS Care. 2011 Mar;23(3):303-14. doi: 10.1080/09540121.2010.507746.
13. Leschenko OY, Genich EV. [The reproductive health and sexual behavior of HIV-infected women: the review]. Probl Sotsialnoi Gig Zdravookhranenniiai Istor Med. 2020 Mar;28(2):294-302. doi: 10.32687/0869-866X-2020-28-2-294-302. [Article in Russian].
14. Kolesnikova LI, Kolesnikov SI, Darenskaya MA, Grebenkina LA, Timofeeva EV, Leshchenko OY, Vanteeva OA, Rashidova MA. [Evaluation of the pro- and antioxidant status of women with HIV or coinfection]. Ter Arkh. 2016;88(11):17-21. doi: 10.17116/terarkh2016881117-21. [Article in Russian].
15. Leshchenko OYa, Genich E. Susceptible hormones in women with HIV-infection and displeasure. BJOG: An International Journal of Obstetrics and Gynaecology. 2019;126(S2): 217-224. doi: 10.1111/1471-0528.20_15703
16. Shapiro K, Ray S. Sexual health for people living with HIV. Reprod Health Matters. 2007 May;15(29 Suppl):67-92. doi: 10.1016/S0968-8080(07)29034-2.

***Corresponding author:** *Olga Ya. Leshchenko, PhD, ScD. Scientific Centre for Family Health and Human Reproduction Problems, Irkutsk, the Russian Federation. E-mail: loyairk@mail.ru*

International Journal of Biomedicine 12(1) (2022) 124-133
http://dx.doi.org/10.21103/Article12(1)_OA13

ORIGINAL ARTICLE

Experimental Medicine

INTERNATIONAL JOURNAL OF BIOMEDICINE

Effectiveness of Experimental Colitis Therapy with Original Vitamin D_3 Rectal Suppositories

M. V. Osikov[1,2]; M. S. Boyko[1*]; A. A. Fedosov[3,4]; M. A. Ilyinykh[1]

[1]*South Ural State Medical University, Chelyabinsk, Russia*
[2]*Chelyabinsk Regional Clinical Hospital, Chelyabinsk, Russia*
[3]*Russian National Research Medical University named after N.I. Pirogov, Moscow, Russia*
[4]*Peoples' Friendship University of Russia (RUDN University), Moscow, Russia*

Abstract

Background: Pathogenesis of inflammatory bowel disease (IBD) is insufficiently explored, while most of the therapeutic agents used for IBD cases have undesirable side effects, which restrict their administration.The aim of this research was to study the influence of vitamin D3 formulated into original rectal suppositories on the parameters of clinical score, morphology, and oxidative lipid and protein destruction in the colonic lesion in the cases of experimental colitis (EC).

Methods and Results: The experiment was performed on 98 Wistar male rats weighing 210-230 g. EC condition was induced by two-phase administration (dermal application and per rectum) of 3% alcohol solution of oxazolone. Originator polyethylene glycol-based suppositories, which contained 1500 ME of vitamin D3, were administered per rectum every 12 hours. Clinical score was defined according to the Disease Activity Index (DAI) scale. Morphometry was run using the software program "ImageScope M" (Russia). Damage of the colonic tissue was estimated on Tissue Damage Index (TDI).

The following parameters were determined in the colonic lesion: neutrophil count (NC), lymphocyte count (LC), eosinophil count (EC), histiocyte count (HC), plasma cell count (PC), fibroblast count (FC), the diameter of the ulcerous defect, TDI, MPO expression, and TNF-α expression. The following parameters were determined in the damaged tissue homogenate: lipid peroxidation product count (LPP) and protein oxidative modification (POM) count.

In cases of oxazolone-induced EC, on Days 2, 4, and 6, we registered clinical and laboratory signs, an ulcerous defect in the damaged area of the colon, all of which are typical for IBD conditions. There was an increase in DAI (peak on Day 6) and TDI (peak on Day 2). We also found an increase in NC (peak on Day 2), LC (peak on Day 6), EC (peak on Day 2), PC (peak on Day 2), HC (peak on Day 2), and FC (peak on Day 2). There was an increase in MPO expression (peak on Day 2) and TNF-α expression (peak on Days 2 and 4). We observed increases in the primary, secondary, and end LPP counts and the early-phase and late-phase POM counts in spontaneous and induced modes.

An administration of 1500 ME vitamin D3 rectal suppositories every 12 hours for 6 days decreased the severity of clinical manifestations and DAI. It reduced the area of the ulcerous defect and decreased the TDI on Days 4 and 6 of the experiment. On the background of using vitamin D3 rectal suppositories, we found a decrease in NC, EC, LC, and PC in the damaged area and an increase in HC and FC on Days 2, 4, and 6 from the start of the experiment. Administration of D3 rectal suppositories decreased MPO expression and TNF-α expression on Days 4 and 6 of EC. In the damaged area of the colon, we observed a decrease in the counts of the primary, secondary, and end LPP on Days 4 and 6 of the experiment. We also documented a decrease in the POM count in spontaneous mode on Day 2 and on Day 6 in induced mode.

Conclusion: Vitamin D3 as a constituent of originator rectal suppositories in total dose 18,000 ME in the pre-clinical phase of EC decreases the intensity of EC clinical manifestations. It reduces the count of the cells that take part in tissue destruction in the colonic wall, of TNF-α and MPO expression levels, and LPP- and POM product count. It increases the count of the cells, which promotes tissue reparation. The obtained results are essential for carrying out further research aimed at elaboration of the mechanism of the D3 effect in cases of IBD and at its possible clinical use.(**International Journal of Biomedicine. 2022;12(1):124-133.**)

Key Words: experimental colitis • rectal suppositories • vitamin D_3 • oxidative stress

For citation: Osikov MV, Boyko MS, Fedosov AA, Ilyinykh MA. Effectiveness of Experimental Colitis Therapy with Original Vitamin D3 Rectal Suppositories. International Journal of Biomedicine. 2022;12(1):124-133. doi:10.21103/Article12(1)_OA13

Abbreviations

DAI, disease activity index; **EC**, experimental colitis; **EC**, eosinophil count; **FC**, fibroblast count; **HC**, histiocyte count; **IBD**, inflammatory bowel disease; **LPP**, lipid peroxidation product; **LC**, lymphocyte count; **NC**, neutrophil count; **OS**, oxidative stress; **POM**, protein oxidative modification; **PC**, plasma cell count; **ROS**, reactive oxygen species; **TDI**, tissue damage index.

Introduction

Inflammatory bowel diseases (IBD) include diseases with multiple etiology, which are characterized by chronic inflammatory-destructive progressive damage of the gastrointestinal tract by the systemic immunological factors under the conditions of immune response dysregulation. The incidence of autoimmune gastrointestinal disorders has only been increasing for the last ten years. The annual rate of increase in the number of IBD cases is 5-20 cases per 100,000 people, and the number is continuing to grow.[1,2,3] Pathogenesis of IBD is insufficiently explored, while most of the therapeutic agents used for IBD cases have undesirable side effects, which restrict their administration. In IBD pathogenesis, the following factors damage the colonic wall: Th2-dependent reactions involving IgM and IgG, as well as Th-1 dependent reactions with increased production of IL-8, TNF-α, and other cytokines; the activation of chemotaxis; absorption and killing activity of neutrophils, monocytes/macrophages; and the production of ROS and nitrogen.

Hyperproduction of ROS in combination with a decreased activity of the antioxidant system leads to the progression of oxidative stress (OS) and accumulation of irreversible products of protein oxidative modification (POM) – i.e. carbonyl derivatives and lipid peroxidation products (LPP).[4] The mentioned changes on the morphological level lead to damaging of distal colonic regions, to the destruction of intestinal glands, to goblet cell hyperplasia, mucous ulceration and fibrosis, which clinically manifest as tenesmus, changes of stool consistency, an admixture of blood in fecal matter, body mass deficiency and other symptoms, including intestinal and extraintestinal complications.[5-7] The essential IBD therapy includes topical and systemic inflammatory inhibitors (5-aminosalicylate, corticosteroids), immunosuppressive agents(azathioprine, 6-mercaptopurine, etc.), and biologic therapy medications(infliximab, adalimumab, golimumab, etc), all of which have a wide variety of undesirable side effects on the gastrointestinal tract, the hemic system, and the reproductive system. These treatments do not guarantee achieving long-term remission. About 30% of IBD patients develop resistance to therapy and medication intolerance in cases of long-term use. Therefore, elaboration of new IBD treatment approaches is urgent.[8,9] In this aspect, vitamin D3 is of certain interest because of its pleiotropic qualities (antioxidative, anti-inflammatory, immunomodulatory, and other).[10-12] Administration of vitamin D3 in cases of multiple sclerosis and psoriasis limits the severity of inflammatory process and clinical signs due to increased IL-10 production and Treg count in blood, and a shift in Th1/Th2 balance to the side of Th2-dependent immune response.[13,14] In the presence of rheumatoid arthritis, vitamin D3 represses the activity of Th17 and the production of IL-17.[15] The stated facts serve as a ground for clinical usage of vitamin D3 in IBD cases.[16] As of now, in the CIS countries, there are no dosage forms for using vitamin D3 locally *per rectum* aimed at the impact on the area of inflammation and the damaged colonic section in cases of IBD. We have developed original rectal D3 suppositories based on a 10% D3 aqueous solution.[17] Formerly we proved that vitamin D3 as a constituent of original rectal suppositories in cases of experimental colitis (EC) has a systemic immunotropic effect, decreases blood neutrophil count, restores absorption and NBT-reducing activity of neutrophils, decreases LC, including CD3+ and CD45RA+, and decreases the concentration of IgM, IgG, IL-6, and IL-8.[18] We assume that the systemic immunotropic effect of vitamin D3 formulated into original rectal suppositories in EC cases is associated with its local protective action in the colonic lesion. The aim of this research was to study the influence of vitamin D3 formulated into original rectal suppositories on the parameters of clinical score, morphology, and oxidative lipid and protein destruction in the colonic lesion in EC cases.

Materials and Methods

The experiment was performed on Wistar male rats weighing 210-230g. All stages of the experiment were carried out in accordance with the requirements of Directive 2010/63/EU of the European Parliament and of the Council of 22 September 2010 on the protection of animals used for scientific purposes.[19]

Ninety-eight rats were randomly divided into three experimental groups: Group 1 included 14 intact animals (control group); Group 2 included 42 animals with EC; Group 3 included 42 animals with EC treated by vitamin D3 rectal suppositories every 12 hours for 6 days until withdrawn from the experiment.

EC condition was induced by two-phase administration of oxazolone ("Sigma-aldrich", USA). In the first phase, sensibilization was performed by a dermal application between the shoulders of 150 µl of 3% alcohol solution of oxazolone. In the second phase, 150 µl of 3% alcohol solution of oxazolone was inserted to the depth of 7-8 cm per rectum (Fig.1).[20] For anesthetic purposes, "Zoletil-100" ("Virbac Sante Animal", France) was administered in a dose of 20 mg/kg. EC diagnosis was verified by estimating the clinical pattern and morphology of the damaged area of the colon.

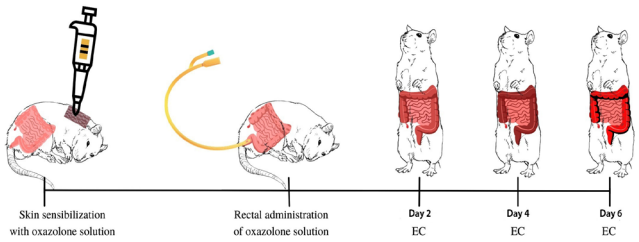

Fig. 1. *EC modeling.*

Vitamin D3 suppositories were based on a 10% aqueous solution of vitamin D3, with a compound of polyethylene glycols with different molecular weights, emulsifier T-2, cremophor RH-40 and kolliphor as excipients. The size and the shape of suppositories answered the specifics of the distal section of rats' colon. The final mass of each suppository was 300 mg; the content of vitamin D3 in each suppository was 1500 ME (Fig,2).[17,21]

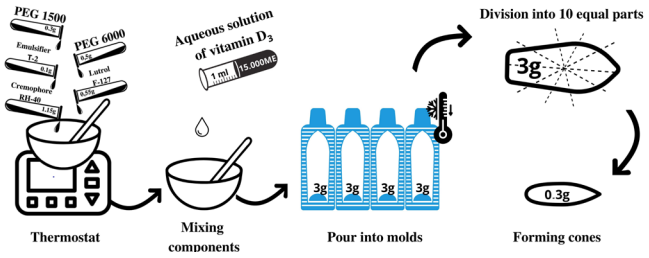

Fig. 2. *Manufacturing technology of vitamin D_3 rectal suppositories.*

The study was run on Days 2, 4 and 6 after EC induction. To estimate clinical score, we used the Disease Activity Index (DAI) scale, which was adapted for rats. It included the following parameters: body mass, stool consistency, and blood admixtures in the excrement.[22] The parameters were calculated daily on a 5-point scale from 0 to 4, with maximum possible DAI – 12.

Segmented intestine distal fragments were fixed in 10% neutral formalin solution; serial sections were stained with H&E. In ten randomly selected fields of vision on a micrograph "Leica DMRXA" (Germany) (×400 magnification), we quantified NC, LC, EC, HC, PC, FC per 1mm^2. At ×100 magnification, we quantified the diameter of the ulcerous defect. Morphometry was run using the software program "ImageScope M" (Russia)

Damage of the colonic tissue was estimated on scale from 0 to 6 with the definition of the relative area of lesion, colonic wall thickness, angiogenesis, goblet cell loss, severity of leucocyte infiltration and Tissue Damage Index (TDI).[23]

Myeloperoxidase (MPO) expression and TNF-α expression in the colon mucosa were estimated by an immunohistochemical test with an antibody kit that was specified for rats ("Cloud. Clon. Corp.", China), and super-adhesive slides with a positively charged surface (Super Frost Plus). The reactions were run in immunohistostainer "Bench Mark XT" (Ventana, USA) with complete adherence to the research protocol. Imaging was carried out in the "Ultra VIEW Universal DAB" system (Ventana, USA) with second-antibody and chromogen complex.

For preparing the 10% colon mucosa homogenate, a proximal part of the segmented intestine was taken from the peritoneal cavity and put into cooled 0.1M phosphate-buffered saline (pH=7.4). After that, approximately 100mg of tissue were homogenized in a glass mechanical homogenizer in a ratio of 1:10 for 3 minutes at a temperature less than 4°C with subsequent generation of 1ml of homogenate.

The LPP level in colon mucosa homogenate was determined by the extraction-and-spectrophotometric method in spectrophotometer "SF-56" ("LOMO-Specter", Russia) according to I.A. Volchegorsky et al.[24,25] The optical density of heptane and isopropanol extracts was measured at 220 nm (isolated double bonds count), 232 nm (diene conjugate count – DC), 278 nm (ketodiene and conjugated triene count – KD and CT), and 400 nm (Schiff's base – SB). Relative LPP count was evaluated in units of oxidation index (u.o.i.): E_{232}/E_{220} (DC), E_{278}/E_{220} (KD and CT), and E_{400}/E_{220} (SB).

POM count in colon mucosa homogenate was defined according to reaction of carbonyl protein compounds with 2,4–dinitrophenylhydrazine in spontaneous and metal-enhanced modes by Fenton's reaction with further spectrometric monitoring of aldehyde-dinitrophenylhydrazine (ADNPH) (early-stage markers of OS) and ketone-dinitrophenylhydrazine (KDNPH) (late-stage markers of OS).[26,27] The results were expressed in optical density units per mg of protein (au/mg).

Statistical analysis was performed using statistical software package SPSS version 23.0 (SPSS Inc, Armonk, NY: IBM Corp). For descriptive analysis, results are presented as median (Me), first quartile (Q1) and third quartile (Q3). A non-parametric Kruskal-Wallis test was used for comparisons of median values among three groups ($P<0.05$), followed by post-hoc testing using un-paired Mann-Whitney U tests. Spearman's rank correlation coefficient (R) was calculated to measure the strength and direction of the relationship between two variables. A probability value of $P<0.01$ was considered statistically significant.

Results and Discussion

Group 2

In cases of EC, on Day 2 of observation, there were the following symptoms: body mass deficiency, frequent defecation, loose stool consistency, and admixture of blood, which could be defined both by the benzidine test and visually.

Table 1.

DAI in the study groups (Me (Q_1; Q_3))

	Group 1 (n=7)	Group 2 Day 2 (n=7)	Group 2 Day 4 (n=7)	Group 2 Day 6 (n=7)	Group 3 Day 2 (n=7)	Group 3 Day 4 (n=7)	Group 3 Day 6 (n=7)
DAI, c.u.	0	7.00 (3.00;7.00)*	8.00 (6.00;10.00)*	11.00 (11.00;11.00)*	5.00 (5.00;5.00)*	4.00 (4.00;5.00)*#	4.00 (4.00;4.00)*#
* - $P<0.01$ with Group 1; # - with Group 2.							

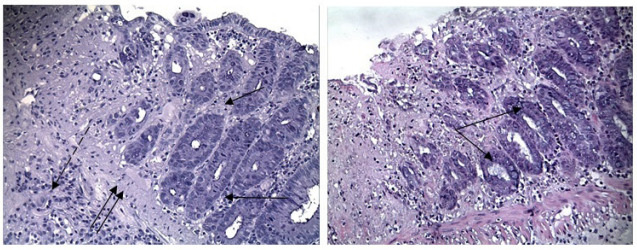

A B

Fig. 3. *Morphological changes in the damaged area of the colon on Day 2 of EC. H&E staining; ×200 magnification. A – Group 2: neutrophil and lymphocyte infiltration of interstitial tissue (arrow), thickening of deep mucosa (double arrow), infiltration of sub-mucous membrane (dotted arrow). B – Group 3: reduced crypts.*

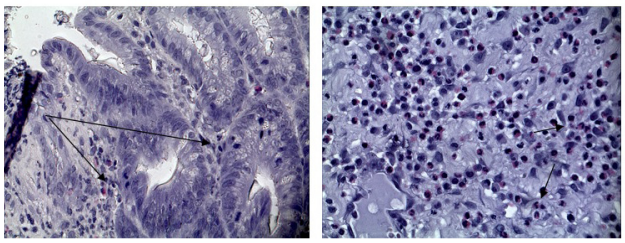

A B

Fig. 4. *Morphological changes in the damaged area of the colon on Day 4 of EC. H&E staining; ×400 magnification. A – Group 2: neutrophil and lymphocyte stromal infiltration with multitude of eosinophil cells. B – Group 3: proliferating fibroblasts.*

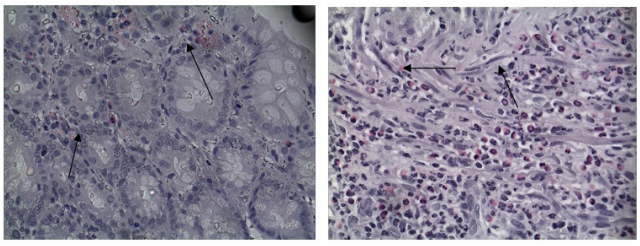

A B

Fig. 5. *Morphological changes in the damaged area of the colon on Day 6 of EC. H&E staining; ×400 magnification. A – Group 2: neutrophil infiltration of connective tissue interlayers. B – Group 3: fibroblast proliferation and fibrillogenesis.*

On Days 4 and 6, the clinical manifestations became more severe. DAI index was scaling up massively on Day 2, on Day 4, and on Day 6 of the experiment. DAI value on Day 6 was higher (P<0.01) than its value on Days 4 and 2 (Table 1).

On Day 2, after EC induction, histological examination of the colonic wall in the place of the lesion showed ulcers with bases situated in deep mucosa (lamina propria) and the surface layers of the submucous membrane. In the same place, we registered cellular infiltration accompanied by interstitial tissue edema, venous and capillary plethora, and crypt epithelium in a state of albuminous degeneration (Fig.3). On Day 4, ulcerative defects, swelling of the interstitial tissue, plethora with leukostasis and leukodiapedesis, plasma impregnation and swelling of the vascular walls, and stromal infiltration persisted (Fig.4). In the depths of ulcerative defects, we observed the proliferation of preserved cambial cells of the intestinal glands. On Day 6, we noticed ulcerous defects with cell debris, edema and maceration of interstitial tissue and vascular plethora (Fig.5). Between the areas of infiltration, there was a distinct proliferation of juvenile fusiform fibroblasts and the initial phase of neoangiogenesis. The edges of the ulcerous defects had distinct signs of epithelialization.

Morphometric evaluation of the cellular composition of the infiltrate in colonic lesions demonstrated a significant increase in NC, LC, PC, FC, in the area of the ulcerous defect, and in the TDI on Days 2, 4, and 6 after EC induction (Table 2). EC progression shows that NC on Day 4 was less (P<0.01) than on Day 2, and on Day 6 less (P<0.01) than on Day 2. LC on Day 6 was higher (P<0.01) than on Day 2 and Day 4. EC, HC, and PC were higher (P<0.01) on Days 4 and 6 than on Day 2. FC on Day 4 was higher (P<0.01) than on Day 2, while FC on Day 6 was higher (P<0.01) than on Days 2 and 4 of the experiment. The area of the ulcerous defect on Days 4 and 6 was bigger (P<0.01) than on Day 2. The peak extent of NC in the lesion was recorded on Day 2, for EC, HC, PC, and FC – on Days 2 and 4, LY – on Day 6 after ES onset.

Expression of MPO and TNF-α increased massively on Days 2, 4, and 6 of EC (Table 3). MPO expression on Day 6 was lower (P<0.01) than on Day 2; TNF-α expression on Day 6 was lower (P<0.01) than on Days 2 and 4.

While estimating LPP count in colonic mucosa lesion homogenate on Day 2, we observed a significant increase in primary, secondary and end LPP count in the heptane phase of the lipid extract. The same applies to the secondary and end LPP count in the isopropanol phase of the lipid extract (Table 4). On Days 4 and 6 of EC, we recorded a significant increase in the primary, secondary and end LPP count in both heptane and isopropanol phases of the lipid extract of colonic mucosa lesion homogenate. With EC progression, in the heptane phase of the lipid extract, the primary LPP count was less (P<0.01) on Day 6 than on Days 4 and 2; the secondary LPP count on Day 4 was higher (P<0.01) than on Days 2 and 6. In the isopropanol phase, the primary LPP count was higher (P<0.01) on Day 4 than on Days 2 and 6; the secondary LPP count was less (P<0.01) on Day 4 than on Day 2, and the secondary LPP count on Day 6 was less (P<0.01) than on Days 4 and 2. In the isopropanol phase, the end LPP count on Day 4 was higher (P<0.01) than on Days 2 and 6.

POM count in the spontaneous mode showed an increase in the total count of protein carbonyl derivatives ADNPH and KDNPH in colonic mucosa lesion homogenate on Days 2, 4, and 6 of EC (Table 5). The total POM count on Day 4 was less (P<0.01) than on Days 2 and 6. The count of ADNPH was less (P<0.01) on Day 4 than on Days 2 and 6. The count of KDNPH was less (P<0.01) on Days 4 and 6 than on Day 2. In the metal-induced mode, we observed the increased total POM count on Days 4 and 6, while the counts

of ADNPH and KDNPH massively increased on Days 2, 4, and 6. With EC progression, total POM count and ADNPH count was higher (P<0.01) on Day 6 than on Days 4 and 2. KDNPH count was higher (P<0.01) on Day 4 than on Day 2, and on Day 6 than on Day 2 (P<0.01) of EC.

Group 3

Under the local application of vitamin D3 in cases of EC, we observed improvement of the rats' clinical condition. There was no decrease in weight; the fecal matter was firmer, an admixture of blood was defined only by a benzidine test.

Table 2.

Morphometric parameters in the damaged area of the colon in the study groups (Me (Q_1; Q_3))

Parameters	Group 1 (n=7)	Group 2 Day 2 (n=7)	Group 2 Day 4 (n=7)	Group 2 Day 6 (n=7)	Group 3 Day 2 (n=7)	Group 3 Day 4 (n=7)	Group 3 Day 6 (n=7)
NC, u/mm^2	204.56 (189.71;223.57)	2651.41 (2558.85;2813.85) *	1518.48 (1121.49;2100.00) *	1333.33 (1213.34;1608.04 *	873.78 (666.67;925.92) *#	550.45 (370.37;1006.03) *#	654.21 (582.53; 804.83) *#
LY, u/mm^2	338.99 (305.14;368.35)	1104.48 (947.67;1333.34) *	1004.55 (880.09;1238.11) *	1667.02 (1302.62;2038.84) *	680.07 (511.78;849.32) *#	710.67 (495.06;733.95) *#	642.19 (582.61;891.11) *#
EC, u/mm^2	146.91 (120.83;176.18)	852.34 (839.46;857.45) *	2671.29 (2352.95;3553.31) *	2380.11 (2110.11;2613.05) *	467.29 (304.57;611.13) *#	852.89 (635.86;1094.25) *#	805.12 (685.42;867.49) *#
HC, u/mm^2	13.47 (13.42;13.65)	571.94 (198.02;750.26) *	1197.11 (1049.31;1614.91) *	1006.03 (970.87;1009.17) *	913.31 (759.37;1102.82) *#	1395.36 (1313.13;1600.00) *	1617.79 (1512.09;1809.04) *#
PC, u/mm^2	13.42 (12.87;13.56)	673.13 (549.12;704.52) *	804.02 (713.06;910.01) *	810.13 (804.82;1210.12) *	480.81 (370.37;560.74) *#	401.06 (372.67;411.77) *#	373.83 (297.03;545.56) *#
FC. u/mm^2	22.66 (13.56;26.82)	512.77 (281.37;711.65) *	1146.77 (866.81;1358.22) *	1685.27 (1523.84;2057.07) *	1821.02 (1817.34;1845.66) *#	2353.94 (2311.23;2401.00) *#	2467.89 (2413.88;3047.61) *#
UD, µm	0	575.00 (305.00; 780.60) *	735.00 (635.52;976.50) *	753.00 (372.00;882.50) *	294.00 (197.00;357.00) *#	242.00 (151.00;539.00) *#	238.50 (169.00;299.00) *#
TDI, c.u.	0	3.71 (3.00;4.00) *	3.57 (3.00;4.00) *	3.42 (3.00;4.00) *	3.00 (3.00;4.00) *	2.17 (1.00;3.00) *#	2.12 (1.00;3.00) *#

* – P<0.01 with Group 1, # - with Group 2; UD - ulcerous defect

Table 3.

MPO count and TNF-α count in the damaged area in the colon in study groups (Me (Q_1; Q_3))

Parameters	Group 1 (n=7)	Group 2 Day 2 (n=7)	Group 2 Day 4 (n=7)	Group 2 Day 6 (n=7)	Group 3 Day 2 (n=7)	Group 3 Day 4 (n=7)	Group 3 Day 6 (n=7)
MPO, u/mm^2	19.16 (0.00;19.16)	1241.37 (967.04;1486.59) *	938.69 (770.15;1109.19) *	775.86 (766.28;814.17) *	1053.64 (977.01;1091.95) *	498.08 (478.92;593.86) *#	287.35 (268.19;287.35) *#
TNF-α, u/mm^2	57.47 (38.31;76.63)	1321.83 (919.54;1475.09) *	1302.68 (1264.36;1321.83) *	752.87 (703.06;814.17) *	766.28 (670.49;957.85) *	727.96 (727.97;766.28) *#	210.72 (172.41;229.88) *#

* – P<0.01 with Group 1, # - with Group 2

Consequently, there was a massive decrease in DAI on Days 4 and 6 of the experiment (Table 1). Thus, DAI on Days 4 and 6 was significantly lower than in Group 2, which indicates partial restoration of the parameter.

In Group 3, histologic examination of the EC colonic wall in the place of the defect on Day 2 of the experiment showed ulcers in lamina propria and in the surface layers of the submucous membrane with venous and capillary plethora. Colonic mucosa was mildly edematic, the crypts were shortened and widened, and their epithelium was in a state of granular dystrophy (Fig.3).

On Day 4 of the experiment, we observed fully-epithelized areas of mucous lesion restoration with the initial formation of intestinal glands and crypts, focal granulocyte infiltration, and proliferation of juvenile fibroblasts (Fig.4). On Day 6 of the experiment, we recorded complete epithelization

Table 4.

LPP count in colonic mucosa lesion homogenate in the study groups (Me (Q_1; Q_3))

Parameters	Group 1 (n=7)	Group 2 Day 2 (n=7)	Group 2 Day 4 (n=7)	Group 2 Day 6 (n=7)	Group 3 Day 2 (n=7)	Group 3 Day 4 (n=7)	Group 3 Day 6 (n=7)
DC (h) u.o.i.	0.63 (0.55;0.65)	0.79 (0.75;0.81)*	0.78 (0.77;0.78)*	0.76 (0.75;0.77)*	0.77 (0.71;0.78)*	0.68 (0.63;0.68)#	0.70 (0.65;0.73)* #
KDCT (h) u.o.i.	0.06 (0.05;0.06)	0.08 (0.07;0.08)*	0.22 (0.21;0.22)*	0.09 (0.09;0.11)*	0.06 (0.06;0.09)	0.19 (0.18;0.19)* #	0.06 (0.05;0.07)#
SB (h) u.o.i.	0.01 (0.01;0.02)	0.03 (0.02;0.04)*	0.02 (0.02;0.05)*	0.05 (0.04;0.06)*	0.03 (0.02;0.04)*	0.01 (0.01;0.01)#	0.02 (0.01;0.03)#
DC (i) u.o.i.	0.34 (0.32;0.36)	0.38 (0.33;0.43)	0.55 (0.52;0.56)*	0.43 (0.43;0.45)*	0.38 (0.33;0.43)	0.51 (0.51;0.51)* #	0.41 (0.39;0.42)* #
KDCT (i) u.o.i.	0.31 (0.29;0.32)	0.72 (0.56;0.91)*	0.51 (0.51;0.57)*	0.48 (0.47;0.49)*	0.72 (0.56;0.91)*	0.42 (0.41;0.43)* #	0.42 (0.41;0.42)* #
SB (i) u.o.i.	0.01 (0.01;0.02)	0.07 (0.07;0.09)*	0.24 (0.21;0.31)*	0.11 (0.11;0.14)*	0.07 (0.07;0.09)*	0.01 (0.01;0.01)#	0.06 (0.05;0.08)* #
* –P<0.01 with Group 1, # - with Group 2. The parameters demonstrate LPP count in heptane (h) and isopropanol (i) phases of lipid extract.							

Table 5.

POM product counts in colonic mucosa lesion homogenate in the study groups (Me (Q_1; Q_3))

Parameters	Group 1 (n=7)	Group 2 Day 2 (n=7)	Group 2 Day 4 (n=7)	Group 2 Day 67 (n=7)	Group 3 Day 2 (n=7)	Group 3 Day 4 (n=7)	Group 3 Day 6 (n=7)
S_{POM}, au/mg (spont)	141.57 (141.28;144.18)	325.31 (251.18;348.01) *	214.59 (169.57;245.21) *	286.83 (165.86;297.74) *	166.74 (151.86;173.73) *#	181.91 (168.31;182.07) *	241.73 (238.92;261.63) *
S ADNPH, au/mg (spont)	131.25 (127.61;152.01)	294.78 (224.58;308.54) *	193.81 (165.47;222.84) *	268.31 (154.66;273.24) *	156.25 (132.91;163.51) #	166.57 (157.22;166.98) *	222.91 (219.25;242.86) *
S KDNPH, au/mg (spont)	12.16 (10.03;13.97)	30.53 (26.59;38.01) *	20.78 (14.39;22.35) *	18.52 (14.21;24.49) *	10.23 (8.94;10.49) #	14.07 (12.04;14.12) #	18.76 (18.76;18.83) *
S_{POM}, au/mg (ind)	266.20 (266.19;317.14)	321.71 (284.89;377.77)	416.51 (325.26;472.92) *	570.79 (526.85;638.48) *	266.02 (237.19;310.61)	328.36 (319.81;600.42) *	470.94 (328.39;470.94) *#
S ADNPH, au/mg (ind)	228.91 (228.81;237.95)	266.69 (264.71;314.21) *	338.86 (258.04;384.07) *	459.72 (422.91;521.53) *	217.64 (202.71;260.77) #	265.29 (253.29;492.93) *	403.12 (238.28;411.66) *#
S KDNPH, au/mg (ind)	37.31 (37.08;39.18)	54.36 (52.81;55.01) *	77.65 (59.35;79.95) *	108.05 (103.93;111.07) *	40.83 (39.84;48.37) *#	63.07 (48.51;107.49) *	59.27 (50.11;59.27) *#
* – P<0.01 with Group 1, # - with Group 2. POM product counts in spontaneous (spont) and induced (ind) modes.							

of the ulcerous defects, focal infiltration, and vast fields of proliferating fibroblasts, newly-formed fibers of connective tissue, and vessels in abundance (Fig.5).

Morphometric study of the cellular composition of the infiltrate in the colonic EC lesion against the background of the vitamin D3 therapy demonstrated that on Day 2, there was a significant decrease in NC, LC, EC, and PC, and an increase in HC and FC. On Day 4, there was a significant decrease in NC, LC, EC and PC, and an increase in FC.

On Day 6, we observed a significant decrease in NC, LC, EC, and PC, and an increase in HC and FC. On Days 2, 4, and 6 of the experiment, we found a decrease in the size of the ulcerous defect, and on Days 4 and 6 a decrease in TDI (Table 2). EC and HC were higher (P<0.01) on Day 4 than on Day 2, and on Day 6 higher (P<0.01) than on Day 2. FC was higher (P<0.01) on Day 4 than on Day 2, and on Day 6 than on Days 4 and 2. TDI was less on Days 4 and 6 (P<0.01) than on Day 2. During all periods of the study, morphometric parameters never reached the parameter values of the intact animals' group; the recovery was only partial.

The use of vitamin D3 in the EC therapy was associated with a decrease in the expression of MPO and TNF-α in the area of the ulcerous defect on Days 4 and 6 (Table 3). The MPO expression on Day 4 was lower (P<0.01) than on Day 2, and on Day 6 lower (P<0.01) than on Days 4 and 2. The TNF expression was lower (P<0.01) on Day 6 than on Days 4 and 2.

In the colonic mucosa lesion homogenate (in the heptane and isopropanol phases of the lipid extract), on Days 4 and 6 of EC with vitamin D3 therapy, there was a significant decrease in the counts of primary, secondary and end LPP (Table 4). In the heptane phase of the lipid extract, the primary LPP count on Days 4 and 6 was less(P<0.01) than on Day 2. The count of the secondary LPP on Day 4 was higher than on Days 2 and 6. The count of the end LPP was less (P<0.01) on Day 4 than on Days 2 and 6. In the isopropanol phase of the lipid extract, the primary LPP count was higher (P<0.01) on Day 4 than on Days 2 and 6. The secondary LPP count was less (P<0.01) on Days 4 and 6 than on Day 2. The count of the end LPP was less (P<0.01) on Day 4 than on Days 2 and 6.

The use of the vitamin D3 rectal suppository led to a significant decrease in the total count of protein carbonyl derivatives (along with decreased counts of ADNPH and KDNPH) on Day 2. On Day 4, we observed a further decrease in the KDNPH count (Table 5). The total count of POM products and ADNPH count were higher (P<0.01) on Day 6 than on Days 4 and 2. The KDNPH count was higher (P<0.01) on Day 4 than on Day 2, and on Day 6 than on Days 4 and 2. In metal-induced mode, on Day 2, we recorded a decrease in the counts of ADNPH and KDNPH. On Day 6, there was a decrease (P<0.01) in total POM count, ADNPH count and KDNPH count. According to EC progression, in metal-induced mode, the total POM count and ADNPH count were higher (P<0.01) on Days 4 and 6 than on Day 2. The KDNPH count was higher (P<0.01) on Days 4 and 6 than on Day 2 of the experiment.

Thus, in cases of EC, there are specific clinical manifestations (loss of weight, loose stool with blood admixture) and morphological patterns, which is typical for IBDs. It makes it possible to apply the suggested model for further research of IBD pathogenesis and IBD experimental therapy.

There is an assumption that oxazolone is similar to haptene in its qualities. Haptene directs the immune response mostly through Th2-dependent way, which is accompanied by increased immunoglobulin (IgG, IgM) secretion and cytokine (IL-6, IL-8, TNF-α, etc.) secretion in blood. It results in leukocyte accumulation in the area of inflammation, damage of the colonic wall, and extension of the secondary alteration area.[28,29] The source of ROS that initiates lipid destruction, protein destruction, and accumulation of LPP and POM in the colonic wall is mostly neutrophils, monocytes/macrophages. Infiltration by the latter is a typical morphological sign of colitis.[30] IL-1, IL-6, TNF-α, and other anti-inflammatory cytokines intensify myelopoiesis and release of mature neutrophils and monocytes from the bone marrow and their migration to the inflammation site.[31] Endotheliocytes can also take part in ROS production due to eNOS activation, NO synthesis, and peroxynitrite synthesis.

In cases of EC with the use of original vitamin D3 rectal suppositories, a decrease in clinical manifestations and morphological signs of damage in the colonic wall can take place due to the vitamin D3 pleiotropic effect.

The correlation analysis showed the average and high strength of the relationship between the severity of clinical manifestations according to DAI and the following parameters: TDI, size of the ulcerous defect, HC, MPO count and TNF-α count in the damaged area (on Days 2, 4, and 6 of EC), PC (on Days 4 and 6 of EC), LC (on Day 6 of EC), and FC (on Day 6 of EC), as well as the primary, secondary and end LPP counts in heptane and isopropanol phases (peak on Days 2 and 4 of EC), and the counts of ADNPH and KDNPH in spontaneous and induced modes (peak on Days 2 and 4 of EC) (Table 6).

We believe that the obtained results are connected to several mechanisms of the vitamin D3 effect in cases of EC. First, the immunotropic effect of vitamin D3 is realized by the active influence of vitamin D3 metabolite calcitriol on T-lymphocyte proliferation and differentiation. It decreases Th1, Th17 count and increases Treg due to decreased synthesis of IL-1, IL-2, IL-6, IL-12, IL-17, IFN-γ, TNF-α, and increased synthesis of IL-10. Vitamin D3 inhibits macrophage migration and macrophage production of IL-1, IL-6, IL-12, as well as chemotaxis and neutrophil accumulation.(30) On the surface of dendritic cells, vitamin D3 inhibits the expression of TLR, CD40, CD80, CD83, and CD86, decreases secretion of IL-2 and IFN-γ by dendritic cells, and increases IL-10 synthesis.[32] It restricts the activity of the inflammation process in the colon and colonic tissue alteration.[33]

Second, vitamin D3 antioxidant effect is achieved directly through activation of transcriptional factor – nuclear factor erythroid 2-related factor 2, which is responsible for the regulation of antioxidant ferment expression, antioxidant ferment synthesis induction, and antioxidant enterocyte protection in conditions of OS.[21,28,33,34] Vitamin D3 indirect antioxidant effect is connected with a decrease in the infiltration of the damaged area by ROS-producer cells

(neutrophils and monocytes/macrophages) in conditions of restoring cooperation of immune-competent cell.

Table 6.

Correlation between DAI and other parameters in Group 3

Parameters	Group 3 Day 2	Group 3 Day 4	Group 3 Day 6
LC, u/mm^2	R=0.34	R=0.22	R=0.55*
NC, u/mm^2	R=0.20	R=0.24	R=0.18
EC, u/mm^2	R=0.24	R=0.15	R=0.15
HC, u/mm^2	R= - 0.58*	R= - 0.52*	R= - 0.56*
PC, u/mm^2	R= 0.41	R= 0.58*	R= 0.78*
FC, u/mm^2	R= - 0.38	R= - 0.35	R= - 0.55*
Ulcerous defect, μm	R=0.54*	R=0.58*	R=0.69*
TDI, c.u.	R=0.79*	R=0.78*	R=0.78*
MPO, u/mm^2	R=0.62*	R=0.67*	R=0.53*
TNF-α, u/mm^2	R=0.60*	R=0.59*	R=0.57*
DC (h), u.o.i.	R=0.72*	R=0.58*	R=0.72*
KDCT (h), u.o.i.	R=0.71*	R=0.82*	R=0.66*
SB (h), u.o.i.	R=0.52	R=0.17	R=0.88*
DC (i), u.o.i.	R=0.73*	R=0.75*	R=0.92*
KDCT (i), u.o.i.	R=0.81*	R=0.76*	R=0.88*
SB (i), u.o.i.	R=0.81*	R=0.31	R=0.72*
S_{PQM}, au/mg (spont)	R=0.71*	R=0.77*	R=0.89*
S ADNPH, au/mg (spont)	R=0.76*	R=0.68*	R=0.38
S KDNPH, au/mg (spont)	R=0.75*	R=0.86*	R=0.50
S_{PQM}, au/mg (ind)	R=0.86*	R=0.85*	R=0.81*
S ADNPH, au/mg (ind)	R=0.74*	R=0.81*	R=0.45
S KDNPH, AU/mg (ind)	R=0.73*	R=0.75*	R=0.37

** – P<0.01*

Third, vitamin D3 activates reparation processes in the damaged area of the colon in cases of EC. In coordination with specific nuclear receptors of colonic epithelial cells, vitamin D3 intensifies the expression of vinculin, zonulin, occludin and claudin – proteins that take part in the formation of epithelial cells.[16,34,35] Increases in histocyte and fibroblast count in the damaged area indicate active reparation processes in the colonic wall. Furthermore, inhibition of vascular-exudative and leucocyte reactions due to anti-inflammation and antioxidant effect activates the reparation process under the conditions of using vitamin D3.

Conclusion

In cases of oxazolone-induced EC, on Days 2, 4, and 6, we registered clinical and laboratory signs, an ulcerous defect in the damaged area of the colon, all of which are typical for IBD conditions. There was an increase in DAI (peak on Day 6) and TDI (peak on Day 2). We also found an increase in NC (peak on Day 2), LC (peak on Day 6), EC (peak on Day 2), PC (peak on Day 2), HC (peak on Day 2), and FC (peak on Day 2). There was an increase in MPO expression (peak on Day 2) and TNF-α expression (peak on Days 2 and 4). We observed increases in the primary, secondary, and end LPP counts and the early-phase and late-phase POM counts in spontaneous and induced modes. An administration of 1500ME vitamin D3 rectal suppositories every 12 hours for 6 days decreased the severity of clinical manifestations and DAI. It reduced the area of the ulcerous defect and decreased the TDI on Days 4 and 6 of the experiment. On the background of using vitamin D3 rectal suppositories, we found a decrease in NC, EC, LC, and PC in the damaged area and an increase in HC and FC on Days 2, 4, and 6 from the start of the experiment. Administration of D3 rectal suppositories decreased MPO expression and TNF-α expression on Days 4 and 6 of EC. In the damaged area of the colon, we observed a decrease in the counts of the primary, secondary, and end LPP on Days 4 and 6 of the experiment. We also documented a decrease in the POM count in spontaneous mode on Day 2 and on Day 6 in induced mode. The severity of EC clinical manifestations diminished, as did TDI, size of the ulcerous defect, MPO and TNF-α in the damaged area, and protein and lipid oxidative breakdown products.

We believe that the obtained results are essential for carrying out further research aimed at elaboration of the mechanism of the D3 effect in cases of IBD and at its possible clinical use.

Competing Interests

The authors declare that they have no competing interests.

References

1. Knyazev OV, Shkurko TV, Kagramanova AV, Veselov AV, Nikonov EL. [Epidemiology of inflammatory bowel disease. The current state of the problem (Literature review)]. Evidence-Based Gastroenterology. 2020;9(2):66–73. doi: 10.17116/dokgastro2020902166. [Article in Russian].
2. Mak WY, Zhao M, Ng SC, Burisch J. The epidemiology of inflammatory bowel disease: East meets west. J Gastroenterol Hepatol. 2020 Mar;35(3):380-389. doi: 10.1111/jgh.14872.
3. Dolgushina AI, Khusainova GM, Vasilenko AG, Kononets VA. [The prevalence of inflammatory bowel disease in the Chelyabinsk region]. Almanac of Clinical

Medicine. 2019;47(6):511-517. doi:10.18786/2072-0505-2019-47-066. [Article in Russian].
4. Tohari AM, Alhasani RH, Biswas L, Patnaik SR, Reilly J, Zeng Z, Shu X. Vitamin D Attenuates Oxidative Damage and Inflammation in Retinal Pigment Epithelial Cells. Antioxidants (Basel). 2019 Aug 24;8(9):341. doi: 10.3390/antiox8090341.
5. Kopecki Z, Yang G, Treloar S, Mashtoub S, Howarth GS, Cummins AG, Cowin AJ. Flightless I exacerbation of inflammatory responses contributes to increased colonic damage in a mouse model of dextran sulphate sodium-induced ulcerative colitis. Sci Rep. 2019 Sep 5;9(1):12792. doi: 10.1038/s41598-019-49129-6.
6. Sitkin SI, Vakhitov TY, Demyanova EV. [The microbiome, colon dysbiosis, and inflammatory bowel disease: when function is more important than taxonomy]. Almanac of Clinical Medicine. 2018;46(5):396–425. doi:10.18786/2072-0505-2018-46-5-396-425. [Article in Russian].
7. Ungaro R, Mehandru S, Allen PB, Peyrin-Biroulet L, Colombel JF. Ulcerative colitis. Lancet. 2017 Apr 29;389(10080):1756-1770. doi: 10.1016/S0140-6736(16)32126-2.
8. Yokoyama Y, Kamikozuru K, Nakamura S. Granulomonocytapheresis as a cell-based therapy in an ulcerative colitis patient complicated by aminosalicylate-induced severe lymphocytopenia and pneumonia. Cytotherapy. 2016 Sep;18(9):1234-6. doi: 10.1016/j.jcyt.2016.05.016.
9. Ivashkin VT, Shelygin YA, Khalif IL, Belousova EA. [Clinical recommendations of the Russian gastroenterological association and the association of coloproctologists of Russia for the diagnosis and treatment of ulcerative colitis]. Coloproctology. 2017;1(59):6-30. [Article in Russian].
10. Šimoliūnas E, Rinkūnaitė I, Bukelskienė Ž, Bukelskienė V. Bioavailability of Different Vitamin D Oral Supplements in Laboratory Animal Model. Medicina (Kaunas). 2019 Jun 10;55(6):265. doi: 10.3390/medicina55060265.
11. Yamamoto E, Jørgensen TN. Immunological effects of vitamin D and their relations to autoimmunity. J Autoimmun. 2019 Jun;100:7-16. doi: 10.1016/j.jaut.2019.03.002.
12. Bakke D, Sun J. Ancient Nuclear Receptor VDR With New Functions: Microbiome and Inflammation. Inflamm Bowel Dis. 2018 May 18;24(6):1149-1154. doi: 10.1093/ibd/izy092.
13. Harrison SR, Li D, Jeffery LE, Raza K, Hewison M. Vitamin D, Autoimmune Disease and Rheumatoid Arthritis. Calcif Tissue Int. 2020 Jan;106(1):58-75. doi: 10.1007/s00223-019-00577-2.
14. Liu J, Wang W, Liu K, Wan D, Wu Z, Cao Z, Luo Y, Xiao C, Yin M. Vitamin D receptor gene polymorphisms are associated with psoriasis susceptibility and the clinical response to calcipotriol in psoriatic patients. Exp Dermatol. 2020 Dec;29(12):1186-1190. doi: 10.1111/exd.14202.
15. Del Pinto R, Ferri C, Cominelli F. Vitamin D Axis in Inflammatory Bowel Diseases: Role, Current Uses and Future Perspectives. Int J Mol Sci. 2017 Nov 7;18(11):2360. doi: 10.3390/ijms18112360.
16. Naderpoor N, Mousa A, Fernanda Gomez Arango L, Barrett HL, Dekker Nitert M, de Courten B. Effect of Vitamin D Supplementation on Faecal Microbiota: A Randomised Clinical Trial. Nutrients. 2019 Nov 27;11(12):2888. doi: 10.3390/nu11122888.
17. Simonyan EV, Osikov MV, Boyko MS, Bakeeva AE. Remedy with vitamin D3 for the treatment of ulcerative colitis in the form of rectal suppositories. Patent RU, No. 2709209. 2019. Bull. #35.
18. Osikov MV, Boyko MS, Simonyan EV, Ushakova VA. [Immunotropic effects of vitamin D3 in original rectal suppositories in experimental ulcerative colitis]. Medical Immunology (Russia). 2021;23(3):497-508. doi: 10.15789/1563-0625-IEO-2176. [Article in Russian].
19. Directive 2010/63/EU of the European Parliament and of the Council of September 22, 2010, on the Protection of Animals Used for Scientific Purposes 2010. Official Journal of the European Union. L 276/33. Available from: https://eur-lex.europa.eu/eli/dir/2010/63/oj.
20. Hoving JC, Keeton R, Höft MA, Ozturk M, Otieno-Odhiambo P, Brombacher F. IL-4 Receptor-Alpha Signalling of Intestinal Epithelial Cells, Smooth Muscle Cells, and Macrophages Plays a Redundant Role in Oxazolone Colitis. Mediators Inflamm. 2020 Jan 17;2020:4361043. doi: 10.1155/2020/4361043.
21. Osikov MV, Boyko MS, Simonyan EV. [The severity of the acute phase reaction to the use in experimental ulcerative colitis under D3 conditions in original rectal suppositories]. Pathological Physiology and Experiment. 2021;65(4):80–88. doi: 10.25557/0031-2991.2021.04.80-88. [Article in Russian].
22. Kim JJ, Shajib MS, Manocha MM, Khan WI. Investigating intestinal inflammation in DSS-induced model of IBD. J Vis Exp. 2012 Feb 1;(60):3678. doi: 10.3791/3678.
23. Yao J, Lu Y, Zhi M, Hu P, Wu W, Gao X. Dietary n-3 polyunsaturated fatty acids ameliorate Crohn's disease in rats by modulating the expression of PPAR-γ/NFAT. Mol Med Rep. 2017 Dec;16(6):8315-8322. doi: 10.3892/mmr.2017.7673.
24. Volchegorskiĭ IA, Nalimov AG, Iarovinskiĭ BG, Lifshits RI. [Comparison of various approaches to the determination of the products of lipid peroxidation in heptane-isopropanol extracts of blood]. Vopr Med Khim. 1989 Jan-Feb;35(1):127-31. [Article in Russian].
25. Lvovskaya EI, Volchegorsky IA, Shemyakov SE, Lifshits RI. [Spectrophotometric determination of LPO end products]. Voprosy Meditsinskoi Khimii. 1991;4:92–93. [Article in Russian].
26. Dubinina EE. Products of oxygen metabolism in the functional activity of cells (life and death, creation and destruction). Physiological and clinical-biochemical aspects. SPb.: "Medical press", 2006. [In Russian].
27. Fomina MA. A method for a comprehensive assessment of the content of products of oxidative modification of proteins in tissues and biological fluids: Guidelines. Ryazan, 2014. [In Russian].

***Corresponding author:** Margarita S. Boyko. South Ural State Medical University, Chelyabinsk, Russia. E-mail: ri-tochka9@list.ru*

28. Larabi A, Barnich N, Nguyen HTT. New insights into the interplay between autophagy, gut microbiota and inflammatory responses in IBD. Autophagy. 2020 Jan;16(1):38-51. doi: 10.1080/15548627.2019.1635384.
29. Lynch WD, Hsu R. Ulcerative Colitis. 2021 Jun 18. In: StatPearls [Internet]. Treasure Island (FL): StatPearls Publishing; 2022 Jan–. PMID: 29083748.
30. Tian T, Wang Z, Zhang J. Pathomechanisms of Oxidative Stress in Inflammatory Bowel Disease and Potential Antioxidant Therapies. Oxid Med Cell Longev. 2017;2017:4535194. doi: 10.1155/2017/4535194.
31. De Schepper S, Stakenborg N, Matteoli G, Verheijden S, Boeckxstaens GE. Muscularis macrophages: Key players in intestinal homeostasis and disease. Cell Immunol. 2018 Aug;330:142-150. doi: 10.1016/j.cellimm.2017.12.009.
32. Murdaca G, Tonacci A, Negrini S, Greco M, Borro M, Puppo F, Gangemi S. Emerging role of vitamin D in autoimmune diseases: An update on evidence and therapeutic implications. Autoimmun Rev. 2019 Sep;18(9):102350. doi: 10.1016/j.autrev.2019.102350.
33. Teixeira TM, da Costa DC, Resende AC, Soulage CO, Bezerra FF, Daleprane JB. Activation of Nrf2-Antioxidant Signaling by 1,25-Dihydroxycholecalciferol Prevents Leptin-Induced Oxidative Stress and Inflammation in Human Endothelial Cells. J Nutr. 2017 Apr;147(4):506-513. doi: 10.3945/jn.116.239475.
34. Fakhoury HMA, Kvietys PR, AlKattan W, Anouti FA, Elahi MA, Karras SN, Grant WB. Vitamin D and intestinal homeostasis: Barrier, microbiota, and immune modulation. J Steroid Biochem Mol Biol. 2020 Jun;200:105663. doi: 10.1016/j.jsbmb.2020.105663.
35. Charoenngam N, Holick MF. Immunologic Effects of Vitamin D on Human Health and Disease. Nutrients. 2020 Jul 15;12(7):2097. doi: 10.3390/nu12072097.

International Journal of Biomedicine 12(1) (2022) 134-137
http://dx.doi.org/10.21103/Article12(1)_OA14

ORIGINAL ARTICLE

Experimental Medicine

INTERNATIONAL JOURNAL OF BIOMEDICINE

Experimental Substantiation of Application of Autoplasma to Reduce Inflammatory Response to Implants in Herniology

Serhiy H. Hryvenko[1], MD, PhD, ScD[*]; Yuriy A. Semenov[1], MD; Mariia A. Behma[2]; Abhijit Mahanta[1], MD, MS; Tamila E. Usmanova[1], MD, PhD; Andrej A. Dovgan[1], MD, PhD

[1]*Medical Academy named after S.I. Georgievsky of Vernadsky CFU, Simferopol, Crimea*
[2]*National Pirogov Memorial Medical University, Vinnytsya, Ukraine*

Abstract

The article represents an experimental assessment of the effectiveness of the author's method of processing polypropylene mesh implants during their implantation in the tissue of the anterior abdominal wall (Patent of Ukraine No. 146133). It has been demonstrated that the use of the proposed new technology for processing polypropylene mesh implants with a biocompatible component, being a simple, safe, and effective method, optimizes reparative processes in the peri-implantation zone without deteriorating the mechanical properties of mesh implants (MI). All the discovered effects make it possible to increase biocompatibility and improve the survival rate of MI. The thickness of the inflammatory shaft around the elements of MI was significantly decreased, on average, by 28.4% (P<0.05) when using autogenous blood plasma. (**International Journal of Biomedicine. 2022;12(1):134-137.**)

Key Words*:* polypropylene • anterior abdominal wall • mesh implants • autogenous blood plasma

For citation: Hryvenko SH, Semenov YuA, Begma MA, Mahanta A, Usmanova TE, Dovgan AA. Experimental Substantiation of Application of Autoplasma to Reduce Inflammatory Response to Implants in Herniology. International Journal of Biomedicine. 2022;12(1):134-137. doi:10.21103/Article12(1)_OA14

Abbreviations

ABP, autogenous blood plasma; **PP**, polypropylene; **AAW**, anterior abdominal wall; **MI**, mesh implants; **IC**, inflammatory changes.

Introduction

In the arsenal of surgeons, more than 300 types of mesh implants (MI) are currently used. It remains unclear why bioinert synthetic materials cause a pronounced inflammatory tissue reaction known as a foreign body reaction.[1-3] One of the main reasons for the development of periprosthetic complications is that the process of MI adaptation in soft tissues is violated as a result of poor biocompatibility and impaired formation of the periprosthetic capsule.[4-6]

Despite the fact that of the materials available in herniology, polypropylene (PP) most fully meets the requirements for anterior abdominal wall (AAW) prosthesis, it has a significant drawback – the ability to cause a pronounced inflammatory reaction from periprosthetic tissues with a predominance of the exudative-infiltrative component.[2,3] In this regard, there is a need to develop MI that cause a slight inflammatory reaction, provided that satisfactory characteristics of strength and production cost are maintained. Experimental data have appeared on the use of PP ligatures after preliminary treatment with a solution of serum albumin during implantation into muscles and for the formation of vascular anastomoses.[7] According to the researchers, this technique led to a significant decrease in the severity of aseptic inflammation around the ligatures, which made it possible to recommend it for clinical

***Corresponding author:** Serhiy H. Hryvenko, MD, PhD, ScD. Medical Academy named after S.I. Georgievsky of Vernadsky CFU, Simferopol, Crimea. E-mail: hryva@mail.ru*

use.[8] This phenomenon has been termed "suture mimicry."[7] And since PP-MI are made from the same chemical as the PP ligatures, it is advisable to study the local inflammatory response to implantation of MI treated with ABP.

The purpose of this study was experimental substantiation of the possibility and feasibility of using autogenous plasma treatment with PP-MI to reduce the manifestations of a local inflammatory reaction.

Materials and Methods

The study was carried out on 24 white nonlinear male rats weighing 200–250g. The animals were kept in the vivarium of the Department of Human Anatomy of the Medical Academy named after V.I. SI Georgievsky in compliance with the rules and international recommendations of the European Convention for the Protection of Animals (1997). The experiment was carried out in compliance with the norms of humane treatment, in accordance with the current legislation on working with laboratory animals, and was approved by the local commission on bioethics.

All animals, under ether anesthesia, were implanted with PP-MI in the AAW tissue. PP mesh "Alfa Vita 90" (Ukraine) in strips up to 1cm² was used as MI. The material was fixed in the AAW tissues with a nylon ligature from four sides. Then the wound was sutured and the integrity of the AAW was restored. The animals were divided into two groups. The main group (MG, n=12) consisted of animals that were implanted with PP-MI after treatment with ABP.[9] The latter was prepared traditionally. The exposure time was 10 minutes. The control group (CG, n=12) consisted of animals that were implanted with MI without pretreatment.

The animals were withdrawn from the experiment on Days 7, 14, 21, and 28 after implantation. After fixation in 10% neutral formaline, histological sections were prepared from the preparations according to the standard technique. Sections were stained with H&E, followed by histological and histomorphometric examination.

The results were evaluated using the Master of Morphology and SPSS computer programs.

Results

According to the data of the study, by Day 7 of the experiment animals of the CG showed a pronounced penetration of leukocytes along the circumference of the PP particles of MI. At the same time, the ontogenesis of granulation tissue along the peripheral areas was observed, accompanied by sporadic lymphocytes and histiocytes (Figure 1). When measuring the thickness of inflammatory changes (IC) in the circumference of the PP-MI fragments, this indicator was 41.607±0.279 μm (Table 1). In the MG in the same period of the experiment, leukocyte infiltration was expressed to a much lesser extent. Lymphocytes, leukocytes and histiocytes were equally represented. The natural growth of granulation tissue was formed (Figure 2). The thickness of IC in the circumference of the PP-MI fragments was 27.497±0.169 μm.

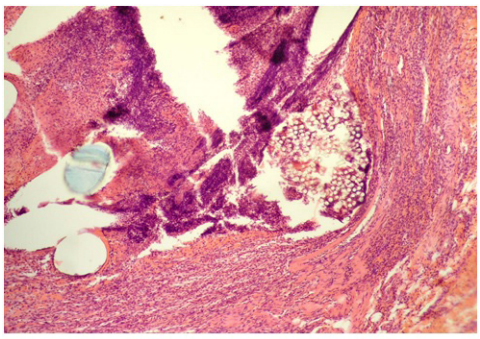

Fig. 1. *AAW of the CG animal by Day 7 of the experiment. Staining with H&E. ×10*

Table 1.

The thickness of inflammatory changes (IC) in the circumference of the PP-MI fragments (μm)

Day of the experiment	CG	MG	*P*-value
Day 7	41,607±0,279	27,497±0,169	0.000
Day 14	46,724±0,310	25,138±0,055	0.000
Day 21	40,012±0,283	23,351±0,102	0.000
Day 28	31,068±0,270	22,247±0,133	0.000

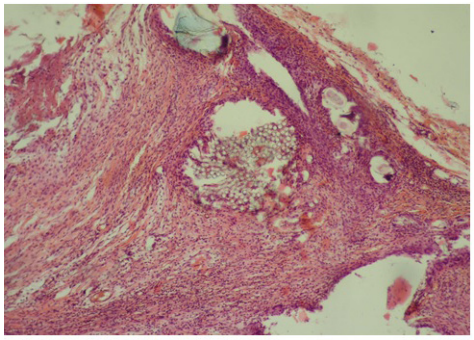

Fig. 2. *AAW of the MG animal by Day 7 of the experiment. Staining with H&E. ×10*

By Day 14 of the experiment, the animals of the CG were diagnosed with a decrease in the population of leukocytes and an increase in the number of histiocytes and lymphocytes. At the same time, sporadic siderophages were visualized, as well as giant cells of phagocytosis (Figure 3). The thickness of IC in the circumference of the PP-MI fragments was 46.724±0.310 μm. In the MG, in contrast to the CG, there was no progress in leukocyte infiltration. At the same time, giant cells of phagocytosis were not diagnosed near the PP-MI (Figure 4). The thickness of IC in the circumference of the PP-MI fragments was 25.138±0.055 μm.

By Day 21, in the CG, the inflammatory manifestations were more pronounced than in the MG. Giant cells of phagocytosis were detected near the PP-MI particles (Figure 5). The thickness of IC in the circumference of the PP-MI fragments was 40.012±0.283 μm. In the MG, giant cells of phagocytosis were also visualized. They frame the fibers of the

PP-MI yarns. In comparison with the CG, the inflammation was much less pronounced (Figure 6). The thickness of IC in the circumference of the PP-MI fragments was 23.351±0.102 μm.

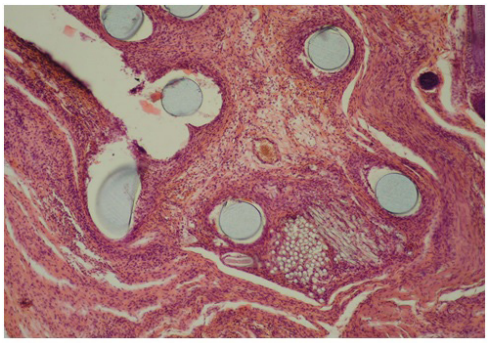

Fig. 3. *AAW of the CG animal by Day 14 of the experiment. Staining with H&E. ×10*

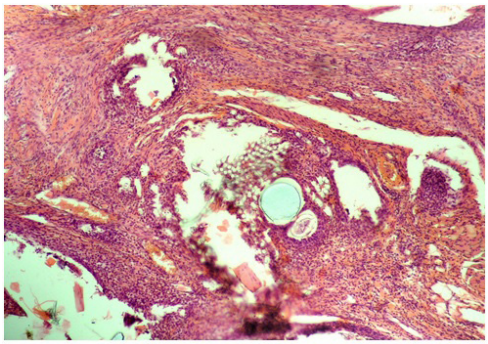

Fig. 4. *AAW of the MG animal by Day 14 of the experiment. Staining with H&E. ×10*

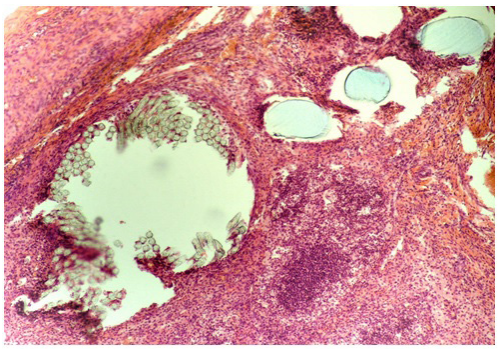

Fig. 5. *The fragment of AAW of the CG animal with elements of PP-MI. Day 21 of the experiment. Staining with H&E. ×10*

By Day 28, in the CG, intense inflammation continued to be recorded near the PP-MI filaments. Both neutrophils and lymphocytes with giant cells of phagocytosis, as well as macrophages, were visualized, as well as a significant number of siderophages (Figure 7). The thickness of IC in the circumference of the PP-MI fragments was 31.068±0.270 μm. In the MG, inflammatory processes were weakened and leukocytes were visualized, as were histiocytes, which, along with lymphocytes, were evenly represented. A fair number of giant cells of phagocytosiswere diagnosed along the circumference of the PP-MI components (Figure 8). In this case, there was a natural growth of granulation tissue. The thickness of IC in the circumference of the PP-MI fragments was 22.247±0.133 μm.

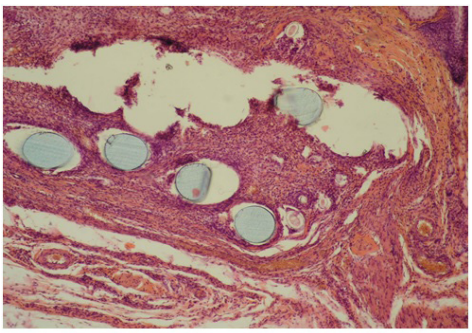

Fig. 6. *The fragment of AAW of the MG animal with elements of PP-MI. Day 21 of the experiment. Staining with H&E. ×10*

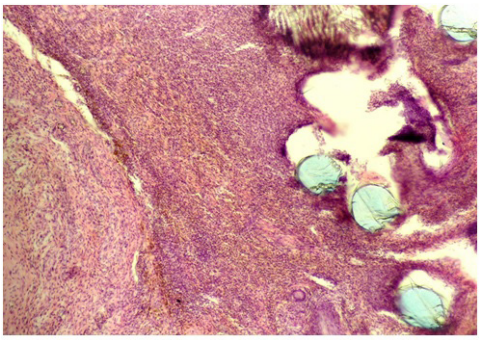

Fig. 7. *The fragment of AAW of the CG animal with elements of PP-MI. Day 28 of the experiment. Staining with H&E. ×10*

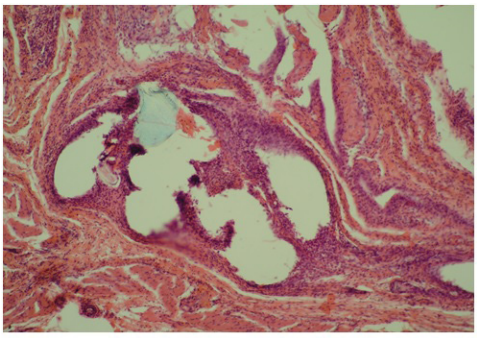

Fig. 8. *The fragment of AAW of the MG animal with elements of PP-MI. Day 28 of the experiment. Staining with H&E. ×10*

Discussion

Thus, the presented results of histological and morphometric studies confirm the fact that implantation of PP-MI causes a local aseptic inflammatory response. However, its intensity differed significantly in different experimental groups of animals at all periods of the experiment. The

greatest local aseptic inflammatory response to the implantation of PP-MI was observed in the CG, and this was true for all periods of observation. To a much lesser extent, the inflammatory reaction was observed in the animals of the MG. Thus, the technological method of treating PP-MI with an anti-inflammatory agent was experimentally substantiated; the agent proposed was ABP. The results of the conducted microscopic studies show the effectiveness of the proposed technology to reduce the local inflammatory response during the implantation of the MI-PP in the AAW tissue. The author's method for treating PP-MI with an anti-inflammatory agent can find application in herniological practice, since it is easily reproducible, and its implementation does not impose serious material requirements. Nevertheless, legal aspects remain cardinal barriers for the subsequent clinical use of the method proposed in the experiment, namely, obtaining permits (licenses) for their clinical trials.

In conclusion, treating PP-MI with ABP creates favorable conditions for their full integration into the muscular-aponeurotic layer of the AAW tissues. The thickness of the inflammatory shaft around the elements of MI is significantly decreased, on average, by 28.4% (P<0.05) when using ABP.

Competing Interests

The authors declare that they have no competing interests.

References

1. Nyhus LM, Schumpelick V. Meshes: benefits and risks. Berlin: Springer Berlin Heidelberg; 2004. p. 161–169.

2. Beets GL, Go PM, van Mameren H. Foreign body reactions to monofilament and braided polypropylene mesh used as preperitoneal implants in pigs. Eur J Surg. 1996 Oct;162(10):823-5.

3. Matyja A, Solecki R, Heitzman J. Local reaction to polypropylene mesh - histopatological findings. In: Hernia recurrences. Proceedings of the 26 International congress of the European Hernia Society. Hernia Recurrences. Praga; 2004.

4. Parfenov IP, Yarosh AL, Soloshenko AV, Bitenskaya EP. [Biocompatibility of the synthetic materials applied in abbominal wall hernia surgery]. Nauchnye vedomosti Belgorodskogo gosudarstvennogo universiteta. Seriya: Medicina. Farmaciya. 2010;12(22):5–13. [Article in Russian].

5. Bogdan VG. [Morphological and clinical features endoprosthesis use in surgery incisional abdominal hernias]. Voennaya medicina. 2015;2(35):14–17. [Article in Russian].

6. Dolzhikov AA, Kolpakov AYa, Yarosh AL, Molchanova AS, Dolzhikova IN. [Giant foreign body cells and tissue reactions on the surface of implants]. Man and His Health. 2017;(3):86–94. doi:10.21626/vestnik/2017-3/15 [Article in Russian].

7. Alekseyeva TA, Beregovoy OV, Gomolyako IV, Lazarenko ON, Yashchuk YuI. Mimicry of the suture material to the patient's body. Klinicheskaia Khirurgiia. 2011;11:3. [Article in Russian].

8. Alekseyeva TA, Beregovoy OV, Borovik DV, Galich SP, Gomolyako IV, Lazarenko ON. [Adaptation of surface of implants towards a recipient tissues]. Klinicheskaia Khirurgiia. 2014;3:52–55. [Article in Russian].

9. Hryvenko SH, Pikalyuk VS, Semenov YuA, Begma MA inventors; Hryvenko SH, Pikalyuk VS, Semenov YuA, Begma MA assignees. Method of surface treatment of polypropylene implants to improve the characteristics of their bioscompatible properties. Ukraine patent UA 146133.2021 January 20. [In Ukrainian].

International Journal of Biomedicine 12(1) (2022) 138-141
http://dx.doi.org/10.21103/Article12(1)_OA15

ORIGINAL ARTICLE

Experimental Medicine

INTERNATIONAL JOURNAL OF BIOMEDICINE

Comparative Evaluation of Isolated and Complex Use of Hexetidine and Photoditazine in Combination with Ultrasound Therapy in the Treatment of Purulent Wounds under Experimental Conditions

Ivan S. Dragovoz, Dmitry S. Zotov, Maria A. Zatolokina*, Arsen Yu. Grigoryan, Ekaterina S. Mishina, Vadim V. Tsymbalyuk

Kursk State Medical University, Kursk, Russia

Abstract

Background: Currently, despite the significant success of the pharmaceutical industry in producing drugs with antibacterial activity, the treatment of soft tissue diseases accompanied by purulent-inflammatory processes within them remains one of the topical problems of general surgery. Not only the widespread introduction of antibacterial agents in practical medicine, but also the steady increase in the resistance of microorganisms to existing drugs leads to the need to search for new combinations aimed at the local treatment of purulent wounds. The purpose of our work was to study the course of the wound process in a purulent wound by using hexetidine and photoditazine in combination with ultrasound treatment.

Methods and Results: This experimental study was carried out on 144 male Wistar rats. The course of the wound process was evaluated on a model of a purulent wound. The animals were divided into 4 equal groups (36 animals in each group), depending on their treatment. Treatment was carried out using daily dressings for 15 days. The dynamics of changes in the area of the wound were assessed by the planimetry method. The percentage of area reduction of the wound was calculated. A histological examination of a skin area (1.0 cm×1.5 cm) taken in the zone of a simulated purulent wound was carried out on Days 5 and 10 of the experiment. Our study confirmed the effectiveness of the use of hexetidine, photoditazine, and a combination of them, along with ultrasound treatment, in the local treatment of a purulent wound. At the same time, the combined effect of an antiseptic and a photosensitizer showed significantly better results in the first and second phases of the course of the wound process than did their isolated use.(**International Journal of Biomedicine. 2022;12(1):138-141.**)

Key Words: purulent wound • hexetidine • photoditazine • ultrasound therapy • methylcellulose

For citation: Dragovoz IS, Zotov DS, Zatolokina MA, Grigoryan AYu, Mishina ES, Tsymbalyuk VV. Comparative Evaluation of Isolated and Complex Use of Hexetidine and Photoditazine in Combination with Ultrasound Therapy in the Treatment of Purulent Wounds under Experimental Conditions. International Journal of Biomedicine. 2022;12(1):138-141. doi:10.21103/Article12(1)_OA15

Abbreviations

UST, ultrasound treatment; **MC**, methylcellulose; **H**, hexetidine; **PD**, photoditazine; **DMTHP**, dioxomethyltetrahydropyrimidine; **CP**, chloramphenicol.

Introduction

At present, the question of treating the purulent-inflammatory process of soft tissues is one of the most urgent. Despite the vast range of treatment options for this process, purulent-inflammatory diseases occupy a leading position. They account for 30%-45% of the conditions and complications in surgical patients, both outpatient and inpatient.[1,2] This problem is associated with the uncontrolled use of antibiotics and the emergence of resistant microorganisms.[3,4] Therefore, at present, interest has increased in antiseptics and photosensitizers, which have proven themselves in the treatment of purulent wounds while not causing resistance in microorganisms.[5] However, despite the variety of different means of treatment, the number

of patients with purulent-inflammatory diseases of soft tissues is not decreasing.[6] In this regard, there is a need to use the latest treatment methods, using physical factors of influence. One of these methods is UST, which has not only a bactericidal and bacteriostatic effect on microorganisms, but also enhances the effect of antiseptics.[7,8] Thus, the search for and development of the most optimal combination of a drug with ultrasound therapy is an urgent and priority task in modern surgery.

The purpose of our work was to study the course of the wound process in a purulent wound by using hexetidine and photoditazine in combination with ultrasound treatment.

Materials and Methods

This experimental study was carried out on 144 male Wistar rats. The course of the wound process was evaluated on a model of a purulent wound.

In vivo experiments were carried out in compliance with the norms of humane treatment, in accordance with the current legislation on working with laboratory animals, and was approved by the Ethics Committee of the Kursk State Medical University (Protocol No. 7 dated November 30, 2018).

The purulent wound (at the withers, with an area about 150 mm^2) was modeled according to P. Tolstykh,[3] in an operating room under isoflurane inhalation anesthesia. Next, a gauze ball soaked in 1 ml of the billionth suspension of *Staphylococcus aureus* was introduced into the wound and sutured. After 24 hours, all animals developed a purulent wound with all the characteristic signs (hyperemia and swelling of the skin around the defect, purulent discharge from the wound). Then the animals were divided into 4 equal groups (36 animals in each group), depending on their treatment: Group 1 (MC[2.0g]+H[0.5g]+UST), Group 2 (MC[2.0g]+PD[1.0g]+UST), Group 3 (MC[2.0 g]+H[0.5g]+PD[1.0g]+UST), and Group 4 (official drug (DMTHP[0.04g]+CP[0.0075g]-ointment)+UST). Treatment was carried out for 15 days. Dressings were performed daily with the study combination. In Groups 2 and 3, daily phototherapy was carried out using the Nevoton apparatus (Nevoton LLC, Russia) (the wavelength of light radiation was 650–670nm). UST was carried out daily, starting from Day 4 after the experiment, using a dual-frequency device (UZT - 1.3.01F - "Med TeKo") in this study, a frequency of 2.64±0.03 MHz was used, the oscillation intensity was 1.0W/cm^2. The duration of each therapeutic exposure was 5 minutes. The dynamics of changes in the area of the wound were assessed by the planimetry method. The percentage of area reduction (PAR) of the wound was calculated according to the formula:

PAR= (W1-Wx)/W1×100%, where W1 is the initial wound area (mm^2), Wx is the area on measurement day (mm^2).

A histological examination of a skin area (1.0 cm×1.5 cm) taken in the zone of a simulated purulent wound was carried out on Days 5 and 10 of the experiment. Light microscopy of the preparations obtained was carried out using a Levenhuk C320 microscope at ×200 and ×400 magnifications, microphotography was performed with a Levenhuk C310 NG digital camera.

Statistical analysis was performed using Microsoft Excel 2010. For descriptive analysis, results are presented as median (Me), first quartile (Q1) and third quartile (Q3). A non-parametric Kruskal-Wallis test was used for comparisons of median values among study groups, followed by post-hoc testing using un-paired Mann-Whitney U tests. A probability value of $P<0.05$ was considered statistically significant.

Results

The study showed that in all observation groups, there was a decrease in the area of the wound surface throughout the entire period of treatment. In Groups 2 and 3, with the use of the photosensitizer the wound was completely healed by day 15. The dynamics of these changes is presented in Table 1.

Table 1.

Dynamics of changes in the area of wounds (PAR, %) (Me (Q_1; Q_3))

Group	Group 1	Group 2	Group 3	Group 4
Day 3 (n=30)	12.2 (8.6; 15.2)*	13.1 (11.9; 14.7)*	35.9 (27.2; 41.6)*^#	8.7 (6.1; 10.6)
Day 5 (n=24)	25.3 (23; 28.1)*	22.8 (21.8; 25.2)*	57.6 (54.9; 63.2)*^#	15.7 (12.8; 17.1)
Day 8 (n=18)	66 (63.7; 66.9)*	48.4 (45; 52.8)	82.7 (80.5; 83.9)*^#	41.7 (38.8; 43.2)
Day 10 (n=12)	80.2 (77.0; 83)*	91.2 (90.4; 91.9)*	97.3 (96.8; 97.3)*^	60.5 (58.7; 64.5)
Day 15 (n=6)	93.7 (93.4; 95.1)*	-	-	81.3 (81.2; 82.1)

*n - Number of animals at the time of the measurement; *– P<0.05 between Group 4 and Groups 1-3; ^– P<0.05 between Group 1 and Groups 2 and 3; # – P<0.05 between Group 2 and Group 3.*

The microscopic examination showed that in **Group 1,** on Day 5 of the experiment (Fig.1A), the outside of the wound defect was covered with a wide scab, the material substrate of which was necrotic masses and fibrin deposits. The tissues surrounding the wound defect showed signs of interstitial edema. Round cell infiltration was visualized far beyond the boundaries of the wound defect. The field of view was dominated by neutrophils and macrophages, which, in turn, are the main structural elements of the leukocyte shaft that delimits the granulation tissue; in the thickness of that shaft, cells of the leukocyte-lymphocytic series were visualized.

On Day 10 (Fig.1B), the wound area was completely covered with stratified squamous keratinized epithelium of heterogeneous thickness throughout the wound defect. The newly formed connective tissue was not mature enough; the border with the intact dermis was well defined. In the field of view, the cellular component predominated over the fibrous component.

In Group 2, on Day 5 of the experiment (Fig.1C), deposits of necrotic and fibrinoid masses were visualized in the area of the wound defect, under which an extensive zone of hemorrhagic impregnation of tissues was determined, separated, in turn, by a leukocyte shaft from the newly formed

granulation fabrics. The infiltration zone was extensive and extended to the muscle tissue. Histiocytic cells were visualized in the field of view. In the bottom of the wound, we observed local accumulations of macrophages and the initial stages of the formation of multinucleated cells.

On Day 10 (Fig.1D), epithelialization of the wound was observed in the form of marginal creeping of the stratified squamous keratinizing epithelium from the side of the lateral edges of the wound defect of the skin inwards. Complete epithelialization was not observed by this time. Outside of the newly formed epidermis, scab elements (necrotic and fibrin deposits) continued to be visualized. The newly formed epithelium was thin without a clear structural organization of the layers and the complete absence of the stratum corneum. There was a clearly defined border between the granulation tissue and the intact dermal tissue.

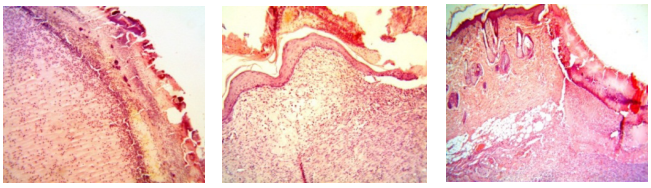

A B C

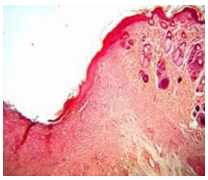

D

Fig. 1. *Micrograph of the skin section in the area of the wound defect. H&E staining, ×100 magnification.*

Group 1: A - on Day 5; B - Day 10.

Group 2: C - on Day 5; D - on Day 10.

In Group 3, on Day 5 of the experiment (Fig.2A), an extensive area of the scab was visualized in the area of the skin defect, the material substrate of which was necrotic masses, fibrin deposits, and cellular detritus. In the area of the newly formed granulation tissue, separated by a leukocytic ridge of the scab, vertically oriented small blood vessels and focal accumulations of adipocytes were determined. The field of view was dominated by inflammatory cells. In the deeper layers of the wound, a macrophage-histiocytic reaction was pronounced.

On Day 10 (Fig.2B), complete epithelialization of the wound defect was observed. The newly formed thin epithelial layer covered the entire area of the wound defect and consisted of well-identified layers of stratified squamous keratinized epithelium. Above the "young" epithelium, elements of the scab containing necrotic masses and degeneratively altered lymphohistiocytic elements continued to be preserved in some areas.

In Group 4, on Day 5 of the experiment (Fig.2C), an extensive zone of round cell infiltration continued to be visualized outside the area of the wound defect. In the newly formed granulation tissue, a large number of vertically oriented blood vessels were determined. The field of view was dominated by the cellular component over the fibrous one.

On Day 10 (Fig.2D), epithelialization of the wound defect of the skin was observed. The wound defect was filled with scar tissue; the fibrous component predominated in the field of view. The border between the cicatricial and intact dermis was well defined, mainly due to the fact that the newly formed fibers were not yet combined into bundles, but were located separately.

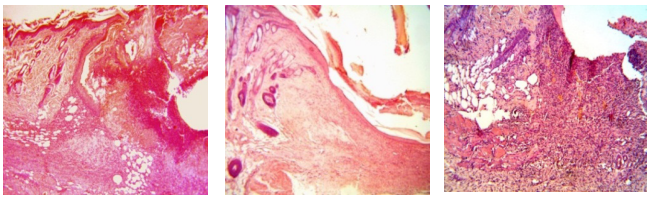

A B C

D

Fig. 2. *Micrograph of the skin section in the area of the wound defect. H&E staining, ×100 magnification.*

Group 3: A - on Day 5; B - Day 10.

Group 4: C - on Day 5; D - on Day 10.

In conclusion, our study confirmed the effectiveness of the use of hexetidine, photoditazine, and a combination of them, along with UST, in the local treatment of a purulent wound. At the same time, the combined effect of an antiseptic and a photosensitizer showed significantly better results in the first and second phases of the course of the wound process than did their isolated use. Thus, this combination of hexetidine with photoditazine can be recommended for further preclinical studies for local treatment of the soft tissue purulent-inflammatory process.

Competing Interests

The authors declare that they have no competing interests.

References

1. Arkhipov DV, Andreev AA, Atyakshin DA, Glukhov AA, Ostroushko AP. [Jet oxygen sorption treatment in the local treatment of purulent wounds of soft tissues]. Bulletin of Experimental and Clinical Surgery. 2020;13(1):41–45. doi:10.18499/2070-478X-2020-13-1-41-45. [Article in Russian].

2. Katorkin SE, Bystrov SA, Lisin OE, Rozanova AA, Bezborodov AI. [Evaluation of the effectiveness of the use of modern dressings in the complex treatment of purulent wounds]. Stationary-Replacing Technologies: Ambulatory Surgery. 2019;1-2:146–152. doi:10.21518/1995-1477-2019-1-2-146-152. [Article in Russian].

3. Bezhin AI, Pankrusheva TA, Zatolokina MA, Grigoryan AYu, Zhilyaeva LV, Kobzareva EV, Mishina ES.

***Corresponding author**: Prof. Mariya A. Zatolokina, PhD, ScD. Department of Histology, Embryology, and Cytology. Kursk State Medical University. Kursk, Russia. E-mail: marika1212@mail.ru*

[Morphological features of wound surface healing when using new preparations based on carboxymethyl cellulose]. Modern Problems of Science and Education. 2015;3. Available from: https://science-education.ru/ru/article/view?id=20333. [Article in Russian].
4. Hoffmann JP, Friedman JK, Wang Y, McLachlan JB, Sammarco MC, Morici LA, et al. *In situ* Treatment With Novel Microbiocide Inhibits Methicillin Resistant *Staphylococcus aureus* in a Murine Wound Infection Model. Front Microbiol. 2020 Jan 23;10:3106. doi: 10.3389/fmicb.2019.03106.
5. Duvansky VA, Eliseenko VI, Shin EF. Influence of photodynamic therapy on the reparative processes of purulent wounds. Proceedings of the 3rd International Congress «Wounds and wound infections.» Moscow;2016:99–100.
6. Belyaeva OA, Luneva AG, Kryzhevsky VV, Karol IV, Zavadetskaya EP, Oleinik EA, Krivenko EA. [Cytological monitoring of the healing of purulent wounds during their treatment using application sorption and NO-therapy. Laboratory diagnostics]. Eastern Europe. 2018;7(3):374–383. [Article in Russian].
7. Muñoz-Sepeda PA, Blatun LA, Paskhalova YuS. The effectiveness of ultrasonic cavitation in the treatment of purulent-necrotic complications of the diabetic foot syndrome. Proceedings of the 4th International Scientific and Practical Congress «Wounds and wound infections.» Moscow;2018:123–124.
8. Conner-Kerr T, Oesterle ME. Current perspectives on therapeutic ultrasound in the management of chronic wounds: a review of evidence. Chronic Wound Care Management and Research. 2017;4:89-98.

International Journal of Biomedicine 12(1) (2022) 142-146
http://dx.doi.org/10.21103/Article12(1)_OA16

ORIGINAL ARTICLE

Adolescent Health

INTERNATIONAL JOURNAL OF BIOMEDICINE

Oxidative Stress Index Levels in Asian Adolescents with Exogenous-Constitutional Obesity

Marina A. Darenskaya, PhD, ScD*; Lyubov V. Rychkova, PhD, ScD; Sergey I. Kolesnikov, PhD, ScD, Member of the RAS; Olga V. Kravtsova, MD; Natalya V. Semenova, PhD, ScD; Anastasia Brichagina; Alexandra Bliznyuk; Natalya Yuzvak; Maria A. Rashidova, PhD; Lyubov I. Kolesnikova, PhD, ScD, Member of the RAS

Scientific Centre for Family Health and Human Reproduction Problems
Irkutsk, the Russian Federation

Abstract

The aim of this research was to evaluate the integral oxidative stress index (OSI) level in Asian girls and boys with exogenous-constitutional obesity.

Methods and Results: A total of 170 Asian adolescents aged 12-18 years were examined: 26 girls and 28 boys with constitutional obesity (main group, MG); 59 girls and 57 boys - healthy adolescents (control group, CG). The levels of lipid peroxidation (LPO) products and antioxidant defense (AOD) parameters were detected using spectrophotometric and fluorometric methods. The level of LPO products and AOD components in the studied groups were assessed to calculate the integral OSI.

Significant increases in the levels of primary LPO products (conjugated dienes by 2.18 times) and secondary LPO products (ketodienes and conjugated trienes by 2.48 times) in the obese Asian girls, compared with the control values, were observed. We found a significant decrease in the parameters of the AOD system in the obese Asian girls, compared with the control values: α-tocopherol (by 1.41 times; P=0.0262), retinol (by 1.12 times; P=0.0306), and SOD activity (by 1.28 times; P=0.0004). In the obese Asian boys, increased values of LPO components were found, compared to controls: conjugated dienes (by 2.13 times; P<0.0001), ketodienes and conjugated trienes (by 3.4 times; P<0.0001), final thiobarbituric acid reactants of LPO (by 1.24 times; P=0.0358). They showed a statistically significant decrease in the level of α-tocopherol (by 1.49 times; P=0.01), compared with the control values. According to the obtained data, OSI in the group of Asian girls with obesity was 15.68 units, in the group of Asian boys with obesity - 22.89 units. The OSI in the group of Asian boys was significantly higher (by 1.46 times; P=0.0492) than in the obese girls.

Conclusion: Certain OSI levels are consistent with the presence of antioxidant insufficiency in exogenous-constitutional obesity and allow us to specify and evaluate the ethnic aspect of the severity of the pathological process more reliably.(**International Journal of Biomedicine. 2022;12(1):142-146.**)

Key Words: adolescents • obesity • lipid peroxidation • oxidative stress index

For citation: Darenskaya MA, Rychkova LV, Kolesnikov SI, Kravtsova OV, Semenova NV, Brichagina A, Bliznyuk A; Yuzvak N, Rashidova MA, Kolesnikova LI. Oxidative Stress Index Levels in Asian Adolescents with Exogenous-Constitutional Obesity. International Journal of Biomedicine. 2022;12(1):142-146. doi:10.21103/Article12(1)_OA16

Abbreviations

AOD, antioxidant defense; **BMI, b**ody mass index; **CDs,** conjugated dienes; **GSH,** reduced glutathione; **GSSG,** oxidized glutathione; **KD-CT,** ketodienes and conjugated trienes; **LPO,** lipid peroxidation; **OS,** oxidative stress; **OSI**, oxidative stress index; **SOD,** superoxide dismutase; **TBARs**, thiobarbituric acid reactants; **WHO,** World Health Organization.

Introduction

Obesity is a chronic disease, heterogeneous according to etiology and clinical data, and has a progressive course, characterized by excessive deposition of adipose tissue in the organism.[1] It has been established that in adolescents with obesity, this diagnosis persists into adulthood in 90% of cases. Various comorbid pathologies are associated with obesity,

including cardiovascular disorders and diabetes mellitus.[2,3] The complications of obesity in childhood and adolescence are no less severe and include disorders of carbohydrate and lipid metabolism, liver morphological changes (fatty hepatosis), arterial hypertension, sexual development disorders, etc.[4]

According to WHO data, about 41 million children under 5 years of age are overweight or obese; 340 million children from 5 to 19 years of age are obese.[1] This trend is equally characteristic for children and adolescents of both sexes.[5] In Russia, more than 500,000 adolescents with obesity have been registered at the present time.[6] There is also a direct correlation between the incidence of obesity and territorial and ethnic factors.[7-11] Thus, the level of adolescent obesity is high in the Volga, Southern, Siberian, Central, and Northwestern Federal Districts.[6] The largest number of obesity cases in rural areas is in the Republic of Adygea, while in the Republic of Mari El, the share of obese children is very low (0.4%).[5] According to the Federal State Statistics Service of the Russian Federation for 2016, the prevalence of obesity in the Siberian Federal District is 14.8 per 1000, in the Republic of Buryatia - 13.8 per 1000, in the Irkutsk region - 18.8 per 1000 population.[12]

The study of the molecular mechanisms of obesity formation in adolescence is topical.[13] One of the pathogenetic mechanisms of obesity is the activation of OS reactions and the decrease of antioxidant defense (AOD) activity.[14-16] The increased content of products of the lipid peroxidation (LPO) process can have a multilateral damaging effect on different cellular structures and contribute to a more severe course of the disease. The calculation of integral index has recently been considered the most optimal way to assess disorders in this system.[10,14] The study of OS reactions in indigenous peoples of the Russian Federation adolescents with obesity is interesting.

The aim of this research was to evaluate the integral oxidative stress index (OSI) level in Asian girls and boys with exogenous-constitutional obesity.

Materials and Methods

A total of 170 Asian adolescents aged 12-18 years were examined: 26 girls and 28 boys with constitutional obesity (main group, MG); 59 girls and 57 boys - healthy adolescents (control group, CG). The WHO classification of obesity in children and adolescents was used.[17] All participants belonged to the Buryat ethnic group and were examined, including anamnestic data collection, physical examination, anthropometric data analysis, laboratory analysis. Body mass index (BMI) was calculated using the Quetelet's formula. The quality, quantity, and regularity of food intake were evaluated. We considered the heredity in relatives of such diseases as type 2 diabetes, obesity, ischemic heart disease, arterial hypertension, and the presence of concomitant diseases. No patients took vitamins during the blood sampling period. Blood was taken from the ulnar vein in accordance with the existing requirements in the morning after an overnight fast.

The study complied with the ethical principles of World Medical Association Declaration of Helsinki (1964, ed. 2013) and it was approved by the Ethic Committee of Scientific Centre for Family Health and Human Reproduction Problems and all patients involved or their parents signed the informed consent agreement to participate in the study.

Blood samples (5 ml) were collected from the ulnar vein in standard vacuum tubes with EDTA. The erythrocyte population was separated from the other blood components by centrifugation at 1500 *g* for 5 min, at 4°C. The erythrocyte pellet was washed 3 times with a 0.9% (wt/vol) NaCl solution. Aliquots of plasma and washed erythrocytes were used immediately or kept frozen at -40°C, not exceeding one month. We estimated the LPO-AOD parameters by plasma concentrations of primary/secondary products of LPO (CDs, KD-CT, and TBARs) and *antioxidant parameters* (SOD activity, GSH, GSSG, α-tocoferol, and retinol). The concentration of CDs and KD-CT was detected at 232nm in plasma heptane extracts.[18] For conversion of absorption units to μmol/L, we used the coefficient of molar absorption ($K=2.2\cdot10^5 M^{-1}C^{-1}$). TBARs levels were detected by fluorometry[19] and estimated in μmol/L. α-tocopherol and retinol levels were detected in plasma by fluorometry. Plasma levels of GSH, GSSG, α-tocopherol and retinol, as well as SOD activity in hemolysate were detected by fluorometry.[20-22] The measurements were conducted with a Shimadzu RF-1501 spectrophotometer (Japan) consisting of two blocks: a UV-1650PC spectrophotometer and a RF-1501 spectrofluorimeter. The level of LPO products and AOD components in the studied groups were assessed to calculate the integral OSI.[14] To measure the intensity of OS, the integral OSI) was calculated (the ratio of the LPO-AOD system indicators in the MG to average indicators in the CG).

Statistical analysis was performed using the Statistica 8.0 software package (Stat-Soft Inc., USA). For descriptive analysis, results are presented as mean±standard deviation (SD). For data with normal distribution, inter-group comparisons were performed using Student's t-test. Differences of continuous variables departing from the normal distribution, even after transformation, were tested by the Mann-Whitney *U*-test. A probability value of $P<0.05$ was considered statistically significant.

Results and Discussion

The level of LPO products and AOD components in the studied groups were assessed to calculate the integral OSI.

Significant increases ($P<0.0001$) in the levels of primary LPO products (CDs by 2.18 times) and secondary LPO products (KD-CT by 2.48 times) in the obese Asian girls, compared with the control values, were observed (Figure 1). We found a significant decrease in the parameters of the AOD system in the obese Asian girls, compared with the control values: α-tocopherol (by 1.41 times; $P=0.0262$), retinol (by 1.12 times; $P=0.0306$), and SOD activity (by 1.28 times; $P=0.0004$) (Figure 1).

In the obese Asian boys, increased values of LPO components were found, compared to controls: CDs (by 2.13 times; $P<0.0001$), KD-CT (by 3.4 times; $P<0.0001$), final TBA-active products of LPO (by 1.24 times; $P=0.0358$) (Figure 2). They showed a statistically significant decrease

in the level of α-tocopherol (by 1.49 times lower; *P*=0.01), compared with the control values.

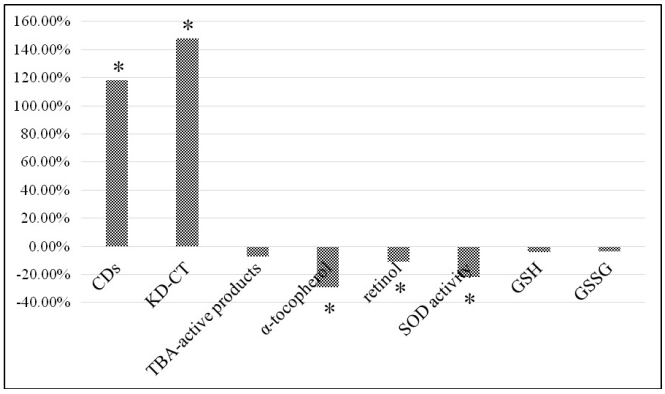

Fig. 1. *Changes in LPO-AOD parameters in the obese Asian girls.*
**-P<0.05 between the obese Asian girls and control values.*

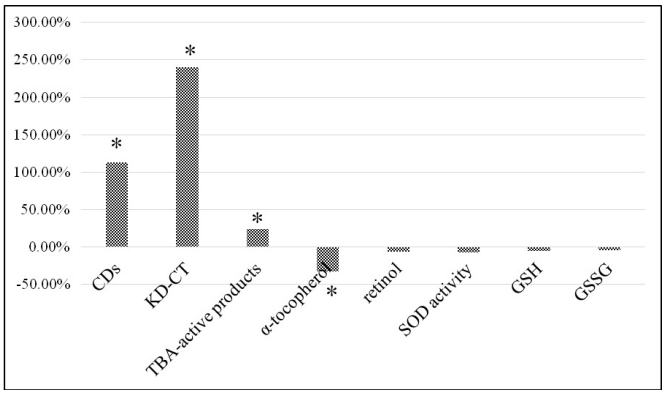

Fig. 2. *Changes in LPO-AOD parameters in the obese Asian boys.*
**-P<0.05 between the obese Asian boys and control values.*

Analysis of changes in LPO products in the adolescents with obesity confirmed the high activity of pro-oxidant reactions in this pathology. Taking into consideration the significance of LPO products as mediators of intercellular interactions, as well as adaptation mechanisms, the increased concentrations of these parameters can also be considered as a factor of disadaptation.[23] The indicated changes were similar to those in obese Caucasians, which we noted in earlier studies.[8,10,15]

In Asian adolescents with obesity, the decrease in AOD factors was also similar to that of Caucasians, with a lower content of fat-soluble vitamins. Obviously, the deficiency of any vitamin, and the combined insufficiency of a number of antioxidants, disturbs the activity of enzymatic processes and depends on the physiological functions that hinder the course of adaptive reactions. Especially, negative consequences can have insufficient antioxidant vitamins in adolescent girls because of the known diverse effects of these factors on the female reproductive system.[24] The important role of antioxidant vitamins as regulators of tissue growth and morphological differentiation is noted, so it is an extremely important registered high tension in this link of metabolism in adolescents with adiposity. Analysis of activity in the enzymatic part of the AOD system showed a decrease in the activity of the antioxidant enzyme SOD in Asian girls with obesity. This enzyme acts at the initial stage of superoxide anion radical neutralization and is the most important factor of the initial effect of the AOD system.[21] A decrease in its activity can be regarded as a factor of more intensive development of antioxidant deficiency.

Several mechanisms for the OS development in obesity have currently been established: an increase in proinflammatory cytokines and free fatty acids as substrates for LPO, and the involvement of biologically active adipokines in the development of pathological processes.[16,23] Activation of LPO reactions in obesity is also associated with a deficiency in exogenous antioxidants, occurring on the background of excessive intake of fats and carbohydrates.[27] Because of the above-mentioned processes, there is an increase of LPO products in the obese patient's blood, which we observed in the Asian adolescent groups.

Due to the frequently occurring, multidirectional changes in the LPO-AOD system in the development of various pathological conditions, it seems optimal to use the integral OSI. For this purpose, we applied the formula to calculate the OSI in our modification.[14] This formula takes into account not only the accumulation of LPO products at various stages but also the activity of various parts of the AOD system.

According to the obtained data, OSI in the group of Asian girls with obesity was 15.68 units, in the group of Asian boys with obesity - 22.89 units (Figure 3). The OSI in the group of Asian boys was significantly higher (by 1.46 times; *P*=0.0492) than in the obese girls.

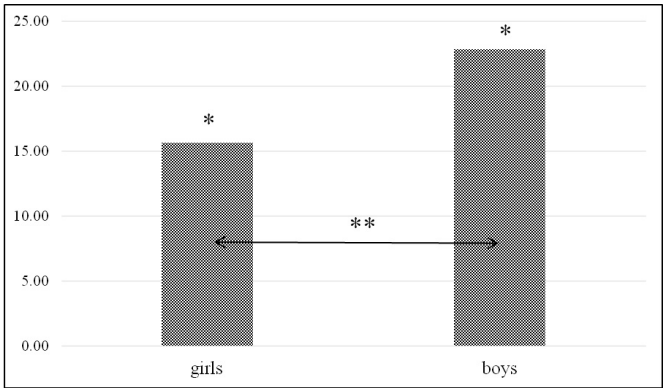

Fig. 3. *OSI in the obese Asian girls and boys*
**-P<0.05 between the obese Asian boys/girls and control values; **-P<0.05 between the obese Asian boys and girls; control group data are taken for 0.*

These results confirm the presence of a pronounced AOD insufficiency against the background of the activation of pro-oxidant factors in obese Asian girls and boys. The revealed differences in the levels of metabolites of the LPO-AOD system in Asians may be associated with general trends in the health status of the indigenous ethnic group of

the Baikal region. Thus, according to our data, an increasing tendency to an increase in body weight has previously been registered among Asian adolescents, especially those living in rural areas.[28] In addition, the metabolic changes can be associated with changes in the diet of the Asian ethnic group, one of the physiological features of which has so far been the protein-lipid nature of the diet.[29] With this type of diet, there are peculiarities of enzymatic reactions at the level of the gastrointestinal tract, liver, and fat depots, and a corresponding increase in concentrations of total cholesterol and atherogenic lipoprotein fractions.[29,30] However, one can state that the nutritional structure of this indigenous population has undergone significant changes in recent decades. Undoubtedly, this can entail a drastic disturbance of established metabolic mechanisms and, consequently, destabilization of the population's health. As a consequence, an excess level of alimentary-dependent nosologies, particularly obesity, has been registered among Asians living in this territory, compared to the average Russian level.[30,31]

In conclusion, certain OSI levels are consistent with the presence of antioxidant insufficiency in exogenous-constitutional obesity and allow us to specify and evaluate the ethnic aspect of the severity of the pathological process more reliably. In the complex treatment of exogenous and constitutional obesity in adolescents, in addition to the normalization of lipid metabolism parameters, the appropriateness of prescribing a complex of antioxidant drugs according to the patient's ethnicity has been shown.

Competing interests

The authors declare that they have no competing interests.

Sources of Funding

This study was supported by the Council for Grants of President of the Russian Federation (Grant No. NSh - 3382.2022.1.4).

References

1. Spinelli A, Buoncristiano M, Kovacs VA, Yngve A, Spiroski I, Obreja G, et al. Prevalence of Severe Obesity among Primary School Children in 21 European Countries. Obes Facts. 2019;12(2):244-258. doi: 10.1159/000500436.
2. Endalifer ML, Diress G. Epidemiology, Predisposing Factors, Biomarkers, and Prevention Mechanism of Obesity: A Systematic Review. J Obes. 2020 May 31;2020:6134362. doi: 10.1155/2020/6134362.
3. Pollack HA. The Problem of Obesity. J Health Polit Policy Law. 2016 Jun;41(3):451-2. doi: 10.1215/03616878-3523996.
4. O'Connor TG, Williams J, Blair C, Gatzke-Kopp LM, Francis L, Willoughby MT. Predictors of Developmental Patterns of Obesity in Young Children. Front Pediatr. 2020 Mar 24;8:109. doi: 10.3389/fped.2020.00109.
5. Tutelyan VA, Baturin AK, Kony IYa, Martinchik AN, Uglitskikh AK, Korostelev MM et al. [Prevalence of overweight and obesity in child population of Russia: multicenter study]. Pediatrics. Journal named after G.N. Speransky. 2014;93(5):28-31. [Article in Russian].
6. Karpova OB, Shchepin VO, Zagoruichenko AA. [The prevalence of adolescent obesity in the world and the Russian Federation in 2012–2018]. Hygiene and Sanitation. 2021;100(4):365-72. [Article in Russian].
7. Soboleva NP. [Bioimpedance screening of the Russian population at health centers: prevalence of overweight and obesity]. Russian Medical Journal. 2014;4:4-13. [Article in Russian].
8. Darenskaya MA, Kolesnikova LI, Rychkova LV, Kravtsova OV, Semenova NV, Kolesnikov SI. Relationship between lipid metabolism state, lipid peroxidation and antioxidant defense system in girls with constitutional obesity. AIMS Molecular Science. 2021;8(2):117-126.
9. Balzhieva VV, Bairova TA, Rychkova LV, Ayurova ZhG, Kolesnikov SI. [Ethnogenetic aspects of obesity in children and adolescents]. Pediatric Nutrition. 2017;15(5):29-34. [Article in Russian].
10. Darenskaya MA, Gavrilova OA, Rychkova LV, Rychkova LV, Kravtsova OV, Grebenkina LA, et al. The assessment of oxidative stress intensity in adolescents with obesity by the integral index. International Journal of Biomedicine. 2018;8(1):37-41. doi: 10.21103/Article8(1)_OA5
11. Kolesnikova LI, Darenskaya MA, Rychkova LV, Grebenkina LA, Semenova NV, Kolesnikov SI. [Lipids metabolism and antioxidant status in exogenous constitutional obesity in girls of Buryatia]. Russian Bulletin of Perinatology and Pediatrics. 2021;66(1):80-86. [Article in Russian].
12. Soboleva NP. [Bioimpedance screening of the Russian population in health centers: the prevalence of overweight and obesity]. Russian Medical Lournal. 2014;4:4-13. [Article in Russian].
13. Zuo L, Prather ER, Stetskiv M, Garrison DE, Meade JR, Peace TI, Zhou T. Inflammaging and Oxidative Stress in Human Diseases: From Molecular Mechanisms to Novel Treatments. Int J Mol Sci. 2019 Sep 10;20(18):4472. doi: 10.3390/ijms20184472.
14. Kolesnikova LI, Semyonova NV, Grebenkina LA, Darenskaya MA, Suturina LV, Gnusina SV. Integral indicator of oxidative stress in human blood. Bull Exp Biol Med. 2014 Oct;157(6):715-7. doi: 10.1007/s10517-014-2649-z.
15. Darenskaya MA, Rychkova LV, Kolesnikov SI, Gavrilova OA, Kravtsova OV, Grebenkina LA, Kolesnikova LI. Oxidative stress parameters in adolescent boys with exogenous-constitutional obesity. Free Radical Biology & Medicine. 2017;112:129-130.
16. Filgueiras MS, Rocha NP, Novaes JF, Bressan J. Vitamin D status, oxidative stress, and inflammation in children and adolescents: A systematic review. Crit Rev Food Sci Nutr. 2020;60(4):660-669. doi: 10.1080/10408398.2018.1546671.
17. Styne DM, Arslanian SA, Connor EL, Farooqi IS, Murad MH, Silverstein JH, Yanovski JA. Pediatric Obesity-Assessment, Treatment, and Prevention: An Endocrine Society Clinical Practice Guideline. J Clin Endocrinol Metab. 2017 Mar 1;102(3):709-757. doi: 10.1210/jc.2016-2573.

***Corresponding author:** Marina A. Darenskaya, PhD, ScD. Scientific Centre for Family Health and Human Reproduction Problems, Irkutsk, the Russian Federation. E-mail: marina_darenskaya@inbox.ru*

18. Volchegorskiĭ IA, Nalimov AG, Iarovinskiĭ BG, Lifshits RI. [Comparison of various approaches to the determination of the products of lipid peroxidation in heptane-isopropanol extracts of blood]. Vopr Med Khim. 1989 Jan-Feb;35(1):127-31. [Article in Russian].
19. Gavrilov VB, Gavrilova AR, Mazhul' LM. [Methods of determining lipid peroxidation products in the serum using a thiobarbituric acid test]. Vopr Med Khim. 1987 Jan-Feb;33(1):118-22. [Article in Russian].
20. Hissin PJ, Hilf R. A fluorometric method for determination of oxidized and reduced glutathione in tissues. Anal Biochem. 1976 Jul;74(1):214-26. doi: 10.1016/0003-2697(76)90326-2.
21. Misra HP, Fridovich I. The role of superoxide anion in the autoxidation of epinephrine and a simple assay for superoxide dismutase. J Biol Chem. 1972 May 25;247(10):3170-5.
22. Cherniauskene RCh, Varshkiavichene ZZ, Gribauskas PS. [Simultaneous fluorometric determination of the concentrations of vitamins E and A in blood serum]. Lab Delo. 1984;(6):362-5. [Article in Russian].
23. Marseglia L, Manti S, D'Angelo G, Nicotera A, Parisi E, Di Rosa G, et al. Oxidative stress in obesity: a critical component in human diseases. Int J Mol Sci. 2014 Dec 26;16(1):378-400.
24. Kolesnikova LI, Darenskaya MA, Semenova NV, Grebenkina LA, Suturina LV, Dolgikh MI, Gnusina SV. Lipid peroxidation and antioxidant protection in girls with type 1 diabetes mellitus during reproductive system development. Medicina (Kaunas). 2015;51(2):107-11. doi: 10.1016/j.medici.2015.01.009.
25. Niki E. Role of vitamin E as a lipid-soluble peroxyl radical scavenger: in vitro and in vivo evidence. Free Radic Biol Med. 2014 Jan;66:3-12. doi: 10.1016/j.freeradbiomed.2013.03.022.
26. Kolesnikova LI, Darenskaia MA, Grebenkina LA, Osipova EV, Dolgikh MI, Natiaganova LV. [The state of the antioxidant status of children of different ages]. Vopr Pitan. 2013;82(4):27-33. [Article in Russian].
27. Calcaterra V, Regalbuto C, Porri D, Pelizzo G, Mazzon E, Vinci F, Zuccotti G, Fabiano V, Cena H. Inflammation in Obesity-Related Complications in Children: The Protective Effect of Diet and Its Potential Role as a Therapeutic Agent. Biomolecules. 2020 Sep 16;10(9):1324. doi: 10.3390/biom10091324.
28. Rychkova LV, Ayurova ZhG, Pogodina AV, Kosovtseva AS. [Risk factors for obesity in adolescents from ethnic groups in rural areas of the Republic of Buryatia: results of a cross-sectional study]. Questions of Modern Pediatrics. 2017;16(6):509-15. [Article in Russian].
29. Kolosov YuA, Kolesnikov SI, Anisshenko AP, Burdukova EV, Gurevich KG. [Overweight and obesity in children, adolescents and adults: Causes of development and risk factors]. Pathogenesis. 2016;14(4):9-14. [Article in Russian].
30. Rychkova LV, Mashanskaja AV., Kravcova OV, Vlasenko AV, Pogodina AV, Mandziak TV, Chramova EE. Issues of prevention, diagnosis, and treatment of obesity in children and adolescents (Guidelines). Irkutsk, 2016. [In Russian].
31. Darenskaya MA. [Features of metabolic reactions in the indigenous and alien population of the north and Siberia]. Acta Biomedica Scientifica (East Siberian Biomedical Journal). 2014;2(96):97-103. [Article in Russian].

International Journal of Biomedicine 12(1) (2022) 147-150
http://dx.doi.org/10.21103/Article12(1)_OA17

ORIGINAL ARTICLE

Dentistry

INTERNATIONAL JOURNAL OF BIOMEDICINE

On Muscular Factor Question in the Correction of Transversal Incisor Occlusion

Natalya M. Didenko[1], PhD; Vladimir V. Gazinskiy[1], PhD; Oleg N. Nikitin[1], PhD; Evgeniy V. Mokrenko[1], PhD; Igor Yu. Kostritsky[1]; Ivan S. Goncharov[1]; Maria I. Suslikova[1], PhD; Larisa R. Kolesnikova[1], PhD, ShD; Isai M. Mikhalevich[2], PhD; Evgeniy V. Genich[3], MD; Yulia O. Sinyova[4], PhD; Marina A. Darenskaya[5], PhD, ShD

[1]*Irkutsk State Medical University*
[2]*Irkutsk State Medical Academy of Postgraduate Education — Affiliated Branch of Russian Medical Academy of Continuing Professional Education*
[3]*Irkutsk State Clinical Hospital №1*
[4]*Irkutsk National Research Technical University*
[5]*Scientific Centre for Family Health and Human Reproduction Problems*
Irkutsk, the Russian Federation

Abstract

The aim of our study was to evaluate the role of the muscle factor and the effectiveness of manual treatment of masticatory muscle dysfunction in patients with transversal incisor occlusion (TIO).

***Methods and Results*:** We examined and treated 35 patients aged 18-25 years with clinical signs of TIO in the clinic of orthopedic dentistry. Diagnostic methods for TIO included an interview, face and oral cavity examination, and clinical functional tests. Occlusion was assessed using anthropometric measurements and examination of plaster jaw models in an articulator for additional diagnostics of the dental factor; a radiological method (jaw orthopantomography with the inclusion of articular joints) was also used for the articular factor diagnostics and examination of masticatory muscles and neck muscles. The treatment methods included manual treatment of masticatory muscle dysfunction: "myofascial trigger point release technique," "stretching-push," and "post-isometric relaxation." All patients' complaints were mainly confined to improper occlusion of the front teeth, namely, a misalignment of the centerline between the upper and lower anterior teeth. Moreover, 71.4% of patients noted intermittent clicking in one or both articular joints of the temporomandibular joint, 42.8% of patients reported pain in the region of one temporomandibular joint, 28.6% of patients noted noise in the ear of the same joint, as well as discomfort while chewing. On external examination, all patients had a slight asymmetry of the lips and cheeks on the habitual chewing side. The apex of the chin was positioned slightly to the side relative to the facial midline. All patients had a disturbed movement trajectory of the lower jaw. During mouth opening, the lower jaw trajectory changed relative to the facial midline: at first, it was straight, for a very short period, and then it deviated sideways, after which it returned to the center. There was a misalignment of the central line of the lower dentition relative to the midline of the face in the anterior region. The radiological picture showed signs of articular joint dysfunction: difference in the size of the articular gaps on the right and left sides. After a single session of manual treatment of masticatory muscles, all patients noted that the improper occlusion of the front teeth was corrected, pain and clicking sensations in the TMJ disappeared in 42.8% of patients, and pain disappeared in the area of one joint, along with noise in the ears and chewing discomfort. Headache in the parietal and temporal areas disappeared. The trajectory of lower jaw movements during mouth opening normalized in all patients after the performed manual treatment.

Conclusion: We can conclude that when diagnosing and treating occlusal disorders, it is necessary to pay attention not only to the position of the teeth and the TMJ elements, but also to the muscular factor – the condition of the masticatory muscles. Special attention should be paid to the condition of the lateral wing muscles.(**International Journal of Biomedicine. 2022;12(1):147-150.**)

Key Words : transversal incisor occlusion • masticatory muscles • manual treatment

For citation: Didenko NM, Gazinskiy VV, Nikitin ON, Mokrenko EV, Kostritsky IYu, Goncharov IS, Suslikova MI, Kolesnikova LR, Mikhalevich IM, Genich EV, Sinyova YuO, Darenskaya MA. On Muscular Factor Question in the Correction of Transversal Incisor Occlusion. International Journal of Biomedicine. 2022;12(1):147-150. doi:10.21103/Article12(1)_OA17

Abbreviations

LWM, lateral wing muscle; **TIO,** transversal incisor occlusion; **TMJ,** temporomandibular joint.

Introduction

In orthopedic dentistry, we often observe a situation in which adult patients with occlusal anomalies and relatively correct dentition complain of an aesthetic defect at the examination.[1,2] This defect consists of misaligning the central line between the antagonist incisors.[2] Moreover, these patients had previously noted that the cosmetic center of their upper and lower teeth coincided.

According to L.S. Persin's classification (1990) of dental row occlusion anomalies, the misalignment of the interincisal line is a sign of a transversal occlusion anomaly in the anterior part of the dental arch; it is the so-called transversal incisor occlusion (TIO) - a disorder of the anterior teeth occlusion in a transversal direction with preserved contact between them.[3]

TIO is an occlusion anomaly complex of the structure of morphofunctional changes in the dentition and occurs in different age periods.[4] This anomaly is manifested by a mismatch of the interincisal line of the upper and lower jaws, accompanied by a violation of the coordinated activity of the masticatory muscles, a decrease in the tone of the masticatory muscles, and, as a result, severe violations of the chewing function.[4-6] Despite much research, there is still a lot of uncertainty on this issue.

The aim of our study was to evaluate the role of the muscle factor and the effectiveness of manual treatment of masticatory muscle dysfunction in patients with TIO.

Materials and Methods

We examined and treated 35 patients aged 18-25 years with clinical signs of TIO in the clinic of orthopedic dentistry during 2010-2021. All patients gave their written informed consent. Diagnostic methods for TIO included an interview, face and oral cavity examination, and clinical functional tests. Occlusion is characterized mainly by three factors: dental, articular, and muscular.[7] We used anthropometric measurements and examination of plaster jaw models in an articulator for additional diagnostics of the dental factor. We also used a radiological method (jaw orthopantomography with the inclusion of articular joints) for the articular factor diagnostics and examination of masticatory muscles and neck muscles, according to the method described by A. Puzin.[8]

The treatment methods included manual treatment of masticatory muscle dysfunction: "myofascial trigger point release technique," "stretching-push," and "post-isometric relaxation." [9,10]

Statistical analysis was performed using the Statistica 10.0 software package (Stat-Soft Inc., USA). The frequencies of categorical variables were compared using Pearson's chi-squared test or Fisher's exact test, when appropriate. A value of $P<0.05$ was considered significant.

Results and Discussion

Patients' complaints were mainly confined to improper occlusion of the front teeth, namely, a misalignment of the centerline between the upper and lower anterior teeth. Moreover, 71.4% of patients noted intermittent clicking in one or both articular joints of the TMJ, 42.8% of patients reported pain in the region of one TMJ joint, 28.6% of patients noted noise in the ear of the same joint, as well as discomfort while chewing. Characteristically, the clicks were mainly on the side opposite habitual chewing. It was also found that 57.14% of patients had a headache in the parietal region on the same side, and 28.57% of patients had slight pain in the temple area on the opposite side. Moreover, patients did not attribute these symptoms to malocclusion of the front teeth. According to the patients, 85.6% had an asymmetrical or late eruption of the first molars on the lower jaw. Also, 42.8% of patients had undergone therapeutic dental treatment for uncomplicated and complicated caries over several months (up to one year) (Table 1). On external examination, all patients had a slight asymmetry of the lips and cheeks on the habitual chewing side. The apex of the chin was positioned slightly to the side relative to the facial midline. All patients had a disturbed movement trajectory of the lower jaw. During mouth opening, the lower jaw trajectory changed relative to the facial midline: at first, it was straight, for a very short period, and then it deviated sideways, after which it returned to the center. The degree of mouth opening did not exceed 2cm in 42.8% of patients.

Table 1.

Results of patient's examination before and after manual therapy

Symptoms	Before manual therapy (n)	After manual therapy* (n)
Improper occlusion of the front teeth	35	0
Clicks in TMJ	25	15
Pain in the area of one joint	15	0
Noise in the ear	10	0
Chewing discomfort	10	0
Headache in the parietal area	20	0
Temporal headache	10	1
Unsymmetrical and late molars eruption	30	0
Fillings, caries	15	0
Soft tissues asymmetry	35	5
Offset of the top of the chin to the facial midline	35	5
Lower jaw trajectory (first sideways and then towards the center)	35	0
Degree of mouth opening less than 2 cm	15	0
Differences in the size of the right and left articular gaps	35	6
Misalignment of the central line of the lower dentition to the midline of the face	35	5
Lack of third molar rudiments	30	0

** - statistically significant differences.*

Examination of dental articulation in the central occlusion position showed the following: The tooth ratio slightly differed from neutral in the lateral sections; a fissure-cusp contact was noted, however, on the side of habitual chewing, the cheek cusps of lower teeth overlapped the cheek cusps of upper teeth with a slight distal shift, approximately to one-fourth of the cusp width; and on the opposite side, the cheek cusps of upper teeth overlapped the cheek cusps of lower teeth somewhat mesially, approximately to the same cusp width.

There was a misalignment of the central line of the lower dentition relative to the midline of the face in the anterior region (Table 1). The anatomical shape of the anterior teeth was not altered, and the sizes on the right and left did not differ significantly. A detailed examination of the state of the occlusal surface of the teeth revealed fillings on the opposite side of the habitual chewing in 42.8% of patients (Table 1).

The radiological picture showed the absence of bone pathology of the TMJ in all patients, but there were signs of articular joint dysfunction: difference in the size of the articular gaps on the right and left sides. There was a lack of third molar rudiments in 30 patients. One 19-year-old patient had a rudiment of the lower third molar removed to prevent asymmetry of the dentition after the expected eruption, which was revealed after the orthopantomogram examination.

After a single session of manual treatment of masticatory muscles, all patients noted that the improper occlusion of the front teeth was corrected (P<0.0001; F-test), pain and clicking sensations in the TMJ disappeared in 42.8% of patients (χ^2=4.73, P=0.030), and pain disappeared in the area of one joint (P<0.0001; F-test), along with noise in the ears (P<0.0001 (F-test)) and chewing discomfort (P<0.0001; F-test). Headache in the parietal (P=0.003; F-test) and temporal (P=0.009; F-test) areas disappeared. The trajectory of lower jaw movements during mouth opening normalized in all patients after the performed manual treatment (P<0.0001; F-test). The degree of mouth opening increased up to 3cm and more (P=0.04; F-test).

In 14.29% of cases, we noted correction of the soft tissues asymmetry and the offset of the top of the chin to the facial midline, a reduction in the differences between the size of the right and the left articular gaps, and the misalignment of the central line of the lower dentition to the facial midline. (χ^2=49.06, P<0.0001) (Table 1).

Examination of the masticatory muscles showed narrowing of the maxillary space (in 100% of cases; χ^2=46.63, P<0.0001), shortening, and hypertonicity of the LWM on the side opposite to habitual chewing in all 35 patients (Table 2). Extraoral palpation of the upper pole of the LWM head revealed trigger points of the inferior head of the LWM (in 100% of cases; χ^2=46.63, P<0.0001), trigger points of the superior head of the lateral pterygoid muscle (in 100% of cases; χ^2=46.63, P<0.0001). At the same time, 42.8% of patients had unilateral clicks on the same side where the trigger points of the LWM upper head were identified, and 28.57% of patients had bilateral clicks intermittently. Palpation of the temporalis and parietal muscles also revealed slight soreness in 28.57% of patients (Table 2).

Table 2.

Results of examination of masticatory muscles.

Symptoms	Before manual therapy	After manual therapy*
Unilateral narrowing of the maxillary space	35 (100%)	5 (14.29%)
Trigger points of the inferior head of the lateral wing muscle	35 (100%)	6 (17.14%)
Trigger points of the superior head of the lateral pterygoid muscle	35 (100%)	0
Clicks in one joint	15	0
Clicks in both joints	10 (28.57%)	2 (5.71%)
Temporal muscle soreness on one side	10 (28.57%)	0
Soreness of the parietal muscle on the opposite side	10 (28.57%)	0

* - *statistically significant differences.*

After a single session of manual treatment of masticatory muscles, no patients noted trigger points of the superior head of the lateral pterygoid muscle (χ^2=70.96, P<0.0001), clicks in one joint (χ^2=16.63, P<0.0001), and soreness (χ^2=9.45, P=0.002). Unilateral narrowing of the maxillary space was noted in 14.29% cases (χ^2=49.06, P<0.0001), trigger points of the inferior head of the lateral wing muscle in 17.14% cases (χ^2=46.16, P<0.0001), and clicks in both joints in 5.71% cases (χ^2=4.93, P=0.026) were noted.

Anatomically, the fascial fibers of one of the poles of the lateral pterygoid muscle superior head are woven into the TMJ capsule and also give off fibers to the interarticular meniscus.[8,11] Obviously, the synchronous movement of the condyle and meniscus in the temporal bone socket will be impaired if the lateral pterygoid muscle spasms. This explains the clicking sound in the articulation during mandibular excursions. Besides, the branch of the mandibular nerve of the same name innervates the lateral pterygoid muscle, which is the third branch of the trigeminal nerve. The sensory fibers passing next to the motor fibers of the lateral pterygoid nerve are the connective branches of the auricular ganglion that approach this parasympathetic node. With the increased tone of one of the heads of the lateral pterygoid muscle, these nerve branches are compressed, which can lead to the formation of noise in the ear. And therapeutic dental treatment for uncomplicated and complicated caries can lead to the formation of the habit of chewing on one side. Also, the asymmetrical or late eruption of the first molars on the lower jaw can be a reason for forming one-sided chewing habits. In the process of forming the habit of chewing on one side, spasm of the lateral pterygoid muscle occurs on the opposite side, mainly in the area of its lower head.[11-14] In our opinion, a patient with the removed embryo of the lower third molar could also have developed the habit of chewing on one side, since such surgical intervention causes pain and discomfort during chewing for a long time.

Pain and soreness in the muscles, spasms, increased tone, and hypertonicity can be the signs that characterize muscle dysfunction.[10]

The zigzagging of the mandibular trajectory during mouth opening is characterized by lateral wing muscle

dysfunction.[1,2,10,12,15-17] At first, the trajectory is straight; it is the first phase – the articulated movement of the condyle under the action of the muscles lowering the lower jaw. And then, in the middle phase, during the linear progressive movement of the lower jaw along the slope of the articular tubercle of the temporal bone, the lateral wing muscles come into action, extending the lower jaw. And if one side of the muscle spasms, the trajectory of the lower jaw movement will be changed to the opposite side. In the lower phase of the movement, the muscles lowering the lower jaw straighten the trajectory of the lower jaw.

I. Klineberg and S. Eckert [15] refer to the term "occlusion" as the dynamic biological interaction of the components of the masticatory system, which determines the teeth' interposition. The driving force for the interaction of the components of this system is the masticatory muscles. L. Persin`s findings [9] show the mismatch between the central position of the lower jaw and its habitual position. Therefore, the mismatch of the central lines between the upper and lower teeth can be explained by the different tones of the lateral wing muscles on the right and left. Special attention should be paid to the condition of the lateral pterygoid muscles; this is confirmed by the words of J. Travel et al.,[10] who called the lateral pterygoid muscle "the key to understanding and correcting functional disorders in the skull and mandible."

Thus, we can conclude that when diagnosing and treating occlusal disorders, it is necessary to pay attention not only to the position of the teeth and the TMJ elements, but also to the muscular factor – the condition of the masticatory muscles. Special attention should be paid to the condition of the lateral wing muscles.

Competing Interests

The authors declare that they have no competing interests.

References

1. Didenko NM, Vyazmin AYa, Mokrenko EV, Gazinskiy VV, Suslikova MI, Darenskaya MA, Andreeva VB, Aksnes D, Gubina MI. Relationship between the types of malocclusion and the localization of headaches in adults. International Journal of Biomedicine. 2021;11(2):197-200.doi: 10.21103/Article11(2)_OA12
2. Didenko NM, Stefanidi AV. Method for determining the causes and methods of prevention of recurrent occlusion disorders in patients with diagnosing and therapy of pathobiodynamic changes of the locomotor system. Patent 2019. RU 2690408 C1.
3. Persin LS. Orthodontics. Diagnosis and treatment of dentofacial anomalies and deformities. Textbook. M.:GEOTAR-Media, 2016;104.
4. Al-Nimri K, Gharaibeh T. Space conditions and dental and occlusal features in patients with palatally impacted maxillary canines: an aetiological study. Eur J Orthod. 2005 Oct;27(5):461-5. doi: 10.1093/ejo/cji022.
5. Militi A, Nucera R, Ciraolo L, Alibrandi A, Fastuca R, Lo Giudice R, Portelli M. Correlation between Caries, Body Mass Index and Occlusion in an Italian Pediatric Patients Sample: A Transverse Observational Study. Int J Environ Res Public Health. 2020 Apr 26;17(9):2994. doi: 10.3390/ijerph17092994.
6. Quast A, Santander P, Leding J, Klenke D, Moser N, Schliephake H, Meyer-Marcotty P. Orthodontic incisor decompensation in orthognathic therapy-success and efficiency in three dimensions. Clin Oral Investig. 2021 Jun;25(6):4001-4010. doi: 10.1007/s00784-020-03730-6.
7. Hiew LT, Ong SH, Foong KW. Optimal occlusion of teeth. The 9th International Conference on Control, Automation, Robotics and Vision. 2006;1-5.
8. Puzin AM, Vyazmin AYa. Pain dysfunction of the temporomandibular joint. M.:Meditsina, 2002.
9. Bertoni A, Zharmeny-Taren K.A. Cranial osteopathy. Technique and treatment protocols. M.:MEDpress-Inform, 2010.
10. Travell DG, Simons DG. Myofascial pain and dysfunction: A guide to trigger points (In 2 volumes). V.1. M.: Meditsina, 2005.
11. Amig ZhP. Dental system. Dental concept. Osteopathic concept. SPb: Nevsky Racurs. 2017;51.
12. Slavichek R. Chewing organ. Functions and dysfunctions. Publishing House Azbuka. 2008:76-101.
13. Fulks BA, Callaghan KX, Tewksbury CD, Gerstner GE. Relationships between chewing rate, occlusion, cephalometric anatomy, muscle activity, and masticatory performance. Arch Oral Biol. 2017 Nov;83:161-168. doi: 10.1016/j.archoralbio.2017.07.020.
14. Deniz DA, Kulak Ozkan Y. The influence of occlusion on masticatory performance and satisfaction in complete denture wearers. J Oral Rehabil. 2013 Feb;40(2):91-8. doi: 10.1111/joor.12015.
15. Klineberg I, Eckert S. Functional Occlusion in Restorative Dentistry and Prosthodontics E-Book. Elsevier Health Sciences, 2015.
16. Murray GM, Phanachet I, Uchida S, Whittle T. The human lateral pterygoid muscle: a review of some experimental aspects and possible clinical relevance. Aust Dent J. 2004 Mar;49(1):2-8. doi: 10.1111/j.1834-7819.2004.tb00042.x.
17. Ferrario VF, Sforza C, Colombo A, Ciusa V. An electromyographic investigation of masticatory muscles symmetry in normo-occlusion subjects. J Oral Rehabil. 2000 Jan;27(1):33-40. doi: 10.1046/j.1365-2842.2000.00490.x.

***Corresponding author:** Marina A. Darenskaya, PhD, ScD. Scientific Centre for Family Health and Human Reproduction Problems, Irkutsk, the Russian Federation. E-mail: marina_darenskaya@inbox.ru*

International Journal of Biomedicine 12(1) (2022) 151-154
http://dx.doi.org/10.21103/Article12(1)_OA18

ORIGINAL ARTICLE

Population Genetics

INTERNATIONAL JOURNAL OF BIOMEDICINE

Analysis of the Association of 5-Hydroxytryptamine Receptor 2A Gene Variants in Nicotine Addiction in the Yakut Population

Nadezhda I. Pavlova, PhD*[1]; Aleksey A. Bochurov[1]; Vladislav A. Alekseev[1]; Aleksandra T. Diakonova[1]; Vladimir V. Dodokhov[2], PhD; Khariton A. Kurtanov[3], PhD

[1]*Yakut Science Center of Complex Medical Problems*
[2]*Arctic State Agrotechnological University*
[3]*Institute for Biological Problems of Cryolithozone of SB of RAS*
Yakutsk, the Republic of Sakha (Yakutia), Russia

Abstract

The aim of this study was to investigate the relationship between the *HTR2A* 1438A/G (rs6311) SNP and the risk of nicotine addiction in Yakuts.

Methods and Results: A total of 292 people of Yakut nationality were tested (77 women and 215 men). Two groups of examined persons were formed: smokers (n=141) and non-smokers (NS, n=151). To determine the association of the studied SNP with the degree of smoking, the smoker group was divided into two subgroups: Heavy smokers (HS) and Light smokers (LS). Subjects who were smokers were classified based on their consumption of cigarettes per day (cpd), as follows: LS (n=10), those who consumed between 1 and 10 cpd, and HS (n=131), those who consumed ≥20 cpd. The study of the *HTR2A* 1438A/G (rs6311) SNP was performed by PCR and RFLP analysis. The A allele of the *HTR2A* 1438A/G (rs6311) SNP was associated with more of a risk for the HS group than the LS. Using the A allele as a risk factor, RR analysis showed a significant association with a risk factor when comparing HS with LS (RR=1.086; 95% CI=1.032-1.142; *P*=0.049). The analysis of the OR and RR between the HS and LS showed that the AA and AG genotypes were associated with an increased risk for heavy smoking (OR=9.714; 95% CI=1.196-78.874; RR =1.126; 95% CI=1.027-1.235; *P*=0.026). We cannot dismiss the possibility that our results may reflect the small sample size. Despite this potential limitation, the significant associations should not be disregarded and merit further investigation for clarification of these results.(**International Journal of Biomedicine. 2022;12(1):151-154.**)

Key Words: HTR2A • rs6311 • SNP • addictive behavior

For citation: Pavlova NI, Diakonova AT, Alekseev VA, Bochurov AA, Dodokhov VV, Kurtanov KhA. Analysis of the Association of 5-Hydroxytryptamine Receptor 2A Gene Variants in Nicotine Addiction in the Yakut Population. International Journal of Biomedicine. 2022;12(1):151-154. doi:10.21103/Article12(1)_OA18

Introduction

Smoking is one of the causes leading to the development of serious diseases that significantly reduce life expectancy. Worldwide, more people die from smoking than from alcohol, cocaine, and heroin, as well as from AIDS, violent death, car and plane crashes combined. The state of dependence on nicotine, alcohol, and drugs is included in one category of ICD-10: "mental and behavioral disorders due to the use of psychoactive substances." According to the World Health Organization, in 2018, Russia ranked 34th in the world in number of tobacco users, which is 28.3% of Russians (34.2 million inhabitants) over 15 years old.(1) As for the regions of Russia, according to Rosstat for 2019, Chukotka has the largest percentage of smokers (39%) of the adult population. In second place is the Jewish Autonomous Region - 37.3%. In the third place - the Trans-Baikal Territory (36.3%). In the Republic of Sakha (Yakutia), the share of the smoking population was 34.4%, that is, in fifth place among the smoking population in Russia. Nicotine addiction is a chronic disease, similar to other types of substance dependence, requiring repeated interventions to achieve and maintain sustainable smoking cessation. The nicotine contained

***Corresponding author:** Nadezhda I. Pavlova, PhD. Yakut Science Center of Complex Medical Problems. Yakutsk, the Republic of Sakha (Yakutia), Russia. E-mail: solnishko_84@inbox.ru*

in tobacco causes the development of a strong commitment to smoking. Research suggests that nicotine is more addictive than cocaine, ethanol, heroin, caffeine, and marijuana, both in terms of physical and psychological dependence. Nicotine acts as a full agonist at nicotinic acetylcholine receptors (n-AChR) in the central nervous system, activates dopaminergic pathways in the mesolimbic system of the brain, and thus promotes craving and addiction.[2,3] Therefore, genes encoding receptors involved in dopaminergic and serotonergic pathways are potential candidates in the mechanisms of nicotine dependence.

The *HTR2A* gene is located on chromosome 13 and includes three exons and two introns with a length of more than 63 kb, and it contains more than 200 single nucleotide polymorphisms (SNPs). This gene has two known functional SNPs, T102C (rs6313) and A1438G (rs6311), which have been associated with smoking addiction. Some studies have found that SNPs rs6311 (1438A/G) in the promoter region and rs6313 (102T/C) in exon 1 may be associated with a higher risk of cigarette smoking among Caucasians. [4-6]

We have studied for the first time the association of the *SLC6A3* rs27072 SNP with nicotine addiction in the smoking population and the *ABCB1* C3435T SNP in Yakuts associated with addictive behavior. An analysis of the association of the *SLC6A3* rs27072 with nicotine addiction indicated the absence of statistically significant differences between carriers of different genotypes, not only in the study group as a whole, but also separately in men and women.[7] It has been shown that nicotine alters the expression of ABCB1 and that 4-methylnitrosamino-1-3-pyridyl-1-butanone, which is an ingredient in cigarette smoke, induces the *ABCB1* gene by expressing mRNA.[8,9] Therefore, it can be hypothesized that *ABCB1* genetic polymorphisms may interact with mechanisms associated with substance addiction, including nicotine addiction.[10]

The aim of this study was to investigate the relationship between the HTR2A 1438A/G (rs6311) SNP and the risk of nicotine addiction in Yakuts.

Materials and Methods

The study was carried out in the Department of Molecular Genetics at the Yakut Scientific Center for Complex Medical Problems (YSC CMP). A total of 292 people of Yakut nationality were tested (77 women and 215 men). Two groups of examined persons were formed: smokers (n=141) and non-smokers (NS, n=151). To determine the association of the studied SNP with the degree of smoking, the smoker group was divided into two subgroups: Heavy smokers (HS) and Light smokers (LS). Subjects who were smokers were classified based on their consumption of cigarettes per day (cpd), as follows: LS (n=10), those who consumed between 1 and 10 cpd, and HS (n=131), those who consumed ≥20 cpd.

The study was approved by the Ethics Committee of the Yakut Science Center of Complex Medical Problems (YSC CMP). Written informed consent was obtained from each research participant.

Genomic DNA samples were isolated from the peripheral blood leukocytes using a commercial kit for DNA isolation Excell biotech (Yakutsk, Russia). The study of the *HTR2A* 1438A/G (rs6311) SNP was performed by PCR and RFLP analysis. Primer sequences, conditions for amplification, restriction enzymes, and the lengths of the restoration fragments are presented in Table 1.

Table 1.

The primers and restriction enzymes used for detection of the HTR2A 1438A/G (rs6311) SNP using PCR-RFLP methods

Primers	Annealing temperature (˚C)	Restriction enzyme	PCR-RFLP results (bp)
5'- AAC CAA CTT ATT TCC TAC CAC -3'	57 °C	MspI	Allele A: 468 Allele G: 244 and 224
5'-AAG CTG CAA GGT AGC AAC AGC -3'			

bp - base pair

PCR products were detected by horizontal electrophoresis in a 2% agarose gel plate with the addition of ethidium bromide, a specific intercalating fluorescent DNA (RNA) dye, using a standard Tris-acetate buffer at a field voltage of ~ 20V/cm for 30 minutes. After PCR, the amplificate was subjected to restriction using MspI endonuclease (OOO SibEnzim, Novosibirsk) for 3 hours at 37°C. RFLP products were detected by horizontal electrophoresis in 4% agarose gel stained with ethidium bromide using a standard Tris-acetate buffer at 120V for 1 hour.

Fragments containing the uncut A allele had a 468-bp band; fragments containing the G allele had two bands of 244 and 224 bp.

Statistical analysis was performed using Microsoft Excel 2010. The comparison of the frequencies of allelic variants/genotypes was performed using the chi-square test with Yates correction. The odds ratio (OR), relative risk (RR) and the corresponding 95% CI were calculated to estimate the strength of the association. A probability value of $P<0.05$ was considered statistically significant.

Results and Discussion

An analysis of the frequency distribution of alleles and genotypes of the *HTR2A* 1438A/G (rs6311) SNP showed that in the studied sample of Yakuts (men and women), the G allele was predominant (75.2%) and the frequency of occurrence of the GG genotype was 53.4%. The frequency of the AA genotype in women was three times higher than in men: 6.5% and 1.9%, respectively (P=0.046) (Table 2).

The frequency distribution of alleles and genotypes of the *HTR2A* 1438A/G (rs6311) SNP did not differ significantly between smokers and non-smokers (Table 3). The A allele frequency for non-smokers was 22.6%-23.7%, while in the smoking group it was 23.7%-31.5%. The highest frequency of the AA genotype was found in female smokers (8.7%), while in male smokers it was the lowest (1.1%). The frequency of the heterozygous AG genotype in all subgroups of smokers was higher than in non-smokers.

Table 2.

The frequency of occurrence of genotypes and alleles of the HTR2A 1438A/G (rs6311) SNP in the Yakut population

Group	Genotype frequency			Allele frequency	
	AA	AG	GG	A	G
Men and women (n=292)	3.1	43.5	53.4	24.8	75.2
Men (n=215)	1.9	43.7	54.4	23.7	76.3
P-value	0.046	>0.05	>0.05	>0.05	>0.05
Women (n=77)	6.5	42.9	50.6	27.9	72.1

The A allele of the *HTR2A* 1438A/G (rs6311) SNP was associated with more of a risk for the HS group than the LS. Using the A allele as a risk factor, RR analysis showed a significant association with a risk factor when comparing HS with LS (RR=1.086; 95% CI=1.032-1.142; *P*=0.049). The analysis of the OR and RR between the HS and LS showed that the AA and AG genotypes were associated with an increased risk for heavy smoking (OR=9.714; 95% CI=1.196-78.874; RR =1.126; 95% CI=1.027-1.235; *P*=0.026). This is consistent with the data of Pérez-Rubio et al.,[4] who found in the Mexican mestizo population that the A allele of the *HTR2A* 1438A/G (rs6311) SNP was associated with cigarette smoking; in addition, the heterozygous GA genotype and the homozygous AA genotype were associated with the risk in the comparison between HS and NS. According to Z. Verde,[11] the allele A of the *HTR2A* 1438A/G (rs6311) SNP, among all smokers, was associated with the number of packs smoked per year (*P*=0.02).

A potential limitation of this study is that smokers self-reported smoking and cigarette consumption levels. Ideally, the amount of nicotine consumed should be measured by serum cotinine levels. This measure is relevant because cigarette consumption affects the level of nicotine in the body. According to power retrospective analysis, the *HTR2A* 1438A/G (rs6311) SNP has low statistical power in our study, probably because the A allele frequency has a relatively rare occurrence that needs to be taken into account and possibly requires later population validation.

We cannot dismiss the possibility that our results may reflect the small sample size. Despite this potential limitation, the significant associations should not be disregarded and merit further investigation for clarification of these results.

Sources of Funding

The study was carried out within the framework of the project “Physiological and biochemical mechanisms of adaptation of plants, animals, humans to the conditions of the Arctic/Subarctic and the development of biological products based on natural northern raw materials that increase the efficiency of the adaptation process and the level of human health in extreme environmental conditions” (No. 0297-2021-0025 registration number AAAA-A21-121012190035-9) and the Scientific - Research Experimental - Design Work “Study of the genetic structure and burden of hereditary pathology of populations of the Republic of Sakha (Yakutia)” using the Unique scientific equipment (USE) “The Genome of Yakutia” (No. USU_507512).

Competing Interests

The authors declare that they have no competing interests.

Table 3.

OR and 95% CI for HTR2 rs6311 (dominant effect of the A allele, AA+AG vs GG) in relation to smokers

Groups and subgroups	Genotype frequency (%)			Allele frequency (%)		OR	RR	*P*	OR (AA+AG)	RR (AA+AG)	*P*
	AA	AG	GG	A	G						
All smokers Men and women	3.5	45.4	51.1	26.2	73.8	1.578 (0.753-3.308)	1.242 (0.947-1.631)	0.303	1.184 (0.746-1.878)	1.099 (0.867-1.393)	0.435
NS Men and women	2.6	41.7	55.6	23.5	76.5						
Women smokers	8.7	45.7	45.7	31.5	68.5	1.578 (0.753-3.308)	1.242 (0.947-1.631)	0.303	1.648 (0.657-4.134)	1.222 (0.844-1.769)	0.286
NS Women	3.2	38.7	58.1	22.6	77.4						
Men smokers	1.1	45.3	53.7	23.7	76.3	0.996 (0.637-1.559)	1.040 (0.804-1.345)	0.922	1.054 (0.614-1.810)	1.030 (0.762-1.392)	0.848
NS Men	2.5	42.5	55	23.7	76.3						
HS Men and women	3.8	48.1	48.1	27.9	72.1	1.257 (0.860-1.836)	1.127 (0.929-1.366)	0.278	1.353 (0.846-2.164)	1.175 (0.915-1.510)	0.207
NS Men and women	2.6	41.7	55.6	23.5	76.5						
HS Men and women	3.8	48.1	48.1	27.9	72.1	7.339 (0.965-55.820)	1.086 (1.032-1.142)	0.049	9.714 (1.196-78.874)	1.126 (1.027-1.235)	0.026
LS Men and women	0	10	90	5	95						

References

1. World Health Organization. 01.17.2022. Age-standardized estimates of current tobacco use, tobacco smoking and cigarette smoking. Data by country. Available from: https://apps.who.int/gho/data/node.main.TOBAGESTDCURR?lang=en
2. Federal State Statistics Service. Selective observation of behavioral factors affecting the health status of the population 2018. Available from: https://burstat.gks.ru/pfczn. [In Russian].
3. Ramos Neto ES, Mágulas JO, Sousa JJ, Moura AC, Pinto GR, Yoshioka FK, Canalle R, Motta FJ. Study of polymorphic variants of the serotonin 2A receptor gene (5-HT2A) and its possible effects on smoking habits of a population from northeastern Brazil. Genet Mol Res. 2014 Oct 20;13(4):8268-77. doi: 10.4238/2014.October.20.3.
4. Pérez-Rubio G, Ramírez-Venegas A, Noé Díaz V, García Gómez L, Elvira Fabián K, García Carmona S, et al. Polymorphisms in HTR2A and DRD4 Predispose to Smoking and Smoking Quantity. PLoS One. 2017 Jan 19;12(1):e0170019. doi: 10.1371/journal.pone.0170019.
5. Ramos Neto ES, Mágulas JO, Sousa JJ, Moura AC, Pinto GR, Yoshioka FK, Canalle R, Motta FJ. Study of polymorphic variants of the serotonin 2A receptor gene (5-HT2A) and its possible effects on smoking habits of a population from northeastern Brazil. Genet Mol Res. 2014 Oct 20;13(4):8268-77. doi: 10.4238/2014.October.20.3.
6. Polina ER, Contini V, Hutz MH, Bau CH. The serotonin 2A receptor gene in alcohol dependence and tobacco smoking. Drug Alcohol Depend. 2009 Apr 1;101(1-2):128-31. doi: 10.1016/j.drugalcdep.2008.11.001.
7. Diakonova AT, Pavlova NI, Solovyeva NA, Varlamova MA, Alexandrova TN, Kurtanov KhA. Molecular-genetic analysis of the connection of the *SLC6A3* gene with nicotine addiction in Yakutia. Yakut Medical Journal. 2018;4(64):6-8. doi: 10.25789/YMJ.2018.64.01. [Article in Russian].
8. Levran O, O'Hara K, Peles E, Li D, Barral S, Ray B, Borg L, Ott J, Adelson M, Kreek MJ. ABCB1 (MDR1) genetic variants are associated with methadone doses required for effective treatment of heroin dependence. Hum Mol Genet. 2008 Jul 15;17(14):2219-27. doi: 10.1093/hmg/ddn122.
9. Hsin CH, Stoffel MS, Gazzaz M, Schaeffeler E, Schwab M, Fuhr U, Taubert M. Combinations of common SNPs of the transporter gene ABCB1 influence apparent bioavailability, but not renal elimination of oral digoxin. Sci Rep. 2020 Jul 27;10(1):12457. doi: 10.1038/s41598-020-69326-y.
10. Pavlova NI, Diakonova AT, Alekseev VA, Borisova YP, Dodokhov VV, Dmitrieva TI, Kurtanov KhA. C3435T Polymorphism of the *ABCB1* Gene in the Yakut Population. International Journal of Biomedicine 11(3) (2021) 367-371. doi: 10.21103/Article11(3) OA15.
11. Verde Z, Santiago C, Chicharro LM, Bandrés F, Gómez-Gallego F, Rodríguez González-Moro JM, de Lucas P. Association of HTR2A-1438G/A Genetic Polymorphism With Smoking and Chronic Obstructive Pulmonary Disease. Arch Bronconeumol (Engl Ed). 2019 Mar;55(3):128-133. doi: 10.1016/j.arbres.2018.07.021.

International Journal of Biomedicine 12(1) (2022) 155-159
http://dx.doi.org/10.21103/Article12(1)_OA19

ORIGINAL ARTICLE

Population Genetics

INTERNATIONAL JOURNAL OF BIOMEDICINE

Frequency of the Risk A Allele of rs17713054 Localized in the 3p21.31 COVID-19 Risk Locus in the Yakut Population

Nadezhda I. Pavlova[1*], PhD; Aleksey A. Bochurov[1]; Vladislav A. Alekseev[1]; Aleksandra T. Diakonova[1]; Vladimir V. Dodokhov[2], PhD; Khariton A. Kurtanov[3], PhD

[1]*Yakut Science Center of Complex Medical Problems*
[2]*Arctic State Agrotechnological University*
[3]*Institute for Biological Problems of Cryolithozone of SB of RAS*
Yakutsk, the Republic of Sakha (Yakutia), Russia

Abstract

Background: Genome-wide association studies identified the region of chromosome 3p21.31 as having the strongest association with the severe COVID-19 and susceptibility to SARS-CoV-2 infection. The aim of our study was to investigate the frequency of the risk A allele of rs17713054 localized in the 3p21.31 COVID-19 risk locus in Yakuts.

***Methods and Results*:** A total of 382 DNA samples from healthy Yakut volunteers (184 men and 198 women; the average age of 41.8±0.05 years) were examined. Our results show that the frequency of the risk A allele of the rs17713054 SNP in the Yakut population occurs at a frequency of 2% and generally corresponds to the frequency of East Asian populations (from 0% to 2%), geographically close to the Yakuts and belonging to the same Mongoloid race. (**International Journal of Biomedicine. 2022;12(1):155-159.**)

Key Words: SARS-CoV-2 • rs17713054 • epithelial-mesenchymal transition • leucine zipper transcription factor like 1

For citation: Pavlova NI, Bochurov AA, Alekseev VA, Diakonova AT, Dodokhov VV, Kurtanov KhA. Frequency of the Risk A Allele of rs17713054 Localized in the 3p21.31 COVID-19 Risk Locus in the Yakut Population. International Journal of Biomedicine. 2022;12(1):155-159. doi:10.21103/Article12(1)_OA19

Abbreviations

EMT, epithelial-mesenchymal transition; **GWAS**, genome-wide association study; **SNP**, single nucleotide polymorphism; **LZTFL1**, leucine zipper transcription factor like 1.

Introduction

The COVID-19 pandemic has killed millions of people worldwide. The predominant cause of death is pneumonia and severe acute respiratory distress syndrome.[1] However, COVID-19 can cause multiple organ failure due to cytokine release, micro- and macrovascular thrombosis, endothelial injury, acute kidney injury, and myocarditis.[2-4] A study of post-mortem lung biopsies from COVID-19 demonstrated widespread epithelial dysfunction with signs of EMT.[5,6]

Two large GWASs [7,8] identified the region of chromosome 3p21.31 as having the strongest association with the severe COVID-19; another study identified this locus as conferring susceptibility to SARS-CoV-2 infection.[9] GWASs have found that the 3p21.31 region is associated with a two-fold increase in the risk of respiratory failure. The influence of the 3p21.31 locus on the early epithelial response may contribute to susceptibility to SARS-CoV-2 infection.[9]

Downes et al.[10] identified the gain-of-function risk A allele of an SNP, rs17713054G>A, as a probable causative variant for the respiratory failure. The authors showed that

***Corresponding author:** Nadezhda I. Pavlova, PhD. Yakut Science Center of Complex Medical Problems. Yakutsk, the Republic of Sakha (Yakutia), Russia. E-mail: solnishko_84@inbox.ru*

the rs17713054-affected enhancer upregulates the interacting gene, leucine zipper transcription factor like 1 (*LZTFL1*). "This gene encodes a ubiquitously expressed protein that localizes to the cytoplasm. This protein interacts with Bardet-Biedl Syndrome (BBS) proteins and, through its interaction with BBS protein complexes, regulates protein trafficking to the ciliary membrane. Nonsense mutations in this gene cause a form of Bardet-Biedl Syndrome; a ciliopathy characterized in part by polydactyly, obesity, cognitive impairment, hypogonadism, and kidney failure. This gene may also function as a tumor suppressor; possibly by interacting with E-cadherin and the actin cytoskeleton and thereby regulating the transition of epithelial cells to mesenchymal cells."[11] The transmembrane protein E-cadherin is one of the critical components for epithelial integrityIn addition.[12] Thus, LZTFL1 is involved in the trafficking of numerous signaling molecules. [13-17]

For the 3p21.31 COVID-19 risk locus, a higher risk is associated with increased expression of the *LZTFL1* gene, a known inhibitor of EMT. Higher levels of the *LZTFL1* gene may delay the positive effects of an acute EMT response by blocking a reduction in the levels of ACE2 and TMPRSS2 and/or by slowing EMT-driven tissue repair.

The *LZTFL1* gene is widely expressed in pulmonary epithelial cells, including ciliated epithelial cells, which have been identified as one of the main cellular targets for SARS-CoV-2 infection.[18] The *LZTFL1* gene was identified as the gene having strong 3C contacts with the rs17713054 enhancer and lung expression quantitative trait loci (eQTL). *LZTFL1* is the most likely direct regulatory target of the rs17713054-containing epithelial–endothelial–fibroblast enhancer.

The aim of our study was to investigate the frequency of the risk A allele of rs17713054 localized in the 3p21.31 COVID-19 risk locus in Yakuts.

Materials and Methods

The study was carried out in the Department of Molecular Genetics at the Yakut Scientific Center for Complex Medical Problems (YSC CMP). For the study, we used DNA samples from the collection of biomaterials of the YSC CMP (Project "The Genome of Yakutia"; No. USE_507512).

A total of 382 DNA samples from healthy volunteers (184 men and 198 women; the average age of 41.8±0.05 years) were examined. The inclusion criteria for the study were Yakuts by ethnicity, living in Yakutia.

The study was approved by the Ethics Committee of the Yakut Science Center of Complex Medical Problems (YSC CMP). Written informed consent was obtained from each research participant.

Genomic DNA was isolated using the standard phenol-chloroform extraction method from frozen whole blood. Genotyping of DNA samples was carried out by analyzing PCR products - amplification of specific regions of the genome, followed by an analysis of restriction fragment length polymorphism. Primer selection was performed using the National Center for Biotechnology Information (NCBI) primer design tool, Primer-BLAST (forward primer: 5'-TGTCTGATTTTAAAGAAGTTTGGGT-3' and reverse primer: 5'- GGAGCAGAGCCCGTCATTAT-3').The sequence of the study site for the primer selection matrix and the primer specificity test were taken from the UCSC Genome Browser database (GRCh38/hg38). The primers were synthesized by Lumiprobe RUS Ltd (Moscow, Russia). The reaction mixture (25 µl) for PCR contained of forward and reverse primer (1.5µl (10 pmol/µl) of each oligonucleotide primer) (Moscow, Russia), ddH2O (13 µl), 10xPCR buffer (2.5 µl), 25 mM MgCl2 (2.5 µl), 2.5 mM dNTP Mix (2.5 µl), Taq polymerase (0.5 µl (1.5 units)), and DNA (1 µl). PCR was performed in an MJ Mini Gradient Thermal Cycler (BioRad). The temperature-time regime for carrying out the amplification of a given nucleotide sequence with the restriction enzyme used and the lengths of the restriction fragments is presented in Table 1. PCR products were detected by horizontal electrophoresis in a 2% agarose gel plate with the addition of ethidium bromide, a specific intercalating fluorescent DNA (RNA) dye, using a standard Tris-acetate buffer at a field voltage of ~ 20V/cm for 30 minutes.

Table 1.

PCR conditions for rs17713054

Temperature protocol for PCR			Restriction enzyme	Interpretation of the PCR-RFLP result bp)
Temperature	Time	Cycles		
95 °C	4 min	1	Zrm I	AA – 210; AG – 210, 125, 85; GG – 125, 85.
94 °C	30 sec	35		
64 °C	30 sec			
72 °C	1 min			
72 °C	10 min	1		

***bp**, base pair*

After PCR, the amplificate was subjected to restriction using ZrmI endonuclease (OOO SibEnzim, Novosibirsk) for 16 hours at 37°C. Restriction endonuclease selection was performed in a NEBcutter V2.0. RFLP products were detected by horizontal electrophoresis in a 3% agarose gel stained with ethidium bromide using a standard Tris-acetate buffer at 120V for 1 hour. Restriction products were visualized under UV light using a gel-documenting system (Vilber Lourmat, France) (Figure 1).

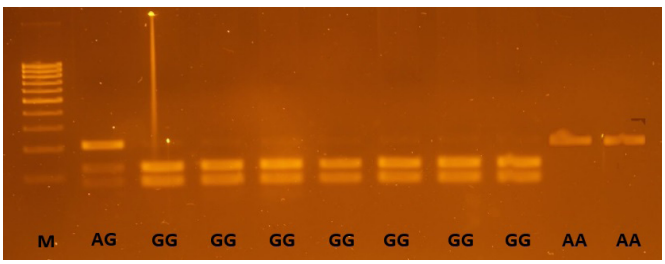

Fig. 1. Electrophoretogram: RFLP products in a 3% agarose gel.

M - marker PUC19 / + Msp I., AG – 210, 125, 85 bp; GG – 125, 85 bp; AA – 210 bp.

Statistical analysis was performed using Microsoft Excel 2010.

Results and Discussion

In our study, the rs17713054 SNP was analyzed in the Yakut population in comparison with the populations of East and South Asia, Africa, America, and Europe.[19] In the Yakut (YKT) population, the frequency of the risk A allele and the G allele of the rs17713054 was 2% and 98%, respectively (Table 2). The genotype distribution was as follows: AG=3.7%, AA=0.5%, GG=95.8%. When compared with an open database of populations from the 1000 Genomes

Table 2.

The frequency of genotypes and alleles of the rs17713054 SNP in the Yakut population and 1000 Genomes Project Phase 3 (population and subpopulations)

Group	ID	Name	Geographic region	Count	Allele freq.		Genotype freq.			Chi-sq.	*P*
					A	G	AA	AG	GG		
All Yakuts	YKT	Yakuts	North-Eastern Siberia	382	0.020	0.980	0.005	0.037	0.958	15.813	0.000
Yakut men				184	0.010	0.990	0	0.027	0.973	0.035	0.852
Yakut women				198	0.033	0.967	0.011	0.045	0.944	15.992	0.000
All 1000 Genomes Project Phase 3 individuals				2504	0.082	0.918	0,019	0.126	0.855	64.538	0.000
East Asian, EAS				504	0.005	0.995	0	0.010	0.990	0.013	0.911
East Asian sub-populations	CDX	Dai	East Asia	93	0.005	0.995	0	0.011	0.989	0.003	0.958
	CHB	Northern Han	East Asia	103	0	1	0	0	1	-	-
	CHS	Southern Han	East Asia	105	0	1	0	0	1	-	-
	JPT	Japanese	East Asia	104	0	1	0	0	1	-	-
	KHV	Kinh	East Asia	99	0.020	0.980	0	0.040	0.960	0.042	0.837
South Asian, SAS				489	0.296	0.704	0,094	0.403	0.503	0.514	0.473
South Asian sub-populations	BEB	Bengali	Central/South Asia	86	0.378	0.622	0.128	0.500	0.372	0.346	0.557
	GIH	Gujarati	Central/South Asia	103	0.267	0.733	0.078	0.379	0.544	0.110	0.741
	ITU	Telugu	Central/South Asia	102	0.289	0.711	0.098	0.382	0.520	0.500	0.479
	PJL	Punjabi	Central/South Asia	96	0.297	0.703	0.094	0.406	0.500	0.069	0.792
	STU	Sri Lankan Tamil	Central/South Asia	102	0.260	0.740	0.078	0.363	0.559	0.330	0.566
European, EUR				503	0.081	0.919	0	0.161	0.839	3.857	0.050
European sub-populations	CEU	European American	Europe	99	0.081	0.919	0	0.162	0.838	0.765	0.382
	FIN	Finnish	Europe	99	0.101	0.899	0	0.202	0.798	1.250	0.264
	GBR	British	Europe	91	0.071	0.929	0	0.143	0.857	0.538	0.463
	IBS	Iberian	Europe	107	0.047	0.953	0	0.093	0.907	0.257	0.612
	TSI	Toscani	Europe	107	0.103	0.897	0	0.206	0.794	1.405	0.236
American, AMR				347	0.043	0.957	0,003	0.081	0.916	0.208	0.648
American sub-populations	CLM	Colombian	Admixed	94	0.064	0.936	0.011	0.106	0.883	1.134	0.287
	MXL	Mexican American	Admixed	64	0.039	0.961	0	0.078	0.922	0.106	0.745
	PEL	Peruvian	Admixed	85	0.029	0.971	0	0.059	0.941	0.078	0.780
	PUR	Puerto Rican	Admixed	104	0.038	0.962	0	0.077	0.923	0.166	0.683
African, AFR				661	0.004	0.996	0	0.008	0.992	0.010	0.922
African sub-populations	ACB	Afro-Caribbean	Admixed	96	0.016	0.984	0	0.031	0.969	0.024	0.876
	ASW	African American	Admixed	61	0.008	0.992	0	0.016	0.984	0.004	0.949
	ESN	Esan	Africa	99	0	1	0	0	1	-	-
	GWD	Gambian	Africa	113	0.004	0.996	0	0.009	0.991	0.002	0.962
	LWK	Luhya	Africa	99	0	1	0	0	1	-	-
	MSL	Mende	Africa	85	0	1	0	0	1	-	-
	YRI	Yoruban	Africa	108	0	1	0	0	1	-	-

ID, population and subpopulation identifier; P - HWE p-value. A probability value of P<0.05 was considered statistically significant.

Project, the Yakuts were similar to the Kinh people of northern Vietnam (KHV subpopulation: A=2%; AA=0 and AG=4%) and the African subpopulation in Barbados (ACB: A=1.6%; AA=0 and AG=3.1%) (Table 2). In the African population (AFR), the risk A allele was absent, except for the aforementioned African subpopulation from the state of Barbados in the Caribbean (ACB) and African Americans from Southwest US (ASW: A=0.8%; AA=0 and AG=1.6%). Probably, in the ACB and ASW populations, the risk A allele is present due to cross-breeding with Europeans. In American populations (AMR), the risk A allele occurs at a frequency of 4% (AA=0.3% and AG=8.1%). Europeans rank second in the world in terms of the prevalence of the risk A allele (EUR: A=8%; AA=0 and AG=16.1%). Among Europeans, a high frequency is observed in Italians (TSI: A=10.3%; AA=0 and AG=20.6%) and Finns (FIN: A=10.1%; AA=0 and AG=20.2%).

A very high frequency of the risk A allele and allele-carrying A genotypes was observed in the South Asian population (SAS: A=30%; AA=9.4% and AG=40.4%), compared with all other considered populations (Table 2). In all the South Asian subpopulations presented, the frequency of the minor allele was high (26%-37.8%), but it should be noted that Bengalis have the highest frequency of the A allele of all analyzed populations (37.8%). The heterozygous AG genotype occurs in 50% of individuals in the Bengal population and 40.6% in the Punjabi population living in Pakistan and the Punjab state of northern India (PJL).

A nationwide cohort study of 29 million adults in England performed by Nafilyan et al.[20] analyzed ethnic differences for the risk of COVID-19-related death in the first and second waves of the pandemic in England. In the first wave, all ethnic minority groups had a higher risk of COVID-19-related death than the White British population. In the second wave, the risk of COVID-19-related death remained elevated for Pakistani (ASMR: 339.9 [95% CI: 303.7-376.2] and 166.8 [141.7-191.9] deaths per 100,000 population in men and women) and Bangladeshi (318.7 [247.4-390.1] and 127.1 [91.1-171.3] in men and women) people, but not for people from Black ethnic groups. Despite a reduction in the increased risk of mortality from COVID-19, after adjusting for socio-demographic characteristics and health status, the risk was significantly higher in people of Bangladeshi and Pakistani origin in both the first and second waves.

In conclusion, our results show that the frequency of the risk A allele of the rs17713054 SNP in the Yakut population occurs at a frequency of 2% and generally corresponds to the frequency of East Asian populations (from 0% to 2%), geographically close to the Yakuts and belonging to the same Mongoloid race. Probably, the risk A allele is present in the Yakut population due to ancient and/or recent miscegenation with Europeans.

Sources of Funding

The study was carried out within the framework of the project "The study of the genetic structure and burden of hereditary pathology of populations of the Republic of Sakha (Yakutia), using the Unique scientific equipment (USE) "The Genome of Yakutia" (Reg. No. USU_507512).

Competing interests

The authors declare that they have no competing interests.

References

1. Marini JJ, Hotchkiss JR, Broccard AF. Bench-to-bedside review: microvascular and airspace linkage in ventilator-induced lung injury. Crit Care. 2003 Dec;7(6):435-44. doi: 10.1186/cc2392.
2. Levi M, Thachil J, Iba T, Levy JH. Coagulation abnormalities and thrombosis in patients with COVID-19. Lancet Haematol. 2020 Jun;7(6):e438-e440. doi: 10.1016/S2352-3026(20)30145-9.
3. Varga Z, Flammer AJ, Steiger P, Haberecker M, Andermatt R, Zinkernagel AS, et al. Endothelial cell infection and endotheliitis in COVID-19. Lancet. 2020 May 2;395(10234):1417-1418. doi: 10.1016/S0140-6736(20)30937-5.
4. Ackermann M, Verleden SE, Kuehnel M, Haverich A, Welte T, Laenger F, et al. Pulmonary Vascular Endothelialitis, Thrombosis, and Angiogenesis in Covid-19. N Engl J Med. 2020 Jul 9;383(2):120-128. doi: 10.1056/NEJMoa2015432.
5. He J, Cai S, Feng H, Cai B, Lin L, Mai Y, et al. Single-cell analysis reveals bronchoalveolar epithelial dysfunction in COVID-19 patients. Protein Cell. 2020 Sep;11(9):680-687. doi: 10.1007/s13238-020-00752-4.
6. Borczuk AC, Salvatore SP, Seshan SV, Patel SS, Bussel JB, Mostyka M, et al. COVID-19 pulmonary pathology: a multi-institutional autopsy cohort from Italy and New York City. Mod Pathol. 2020 Nov;33(11):2156-2168. doi: 10.1038/s41379-020-00661-1.
7. Severe Covid-19 GWAS Group, Ellinghaus D, Degenhardt F, Bujanda L, Buti M, Albillos A, Invernizzi P, et al. Genomewide Association Study of Severe Covid-19 with Respiratory Failure. N Engl J Med. 2020 Oct 15;383(16):1522-1534. doi: 10.1056/NEJMoa2020283.
8. Pairo-Castineira E, Clohisey S, Klaric L, Bretherick AD, Rawlik K, Pasko D, et al.; GenOMICC Investigators; ISARIC4C Investigators; COVID-19 Human Genetics Initiative; 23andMe Investigators; BRACOVID Investigators; Gen-COVID Investigators, Shen X, Ponting CP, Fawkes A, Tenesa A, Caulfield M, Scott R, Rowan K, et al. Genetic mechanisms of critical illness in COVID-19. Nature. 2021 Mar;591(7848):92-98. doi: 10.1038/s41586-020-03065-y.
9. COVID-19 Host Genetics Initiative. Mapping the human genetic architecture of COVID-19. Nature. 2021 Dec;600(7889):472-477. doi: 10.1038/s41586-021-03767-x.
10. Downes DJ, Cross AR, Hua P, Roberts N, Schwessinger R, Cutler AJ, et al.; COvid-19 Multi-omics Blood ATlas (COMBAT) Consortium, Gill DR, Hyde SC, Knight JC, Todd JA, Sansom SN, Issa F, Davies JOJ, Hughes JR. Identification of LZTFL1 as a candidate effector gene at a COVID-19 risk locus. Nat Genet. 2021 Nov;53(11):1606-1615. doi: 10.1038/s41588-021-00955-3.
11. NCBI Resources. LZTFL1 leucine zipper transcription factor like 1 [Homo sapiens (human)]. Available from: https://www.ncbi.nlm.nih.gov/gene/54585

12. Ramirez Moreno M, Stempor PA, Bulgakova NA. Interactions and Feedbacks in E-Cadherin Transcriptional Regulation. Front Cell Dev Biol. 2021 Jun 28;9:701175. doi: 10.3389/fcell.2021.701175.
13. Wei Q, Zhou W, Wang W, Gao B, Wang L, Cao J, Liu ZP. Tumor-suppressive functions of leucine zipper transcription factor-like 1. Cancer Res. 2010 Apr 1;70(7):2942-50. doi: 10.1158/0008-5472.CAN-09-3826.
14. Promchan K, Natarajan V. Leucine zipper transcription factor-like 1 binds adaptor protein complex-1 and 2 and participates in trafficking of transferrin receptor 1. PLoS One. 2020 Jan 2;15(1):e0226298. doi: 10.1371/journal.pone.0226298.
15. Starks RD, Beyer AM, Guo DF, Boland L, Zhang Q, Sheffield VC, Rahmouni K. Regulation of Insulin Receptor Trafficking by Bardet Biedl Syndrome Proteins. PLoS Genet. 2015 Jun 23;11(6):e1005311. doi: 10.1371/journal.pgen.1005311.
16. Wei Q, Gu YF, Zhang QJ, Yu H, Peng Y, Williams KW, et al. Lztfl1/BBS17 controls energy homeostasis by regulating the leptin signaling in the hypothalamic neurons. J Mol Cell Biol. 2018 Oct 1;10(5):402-410. doi: 10.1093/jmcb/mjy022.
17. Seo S, Zhang Q, Bugge K, Breslow DK, Searby CC, Nachury MV, Sheffield VC. A novel protein LZTFL1 regulates ciliary trafficking of the BBSome and Smoothened. PLoS Genet. 2011 Nov;7(11):e1002358. doi: 10.1371/journal.pgen.1002358.
18. Ravindra NG, Alfajaro MM, Gasque V, Huston NC, Wan H, Szigeti-Buck K, et al. Single-cell longitudinal analysis of SARS-CoV-2 infection in human airway epithelium identifies target cells, alterations in gene expression, and cell state changes. PLoS Biol. 2021 Mar 17;19(3):e3001143. doi: 10.1371/journal.pbio.3001143.
19. Reference SNP (rs) Report (rs1773054). Available from: https://www.ncbi.nlm.nih.gov/snp/rs17713054?horizontal_tab=true
20. Nafilyan V, Islam N, Mathur R, Ayoubkhani D, Banerjee A, Glickman M, Humberstone B, Diamond I, Khunti K. Ethnic differences in COVID-19 mortality during the first two waves of the Coronavirus Pandemic: a nationwide cohort study of 29 million adults in England. Eur J Epidemiol. 2021 Jun;36(6):605-617. doi: 10.1007/s10654-021-00765-1.

International Journal of Biomedicine 12(1) (2022) 160-163
http://dx.doi.org/10.21103/Article12(1)_OA20

ORIGINAL ARTICLE

Laboratory Diagnostics

INTERNATIONAL JOURNAL OF BIOMEDICINE

Serous Effusion Cytology in Sudanese Patients

Muaz Osman Fagere[1]; Shawgi A. Elsiddig[2];
Anass M. Abbas[2]; Manar G. Shalabi[2]; Asaad M. A. Babker[3*]

[1]*Department of Clinical Laboratory Sciences, College of Applied Medical Sciences, Imam Abdulrahman Bin Faisal University, Dammam, Saudi Arabia*
[2]*Department of Clinical Laboratory Sciences, College of Applied Medical Sciences, Jouf University, Kingdom of Saudi Arabia*
[3]*Department of Medical Laboratory Sciences, College of Health Sciences, Gulf Medical University, Ajman, United Arab Emirates*

Abstract

The purpose of this study was to determine the etiology and cytological patterns of serous effusions among Sudanese patients.

***Methods and Results*:** This descriptive study was carried out in hospitals of Khartoum state in the period from February 2019 to June 2020. One hundred and seventy-eight patients "clinically and/or radiological" diagnosed as having an accumulation of serous effusions were included in this study. Smears were prepared and stained according to the conventional pap staining procedure.

The majority of the study population (121[68%]) had malignant effusion (MEs), and the other group (57[32%]) - benign effusions (BEs). Among patients with MEs, breast cancer was the major etiology (75[62%]), followed by lung (23[19%]), GIT (12[9.9%]), and thyroid cancers (11[9.1%]), while among patients with BEs, parapneumonic conditions were the main factor (28[49.1%]), followed by tuberculosis (18[31.6%]) and pulmonary embolism (11[19.3%]). The majority of patients with MEs were pleural effusion (109[90.1%]), followed by peritoneal effusion (12[9.9%]), whereas no patients in this group had pericardial effusion. Pleural effusion (29[50.9%]) was also the major one among patients with BEs, followed by peritoneal (21[36.8%]) and pericardial effusions (7[3.9%]).

Conclusion: Malignant serous effusion is commonly seen among patients with malignant tumors; pleural effusions presented a large proportion, especially among females with breast cancer. Thoracentesis and cytological methods (i.e., conventional smear and cell block technique) should be the first line for the diagnosis of malignant pleural effusions, along with confirmatory adjunct techniques such as immunohistochemistry and immunocytochemistry.**(International Journal of Biomedicine. 2022;12(1):160-163.)**

Key Words: serous effusion • malignancy • cytology • malignant effusion • benign effusion

For citation: Fagere MO, Elsiddig SA, Abbas AM, Shalabi MG, Babker AMA. Serous Effusion Cytology in Sudanese Patients. International Journal of Biomedicine. 2022;12(1):160-163. doi:10.21103/Article12(1)_OA20

Abbreviations

ME, malignant effusion: **BE**, benign effusion; **MPE**, malignant pleural effusions

Introduction

The pleural, pericardial, and peritoneal cavities are serous cavities. The visceral and parietal surfaces of each cavity are lined by the mesothelium. Each cavity contains only a small volume of lubricant fluid known as serous fluid. This fluid facilitates the movement of the lungs, heart, and digestive tract.[1] Different pathological conditions may lead to excess accumulation of fluid in body cavities; inflammatory conditions and malignant tumors "primary and/or secondary" are considered to be the major underlying causes.[2,3] Many types of tumors, especially carcinomas, may spread and find their way to serous membranes, and they become disseminated with the effusion. Many studies reveal that patients with lung

and breast cancers are more likely to develop pleural effusion during their disease course. Adenocarcinomas of the breast, lung, ovary, and GIT are the commonest primary, malignant tumors with high susceptibility to metastasize in the serous cavities.[4] The incidences of BEs are twofold common than MEs and have different causes and expressions.[5] BEs can be associated with a wide scale of pathological conditions; congestive heart failure is the most common one.[6] Other causes include rheumatoid disease, systemic lupus erythematosus, pulmonary infarct, pneumonia, pneumothorax, tuberculosis, hepatic cirrhosis, and viral infections.

In Sudan, the major underlying causes of serous effusions vary from inflammatory conditions to metastasized tumors, while cases of primary malignant mesothelioma were not reported among patients.[7] Although the liquid-based approach has advantages, such as uniform fixation and clearer background, because the cellular and background features essential for morphological assessment and diagnosis are better maintained in cytospin, it is thought to be better to utilize this approach in conjunction with conventional cytological technique.[3]

The purpose of this study was to determine the etiology and cytological patterns of serous effusions among Sudanese patients.

Materials and Methods

This descriptive study was carried out in hospitals of Khartoum state in the period from February 2019 to June 2020. One hundred and seventy-eight patients "clinically and/or radiological" diagnosed as having an accumulation of serous effusions were included in this study. From these patients, 178 cytological specimens' effusions were collected. Patients with effusion accumulation were subjected to needle aspiration to collect samples; the collected effusions were then delivered to the laboratory. Smears were prepared and stained according to the conventional pap staining procedure. The collected effusions were centrifuged at 2000 rpm for 7 minutes from the deposited cells; smears were prepared and fixed while they were wet by 95% ethyl alcohol. They were then hydrated through downward grades of ethyl alcohol concentrations (absolute, 90%, 80%, and 75%) to distilled water for 2 minutes/stage. Nuclei were stained with Harris Hematoxylin for 5 minutes, differentiated in 1% acid alcohol 5-7 seconds controlled microscopically, and rinsed in distilled water. Next, the smear was blued in alkaline water for 5 seconds, then dehydrated in ascending grades of alcohol concentrations for 2 minutes/stage. The cytoplasm was counter-stained with orange G6 for 2 minutes, rinsed in 95% alcohol, then treated with Eosin Azour 50 for 3 minutes, Dehydrated, cleared, and mounted in DPX. Data regarding the population that participated in this study, such as age, gender, clinical data, and other laboratory findings, were collected by checklist method. The disease factors data underlying the causes of BEs and MEs were collected from the patient's medical records.

Statistical analysis was performed using the standard Statistical Package for the Social Sciences (IBM SPSS Statistics for Windows, Version 21.0. Armonk, NY: IBM Corp). Written informed consent was obtained from all participants.

Results

In this study, a descriptive analysis for serous effusions among 178 Sudanese patients (age ranged from 20 to 78, with a mean age of 58 years) was carried out. Two groups of individuals were classified according to the diagnostic yields of their effusions. The majority of the study population (121[68%]) had MEs, and the other group (57[32%]) - non-malignant effusions. Most patients with MEs were female - 75(62%), while males constituted 46(38%). In the patients with BEs, most were female - 32(56.1%) vs. 25(43.9%) male. Table/Figure 1 presents the distribution of the study population by malignancy and gender. In patients with MEs, the majority of patients were in the age group of 36-50 years (44[36.4%]), followed by the age groups of 51-65 (42[34.7%]), 66+ (21[17.4%]), and 20-35 years (14[11.6%]). In contrast, among patients with BEs, the majority of patients were in the age group of 51-65 years (22[38.6%]), followed by the age groups of 36-50(20[35.1%]), 20-35(10[17.5%]), and 66+(5[8.8%]) years.

Gender	Malignant		Non-malignant		Total	
	No.	%	No.	%	No.	%
Female	75	62.0%	32	56.1%	107	60.1%
Male	46	38.0%	25	43.9%	71	39.9%
Total	121	68.0%	57	32.0%	178	100.0%

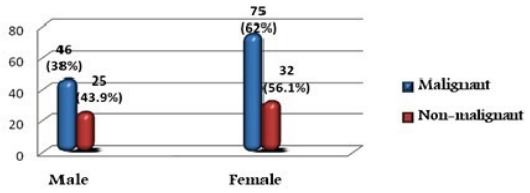

Table/Fig 1. *The distribution of the study population by malignancy and gender.*

Table/Figure 2 presents the distribution of the study population by malignancy and age.

Age	Malignant		Non-malignant		Total	
	No.	%	No.	%	No.	%
20-35	14	11.6%	10	17.5%	24	13.5%
36-50	44	36.4%	20	35.1%	64	36.0%
51-65	42	34.7%	22	38.6%	64	36.0%
66+	21	17.4%	5	8.8%	26	14.6%
Total	121	68.0%	57	32.0%	178	100.0%

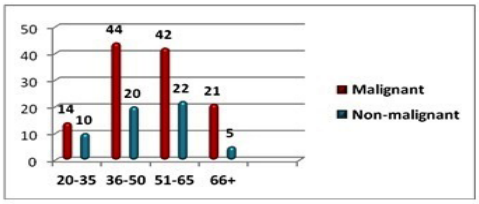

Table/Fig. 2. *The distribution of the study population by malignancy and age.*

Among patients with MEs, breast cancer was the major etiology (75[62%]), followed by lung (23[19%]), GIT (12[9.9%]), and thyroid cancers (11[9.1%]), while among patients with BEs, parapneumonic conditions were the main factor (28[49.1%]), followed by tuberculosis (18[31.6%]) and pulmonary embolism(11[19.3%]) (Table/Figure 3). Table/Figure 4 presents the distribution of the study population by malignancy and effusion site. The majority of patients with MEs were pleural effusion (109[90.1%]), followed by peritoneal effusion (12[9.9%]), whereas no patients in this group had pericardial effusion. Pleural effusion (29[50.9%]) was also the major one among patients with BEs, followed by peritoneal (21[36.8%]) and pericardial effusions (7[3.9%]).

Aetiology	Malignant		Non-malignant		Total	
	No.	%	No.	%	No.	%
Breast Cancer	75	62.0%	0	.0%	75	42.1%
Lung Cancer	23	19.0%	0	.0%	23	12.9%
GIT Cancer	12	9.9%	0	.0%	12	6.7%
Thyroid Cancer	11	9.1%	0	.0%	11	6.2%
Para-pneumonic	0	.0%	28	49.1%	28	15.7%
Tuberculosis	0	.0%	18	31.6%	18	10.1%
Pulm. Embolism	0	.0%	11	19.3%	11	6.2%
Total	121	68.0%	57	32.0%	178	100.0%

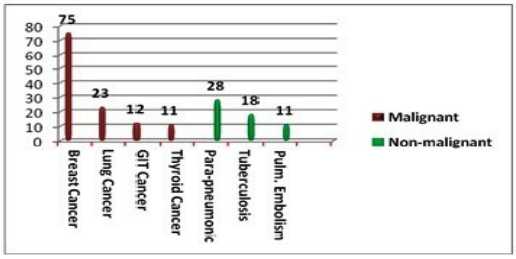

Table/Fig.3. *The distribution of the study population by malignancy and etiology.*

Effusion site	Malignant		Non-malignant		Total	
	No.	%	No.	%	No.	%
Pleural	109	90.1%	29	50.9%	138	77.5%
Peritoneal	12	9.9%	21	36.8%	33	18.5%
Pericardial	0	0.0%	7	3.9%	7	3.9%
Total	121	68.0%	57	32.0%	178	100.0%

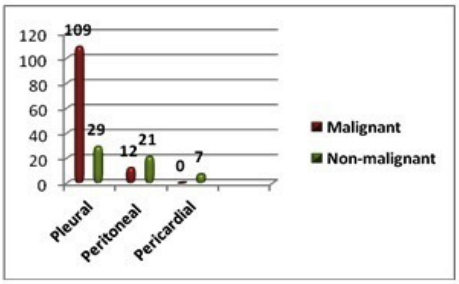

Table/Fig 4. *The distribution of the study population by malignancy and effusion site.*

Discussion

Serous effusion cytology is widely employed in the initial evaluation of the etiology of effusions with high diagnostic sensitivity.[8] This study evaluates the rate of incidence of serous effusions and describes its onset pattern among Sudanese patients. Out of 178(100%) patients with accumulated serous effusion, MEs due to metastatic malignant cells were detected in 121(68%) patients; this relatively high percentage was due to increased incidence of malignant cases, which resulted in the disease being metastasized to different body cavities, causing MEs. These findings support several studies that reported that malignant serous effusion commonly occurs as a secondary manifestation due to the metastatic involvements of malignant cells from diverse body organs to different body cavities.[9-11] Also, the present study finds that the majority of study patients with MEs were females 75(62.0%), and we assume this is associated with the increased incidence of breast cancer among Sudanese females. This finding agrees with a study by Amany et al.,[12] Shalabi et al.,[13] and Abbas et al.,[14] who concluded that breast cancer continues to be the most common cancer among women in Sudan, as well as with Aydogmus et al.[15] and Tremblay et al.,[16] who concluded that breast cancer is the second most common cause, after lung cancer, of MPEs, accounting for approximately one-third of all MPEs.

The present results showed that the accumulation of malignant serous effusion was detected mainly in the pleural cavity. Our results agree with other studies conducted by Antony et al.[17] and Sahn,[18] which elucidate the increased incidence of malignant serous effusion, especially in the pleural cavity.

Conclusion

Based on this study and review of other studies, it could be concluded that malignant serous effusion is commonly seen among patients with malignant tumors; pleural effusions presented a large proportion, especially among females with breast cancer. Therefore, more efforts in awareness of breast cancer should be given to the populations so as to decrease the late cases, which are represented with malignant effusions. Thoracentesis and cytological methods (i.e., conventional smear and cell block technique) should be the first line for the diagnosis of MPEs, along with confirmatory adjunct techniques such as immunohistochemistry and immunocytochemistry.

Competing Interests

The authors declare that they have no competing interests.

References

1. Michailova KN, Usunoff KG. Serosal membranes (pleura, pericardium, peritoneum). Normal structure, development

***Corresponding Author:** Asaad M. A. Baker, Associate Prof. of Hematology, Department of Medical Laboratory Sciences, College of Health Sciences, Gulf Medical University, Ajman, United Arab Emirates. E-mail: azad.88@hotmail.com*

and experimental pathology. Adv Anat Embryol Cell Biol. 2006;183:i-vii, 1-144, back cover. PMID: 16570866.
2. Davidson B. Malignant effusions: from diagnosis to biology. Diagn Cytopathol. 2004 Oct;31(4):246-54. doi: 10.1002/dc.20133.
3. Baykus N, Özekinci S, Erdem ZB, Vurgun E, Yildiz FR. Comparison of Morphological Similarities and Differences between Liquid-Based Cytology and Conventional Techniques of Serous Effusion Cytology Specimens. Acta Cytol. 2021 Dec 30:1-6. doi: 10.1159/000521052.
4. Heffner JE, Nietert PJ, Barbieri C. Pleural fluid pH as a predictor of survival for patients with malignant pleural effusions. Chest. 2000 Jan;117(1):79-86. doi: 10.1378/chest.117.1.79.
5. Thomas R, Lee YC. Causes and management of common benign pleural effusions. Thorac Surg Clin. 2013 Feb;23(1):25-42, v-vi. doi: 10.1016/j.thorsurg.2012.10.004.
6. Light RW. Pleural effusions. Med Clin North Am. 2011 Nov;95(6):1055-70. doi: 10.1016/j.mcna.2011.08.005.
7. Fagere MOM. Diagnostic utility of AgNORs staining of serous effusion among Sudanese patients. International Journal of Science and Technology. 201;5(1):36-42.
8. Pinto D, Chandra A, Schmitt F. The International System for Reporting Serous Fluid Cytopathology: How to Incorporate Molecular Data in Cytopathology Reports. Journal of Molecular Pathology. 2021;2(2):66-76. doi: 10.3390/jmp2020007
9. Politi E, Kandaraki C, Apostolopoulou C, Kyritsi T, Koutselini H. Immunocytochemical panel for distinguishing between carcinoma and reactive mesothelial cells in body cavity fluids. Diagn Cytopathol. 2005 Mar;32(3):151-5. doi: 10.1002/dc.20203.
10. Lozano MD, Panizo A, Toledo GR, Sola JJ, Pardo-Mindán J. Immunocytochemistry in the differential diagnosis of serous effusions: a comparative evaluation of eight monoclonal antibodies in Papanicolaou stained smears. Cancer. 2001 Feb 25;93(1):68-72.
11. Ahuja S, Malviya A. Categorisation of serous effusions using the International System for Reporting Serous Fluid Cytopathology and assessment of risk of malignancy with diagnostic accuracy. Cytopathology. 2021 Dec 15. doi: 10.1111/cyt.13089.
12. Elamin A, Ibrahim ME, Abuidris D, Mohamed KE, Mohammed SI. Part I: cancer in Sudan—burden, distribution, and trends breast, gynecological, and prostate cancers. Cancer Med. 2015 Mar;4(3):447-56. doi: 10.1002/cam4.378.
13. Shalabi MG, Abbas AM, Mills J, Kheirelseid MA, Elderdery AY. The Prognostic Value of Estrogen Receptor β Isoform With Correlation of Estrogen Receptor α Among Sudanese Breast Cancer Patients. Breast Cancer (Auckl). 2021 Feb 25;15:1178223421998354. doi: 10.1177/1178223421998354.
14. M Abbas A, Shalabi MG, A Elsiddig S, Eltahir Z, M A Babker A, G Ahmed H. Evaluation of Angiogenesis by Using CD105 and CD34 in Sudanese Breast Cancer Patients. Pak J Biol Sci. 2021 Jan;24(11):1144-1151. doi: 10.3923/pjbs.2021.1144.1151.
15. Aydogmus U, Ozdemir S, Cansever L, Sonmezoglu Y, Kocaturk CI, Bedirhan MA. Bedside talc pleurodesis for malignant pleural effusion: factors affecting success. Ann Surg Oncol. 2009 Mar;16(3):745-50. doi: 10.1245/s10434-008-0263-x.
16. Tremblay A, Michaud G. Single-center experience with 250 tunnelled pleural catheter insertions for malignant pleural effusion. Chest. 2006 Feb;129(2):362-368. doi: 10.1378/chest.129.2.362.
17. Antony VB, Loddenkemper R, Astoul P, Boutin C, Goldstraw P, Hott J, Rodriguez Panadero F, Sahn SA. Management of malignant pleural effusions. Eur Respir J. 2001 Aug;18(2):402-19. doi: 10.1183/09031936.01.00225601.
18. Sahn SA. Malignant pleural effusions. Semin Respir Crit Care Med. 2001 Dec;22(6):607-16. doi: 10.1055/s-2001-18796.

International Journal of Biomedicine 12(1) (2022) 164-166
http://dx.doi.org/10.21103/Article12(1)_CR

CASE REPORT

INTERNATIONAL JOURNAL OF BIOMEDICINE

Homozygous LOXHD1 Nonsense Mutation (c.1787G>A; p.W596X) is Associated with Hearing Loss in an Iranian Family: A Case Report*

Mostafa Neissi*[1,2]; Husham Khirullah Abdulzahra[3]; Motahareh Sheikh-Hosseini[4]; Hadideh Mabudi[5]; Javad Mohammadi-Asl[6]; Raed Abdulelah Al-Badran[3]

[1]*Department of Genetics, Khuzestan Science and Research Branch, Islamic Azad University, Ahvaz, Iran*
[2]*Department of Genetics, Ahvaz Branch, Islamic Azad University, Ahvaz, Iran*
[3]*Department of Genetics, Science and Research Branch, Islamic Azad University, Tehran, Iran*
[4]*Department of Medical Genetics, Institute of Medical Biotechnology, National Institute of Genetic Engineering and Biotechnology (NIGEB), Tehran, Iran*
[5]*Department of Biotechnology, Ahvaz Branch, Islamic Azad University, Ahvaz, Iran*
[6]*Department of Medical Genetics, School of Medicine, Ahvaz Jundishapur University of Medical Sciences, Ahvaz, Iran*

Abstract

Hereditary hearing loss is the most common sensory neural disorder, which has been revealed to have high genetic heterogeneity. Herein, we aimed to figure out the underlying genetics of the subject from an Iranian deaf family. Next-generation sequencing (NGS) of all known hearing loss genes was carried out in the proband of the family, followed by a cosegregation analysis of all members of the family. We recognized a novel homozygous pathogenic nonsense mutation, NM_001145472: c.1787G>A; p.W596X, in the LOXHD1 gene, and Sanger sequencing verified that this mutation segregated with the ARNSHL in the family. Our study showed a contribution of LOXHD1 variants to the NSHL in Iranian patients and provided a better understanding of the mutation spectrum of deafness in the Iranian population. Also, the present investigation supports the application of genetic testing in the clinical diagnosis and genetic counseling of deafness.(**International Journal of Biomedicine. 2022;12(1):164-166.**)

Key Words: hearing loss • LOXHD1 • mutation

For citation: Neissi M, Abdulzahra HKh, Sheikh-Hosseini M, Mabudi H, Mohammadi-Asl J, Al-Badran RA. Homozygous LOXHD1 Nonsense Mutation (c.1787G>A; p.W596X) is Associated with Hearing Loss in an Iranian Family: A Case Report. International Journal of Biomedicine. 2022;12(1):164-166. doi:10.21103/Article12(1)_CR

**Published without substantive editing per OFAC Guidance.*

Abbreviations

AD, autosomal dominant; **AR**, autosomal recessive; **ExAC**, exome aggregation consortium; **FCD**, fuchs corneal dystrophy; **HGMD**, human gene mutation database; **HHL**, hereditary hearing loss; **LOXHD1**, lipoxygenase homology domains 1; **NGS**, next-generation sequencing; **NSHL**, non-syndromic hearing loss; **PCR**, polymerase chain reaction; **PTA**, pure-tone audiometry; **SHL**, syndromic hearing loss; **WES**, whole exome sequencing.

Introduction

Hearing loss is the most frequent sensory deficit disorder, accounting for a high prevalence of disability.(1) Hearing loss is considered as an etiologically heterogeneous sensory disorder with a prevalence of 1 in 1000 live births around the world.(2) Based on hearing loss combined with the presence or absence of anomalies of the external auditory canal, hereditary hearing loss (HHL) may be divided into a syndromic hearing loss (SHL) and non-syndromic hearing loss (NSHL).(3) About 70% of HHL patients may be attributed to NSHL, and 50% of NSHL patients have Mendelian disease.(4,5) The mode of inheritance of non-syndromic hereditary hearing loss is classified into autosomal dominant (AD), autosomal recessive (AR), X-linked, and

mitochondrial. It is expected that 80% of the inheritance mode of NSHL is AR (ARNSHL), and the remaining 20% is AD (ADNSHL).[6,7] Also, in view of the consanguineous marriages' high rate in the Middle East, ARNSHL is reportedly more common in some western countries.[8]

At present, more than 60 genes and more than 145 chromosomal loci have been reported in cases affected with ARNSHL (https://hereditaryhearingloss.org/). The genes are most frequently implicated in ARNSHL, including GJB2, SLC26A4, MYO15A, OTOF, and CDH23.[6] Genetic heterogeneity of disease has been admittedly known as the most critical challenge in molecular diagnosis of NSHL. Screening for gene variants with traditional Sanger direct sequencing is time-consuming and costly.

With the advent of newer specific technologies that rely on massive parallel such as whole-exome sequencing (WES) based on next-generation sequencing (NGS), genetic heterogeneous diseases have become accessible for the detection of the causative genes and diagnosis.[9]

In the present study, we identified a novel lipoxygenase homology domain 1 (LOXHD1) c.1787G>A; p.(W596X), mutation by WES in a consanguineous Iranian pedigree with HL. To the best of our knowledge, this mutation has not been observed in any of the mutation databases.

Case Presentation

The present study was performed in a consanguineous Iranian pedigree presenting as autosomal recessive NSHL. Informed written consent was obtained from the family members in accordance with the Helsinki Declaration.

The index patient, a 26-year-old female, showed a recessively NSHL, which was symmetrical bilateral, and severe degree (Fig. 1A). The proband was further subjected to clinical examinations of the inner ear accompanied by pure-tone audiometry (PTA). The probands' parents had normal hearing, and no other additional symptoms were complained by the family members.

In order to find out the pathogenic variant in an Iranian family, a standard salting-out method was used to obtain genomic DNA from the peripheral blood samples. Whole exome sequencing was used to screen mutations from candidate genes to hereditary deafness in the genomic DNA of the index patient by Macrogen, Seoul, South Korea. The novel pathogenic variations were analyzed by the 1000 Genomes Project (https://www.internationalgenome.org/) and Exome Aggregation Consortium (ExAC). Only variants with a frequency below 1% were selected. Finally, the candidate variant was checked in the Human Gene Mutation Database (HGMD) and Clinvar.

After preliminary recognition of variant by WES, polymerase chain reaction (PCR) amplification and direct Sanger sequencing of the detected variant were used for confirmation of the co-segregation in the studied family. Also, the identified variant was checked in the healthy control database for the same ethnic group (Iranome; http://www.iranome.ir/).

WES was carried out on the genomic DNA from the proband. A variant rate equal to or less than 0.01 in CNGMD was utilized as the frequency cut-offs. As shown in Figure 1B, a novel homozygous mutation c.1787G>A (TGG>TAG) was detected in exon 15 of the LOXHD1 gene, which was recognized co-segregated with the phenotype in a consanguineous Iranian family. This variant has not been described in 1000 Genome and ExAC databases. Based on the ACMG guidelines, the c.1787G >A mutation is classified as pathogenic.

To confirm the results, direct Sanger sequencing was carried out on the DNA of the family members. The results demonstrated that the affected case was homozygous for this nonsense mutation, and each of her healthy parents carried a heterozygous LOXHD1 c.1787G>A (p.W596X) variant.

The nonsense mutation detected in exon 15 of the LOXHD1 gene (c.1787G>A) leads to the tryptophan stop codon substitution (Trp596Ter), which was located in the polycystin-1/lipoxygenase/alpha-toxin (PLAT) 5 domain of the LOXHD1 protein (Fig. 1C).

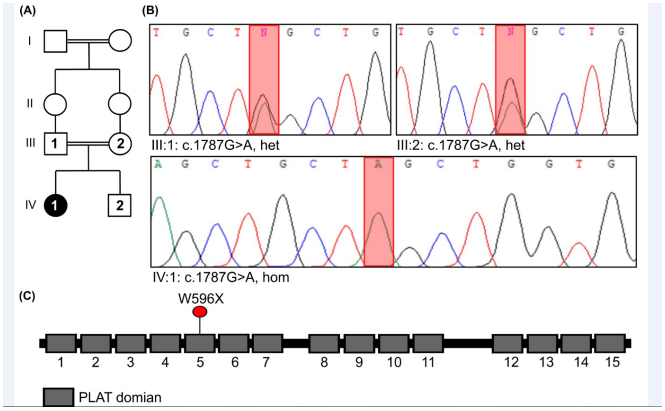

Fig.1. *(A) Pedigree of family with ARNSHL. The black-solid circle (IV:1) represents the affected female patient. The mother and father (III:1 and III:2) are first cousins. (B) Sequence electropherograms showing homozygous change in the proband and parents as heterozygous carriers. (C) Zoomed-in view of region containing the variant. The p.W596X stop mutation is located at the 5th PLAT domain of the LOXHD1 protein.*

Its substitution for a stop codon could result in either a severely truncated protein or the absence of the LOXHD1 protein secondary to nonsense-mediated decay (NMD). Multiple orthologous sequence alignment (MSA) around codon 596 showed this, and neighboring amino acids are evolutionarily highly conserved residues in LOXHD1. In addition, prediction tools, including SIFT and MutationTaster software, predicted that this variant is disease-causing. Thus, it is recommended that the p.W596X residue is important for proper protein function.

Discussion

In the present research, a mutation in the LOXHD1 gene was recognized by targeted WES in an Iranian family. Mutations in the LOXHD1 gene are the pathogenic cause for both Fuchs corneal dystrophy (FCD) and ARNSHL (DFNB77).[10] Patients with FCD usually carry LOXHD1 heterozygous mutations, whereas individuals with DFNB77 usually have homozygous mutations in any domain.[10]

Until now, about 80 pathogenic mutations of the LOXHD1 have been described in patients with FCD and DFNB77 in international mutation databases. Ethnic variety of genetic variance has been described in HL gene LOXHD1.[11] Though, one of these mutations was identified in the Iranian family.

In the present study on a family with severe HL, one nonsense homozygous mutation (c. 1787G>A (p.W596X)) in LOXHD1 was recognized by targeted WES. Subsequently, Sanger sequencing further confirmed the existence of this mutation, which revealed co-segregated with HL. The normal-hearing members in the family were heterozygous for the detected mutation and no visual problems and vestibular dysfunction were shown in any of them.

The LOXHD1 gene (NM_001145472), which is located at 18q12-q21, spans about 35–56 Mb of DNA, and consists of 43 exons. This gene encodes a 2,211-amino acid protein, which is made up of 15 polycystin /lipoxygenase /alpha-toxin (PLAT) domains.[12] The LOXHD1 protein function is unclarified though PLAT domains are predominantly located along the membrane of hair cell stereocilia and believed to be involved in protein-protein and protein-lipid interactions, demonstrating its role in maintaining normal hearing.[12] PLAT domains are approximately 120 amino acids long, form a beta-sandwich including 2 sheets of 4 strands each, and show to function in plasma membrane targeting.[13] PLAT domains share structural similarities to eukaryotic Ca2+-binding C2 domains. Studies recognized LOXHD1 orthologs in vertebrates, cephalochordates, and urochordates, but not in arthropods or nematodes.[14]

Protein structure analyses propose that the first 11 PLAT domains of the LOXHD1 protein are highly conserved from Danio rerio to humans; mutations in these domains perturb LOXHD1 and might damage the interactions and destabilize LOXHD1 protein structure affecting the proper function of the protein.[15] We, therefore, propose that the W596X mutation, which damages the 5th PLAT domain, is the cause of the hearing impairment in our patient.

In conclusion, we successfully recognized a novel and pathogenic mutation in an Iranian family by the targeted WES. Our finding shows that this new method is a highly effective genetic diagnostic technology for this heterogeneous disease.

Acknowledgments

The authors thank the family members for their participation in this study.

Competing Interests

All authors declare that they have no conflict of interest.

Ethics approval and consent to participate

All procedures performed in this study were in accordance with the ethical standards of the institutional and/or national research committee and with the 1964 Helsinki declaration and its later amendments.

References

1. Sheffield AM, Smith RJH. The Epidemiology of Deafness. Cold Spring Harb Perspect Med. 2019 Sep 3;9(9):a033258. doi: 10.1101/cshperspect.a033258.
2. Motavaf M, Soveizi M, Maleki M, Mahdieh N. MYO15A splicing mutations in hearing loss: A review literature and report of a novel mutation. Int J Pediatr Otorhinolaryngol. 2017 May;96:35-38. doi: 10.1016/j.ijporl.2017.03.008.
3. Kremer H. Hereditary hearing loss; about the known and the unknown. Hear Res. 2019 May;376:58-68. doi: 10.1016/j.heares.2019.01.003.
4. Vona B, Müller M, Dofek S, Holderried M, Löwenheim H, Tropitzsch A. A Big Data Perspective on the Genomics of Hearing Loss. Laryngorhinootologie. 2019 Mar;98(S 01):S32-S81. English, German. doi: 10.1055/a-0803-6149.
5. Talebi F, Ghanbari Mardasi F, Mohammadi Asl J, Tizno S, Najafvand Zadeh M. Identification of Novel PTPRQ and MYO1A Mutations in An Iranian Pedigree with Autosomal Recessive Hearing Loss. Cell J. 2018 Apr;20(1):127-131.
6. Hilgert N, Smith RJ, Van Camp G. Function and expression pattern of nonsyndromic deafness genes. Curr Mol Med. 2009 Jun;9(5):546-64. doi: 10.2174/156652409788488775.
7. Mohammadi-Asl J, Saki N, Dehdashtiyan M, Neissi M, Ghanbari Mardasi F. Identification of a Novel WFS1 Mutation Using the Whole Exome Sequencing in an Iranian Pedigree with Autosomal Dominant Hearing Loss. Iran J Otorhinolaryngol. 2021 May;33(116):173-176. doi: 10.22038/ijorl.2021.
8. Najmabadi H, Kahrizi K. Genetics of non-syndromic hearing loss in the Middle East. Int J Pediatr Otorhinolaryngol. 2014 Dec;78(12):2026-36. doi: 10.1016/j.ijporl.2014.08.036.
9. Talebi F, Ghanbari Mardasi F, Mohammadi Asl J, Bavarsad AH, Tizno S. Identification of a novel missence mutation in FGFR3 gene in an Iranian family with LADD syndrome by Next-Generation Sequencing. Int J Pediatr Otorhinolaryngol. 2017 Jun;97:192-196. doi: 10.1016/j.ijporl.2017.04.016.
10. Riazuddin SA, Parker DS, McGlumphy EJ, Oh EC, Iliff BW, Schmedt T, et al. Mutations in LOXHD1, a recessive-deafness locus, cause dominant late-onset Fuchs corneal dystrophy. Am J Hum Genet. 2012 Mar 9;90(3):533-9. doi: 10.1016/j.ajhg.2012.01.013.
11. Bai X, Zhang C, Zhang F, Xiao Y, Jin Y, Wang H, Xu L. Five Novel Mutations in LOXHD1 Gene Were Identified to Cause Autosomal Recessive Nonsyndromic Hearing Loss in Four Chinese Families. Biomed Res Int. 2020 Feb 18;2020:1685974.
12. Grillet N, Schwander M, Hildebrand MS, Sczaniecka A, Kolatkar A, Velasco J, et al. Mutations in LOXHD1, an evolutionarily conserved stereociliary protein, disrupt hair cell function in mice and cause progressive hearing loss in humans. Am J Hum Genet. 2009 Sep;85(3):328-37.
13. Aleem AM, Jankun J, Dignam JD, Walther M, Kühn H, Svergun DI, Skrzypczak-Jankun E. Human platelet 12-lipoxygenase, new findings about its activity, membrane binding and low-resolution structure. J Mol Biol. 2008 Feb 8;376(1):193-209. doi: 10.1016/j.jmb.2007.11.086.
14. Recacha R, Boulet A, Jollivet F, Monier S, Houdusse A, Goud B, Khan AR. Structural basis for recruitment of Rab6-interacting protein 1 to Golgi via a RUN domain. Structure. 2009 Jan 14;17(1):21-30. doi: 10.1016/j.str.2008.10.014.
15. Edvardson S, Jalas C, Shaag A, Zenvirt S, Landau C, Lerer I, Elpeleg O. A deleterious mutation in the LOXHD1 gene causes autosomal recessive hearing loss in Ashkenazi Jews. Am J Med Genet A. 2011 May;155A(5):1170-2.

***Corresponding author**: Mostafa Neissi. Department of Genetics, Khuzestan Science and Research Branch, Islamic Azad University, Ahvaz, Iran. E-mail: iammostafaneissi@gmail.com*

IJBM

INTERNATIONAL JOURNAL OF BIOMEDICINE

Instructions for Authors

International Journal of Biomedicine (IJBM) publishes peer-reviewed articles on the topics of basic, applied, and translational research on biology and medicine. International Journal of Biomedicine welcomes submissions of the following types of paper: Original articles, Reviews, Perspectives, Viewpoints, and Case Reports.

All research studies involving animals must have been conducted following animal welfare guidelines such as *the National Institutes of Health (NIH) Guide for the Care and Use of Laboratory Animals*, or equivalent documents. Studies involving human subjects or tissues must adhere to the *Declaration of Helsinki and Title 45, US Code of Federal Regulations, Part 46, Protection of Human Subjects*, and must have received approval of the appropriate institutional committee charged with oversight of human studies. Informed consent must be obtained.

Pre-submissions

Authors are welcome to send an abstract or draft manuscript to obtain a view from the Editor about the suitability of their paper. Our Editors will do a quick review of your paper and advise if they believe it is appropriate for submission to our journal. It will not be a full review of your manuscript.

Manuscript Submission

Manuscript submissions should conform to the guidelines set forth in the Recommendations for the Conduct, Reporting, Editing and Publication of Scholarly Work in Medical Journals (ICMJE Recommendations), available from www.ICMJE.org.

Original works will be accepted with the understanding that they are contributed solely to the Journal, are not under review by another publication, and have not previously been published except in abstract form.

All manuscripts must be submitted through the International Journal of Biomedicine`s online submission system (www.ijbm.org/submission.php). Manuscripts must be typed, double-spaced using a 14-point font, including references, figure legends, and tables. Leave 1-inch margins on all sides. Assemble the manuscript in this order: Title Page, Abstract, Key Words, Text (Introduction, Methods, Results, and Discussion), Acknowledgments, Sources of Funding, Disclosures, References, Tables, Figures, and Figure Legends. References, figures, and tables should be cited in numerical order according to first mention in the text.

The preferred order for uploading files is as follows: Cover letter, Full Manuscript PDF (PDF containing all parts of the manuscript including references, legends, figures and tables), Manuscript Text File (MS Word), Figures (each figure and its corresponding legend should be presented together), and Tables. Files should be labeled with appropriate and descriptive file names (e.g., SmithText.doc, Fig1.eps, Table3.doc). Text, Tables, and Figures should be uploaded as separate files. (Multiple figure files can be compressed into a Zip file and uploaded in one step; the system will then unpack the files and prompt the naming of each figure. See www.WinZip.com for a free trial.)

Authors who are unable to provide an electronic version or have other circumstances that prevent online submission must contact the Editorial Office prior to submission to discuss alternate options (editor@ijbm.org).

Cover Letter

The cover letter should be saved as a separate file for upload. In it, the authors should (1) state that the manuscript, or parts of it, have not been and will not be submitted elsewhere for publication; (2) state that all authors have read and approved the manuscript; and (3) disclose any financial or other relations that could lead to a conflict of interest. If a potential conflict exists, its nature should be stated for each author. When there is a stated potential conflict of interest a footnote will be added indicating the author's equity interest in or other affiliation with the identified commercial firms.

The corresponding author should be specified in the cover letter. All editorial communications will be sent to this author. A short paragraph telling the editors why the authors think their paper merits publication priority may be included in the cover letter.

Types of articles

Original articles

Original articles present the results of original research. These manuscripts should present well-rounded studies reporting innovative advances that further knowledge about a topic of importance to the fields of biology or medicine. These can be submitted as either a full-length article (no more than 6,000 words, 4 figures, 4 tables) or a Short Communication (no more than 2,500 words, 2 figures, 2 tables). An original

article may be Randomized Control Trial, Controlled Clinical Trial, Experiment, Survey, and Case-control or Cohort study.

Case Reports

Case reports describe an unusual disease presentation, a new treatment, a new diagnostic method, or a difficult diagnosis. The author must make it clear what the case adds to the field of medicine and include an up-to-date review of all previous cases in the field. These articles should be no more than 5,000 words with no more than 6 figures and 3 tables. Case Reports should consist of the following headings: Abstract (no more than 100 words), Introduction, Case Presentation (clinical presentation, observations, test results, and accompanying figures), Discussion, and Conclusions.

Reviews

Reviews analyze the current state of understanding on a particular subject of research in biology or medicine, the limitations of current knowledge, future directions to be pursued in research, and the overall importance of the topic. Reviews could be non-systematic (narrative) or systematic. Reviews can be submitted as a Mini-Review (no more than 2,500 words, 3 figures, and 1 table) or a long review (no more than 6,000 words, 6 figures, and 3 tables). Reviews should contain four sections: Abstract, Introduction, Topics (with headings and subheadings, and Conclusions and Outlook.

Perspectives

Perspectives are brief, evidenced-based and formally structured essays covering a wide variety of timely topics of relevance to biomedicine. Perspective articles are limited to 2,500 words and usually include ≤10 references, one figure or table. Perspectives contain four sections: Abstract, Introduction, Topics (with headings and subheadings), Conclusions and Outlook.

Viewpoints

Viewpoint articles include academic papers, which address any important topic in biomedicine from a personal perspective than standard academic writing. Maximum length is 1,200 words, ≤70 references, and 1 small table or figure.

Manuscript Preparation

Title Page

The first page of the manuscript (title page) should include (1) a full title of the article, (2) a short title of less than 60 characters with spaces, (3) the authors' names, academic degrees, and affiliations, (4) the total word count of the manuscript (including Abstract, Text, References, Tables, Figure Legends), (5) the number of figures and tables, and (6) the name, email address, and complete address of corresponding author.

Disclaimers. An example of a disclaimer is an author's statement that the views expressed in the submitted article are his or her own and not an official position of the institution or funder.

Abstract

The article should include a brief abstract of no more than 200 words. Limit use of acronyms and abbreviations. Define at first use with acronym or abbreviation in parentheses. The abstract should be structured with the following headings: Background, Methods and Results, and Conclusions. The Background section should describe the rationale for the study. Methods and Results should briefly describe the methods and present the significant results. Conclusions should succinctly state the interpretation of the data. Authors should supply a list of up to four key words not appearing in the title, which will be used for indexing. The key words should be listed immediately after the Abstract. Use terms from the Medical Subject Headings (MeSH) list of Index Medicus when possible.

Main text in the IMRaD format

Introduction should describe the purpose of the study and its relation to previous work in the field; it should not include an extensive literature review.

Methods should be concise but sufficiently detailed to permit repetition by other investigators. Previously published methods and modifications should be cited by reference. A subsection on statistics should be included in the Methods section.

Results should present positive and relevant negative findings of the study, supported when necessary by reference to Tables and Figures.

Discussion should interpret the results of the study, with emphasis on their relation to the original hypotheses and to previous studies. The importance of the study and its limitations should also be discussed.

The IMRaD format does not include a separate Conclusion section. The conclusion is built into the Discussion. More information on the structure and content of these sections can be found in the Recommendations for the Conduct, Reporting, Editing and Publication of Scholarly Work in Medical Journals (ICMJE Recommendations), available from www.ICMJE.org.

Acknowledgments, Sources of Funding, and Disclosures

Acknowledgments : All contributors who do not meet the criteria for authorship should be listed in an acknowledgments section. Examples of those who might be acknowledged include a person who provided purely technical help, writing assistance, or a department chairperson who provided only general support. Authors should declare whether they had assistance with study design, data collection, data analysis, or manuscript preparation. If such assistance was available, the authors should disclose the identity of the individuals who provided this assistance and the entity that supported it in the published article.

Sources of Funding: All sources of financial support for the study should be cited on the title page, including federal or state agencies, nonprofit organizations, and pharmaceutical or other commercial sources.

Disclosure and conflicts of interest: All authors must disclose any financial or other relations that could lead to a conflict of interest. If a potential conflict exists, its nature should be stated for each author. All sources of financial support for the study should be cited, including federal or state agencies, nonprofit organizations, and pharmaceutical or other commercial sources. Please use ICMJE Form for Disclosure of Potential Conflicts of Interest (http://www.icmje.org/conflicts-of-interest/).

References

References should follow the standards summarized in the NLM's International Committee of Medical Journal Editors (ICMJE) Recommendations for the Conduct, Reporting,

Editing and Publication of Scholarly Work in Medical Journals: Sample References webpage (www.nlm.nih.gov/bsd/uniform_requirements.html) and detailed in the NLM's Citing Medicine, available from www.ncbi.nlm.nih.gov/books/NBK7256/. MEDLINE abbreviations for journal titles (www.ncbi.nlm.nih.gov/nlmcatalog/journals) should be used. The first six authors should be listed in each reference citation (if there are more than six authors, "et al" should be used following the sixth). Periods are not used in authors' initials or journal abbreviations. Examples of journal reference style:

Journal Article: Serruys PW, Ormiston J, van Geuns RJ, de Bruyne B, Dudek D, Christiansen E, et al. A Polylactide Bioresorbable Scaffold Eluting Everolimus for Treatment of Coronary Stenosis: 5-Year Follow-Up. J Am Coll Cardiol. 2016;67(7):766-76. doi: 10.1016/j.jacc.2015.11.060.

Book: Murray PR, Rosenthal KS, Kobayashi GS, Pfaller MA. Medical Microbiology. 4th ed. St. Louis: Mosby; 2002.

Chapter in Edited Book: Meltzer PS, Kallioniemi A, Trent JM. Chromosome alterations in human solid tumors. In: Vogelstein B, Kinzler KW, editors. The Genetic Basis of Human Cancer. New York: McGraw-Hill; 2002:93–113.

References should be numbered consecutively in the order in which they are first mentioned in the text. Identify references in text, tables, and legends by Arabic numerals in parentheses and listed at the end of the article in citation order.

Tables

Tables should be comprehensible without reference to the text and should not be repetitive of descriptions in the text. Every table should consist of two or more columns; tables with only one column will be treated as lists and incorporated into the text. All tables must be cited in the text and numbered in order of appearance. Tables should include a short title. Place explanatory matter in footnotes, not in the heading. Explain all nonstandard abbreviations in footnotes, and use symbols to explain information if needed. Each table submitted should be double-spaced, each on its own page. Each table should be saved as its own file as a Word Document. Explanatory matter and source notations for borrowed tables should be placed in the table footnote.

Figures and Legends

All illustrations (line drawings and photographs) are classified as figures. All figures should be cited in the text and numbered in order of appearance. Figures should be provided in .tiff, .jpeg or .eps formats. Color images must be at least 300 dpi. Gray scale images should be at least 300 dpi. Line art (black and white or color) and combinations of gray scale images and line art should be at least 1,000 dpi. The optimal size of lettering is 12 points. Symbols should be of a similar size. Figures should be sized to fit within the column (86 mm) or the full text width (180 mm). Line figures must be sharp, black and white graphs or diagrams, drawn professionally or with a computer graphics package. Legends should be supplied for each figure and should be brief and not repetitive of the text. Any source notation for borrowed figures should appear at the end of the legend. Figures should be uploaded as individual files.

Units of Measurement

Measurements of length, height, weight, and volume should be reported in metric units (meter, kilogram, or liter) or their decimal multiples. Temperatures should be in degrees Celsius. Blood pressures should be in millimeters of mercury. All measurements must be given in SI or SI-derived units. Drug concentrations may be reported in either SI or mass units, but the alternative should be provided in parentheses where appropriate.

Style and Language

The journal accepts manuscripts written in English. Spelling should be US English only. The language of the manuscript must meet the requirements of academic publishing. Reviewers may advise rejection of a manuscript compromised by grammatical errors. Non-native speakers of English may choose to use a copyediting service.

Abbreviations and Symbols

Use only standard abbreviations; use of nonstandard abbreviations can be confusing to readers. Avoid abbreviations in the title of the manuscript. The spelled-out abbreviation followed by the abbreviation in parenthesis should be used on first mention unless the abbreviation is a standard unit of measurement.

Drugs should be referred to by their generic names. If proprietary drugs have been used in the study, refer to these by their generic name, mentioning the proprietary name, and the name and location of the manufacturer, in parentheses.

Permissions

To use tables or figures borrowed from another source, permission must be obtained from the copyright holder, usually the publisher. Authors are responsible for applying for permission for both print and electronic rights for all borrowed materials and are responsible for paying any fees related to the applications of these permissions. This is necessary even if you are an author of the borrowed material. It is essential to begin the process of obtaining permission early, as a delay may require removing the copyrighted material from the article. The source of a borrowed table should be noted in a footnote and of a borrowed figure in the legend. It is essential to use the exact wording required by the copyright holder. A copy of the letter granting permission, identified by table or figure number, should be sent along with the manuscript. A permission request form is provided for the authors use in requesting permission from copyright holders.

Open Access Policy

All articles published by International Journal of Biomedicine are made freely and permanently accessible online immediately upon publication, without subscription charges or registration barriers. Articles published under an IMRDC user license are protected by copyright and may be used for non-commercial purposes. A copy of the full text of each Open Access article is archived in an online repository separate from the journal. The International Journal of Biomedicine's articles are archived in Scientific Electronic Library (Russian Science Citation Index). The authors can also self-archive the final publisher's version/PDF on personal website, departmental website, institutional repository with a link to publisher version.

Users may access, download, copy, translate, text and data mine (but may not redistribute, display or adapt) the articles for non-commercial purposes provided that users cite the article using an appropriate bibliographic citation (i.e. author(s), journal, article title, volume, issue, page numbers, DOI and the link to the definitive published PDF version on www.ijbm.org).

Article Processing Charges

When a paper is accepted for publication, the author is issued an invoice for payment of Article Processing Charge (APC). APC can be paid by the author or on their behalf, for example, by their institution or funding body.

APC helps IMRDC recover the costs of publication—including peer review management, production of the journal printed version, and online hosting and archiving, as well as inclusion in citation databases, enabling electronic citation in other journals that are available electronically. IJBM publishes all content Open Access and makes the content freely available online for researchers and readers.

IJBM charges a processing fee of $115.00 per printed black and white journal page and $230.00 per printed page of color illustrations. IJBM charges a processing fee of $94.00 per page in the case of online-only publications. For online-only publications, all illustrations submitted in color will be published in color online, at no cost to the author.

Under IJBM's existing policy, certain categories of authors are eligible for a discount. The amount of discount depends on factors such as country of origin, position of the author in the institute and quality and originality of the work. Young researchers and first time authors may also qualify for a discount. To apply for a discount, please contact our office using the 'Contact Us' page or send email to the Publisher (editor@ijbm.org) with the following information:

- Your name and institution with full address details
- Reason for applying for a waiver
- Title of your paper
- Country of residence of any co-authors.

Page Proofs

Page proofs are sent from the Publisher electronically and must be returned within 72 hours to avoid delay of publication. Generally, peer review is completed within 3-4 weeks and the editor's decision within 7-10 days of this. It is therefore very rare to have to wait more than 6 weeks for a final decision.

IMRDC Author Services

If you need help preparing a manuscript for submission, our publisher, IMRDC, offers a range of editorial services for a fee, including Advanced Editing and Translation with Editing. Please note that use of IMRDC Author Services does not guarantee acceptance of your manuscript.

It is important to note that when citing an article from IJBM, the correct citation format is **International Journal of Biomedicine.**